New Perspectives on the Chronostratigraphy and Magmatic Evolution of the Auckland Volcanic Field, New Zealand

Jenni L. Hopkins

A thesis submitted to Victoria University of Wellington

in fulfilment of the requirements for the degree of

Doctor of Philosophy (Geology)

Victoria University of Wellington, 2015

Abstract

Understanding the eruptive history of a volcanically active region is critical in assessing the hazard and risk posed by future eruptions. In regions where surface deposits are poorly preserved, and ambiguously sourced, tephrostratigraphy is a powerful tool to assess the characteristics of past eruptions. The city of Auckland, New Zealand's largest urban centre and home to ca. 1.4 million people, is built on top of the active Auckland Volcanic Field (AVF). The AVF is an intraplate monogenetic basaltic volcanic field, with ca. 53 eruptive centres located in an area of ca. 360 km^2. Little is known however, about the evolution of the field because the numerical and relative ages of the eruptions are only loosely constrained, and therefore the precise order of many eruptions is unknown. Here I apply tephrostratigraphic and geochemical techniques to investigate the chronology and magmatic evolution of the AVF eruptions.

First, I present an improved methodology for in-situ analysis of lacustrine maar cores from the AVF by employing magnetic susceptibility and X-ray density scanning on intact cores. These techniques are coupled with geochemical microanalysis of the tephra-derived glass shards to reveal details of reworking within the cores. These details not only allow assessment of the deposit relationships within cores (e.g. primary vs. reworked horizons), but also to correlate tephra horizons between cores. Through the correlation of tephra units across cores from a variety of locations across the field, an improved regional tephrostratigraphic framework for the AVF deposits has been established.

Following on from this, I detail the methods developed in this study to correlate tephra horizons within the maar cores back to their eruptive source. This technique uses geochemical fingerprinting to link the glass analyses from tephra samples to whole rock compositions. Such an approach has not been previously attempted due to the complications caused by fractional crystallisation, which affects concentrations of certain key elements in whole rock analyses. My method resolves these issues by using incompatible trace elements, which are preferentially retained in melt over crystals, and therefore retain comparable concentrations and concentration ratios between these two types of sample. Because of the primitive nature of the AVF magmas, their trace element signature is largely controlled by the

involvement of several distinct mantle sources. This leads to significant variability between the volcanic centres that thus can be used for individually fingerprinting, and correlating tephra to whole rocks. Nevertheless, in some cases geochemistry cannot provide an unambiguous correlation, and a multifaceted approach is required to allow the correlation of the tephra horizons to source. The other criteria used to correlate tephra deposits to their source centre include, Ar-Ar ages of the centres, modelled and calculated ages of the tephra deposits, the scale of eruption, and the deposit locations and thicknesses.

The results of this research outline the methodology for assessing occurrence and characteristics of basaltic tephra horizons within lacustrine maar cores, and the methodology for correlating these horizons to their eruptive source. In doing this the relative eruption order of the AVF is accurately determined for the first time. Temporal trends suggest acceleration of eruption repose periods to 21 ka followed by deceleration to present. Although no spatial evolution is observed, coupling of some centres is seen when spatial and temporal evolution are combined. The geochemical signature of the magmas appears to evolve in a cyclic manner with time, incorporating increasing amount of a shallow source. This evolution is seen both during a single eruption sequence and throughout the lifespan of the AVF.

Finally, pre-eruptive processes are assessed as part of the study of the magmatic evolution of the AVF. The effects of contamination from the crust and lithosphere through which the magma ascends are evaluated using the Re-Os isotope system. The results show there are variable inputs from crustal sources, which have previously not been identified by traditional isotope systems (e.g. Pb-Sr-Nd isotopes). Two sources of contamination are identified based on their Os systematics relating to two terranes beneath the AVF: the metasedimentary crust and the Dun Mountain Ophiolite Belt. The identification of this process suggests there is interaction of ascending melt with the crust, contrary to what previous studies have concluded. This body of research has provided a detailed reconstruction of the chronostratigraphy and magmatic evolution of the AVF to aid accurate and detailed risk assessment of the threat posed by a future eruption from the Auckland Volcanic Field.

Acknowledgements

I would first like to thank my supervisors Prof. Colin Wilson, Dr. Graham Leonard, and Dr. Christian Timm for their support and guidance throughout this project. The last few years have been an absolute pleasure. I also owe a great deal of thanks to my advisor Marc-Alban Millet, thank you for continuing to offer essential advice and support to this research.

I am grateful to GNS and the DEVORA team for providing me with the funding and the scope for the project; and for the financial support from VUW submission scholarship and faculty strategic research grants, to allow continued research and travel.

This research would not have been completed without the technical assistance from various people in a number of institutions. At VUW my thanks go to Sabrina for always being ahead of the game in the geochem labs - you are a superstar; to Stewart for training and assistance in sample preparation; to Richard Wysoczanski for teaching me how to use the probe; to Ian Schipper for continued probe assistance; and Monica Handler for ICP-MS assistance. Thanks also to Helen Neil and Alan Orphin (NIWA) for their assistance and discussions in relation to core analysis techniques; to Andrè Poirier (UQAM) for teaching me how to do complex isotope chemistry and analysis on Re and Os; to Michael Palin and Malcolm Reid (UoO) for their assistance with LA-ICP-MS techniques; to Phil Shane (UoA) for providing thought provoking discussion on AVF tephra deposits, and supplying some of the samples and data used in this thesis. I also thank Lucy McGee for also providing essential data, samples, and advice. Finally a huge thanks to Elaine Smid (UoA/DEVORA) - field assistant, colleague, and confidante, good luck for your PhD!

I would like to also thank the friends I have made throughout the PhD journey, VGP group students old and new, fifth floor/ARC representatives, and housemates old and new - you have to play hard to work hard! With a special mention to my PhD twin Chris ‘Condor’ Conway (you didn’t have to break your collar bone just to keep up). To office mates past and present, Maria, Jess, Connie, and Denise, I couldn’t have asked for a nicer environment to work in. To Loretta, the constant throughout my time at VUW, thank you for being a great wing(wo)man to ride the PhD rollercoaster with. Finally, to Becca, thank you for your support both here and over Skype, I couldn’t ask for a better, more understanding best friend.

To my family, thank you for understanding and accepting my need to be at the other side of the world, I am sorry it has meant I have missed out on some important family moments. Your support and pride has kept me going.

Finally, Shaun, I was prepared for moving to New Zealand to be a life-changing adventure, I wasn’t prepared for meeting you, my life changer.

Table of Contents

Appendices (electronic)

List of Figures

Chapter 1

Chapter 2

Chapter 3

Chapter 4

Chapter 5

Chapter 6

List of Tables

Chapter 5

Chapter 6

List of Abbreviations

AFC – Assimilation Fractional Crystallisation
AR – Analytical reagent
AVF – Auckland Volcanic Field
BMS – Base Metal Sulphides
ca. - from the Latin circa meaning approximately
cal. yr BP – Calendar years before present (taken as 1950)
CEVP – Central European Volcanic Province
conc. – concentration
DEVORA – DEtermining VOlcanic Risk in Auckland
DMM – Depleted MORB Mantle
DMOB – Dun Mountain Ophiolite Belt
DRE – Dense Rock Equivalent
DU – Durham University
EDS – Energy-dispersive spectrometry
EM – Enriched Mantle
GNS – Institute of Geological and Nuclear Science
HIMU - high μ; μ = $^{238}U/^{204}Pb$ isotope ratio
HREE – Heavy Rare Earth Elements (Y, Tb, Dy, Ho, Er, Tm, Yb, Lu)
JMA – Junction Magnetic Anomaly
ka – kiloannum, thousand years
Kk – Kawakawa (Oruanui) rhyolitic marker horizon
LA-ICP-MS – Laser Ablation-Inductively Coupled Plasma – Mass Spectrometry
LGM – Last Glacial Maximum
LILE – Large Ion Lithophile Elements (K, Rb, Cs, Sr, Ba, Pb^{2+}, Eu^{2+})
LOI – Loss-on-ignition
LREE – Light Rare Earth Elements
Ma – Megaannum, million years
MC-ICP-MS – Multi Collector - Inductively Coupled Plasma – Mass Spectrometry'
Mg# - Magnesium number = (Mg^{2+}/ (Mg^{2+} +Fe^{2+})) x 100
MI – Mayor Island volcano
mL – millilitre
MORB – Mid Ocean Ridge Basalt
MQ – MilliQ water
MVF – Monogenetic Volcanic Field
NIWA – National Institute of Water and Atmospheric Research
nm – nanometer
NZ – New Zealand
OB – Orakei Basin
OIB – Ocean Island Basalt
On – Onepoto
Ok – Okareka rhyolitic marker horizon
OVC – Okataina Volcanic Centre
PGEs – Platinum Group Elements
ppm – parts per million
Re – Rotoehu rhyolitic marker horizon
Rk – Rerewhakaaitu rhyolitic marker horizon
RMH – Rhyolitic Marker Horizon
SAVF – South Auckland Volcanic Field
SB – Sub Boiled
SF-ICP-MS – Sector Field - Inductively Coupled Plasma – Mass Spectrometry
SMLM – Subduction Metasomatised Lithospheric Mantle
SS – Sea Star
TgVC – Tongariro Volcanic Centre
Tk – Mt Taranaki volcano
TVZ – Taupo Volcanic Zone
UK – United Kingdon
μL – microliter
μm – micrometer (micron) $1x10^{-6}$ of a meter
UoA – University of Auckland
UoO – University of Otago
UQAM – L'Université du Québec à Montréal
VEI - Volcanic Explosivity Index
VUW – Victoria University of Wellington
WDS – Wavelength Dispersive Spectrometry
wt.% - weight percent
XRF – X-ray Fluorescence

Chapter 1

Monogenetic basaltic volcanism and the Auckland Volcanic Field

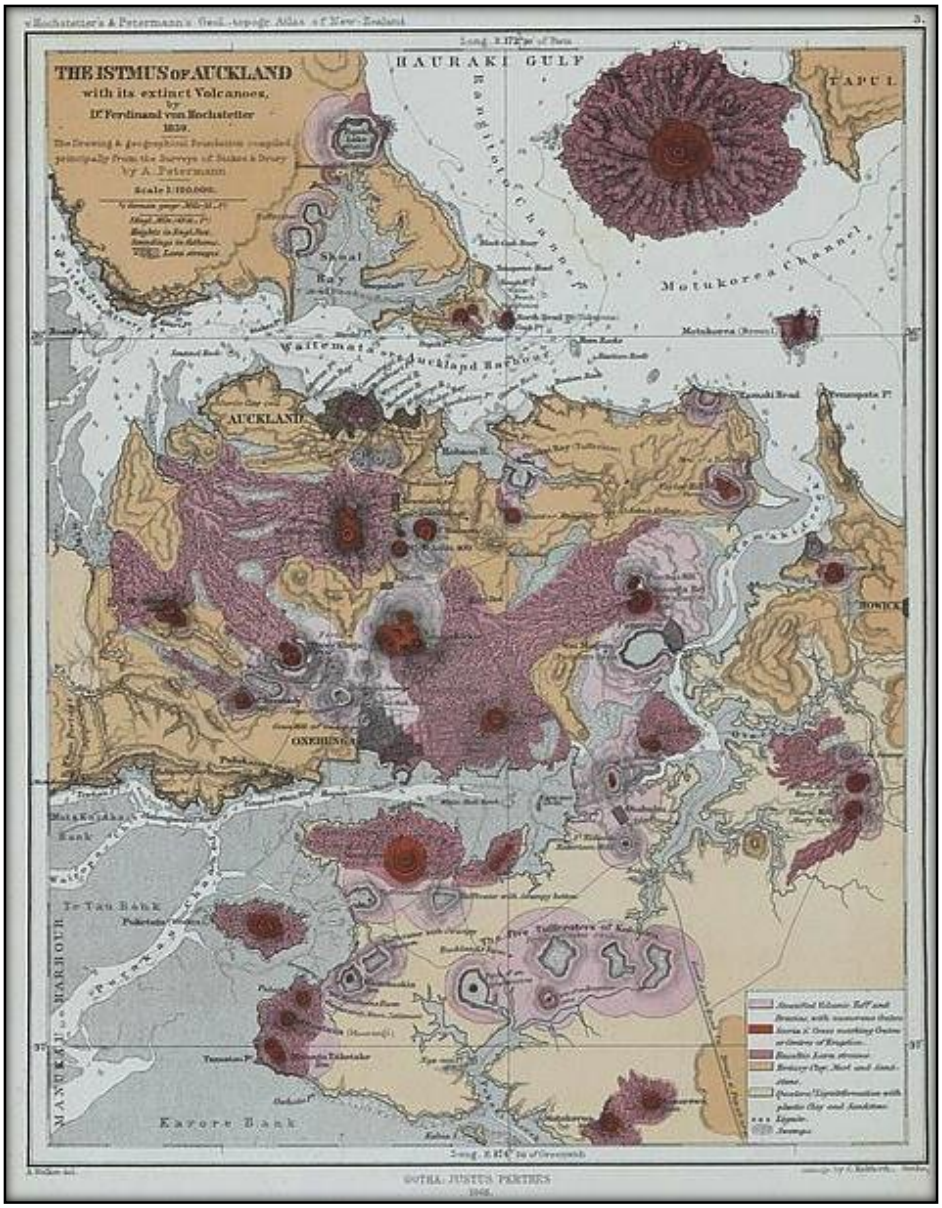

The isthmus of Auckland prior to urbanization with its extinct volcanoes Ferdinand von Hochstetter, published by T. Delattre, Auckland, 1864. Sourced from the National Library of Australia.

A purely local set of happenings that produced a unique set of characteristics Professor E. J. Searle (1909-1996).

1.1. General Introduction

Volcanism is one of many naturally occurring events that fall under the umbrella term of 'natural hazards'. Natural hazards are defined as naturally occurring elements of the physical environment, which have an adverse affect on people, infrastructure, and environment. The sub categories of which include, geological (e.g., volcanic eruption, earthquake, tsunami), meteorological (e.g., storms, drought, heat wave), and biological (e.g., disease, infestation) (Bryant, 2005). Amongst these natural hazards volcanism is often considered one of the most complex in affecting people, and causing costly damage to the urban and rural environments (Rymer, 2000). This is in part due to the association of active volcanism with a multitude of related hazards such as earthquakes, lahars, or ash fall. But in addition, due to the ever-increasing urbanisation in close proximity to active volcanic centres (Rymer, 2000).

Volcanic hazards are subdivided into two categories: primary hazards including lava flows, pyroclastic flows, lahars, and ash fall; and secondary hazards that occur as a result of the primary hazards, for example contamination of water supplies, or impact on aviation and those industries that rely on it (Rymer, 2000). Of the hazards associated with volcanic eruptions, ash fall has the potential to affect the largest areas, and often be the most frequent, disruptive, and costly (Miller and Casadevall, 2000). As well as the immediate effects of ash fall (from damage to buildings and transport links, to destruction of crops and livestock), man-made or natural remobilisation and re-suspension means that volcanic ash may continue to be a hazard for years to decades after an eruption (Horwell and Baxter, 2006).

The most costly impacts from volcanic ash are to the aviation industry (Miller and Casadevall, 2000), as the effects can become a global problem once ash is airborne, and reaches the stratosphere. The April-May 2010 eruption of Eyjafjallajökull, Iceland, sent ash hundreds of kilometres downwind covering much of the UK, Scandinavia, northern Europe, and western Russia. All European and north Atlantic airspace was closed, cancelling ca. 100,000 flights in 8 days (Oxford Economics, 2010). The resultant secondary global impacts on commerce and trade caused economic losses totalling ca. US $5 billion (Oxford Economics,

2010), made up of loss in the aviation sector, loss to revenue in the hospitality and tourism sectors, and losses in economical productivity. Similarly, in the southern hemisphere the eruption of Puyehue-Cordón Caulle volcano, Chile, in 2011 caused problems for New Zealand aviation, causing 7 days of disruption, with 60 flights cancelled and 7000 passengers stranded (New Zealand Transport Agency, 2011).

Although the impact on the economy is costly, one of the more researched topics in relation to ash fall hazards is the impact on respiratory health, both acute short-term effects (directly after eruptions), and more persistent long-term risks (as a result of long-term exposure). These health impacts are heavily dependent on particle size and ash composition. The highest toxic potential is attributed to shards of <4 μm that can travel into the alveoli in the lungs, and cause chronic diseases such as silicosis and pneumoconiosis, or larger particles (4-10 μm) that, when trapped in the nasal cavities or airways, can cause laryngitis or bronchitis (Beckett, 2000). In comparison to natural dusts, fresh ash is a lot more toxic due to its unweathered surfaces that can carry condensed volatiles, trace metals and acids that add to irritations caused in the airways (Horwell *et al.,* 2003). The toxicity and reactivity of the fresh surfaces of ash also has a exceptionally high leaching potential, and as well as the primary respiratory health issues, the secondary leaching of fresh ash into waterways can cause contamination of both drinking and irrigation water.

The superimposition of many urban areas on volcanically active regions, mean information is primarily required regarding future eruption potential and characteristics. Previous volcanic ash deposits are important in these instances for providing information about past eruption types, scale, composition, age and re-occurrence rates of an active volcanic regions. The information gathered is often crucial to assess the characteristics and evolution of a volcanic hazard through time, to allow predictions about potential future eruptions to be developed, and hazard and risk programmes to be implemented.

In 2008 the seven-year collaborative project ‘DEVORA’ (DEtermining VOlcanic Risk in Auckland) was set up between the University of Auckland (UoA) and GNS Science, with links to Victoria University of Wellington (VUW) and

Massey University (Palmerston North). The project was developed with the aim of better understanding the monogenetic Auckland Volcanic Field in terms of the hazard and risk it poses to the people and infrastructure of Auckland city. Auckland is New Zealand's largest urban centre, housing over one third of the country's population, and is the main control point for the country's economic activity. Auckland's physical geographic setting between the Manukau and Waitemata harbours mean that major transport and infrastructure corridors are forced into very restricted areas. When all these aspects are coupled with its location on top of an active volcanic field, it was perceived that a better understanding of the potential volcanism was essential.

As with many geological studies uniformitarianism plays a key role in allowing reconstruction of the past to inform forecasts for the future. Where the eruptive history of a region is unknown, and there is a direct threat to a large population, tephrostratigraphic and geochemical reconstructions can provide critical insight into the magma source and evolution of an active volcanic area. Thereby providing accurate information that can be used to make hazard and risk predictions of future volcanic activity.

1.2. Scientific Rationale

Monogenetic volcanic fields by their nature often have very complex eruption histories. The deposition and preservation of the eruptive products from individual eruptions can allow a more informed reconstruction of the previous activity. In particular, distal pyroclastic deposits provide a time-resolvable record of activity. Therefore the examination and correlation of these deposits to their individual volcanoes gives the opportunity to build a precise picture of the temporal, spatial and geochemical evolution of the field.

Due to their primitive nature, analysis of basaltic eruptive products (e.g., lava, pyroclastic material) also permits investigation of the mantle processes that are occurring beneath the volcanic fields. Primitive melts are the product of initial melting of a rock with only minor amounts of differentiation or interaction with other

rocks, and therefore the study of primitive basalts has the potential to give insights on the mantle source characteristics (Winter, 2010).

The over-arching goal of this thesis is to provide evidence for geological processes that are relevant to the development of hazard and risk management schemes for the city of Auckland. The composition of the mantle source, the eruption characteristics, and the absolute sequence of events in the field are all critical to understanding the hazards posed by a future eruption. All these aspects remained outstanding questions at the inception of this thesis (refer to **section 1.6**).

This introductory chapter provides the necessary background information for this research. It begins with a broad view of global monogenetic basaltic volcanism, the associated settings, the ranges of geochemistry, and the current models for the inception, and eruption, of these small-scale magmatic systems. The focus of this study, the monogenetic basaltic Auckland Volcanic Field (AVF), is then introduced including the regional tectonic setting, the local setting of the individual centres, and details of previous studies that have focused on the age and geochemistry of the field. The chapter then introduces tephrochronology, and focuses on previous tephra studies of the AVF. This introductory review from the larger picture of monogenetic volcanism, to the smaller-scale picture of the AVF characteristics, will highlight the reasoning and significance this study. Leading into the final section of **Chapter 1,** which describes the aims and key questions to be addressed, and finally outlines the structure of the research chapters in this thesis.

1.3. Monogenetic Basaltic Volcanism

1.3.1. Definitions and descriptions

The term ‘monogenetic’ is applied to volcanoes that only erupt once, unlike ‘polygenetic’ volcanoes where eruptions occur repeatedly from one centre (Walker, 2000). Polygenetic and monogenetic systems are the end-member eruptive styles of volcanic behaviour, however natural systems often display a mixture of both style types. For the monogenetic end-member the volcanism is characterised by individual magma batches that are small (0.0001 to 4 km^3) (e.g., Guilbaud *et al.,* 2012) and erupt infrequently (global average ≤ 0.0001 eruption/yr.) (Connor and Conway, 2000). The pathway to the vent does not remain a favoured route for continuing activity, and therefore does not remain active for more than one episode of volcanism, which may last from only a few days to years (Connor and Conway, 2000). The magma batches generally erupt in close proximity to one another and therefore form clusters of volcanic structures creating fields of volcanism, suggesting their plumbing systems are more complex and dispersed compared to a polygenetic system (Francis and Oppenheimer, 2004). Compared to other volcanic systems which erupt basaltic magma (e.g., mid ocean ridges or larger intraplate volcanoes), monogenetic volcanic fields have the lowest output volume of eruptive products, on the order of tens of km^3 in total (Connor and Conway, 2000). The eruption products that occur tend to vary widely with the degree to which there is water interaction with the upwelling magma. Magma interacting with sub-surface water results in explosive phreatomagmatic eruptions excavating maars and forming associated tuff rings. In comparison in ‘dry’ eruption the magma does not interact with water, and forms scoria cones and lava flows. Some centres erupt products of both ‘dry’ and ‘wet’ styles, showing that the eruption style can sometimes change over the course of an event.

1.3.2. Scale, rate and longevity

Table 1.1 outlines examples and summarises the characteristics of monogenetic fields worldwide, and **Figure 1.1** locates the currently active intraplate basaltic monogenetic fields. On a global scale the AVF is classed as relatively small with <55 centres spanning an area of <1000 km^2 (Connor and Conway, 2000). Larger fields are defined as having >100 centres over >1000 km^2; for example, the Michoacán-Guanajuato part of the Trans-Mexican volcanic belt, which contains over 1000 centres and covers an area of >40,000 km^2 (Connor, 1990).

In general, no apparent correlation exists on a global scale between the longevity of the field and the number of vents that are produced. For example, the Springerfield volcanic field (Arizona, USA) contains >400 vents that have been produced in the last 2 Myr (Condit and Connor, 1996) whereas the Cima volcanic field (California, USA) has only 70 vents formed over 4.5 Myr (Dohrenwend *et al.,* 1986). The AVF has produced 53 vents in ca. 200 ka (Lindsay *et al.,* 2011) making it comparatively quite active. However, within all given examples of fields, volcanic activity has waxed and waned over time, with periods of heightened activity and periods of quiescence, which is considered typical for basaltic volcanic fields (Connor and Conway, 2000).

A large majority of the volcanic fields identified in **Figure 1.1** lie in close proximity to large urban centres (e.g., Michoacán-Guanajuato, Mexico City), and therefore most recent studies have focused on the hazard and risk implications as a result of the field's settings. Investigations have focused on finding patterns in vent distributions and considering eruptive reoccurrence rates (e.g., Conway *et al.,* 1998), as well as understanding the processes that govern the magma supply and ascent (e.g., Berghuijs and Mattsson, 2013). Others, in order to predict future eruption styles, have recorded the detailed petrological evolution of the field through time (e.g., Blondes *et al.,* 2008). Studies on volcanic fields have focused on both single centres (e.g., Udo, Jeju Island, Korea: Brenna *et al.,* 2010), multiple centres (e.g., Mt. Gambier and Mt. Schank in the Newer Volcanics Province of eastern Australia: Demidjuk *et al.,* 2007)) and whole fields (e.g., South Auckland Volcanic Field, New Zealand: Cook *et al.,* 2005).

Table 1.1. *Features of major monogenetic volcanic fields world wide, with references; * McGee (2012); a Nicholls and Joyce (1989); b Condit and Connor (1996); c Conway et al. (1998); d Hwang et al. (2005); e Shaw (2004); f Delcamp et al. (2014); g Brenna et al. (2012); h Connor (1990); i Gutmann (2007); j Dohrenwend et al. (1986).*

Name	Location	Primary volcano type	Composition of eruptive products	Minimum number of centres	Total area (km^2)	Last known eruption	Reference
Auckland Volcanic Field	**North Island, New Zealand**	**scoria cones, maars**	**nephelinite to alkalic basalt**	**53**	**360**	**Rangitoto ca. 500 yrs. BP**	*
Newer Volcanics Province	Victoria, Australia	shields, scoria cones, maars	trachybasalt/ tephrite basinite	400	15000	Mt Gambier 2900 yrs. BP	a
Springerville	Arizona, USA	scoria cones	basaltic - tholeiitic	409	3000	0.3 Ma	b
San Francisco	Arizona, USA	scoria cones, lava domes	basalt, rhyolite, dacite	606	5000	Sunset Crater 950 yrs. BP	c
Wudalianchi	NE China	scoria cones	trachybasalt/ tephrite basanite	14	800	1776	d
Eifel	Rhineland, Germany	scoria cones, maars & tuff rings	foidite	323	1000	8300 yrs. BP	e
Chaine des Puys	Central massif, France	lava domes	basalt/ picro basalt	100	50	4040 yrs. BP	f
Jeju Island	South Korea	shield	basaltic to trachytic	300	700	1007 yrs. BP	g
Michoacan-Guanajuato	Mexico	cinder cones	andesite / basaltic andesite	1000	40000	Paricutin 1952	h
Pinacate	Mexico	cinder cones, maars & tuff rings	basalt / picro-basalt	408	1500	unknown	i
Cima	California, USA	cinder cones	basalt to basanite	70	150	ca. 10,000 yrs. BP	j

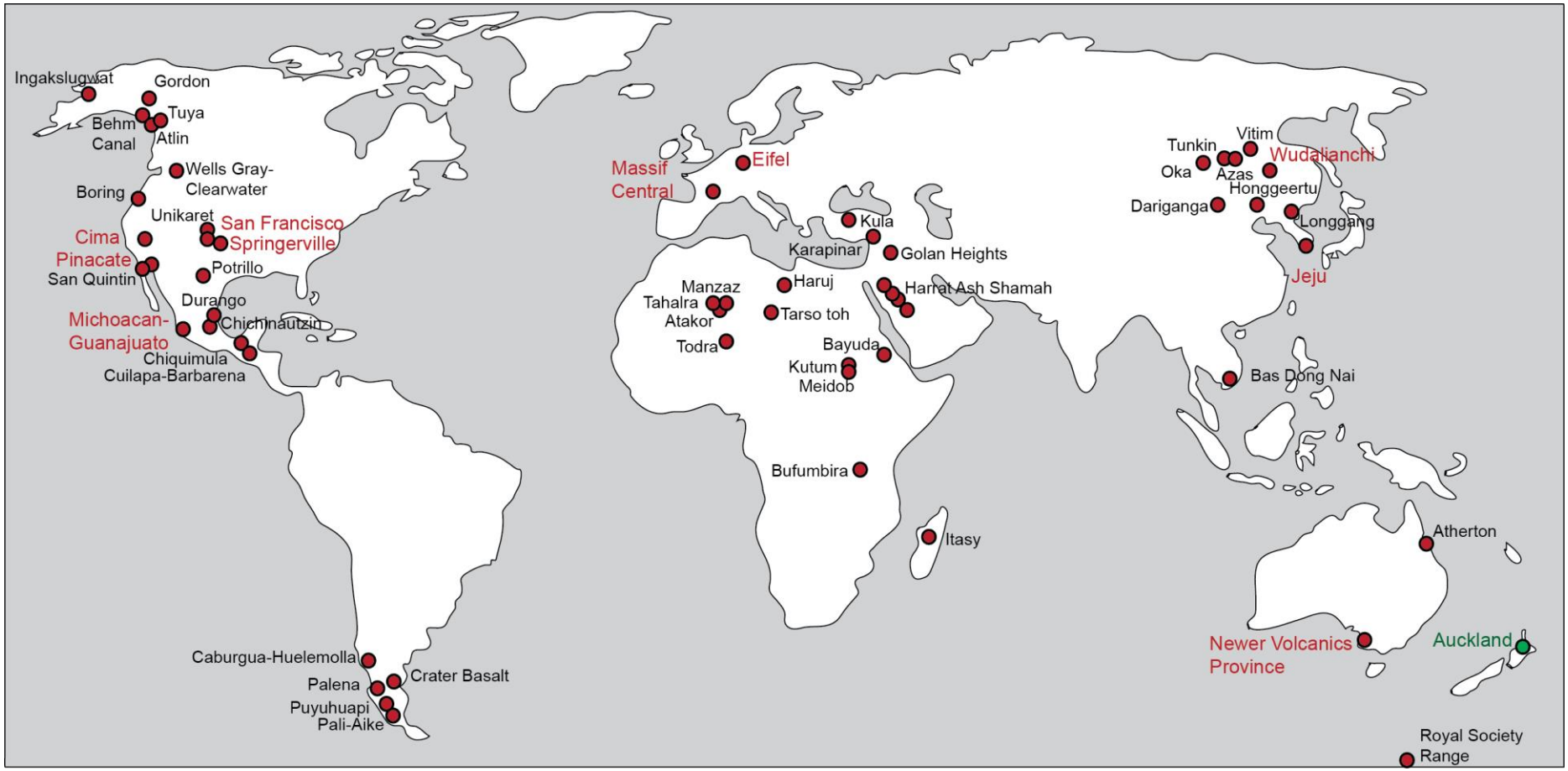

Figure 1.1. *Location map for major, currently active, or dormant intraplate basaltic monogenetic volcanic fields globally. Highlighted in green is the Auckland Volcanic field, and in red are the major fields detailed in* ***Table 1.1***

1.3.3. Tectonic Settings

The tectonic setting of monogenetic fields has traditionally been linked to regions of crustal extension coupled with low rates of magma production (Connor and Conway, 2000); however, increasing numbers of studies have found that monogenetic basaltic fields occur in a variety of tectonic environments. These environments vary, for example, from purely subduction related upwelling (e.g., the Michoacán-Guanajuato Field, Mexico, on the Cocos and Rivera plates; Ortega-Gutierrez *et al.,* 2014), through to text-book examples of extensional intraplate settings, often associated with plume-like upwelling that results in rifting of the region (e.g., Eifel Volcanic Field, Germany; Shaw, 2004). Although the eruption of an individual monogenetic volcano can be short lived (days to years) and the total eruptive products are of low volume, a monogenetic field can have a long life span (e.g., 4.5 Ma, Cima volcanic field; Dohrenwend *et al.,* 1986) and create a large cumulative volume of *total* eruptive products (Németh, 2010).

On a smaller scale, the geomorphologic analysis of fields worldwide has indicated that commonly a relationship is found between the structural environment and the spatial orientation of the centres (e.g., Timm *et al.,* 2010; Le Corvec *et al.,* 2013). For example, individual centres form along known fault traces (e.g., Springerville, Arizona, USA; Condit and Connor, 1996), or migrate relative to plate motion (e.g., San Francisco, Arizona, USA; Tanaka *et al.,* 1986). Other examples include the formation of monogenetic fields on top of pre-existing polygenetic centres (e.g., Higashi-Izu, Japan; Hasebe *et al.,* 2001), or the existence of both monogenetic and polygenetic centres erupting coevally in a single field (e.g., Wudalianchi, NE China; Hwang *et al.,* 2005). These factors show the highly individual characteristics of the volcanic fields worldwide, and it is therefore considered that generic volcanic principles cannot always be applied to monogenetic fields (Connor and Conway, 2000; Németh, 2010).

1.3.4. General petrology and geochemistry of monogenetic fields

Volcanic products of monogenetic fields are dominated volumetrically by basaltic (SiO_2 ≤ 52 wt.%) and basaltic-andesitic (SiO_2 52-56 wt.%) compositions (Valentine and Gregg, 2008). Although minor siliceous andesitic to rhyolitic dome complexes occur (e.g., San Francisco volcanic field: Tanaka *et al.,* 1986). In some

cases entire fields can display unique chemical characteristics, for example the products of Wudalianchi volcanic field, China, all have high K compositions (Zou *et al.,* 2008). Enrichment in incompatible elements (such as large ion lithophile elements (LILE) and light rare earth elements (LREE) relative to mid-ocean ridge basalts (MORB)) is also common, attributed by most studies to the small degrees of melting that generate the magma batches (e.g., South Auckland Volcanic Field (SAVF); Cook *et al.,* 2005; Newer Volcanics Province; Vogel and Keays 1997). Other studies attribute incompatible element enrichment to alternative processes acting on the ascending magma, for example when mantle plume-related melts interact with the surrounding continental lithosphere and crust (e.g., Central European Volcanic Province (CEVP), Germany; Jung *et al.,* 2011) or interaction of ascending melts with subduction-metasomatised lithosphere mantle (e.g., AVF; McGee *et al.,* 2013). Studies of lava major and trace element and isotopic compositions globally (e.g., Sr-Nd-Pb) reveal that heterogeneous mantle sources and/or crustal assimilation (e.g., Harrat Al-Madinah volcanic field, Saudi Arabia; Moufti *et al.,* 2012) are required to explain observed geochemistry at basaltic monogenetic fields, indicating that the mantle sources beneath monogenetic volcanic fields are rarely homogeneous (see **Chapter 5 and 6** for more detail). These geochemical variations, both field-wide and for a single centre, have led a number of authors to question the term ‘monogenetic’ in favour of terms such as ‘polymagmatic’ (e.g., Brenna *et al.,* 2010; McGee 2012).

Systematic changes in geochemical composition throughout a single eruption have also been identified, including: (1) gradual evolution through time to a more primitive composition, (2) a bimodal composition, where an initial evolved composition is followed by a primitive composition, and (3) an initial primitive composition followed by a more evolved composition (Smith *et al.,* 2008). Three broad models are used to explain these changes; for (1) a single uninterrupted eruption (Smith *et al.,* 2008), for (2) magma stalling at a rheological boundary or density barrier (e.g., brittle-ductile boundary between upper and lower crust) causing the more evolved magma to be pushed ahead by the upwelling of more primitive melt (Németh *et al.,* 2003), and for (3) initial deep source eruption followed by stalling over months to years and a ‘second’ eruption of this more evolved magma over time (Johnson *et al.,* 2008).

1.3.5. Melting models for inception of eruptions

Initial models to explain the formation of volcanic fields linked crustal weaknesses (e.g., faults or fractures) to widespread, high degrees of partial melting and upwelling of the mantle (Connor and Conway, 2000). Studies of the petrogenesis of most volcanic fields question this model and instead suggest that melt production can occur at different levels within the mantle, and usually involves low degrees of partial melting undergoing limited fractional crystallisation (Erlund *et al.,* 2010). The combination of these factors implies that volcanic fields do not develop large magma chambers and therefore their melts are relatively primitive in composition (e.g., Johnson *et al.,* 2010).

Monogenetic fields can be separated into two overarching groups: (1) low eruptive volume flux predominately controlled by tectonism (e.g., south-western Nevada volcanic field; 0.5 km^3/Myr; Valentine and Perry, 2007), (2) a high eruptive volume flux primarily controlled by magma volume (e.g., Eastern Snake River Plain field; 2.8 km^3/kyr: Kuntz *et al.,* 1986). Based on these characteristics Németh (2010) proposed that a close link exists between the output rates of the eruptive products, the local crustal thickness, the tectonic setting, the magma composition and melt generation rates.

Petrogenetic studies of monogenetic fields have aided the development of melting models aiming to describe the origin of the magma batches. The current understanding (e.g., Connor and Conway, 2000; Németh e*t al.,* 2003; Valentine and Perry, 2007; Smith e*t al.,* 2008; Erlund *et al.,* 2010; McGee e*t al.,* 2011; McGee *et al.,* 2013; McGee *et al.,* 2015) links a consistent low level of partial melting and melt production from a number of levels within the asthenosphere, lithosphere or a mixture of the two. Most recently McGee et al. (2015) have highlighted evidence for a relationship between physical eruption properties (e.g., volume and explosivity) and chemistry of erupted products in monogenetic volcanic fields (e.g., AVF, Wudalianchi volcanic field, and selected Hawaiian examples). These more recent findings support the model proposed by McGee et al. (2015) outlined above. This is discussed in more detail in **Chapter 4** and **5**.

From this brief overview, we can see the complexities involved in understanding monogenetic volcanism, and the range of factors that must be

considered when working towards an improved knowledge of the systems. It is fundamental to understand that volcanic fields are as much individual in their global context as they are within their contained system, and that the term 'monogenetic' has the potential to be misleading.

1.4. The Auckland Volcanic Field

1.4.1. Regional geology

The focus of this study is the basaltic monogenetic Auckland volcanic field (AVF), located in the north-west of North Island, New Zealand. Since late Pliocene times, the broader north-west region of North Island has hosted a series of basaltic volcanic fields migrating south to north: Ngatutura/Okete ca. 2.7-1.5 Ma (Briggs *et al.,* 1994), South Auckland ca. 1.59-0.51 Ma (Cook *et al.,* 2005), and Auckland ca. 200-0.5 ka (Lindsay *et al.,* 2011). The Auckland Volcanic Field (AVF) is located ca. 250 km west of (behind) the current active arc - The Taupo Volcanic Zone (TVZ) - and ca. 400 km behind the active subduction margin of the Pacific Plate, which is migrating westward beneath the North Island of New Zealand along the Kermadec trench (**Fig.1.2.A**).

The regional basement is composed of two broadly coeval but contrasting Triassic to Jurassic shallow marine sedimentary terranes, the Waipapa and Murihiku groups, brought together as part of the Gondwana margin. The Permian ultramafic Dun Mountain ophiolite belt forms a suture between these two terranes, and runs continuously (apart from the 460 km offset of the Alpine Fault) throughout New Zealand. Although there is only one small outcrop of Dun Mountain ophiolite in the Auckland region, it appears as a series of prominent positive gravity anomalies, interpreted to be a series of eastward dipping serpentinised shear zones running northwest-southeast at ≥1.5 km beneath the Auckland Isthmus (Eccles *et al.*, 2005; **Fig.1.2.A**). During the early Miocene the Auckland region was once again a marine basin, and deposited sands and muds form the now uplifted surface rocks of the region, the Waitemata Group (Kermode, 1992). Finally, atop this is the Quaternary monogenetic basaltic Auckland volcanic field.

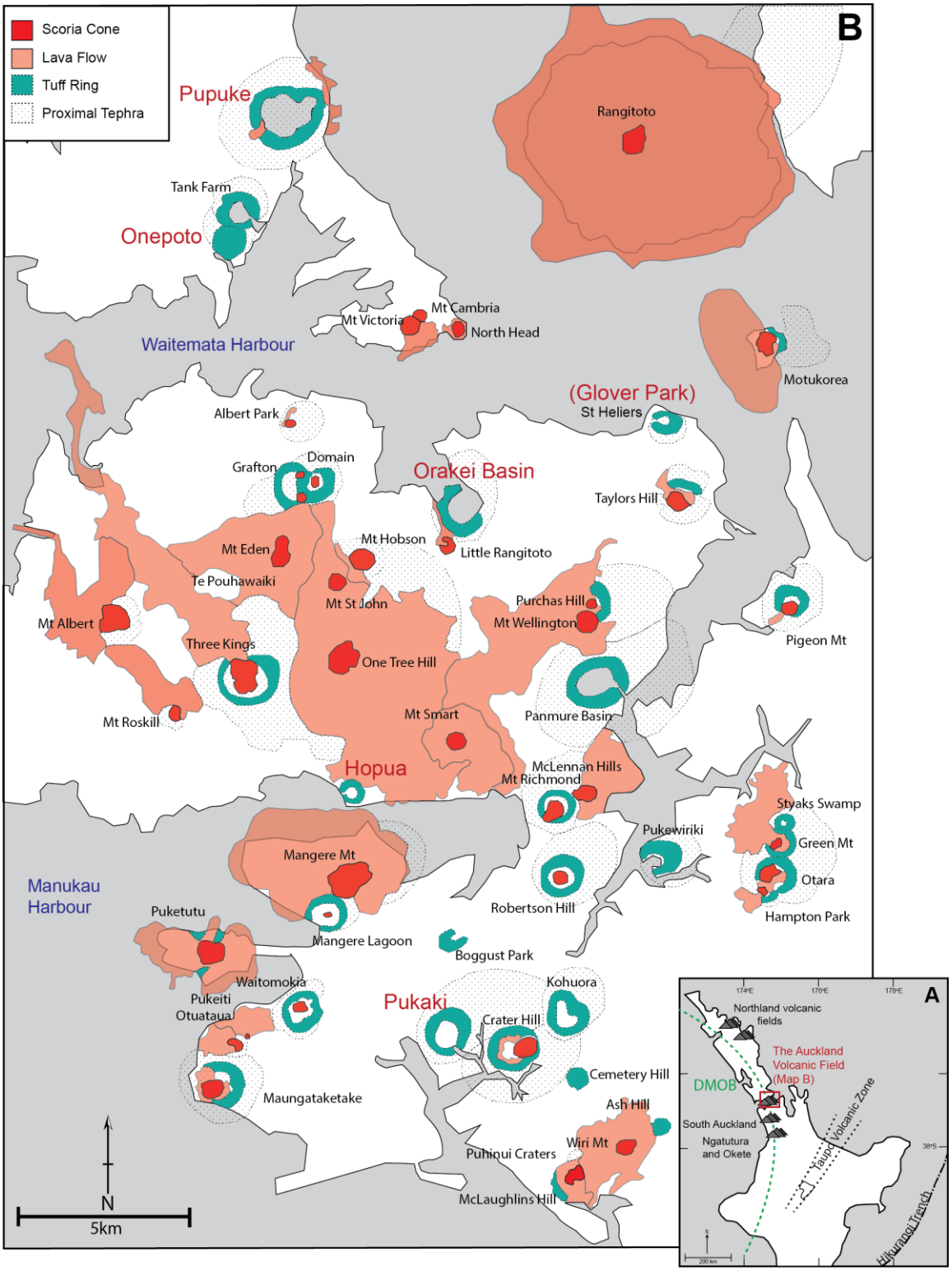

Figure 1.2. *A) Regional setting of the AVF in the North Island, New Zealand, including the older volcanic fields, and the location of the Dun Mountain ophiolite belt (DMOB). B) Local setting map of the individual AVF centres, their associated volcanic products, and maars from which the cores were retrieved (red font). Figure modified from Hayward et al. (2011).*

1.4.2. Local setting

The term monogenetic is widely used in connection with the AVF, on the basis that each centre represents the rise and eruption of a single batch of magma that is confined in time. Each centre in the AVF is individual in terms of its physical characteristics and geochemical signatures, suggesting a complex inter-relationship between source characteristics and transport mechanisms (Smith *et al.,* 2008; Needham *et al.,* 2011; McGee *et al.,* 2011).

There are currently 53 identified centres in the AVF, including three newly discovered centres, Boggust Park, Cemetery Hill, and Puhinui Craters (Hayward *pers. comm.* 2014). Cemetery Hill and Puhinui Craters, however, have no data (age or geochemistry) associated with their eruptions. Of the 53 centres (identified on **Fig.1.2.A**), ten show purely phreatomagmatic eruption styles producing just maar craters and tuff rings. These centres are formed as a result of wet explosive eruptions where the ascending magma interacted with ground water (Ash Hill, Boggust Park, Hopua, Kohuora, Onepoto, Orakei Basin (pictured **Fig. 1.3.A**), Pukaki, St Heliers, Styaks Swamp, and Tank Farm). Twelve centres show evidence of only magmatic eruptions (with both effusive and explosive activity) with small scoria cones and some small lava flows. These centres generally have slightly larger volumes and form as a result of dry, fire fountaining eruptions (e.g., Mangere Mt, Mt. Eden (pictured **Fig. 1.3.B**), Mt. Victoria). The remaining twenty-nine include the largest centres and show evidence for both phreatomagmatic and magmatic styles (both effusive and explosive) of eruption. All, except one (Pupuke), show a general progression from phreatomagmatic to magmatic and effusive eruption styles. These centres often have poorly exposed tuff rings, usually buried by lava flows, and scoria cones built within the explosion craters (e.g., Motukorea; pictured **Fig. 1.3.C**). Two remain (Puhinui Craters and Cemetery Hill) yet to be fully investigated and classified (Hayward *et al*., 2011).

Figure 1.3. *Pictures taken from Hayward et al. (2011), accredited to Alastair Jameson to show examples of the types of volcanic landforms associated with volcanoes of the AVF. Included are, A) Orakei Basin crater (maar) and the surrounding tuff ring formed through phreatomagmatic, wet, explosive eruptions. B) Mt Eden scoria cone and lava flows created through dry fire fountaining and magmatic effusive styles of eruption. C) Motukorea an example where all eruption types are identified within one centre – remnants of the tuff ring can be seen in the top right of the picture, the scoria cone is very obvious in the middle of the picture, and lava flows extend out from the island.*

Current data, based on model simulations, suggest the AVF has a total eruptive output of 1.7 km^3 dense rock equivalent (DRE) magma (Kereszturi *et al.,* 2013) which is about half of the previous study's approximation of 3.4 km^3 (Allen and Smith, 1994). In both these volume estimates the largest 5 centres include Rangitoto, One Tree Hill, Mt Eden, Mt Wellington and Three Kings, which make up ca. 69% of the field's eruptive products. Herein we used the more recently published values; for example Rangitoto, the largest Auckland volcanic centres, comprise ca. 41% (or 0.7 km^3) of the total DRE. The majority of centres have eruptive material between 0.001-0.01 km^3 (ca. 43 centres). For the cases of eruptions that exhibit both wet and dry eruptive styles the majority of the volume is made up from products of the dry eruption lava flows and scoria cones. The smallest centre (Kereszturi *et al.,* 2013) is Ash Hill with total eruptive material of 0.000076 km^3. All volume estimates are outlined and discussed in **Chapter 5**.

1.4.3. Previous Studies

1.4.3.1. General

Research on the AVF began with mapping by Charles Heaphy in 1857, followed shortly by a more in-depth geological survey by Ferdinand von Hochstetter resulting in the publication in 1864 of a full colour geologic map (shown on the title page of this chapter) (Hayward *et al*., 2011). This map shows 63 volcanoes with 27 explosion craters, a number of which have since been disproven. Hochstetter's memoirs remain useful today in giving information about sizes and locations of destroyed or hidden volcanoes of the field.

The next major phases of research on the AVF occurred nearly 100 years later with works from Ernie Searle in the 1950s and 60s (Searle, 1959a;,1959b; 1961a; 1961b; 1964; 1965), and Les Kermode in the 1960s-90s (Kermonde, 1975; 1992; Kermode *et al.,* 1992). Searle undertook much of the initial petrographic work classifying the AVF rocks as basalts with phenocrysts of olivine and clinopyroxene. Heming and Barnet (1986) later confirmed these conclusions, with geochemical analysis identifying the rocks as predominantly alkali basalts.

Since the 1990s volcanological and geochemical research on the AVF has been predominantly based at the University of Auckland, with ever improving analytical techniques and methods allowing new aspects and details of the field to

be investigated. Many studies have focused on geochemistry, and form a basis for the collation of geochemical data for this thesis (**Chapter 4**). These studies include MSc work from Bryner (1991), Miller (1996), Franklin (1999), Hookway (2000), Spargo (2007), Eade (2009) and Needham (2009). Most recently of note is the PhD work of McGee (2012) and associated papers (McGee *et al.,* 2011; 2012; 2013; 2015), which significantly increased the set of geochemical data available and improved the understanding of the complexities both within centres and across the field. A summary of the geochemical database prior to this thesis research is shown and critically discussed in **Chapter 4**. Some studies have also primarily focused on the tephra and core deposits from the AVF, most notably Sandiford et al. (2001), Hoverd et al. (2005), Shane and Hoverd (2002), Molloy (2008), Molloy et al. (2009) and Zawalna-Geer (2012); this topic is discussed further in **Section 1.5**.

The purely monogenetic classification of the AVF has been brought into question by the work of Needham et al. (2011) and Spargo (2007) and more recently by Shane et al. (2013). Rangitoto is the youngest and the largest eruptive centre of the field. It is considered to reflect a change in eruption style at the AVF, and has therefore been the focus of many studies. The MSc thesis of Needham (2009) was the first to uncover evidence for two eruptions from Rangitoto, around 50 years apart (^{14}C dates of 553±7 and 504±5 cal. yr. BP), with each eruption (Rangitoto1 and Rangitoto2) showing a different geochemical signature. Most recently tephrochronology on Rangitoto deposits from Shane et al. (2013) suggested that rather than two eruptions there is evidence within cryptotephra for multiple periodic eruptions over ca. 1000 years. However, this hypothesis is currently not supported by any other tephra work or physical volcanology on Rangitoto deposits, and thus remains uncertain. In either case, Rangitoto shows the simple 'monogenetic' nature of the AVF may be changing, or may be an over-simplification. For example, the older centres simply do not have the same chronological resolution as for Rangitoto. These observed changes in the characteristics of the field have made it necessary to conduct a more detailed and comprehensive study in order to better understand the evolutionary history of the field as a whole, and create better constraints to the hazards and risks posed on the city.

1.4.3.2. Age studies

In order to assess volcanic hazards a critical first step is to determine eruption magnitude-frequency relationships (e.g., Lindsay *et al*., 2011 for a review in the specific case of the AVF). This analysis has been hampered in the AVF due to the lack of accurate age determinations (Magill *et al.,* 2005).

^{14}C dating is of limited use, due to the age of many of the eruptions (>40 ka) and the lack of carbonised material within the deposits. Early attempts at carbon dating (Fergusson and Rafter, 1959; Searle, 1961a) are helpful to some extent in ordering event timings but not necessarily allowing specific dates to be applied. Currently only 5 AVF centres are assigned ages through ^{14}C techniques (Rangitoto1 and 2, Mt Wellington, Purchas Hill, Three Kings, and Ash Hill). K-Ar techniques are also of limited value as excess radiogenic Ar within the samples commonly leads to false ages that are older than the inferred age derived by other means (Lindsay *et al.,* 2011). Mochizuki et al. (2004) present further results from K-Ar technique, however, more recently the developments in $^{40}Ar/^{39}Ar$ dating technology (Cassata *et al.,* 2008) have opened a new chapter on the 'date-ability' of the AVF. This new $^{40}Ar/^{39}Ar$ dating technique has increased the number of *reliable (to reasonably reliable)* ages dates from 11 to 33 (Lindsay *et al.,* 2011). For four centres the original Ar-Ar data from Cassata et al. (2008) are maintained (Wiri Mt., Puketutu, Crater Hill and Hampton Park). However, most recently an extensive campaign undertaken by Leonard et al (*in prep.* **Appendix D)** has added 24 Ar-Ar ages to the database (all AVF centre ages are outlined and discussed in **Chapter 5**).

Six centres remain totally undated (Mt Robertson, Otuataua, Pigeon Mt, Puhinui Crater, Cemetery Hill and Boggust Park), and the remaining 14 have their ages constrained by tephrostratigraphy (n=6) or morphostratigraphy (n=8). These constraints are discussed in detail in **Chapter 5**. Age estimates are therefore now available for ca. 46 of the centres (**Chapter 5, Table 5.1**) although, many of these centres are indistinguishable within uncertainty due to the errors associated with the analytical techniques, and thus have no definitive, relative eruption order. As a result we do not have the ability to assess the temporal and spatial evolution of the field as a whole.

1.4.3.3. Geochemical studies

The geochemistry of the AVF is outlined and discussed in detail in **Chapters 4** and **5**, therefore this section just provides a brief overview of previously published work and key findings. Most of the bulk rocks of the AVF are classified as olivine-rich basalts and basinites (**Fig.1.4**.). They are mostly composed of olivine, clinopyroxene, feldspar, minor apatite, and Fe-Ti accessory oxides. The most common phenocrysts are olivine followed by clinopyroxene (Searle, 1961a; Heming and Barnet, 1986). The groundmass exhibited in bulk rocks shows a fine grained to glassy texture, with vesicularity observed in the upper parts of flow units. Groundmass crystals are plagioclase, clinopyroxene, olivine, and accessory Fe-Ti oxides (Searle, 1961a). Variations on this pattern include; nepheline found at the Domain tuff; amphibole (cummingtonite) found in Three Kings basalts (Searle, 1961a); biotite found in the groundmass of lavas at Mt Wellington and Pigeon Mt (Heming and Barnet, 1986); and subalkalic-tholeiitic products found in the second eruption of Rangitoto (Needham *et al.,* 2011).

A number of centres have erupted xenolithic material, (reported in Jones, 2007; Spörli and Black, 2013; Spörli *et al.,* 2015) including Glover Park and Taylors Hill. The xenoliths are thought to represent mid to lower crustal lithologies that have been linked to the Maitai terrain, a suture between greywacke basements (Jones, 2007). Xenocrystic olivines have also been found in eruptives from Lake Pupuke and Onepoto, they have a Cr-spinel composition that has suggested subduction related origins (Spargo, 2007).

The SiO_2 content of the field is <50 wt.%, and the total alkali (Na_2O+K_2O) contents generally range between 4-7 wt.% (**Fig.1.4.**). The general relationship for total alkali vs. silica (TAS) shows a negative trend for these elements (**Fig.1.4.**). MgO content of the field is ca. 7.5-13.5 wt.% with the corresponding Mg numbers (Mg#) ranging from 52-70 (McGee *et al.,* 2013). Varying trends are observed in the major elements between the centres, the majority showing variable negative trends for example MgO vs. Al_2O_3 (McGee *et al.,* 2013). Major element trends and relationships are fully discussed and explored in **Chapter 4** and **5**.

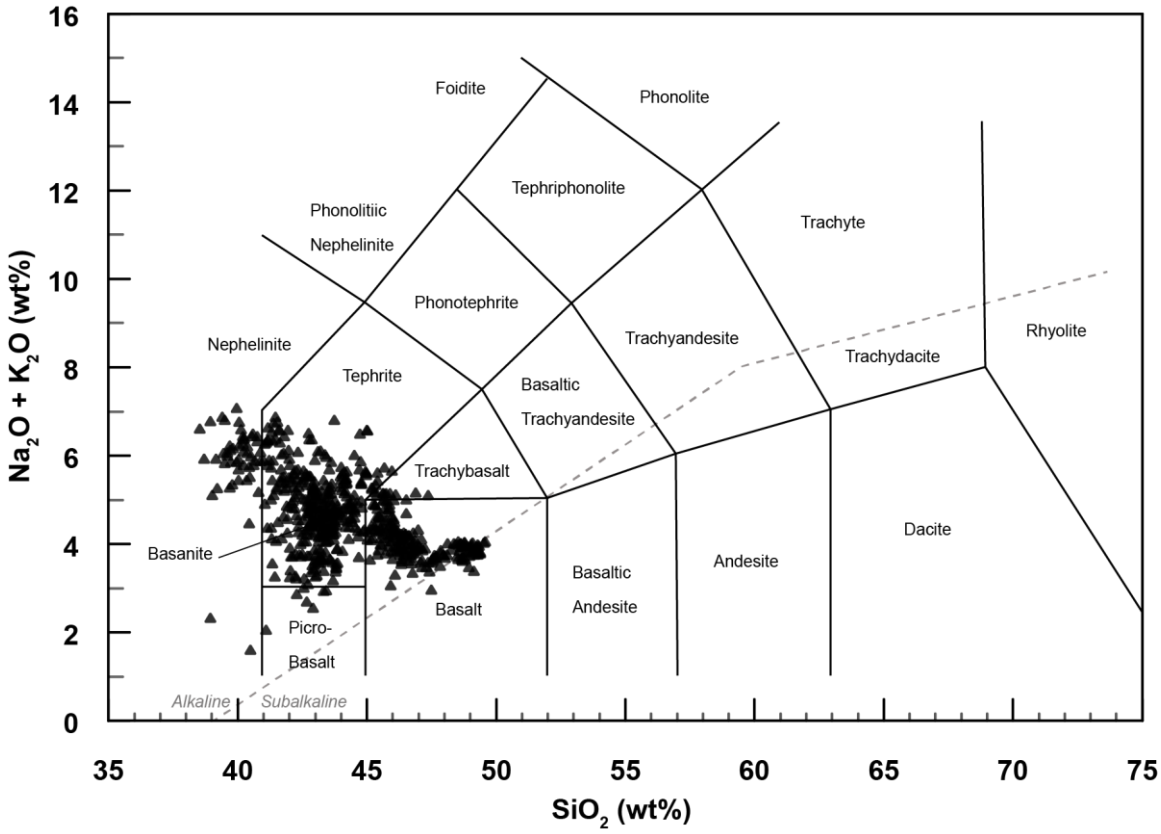

Figure 1.4. *Total alkalis (K_2O+Na_2O) vs. SiO_2 for all whole rock analysis for all centres within the AVF prior to this research, database collated by McGee (2012).*

In general the AVF lavas show trace element signatures that exhibit primitive-normalised multi-element trends similar to Ocean Island Basalts (OIB) (**Fig.1.5.B**). The range in trace element composition for the AVF as whole is large; for example La ranges from ca. 10-60 ppm, Ba from ca. 90-360 ppm, and Nb ca. 15-90 ppm, with the incompatible trace elements showing the largest range in variability across the centres. McGee et al. (2013) noted that in general there is enrichment in the heavy rare earth elements (HREE) in comparison to OIB values, with pronounced anomalies noted in U and Pb (Smith *et al.,* 2009) and K and Sr (McGee *et al.,* 2012; McGee *et al.,* 2013; McGee *et al.,* 2015) (**Fig.1.5**.).

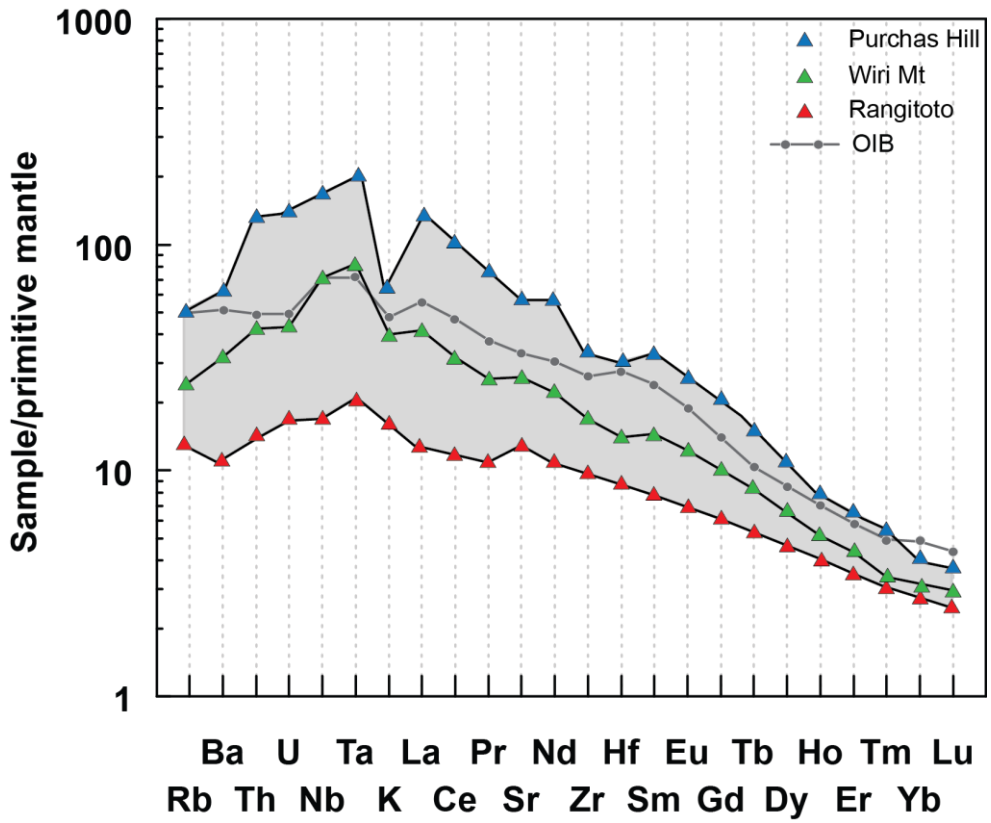

Figure 1.5. *Primitive mantle-normalised multi-element plots for pre-existing whole rock samples from the AVF (data from McGee et al., 2013). Pale grey shows the entire range in the field, colour symbols indicate the three proposed compositional end members, (c.f.* ***Fig 1.6.****) for Rangitoto (red), Wiri Mt. (green), and Purchas Hill (blue). Normalisation and OIB values are from McDonough and Sun (1995).*

Only a minor amount of isotopic data has been obtained for the AVF volcanic products (e.g., Huang *et al.,* 1997; McGee *et al.,* 2011; McGee *et al.,* 2013). Studies have focused on the Sr-Nd-Pb (McGee *et al.,* 2013) and U-Th-Ra (McGee *et al.,* 2011; McGee *et al.,* 2013) systems. The $^{87}Sr/^{86}Sr$ composition range from 0.702710 to 0.703125, and the $^{143}Nd/^{144}Nd$ from 0.512931 to 0.512971 (**Fig.1.6.**). These two systems display only a minimal relationship (McGee *et al.,* 2013), with the Rangitoto eruptions showing a broader range in $^{87}Sr/^{86}Sr$ than the other centres, and exhibiting a higher $^{87}Sr/^{86}Sr$ ratio at similar $^{143}Nd/^{144}Nd$ values. The Pb isotopes show $^{206}Pb/^{204}Pb$ range from 19.039 to 19.416, $^{207}Pb/^{204}Pb$ from 15.574 to 15.617 and $^{208}Pb/^{204}Pb$ vary from 38.781 to 39.009. When looked at in more detail the $^{206}Pb/^{204}Pb$ vs. $^{207}Pb/^{204}Pb$ plot in a mixing triangle (**Fig.1.6.A**), with Purchas Hill, Rangitoto, and Wiri/ Puketutu defining the end-members. A plot

of $^{206}Pb/^{204}Pb$ vs. $^{208}Pb/^{204}Pb$ produces a linear trend with Rangitoto and Purchas Hill again defining the limits of this diagram (**Fig.1.6.B**). There is no relationship exhibited between $^{143}Nd/^{144}Nd$ and $^{206}Pb/^{204}Pb$, and a negative trend is seen when $^{87}Sr/^{86}Sr$ is plotted against $^{206}Pb/^{204}Pb$ (**Fig.1.6.C&D**).

U-Th-Ra isotope analysis was undertaken on the four most recent eruptions from the AVF; the two Rangitoto eruptions (McGee *et al.,* 2011) followed by Purchas Hill and Mt Wellington (McGee *et al.,* 2013). These analyses covered both the largest (Rangitoto 2) and one of the smallest (Purchas Hill) centres of the AVF. The results show that Purchas Hill displays the highest $^{230}Th/^{232}Th$ ratio of 1.380 and Rangitoto 2 the lowest at 1.140. The data show two clusters, one from Rangitoto 2 which has a high $^{238}U/^{232}Th$ ratio and a lower $^{230}Th/^{232}Th$ ratio, and the other encompassing Rangitoto1, Purchas Hill and Mt Wellington exhibiting a lower $^{238}U/^{232}Th$ and a more variable $^{230}Th/^{232}Th$. McGee et al. (2011) concluded this variability was created by two differing magmatic processes (discussed further in **Chapter 5**) causing the eruptions, and overall show that these measurements are some of the highest $^{230}Th/^{232}Th$ ratios measured for ocean island and continental intraplate volcanic field basalts.

Some centres show compositional variation throughout their eruptive products, with Crater Hill (Smith *et al.,* 2008) and Motukorea (McGee *et al.,* 2012) studied in detail. Those which have had their deposits sampled stratigraphically all show a similar evolution through time of low-Si, low-Mg, high-incompatible trace elements in the early eruptive phases, through to high-Si, high-Mg and low incompatible element contents towards the end of the eruptions (Smith *et al.,* 2009). In general terms, the AVF centres show the broadest geochemical variation within the incompatible trace elements, and this variation is (most commonly) larger on a field-wide scale, than on an individual centre scale.

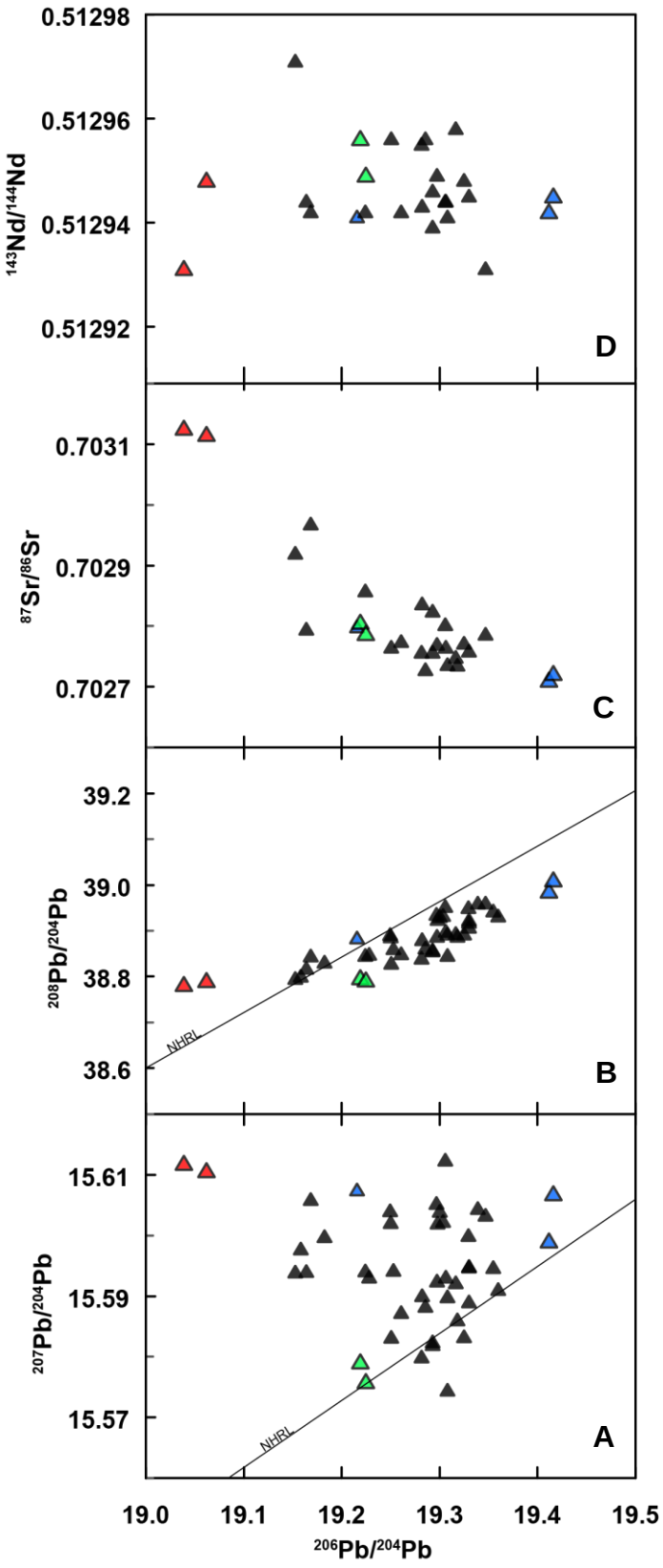

Figure 1.6. *Isotope data from McGee et al., 2013, showing an overview of the field's characteristics. This data set includes samples from 10 centres. Highlighted in red are Rangitoto samples, blue Purchas Hill samples and, green Wiri Mt, proposed as the end members. Northern Hemisphere Reference Line (NHRL) is calculated after Hart (1984).*

1.5. Tephrochronology

Tephrochronology is a method of correlating and dating volcanic activity, and other geological events, using tephra deposits. It has been widely used both in New Zealand and around the world to study volcanic eruptions, and is a major source of data for eruption frequency, timing and geochemistry of volcanic events (Shane, 2000; Lowe, 2011). The term 'tephra' itself comes from the Greek word *tephra* meaning 'ashes'. It encompasses all unconsolidated explosively erupted pyroclastic material irrespective of size, shape, or composition, and includes ash (particles <2 mm in diameter), lapilli (2-64 mm) and volcanic blocks and bombs (>64mm) (Lowe, 2011).

Where individual tephra deposits can be accurately correlated across an area, they can be used as isochronous marker horizons, allowing detailed and accurate stratigraphic frameworks to be constructed. The correlation and thus construction of a stratigraphic framework of deposits relies on the similarity of their lithologies, stratigraphic positions, and geochemistries (e.g., Shane, 2000; Alloway *et al.,* 2004; Lowe *et al.,* 2008; Lowe, 2011). The difficulties with correlations are two fold, they rely on the ability to link deposits by 1) dating the tephra using radiometric methods and/or 2) correlate tephra beds for example using lithology, geochemistry and/or petrology. In recent years, increasing emphasis has been placed on the latter of these two factors because the geochemical and petrological characteristics are likely to be more individual for a particular eruption, and thus more easily unambiguously correlated between individual deposits. In addition appropriate material for dating is often not present or difficult to find, for example a high enough quantity of specific minerals required for $^{40}Ar/^{39}Ar$ analysis, or organic material for ^{14}C analysis (Shane, 2000).

In the last decade, increasing improvements in single shard analysis techniques (e.g., Pearce *et al.,* 2004; 2007; 2008) is allowing accurate measurements of both major and trace element concentrations of very small shards (<30μm). This allows tephra horizons to have their geochemical compositions individually fingerprinted to produce more reliable and robust tephrostratigraphic frameworks. The ability to cross correlate tephra deposits to create isochronous horizons not only allows constraints on the stratigraphic

ordering of eruptions, but can also give details about tephra dispersal and deposit thicknesses, both of which are essential pieces of information for hazard and risk management planning.

1.5.1. Tephrostratigraphy in the AVF

In contrast to the extensive studies of rhyolitic (Allan *et al.,* 2008; Lowe, 2011; Lowe *et al.,* 2013; Vandergoes *et al.,* 2013; and many previous studies summarised therein) and andesitic (Alloway *et al.,* 1995; Shane, 2000; Shane, 2005; Turner *et al.,* 2009) deposits of New Zealand, the proximal AVF basaltic deposits have received less attention (e.g., Molloy *et al*., 2009). This is due primarily to the scarcity of exposed tephra beds, coupled with the urbanisation of the region.

Shane and Smith (2000) studied a small number of proximal tephra compositions in relation to specific centres in the AVF as a potential tool for fingerprinting the centres. Previously this method has successfully been used to correlate distal tephra deposits with their source volcanoes in both New Zealand and worldwide (e.g., Westgate and Gorton, 1981; Shane, 2000; Lowe, 2011). However, Shane and Smith (2000) suggest limitations to the usability of subaerial AVF tephra deposits due to the rapid weathering of basaltic glass. They also note the limited presence of distal basaltic tephra due to poor preservation and low dispersal of small-scale eruptive events. It is for this reason that tephra from the AVF has mostly been studied from within sediment cores.

Most recently Molloy et al. (2009) studied andesitic, rhyolitic and basaltic tephra within the maar lake cores from Orakei, Pupuke, Onepoto and Hopua (highlighted on **Fig 1.2.**). Using visual observations they identified 24 basaltic tephra horizons that ranged from a few mm up 50 cm in thickness, and are composed of dark grey to black ash, lapilli and accidental ejecta. The individual horizons had sharp upper and basal contacts and exhibited normal and reverse graded beds. Two petrographic types were identified: one predominantly composed of glass shards (vesicular scoria-fluidal teardrops) and a small proportion of minerals (olivine plus plagioclase and clinopyroxene), the other consist of 30-60% accidental ejecta (quartz, glauconite, shell fragments and sedimentary lithics), the same mineral assemblage as for the first type and

subordinate juvenile glass shards. The former was thought to have originated from magmatic or effusive activity whereas the latter was attributed to phreatomagmatic activity. As many of the deposits were not thick enough to have any internal structures related to them, the designation between fall and pyroclastic density current deposits was not defined. The distance over which some of the deposits occurred and the thicknesses observed for some deposits suggests the occurrence of prolonged eruption sequences and variable wind directions.

1.5.2. Previous correlations of the AVF tephra horizons

Correlation of the AVF tephra has been attempted both across cores, and in a few cases to the individual proximal source deposits. Most recently Green et al. (2014) used a statistical approach based on stochastic local optimization technique. This method input stratigraphic, mineralogical and geochemical data (obtained from previous studies on 5 cores (Onepoto (Shane and Hoverd, 2002), Pukaki (Sandiford *et al.,* 2001), Orakei, Hopua, and Pupuke (Molloy *et al*., 2009)), in order to correlate and date the tephra deposits. The main basis of the basaltic tephra correlations was 'age dated tephra' which came from estimates on rhyolitic and andesitic deposits constrained by depositional rates, ^{14}C dates, and tephrochronology. The outcome assigned ages to basaltic horizons within the cores and then, using the ages it assigned, correlated across the cores the most closely matched ages. Potential correlations were then further constrained using major element glass chemistry (from Sandiford *et al.,* 2001; Shane and Hoverd, 2002; and Molloy *et al*., 2009). The ages applied to the tephra horizons were then used to link the deposits to dated source centres (ages modelled by Bebbington and Cronin, 2011). Although, the errors associated with the age estimates for the sources mean that, especially with eruptions in the 35-24 ka range, a number of centres could be associated with each deposit. At the time of Green et al. (2014), the individual centres were not well dated (Bebbington and Cronin, 2011) and thus the justifications to pick which centres fitted within the correct age range were poorly constrained.

Attempts to correlate tephra to source have to date relied only upon poorly constrained ages of both the centres *and* the tephra horizons. Bebbington and Cronin (2011) noted the difficulty in correlation based on geochemistry due to the low variability in magma compositions in the AVF (Smith *et al.,* 2008), and the

limited appropriate proximal data set (Sandiford *et al.,* 2001). This is true when based purely on major element chemistry, however, to date no study has looked into the potential of using trace elements as a geochemical fingerprinting tool for the AVF tephras. If the recent study of bulk rock trace element chemistry (McGee *et al*., 2013) is taken into account, it would seem that the potential variation in geochemistry could be broad enough across the field, but narrow enough for individual centres, to help better distinguish and correlate horizons across cores and to their specific centres of origin. Highlighted within past studies on the AVF tephra horizons (Shane and Smith, 2000; Sandiford *et al.,* 2001; Smith *et al.,* 2008; Smith *et al.,* 2009; Molloy *et al.,* 2009; Bebbington and Cronin, 2011) are some specific problems that will need to be addressed when correlating tephra. These are outlined in **table 1.2** coupled with the ways in which this study aims to overcome these limitations.

Table 1.2. *Limitations outlined from previous tephra studies within the AVF and how this study aims to overcome these limitations.*

Potential limitations as highlighted by previous studies:	**How this study aims to overcome these limitations:**
Geochemical variability within single eruptions	Limited by using incompatible trace element ratios and interpretation of multiple analyses
Limited geochemical variability across the field	Increased by using incompatible trace element ratios
Microcrystalline nature of glass shards	Careful analysis of shards and placement of probe/laser beam, geochemical spikes from microcrysts are clearly visible in results and these analyses are discarded.
Limited dispersal of tephra	Coverage of multiple cores in a range of localities across the field
Deposition highly dependent on wind direction which is variable	Taken into account where possible based on morphostratigraphy
Preservation potential of tephra	Coverage of multiple cores in a range of localities across the field
Contamination by accidental ejecta	Analysis of distal deposits aims to limit their inclusion coupled with careful shard selection process
Limited proximal geochemical data	Increased by this study
Limited reliable age data	Increased by Leonard *et al.* (*in prep*. Appendix D)

1.5.3. Geochemistry of the AVF tephra

Basaltic glass shards from the AVF often contain abundant microcrystalline phases (unlike rhyolitic glass that is predominantly microcryst free) including plagioclase, pyroxene, olivine, and a small proportion of Fe-Ti oxides. Microcrysts in the AVF tephra result from rapid elemental diffusion in high temperature, low viscosity, basaltic melts (Shane and Zawalna-Geer, 2011), allowing the rapid growth of small crystals during conduit ascent (Smith *et al.,* 2008). Similar to fractional crystallisation in magma chambers, growth of microcrysts can affect the residual melt composition and thus could result in a large compositional spectrum in glasses quenched from a geochemically homogeneous magma. However, Shane and Zawalna-Geer (2011) showed from EDS microprobe analyses that, in the case of the Mt. Wellington centre, the major element variations were not significant (±1% SiO_2) between different tephra samples from the same centre, and that with careful positioning of probe beam for analysis there is little detectable difference in the resulting chemistry between microcryst rich and poor glass shards (Shane and Smith 2000).

As previously discussed (**sect. 1.4.3.4**), a limited number of studies have analysed proximal (Shane and Smith, 2000) and distal (maar deposits, e.g., Sandiford *et al.,* 2001; Hoverd *et al.,* 2005) tephra-derived glass chemistry from the AVF. All studies measured major elements using in-situ EMPA methods (e.g., Molloy *et al.,* 2009) with only Needham et al. (2011) also measuring a limited selection of trace elements on tephra-derived glass. All these studies show comparable results between AVF tephra deposits. Major element compositions range for SiO_2 42-53 wt.%, Al_2O_3 12-17 wt.%, FeO 8-14 wt.%, CaO 8-12 wt.% and Na_2O 4-7 wt.% and K_2O 1.5-3 wt.%. The general relationship between elements shows increasing Al_2O_3 and FeO with SiO_2 and decreasing CaO, Na_2O, K_2O, and P_2O_5. MnO showed no consistent trend and, in some cases MgO show no trend (Shane and Smith, 2000) but in others it showed positive (Németh *et al.,* 2012) or negative (Shane and Zawalna-Geer, 2011) trends with SiO_2. For studies that analysed multiple deposits, often evidence for two geochemical populations was found (initially by Hoverd *et al.,* 2005), for example:

1) A low SiO_2 group (<45 wt.%) with high CaO and K_2O, and

2) A high SiO_2 group (>45 wt.%) with lower CaO and K_2O.

The geochemical data presented by Needham et al. (2011) for Rangitoto show this bimodal geochemical grouping, however in all other studies this bimodality was identified over the whole data set of multiple centres (Hoverd *et al.,* 2005, Shane *et al.,* 2013), not just within a single centre's deposit.

Initial studies by Shane and Smith (2000) on proximal deposits suggested that tephra horizons are commonly geochemically homogeneous, demonstrated by little geochemical variation between individual tephra-derived glass shards (e.g., SiO_2 ±0.5 wt.%). However, more recent studies (Shane and Hoverd, 2002; Shane, 2005; Hoverd *et al.,* 2005; Molloy *et al.,* 2009) have shown for more distal deposits (maar cores) the inter-shard major element composition in a single horizon can vary substantially (e.g., up to SiO_2 ±5 wt.%) (6 wt.% in Hoverd *et al.,* 2005, but this was attributed to shard reworking). This variability has been interpreted to represent heterogeneity of magma composition and a rapid ascent rate resulting in little time for homogenisation (e.g., Molloy *et al.,* 2009). Németh et al. (2012) further suggest that the variability in tephra geochemical composition seen within certain deposits could be related to some of the larger more complex eruptions, for example, Orakei (a small magma batch) showed minimal geochemical variation in all deposit types (lapilli/scoria/tephra). In comparison, Mt Eden (a volumetrically large centre) shows a very broad range in geochemical composition.

To date, very little is known about the trace element chemistry of the AVF tephra. Needham et al. (2011) published trace element contents from 4 Rangitoto tephras, which are the only tephra trace element data available from AVF. Their results showed the whole rock samples and tephra-derived glass samples had comparable trace element contents and ratios. The indication from the whole rock analysis, coupled with these results from Needham et al. (2011), show that there is a much wider range in variability of the trace elements concentrations (especially incompatible elements; McGee *et al.,* 2013) in comparison to the major element concentrations for the AVF volcanic deposits.

1.6. Aims and Approach

Literature reviews have highlighted the need to gain more detailed information about the potential hazard and risk posed to the city of Auckland by a future eruption from the monogenetic Auckland volcanic field. Reconstructing the chronology and magmatic evolution of the field as a whole is essential in order to forecast the characteristics of a future eruption. Specific gaps are found relating to the temporal eruption sequence, leading to an inability to resolve the spatial or geochemical evolution of the field. Recent methodological and technological advances in tephrochronology, including the accurate identification of basaltic tephra horizons within sediment cores, and geochemical fingerprinting of individual glass shards, have proven to be a very effective method for building reliable tephrostratigraphic framework for a region. If the cross-correlated horizons within this framework can be linked back to their individual source centre, we can build a more definitively sequenced eruption history of the AVF centres.

This project therefore has four key aims expressed as the following research questions:

1. Can a more detailed basaltic tephrostratigraphy for the Auckland Volcanic Field be produced from the maar deposits using newly improving tephra-derived glass shard analysis methods? (**Chapter 3**)

2. Can individual tephra horizons be linked to their source centre? (**Chapters 3, 4 and 5**)

3. What was the spatial, temporal, and geochemical evolution of Auckland Volcanic Field? (**Chapter 5**)

4. What can the eruptive products of the Auckland Volcanic Field tell us about the pre-eruptive processes which act on the magma? (**Chapter 6**)

1.7. Thesis Structure

Chapter 1 details background information, and a summary of previous work, surrounding the research topic.

Chapter 2 outlines all the methods used in this study from insitu tephra-derived glass shard analysis for major and trace element compositions using electron microprobe analysis (EMPA) and laser ablation inductively coupled mass spectrometry (LA-ICP-MS), to whole rock analysis using X-ray fluorescence (XRF) for major element compositions and solution-ICP-MS for trace element compositions. It also outlines Pb column chemistry, and Re-Os extraction and measurement methods for isotope analysis. The final section of **Chapter 2** reviews the analytical accuracy, precision, and consistency of the analyses run throughout this PhD project.

Chapter 3 gives details about the improved analytical procedures for core analysis and basaltic horizon detection. It also outlines the procedure for analysing tephra-derived glass shards for major and trace elements, and the method by which the tephra-derived glass shards are geochemically fingerprinted and correlated across the cores. This cross correlation builds up a detailed tephrostratigraphic framework for the Auckland Volcanic Field eruptive history, and was a pre-requisite for the accurate correlation of tephra deposits to their source centres.

Chapter 4 outlines the collation of pre-existing geochemical whole rock data from a number of sources including published and unpublished work, and MSc and PhD theses. It details new whole rock data collected and analysed by this thesis which are combined with the pre-existing data in order to produce the most holistic database for AVF whole rock geochemistry.

Chapter 5 uses the tephra horizon correlations and the tephra-derived glass shard geochemistry determined in **Chapter 3**, coupled with pre-existing and additional complimentary geochemical data for whole rock analysis (collated in **Chapter 4**) to develop and detail the method to correlate the tephra horizons to their source centres, thereby creating a stratigraphically well-constrained chronology for the eruptions of the AVF. The results not only allow conclusions to be made in relation

to tephra dispersal and deposition, but also provide the temporal, spatial, and geochemical evolution of the field.

Chapter 6 builds on conclusions made and highlighted by the previous chapters, which suggest that pre-eruptive processes and the geochemical evolution at the AVF remain poorly understood. This chapter aims to assess the interplay between crustal and mantle processes which produce the geochemical variability seen in the AVF.

Chapter 7 outlines and discusses the synthesis and conclusions as a result of the analyses undertaken by this research. It details how these address the aims outlined in the introduction, and the original contributions made by this work. Finally a number of potential future research avenues are discussed, highlighted by the findings of this research.

Chapter 2

Methodology

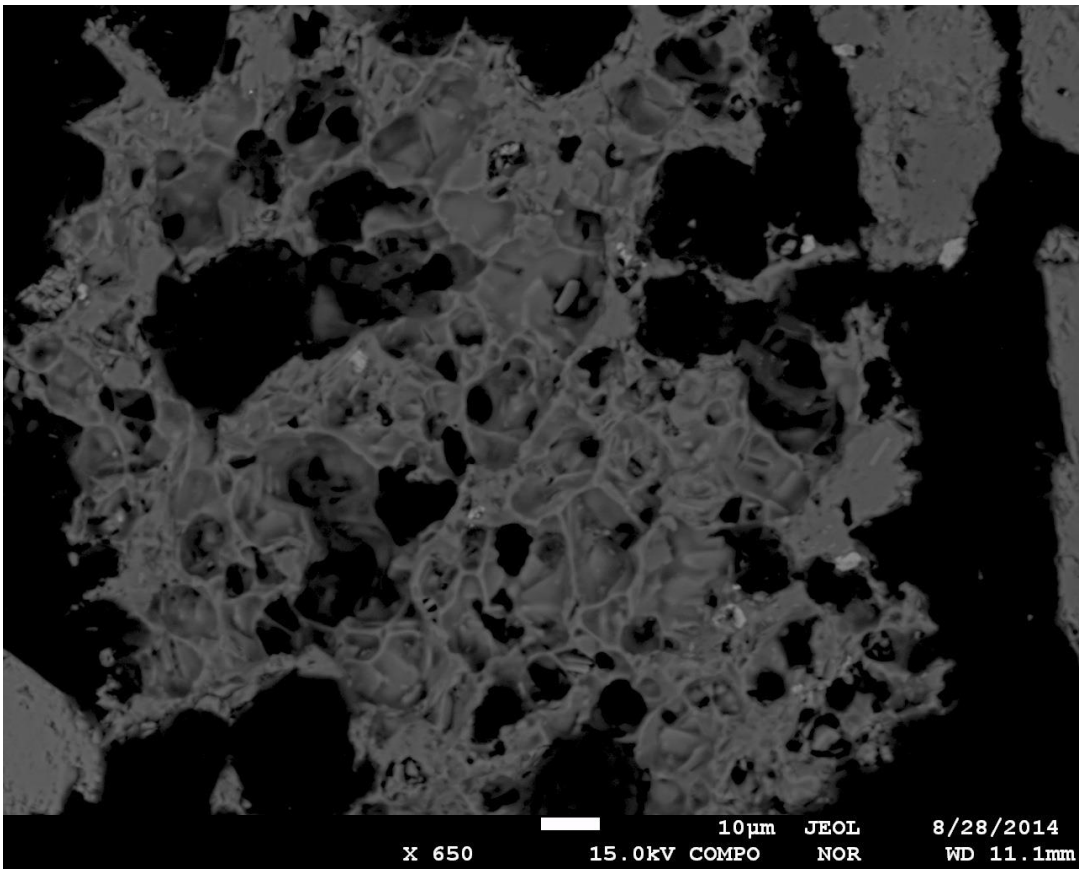

Glass shard from Glover Park core ca. 60 ka. yrs old, perfectly and intricately preserved (image by Hopkins, J.L.).

2.1. Introduction

This chapter is separated into four parts (A-D). Section A details the sample selection, and method developed to analyse basaltic glass shards from within cores. Section B details the collection and analysis of whole rock samples for both major and trace elements. Section C details the analysis of rhenium, osmium and lead concentrations and isotopes from bulk rock data from a selection of centres in the AVF, and Section D presents and reviews the quality of the data obtained for this thesis. It also discusses specifically the ability to compare results measured by multiple types of machine at multiple institutes.

The data presented in this thesis were generated using various instruments in different laboratories:

- For the tephra, X-ray, core sampling and magnetic susceptibility on the Onepoto and Orakei cores was undertaken at the National Institute of Water and Atmospheric Science (NIWA), Wellington. Sampling of the Glover Park core was undertaken at GNS Science, Wellington. Tephra-derived glass sample preparation, mounting, polishing, and insitu major element analysis by electron microprobe (EMPA) were all undertaken at Victoria University (VUW). Trace element analysis by laser ablation (LA)-ICP-MS was undertaken partly at VUW and partly at the University of Otago (UoO), Dunedin. Cores were available for Orakei Basin (OB), Onepoto (On) and Glover Park (GP) and these were therefore analysed and sampled; for Hopua and Pupuke, cores were not available, but mounts made by Molloy (2008) were available, therefore these were analysed by EMPA and LA-ICP-MS; and for Pukaki core neither samples, nor core was available therefore data (major element only) was taken from Sandiford et al. (2001), and supplied by P. Shane *pers. comm,* (2014).

- For the whole rock analyses sample preparation, crushing and powdering was undertaken at VUW. 17 new centres were sampled (Boggust Park, Little Rangitoto, Mt Albert, Mt Cambria, Mt Hobson, Mt Roskill, Mt Smart, Onepoto, Otuataua, Pigeon Mt, Pukaki, Pukeiti, Pupuke, Robertson Hill, St Heliers, Taylors Hill and Te Pou Hawaiki) and analysed for both major and trace

elements. For 7 centres (Green Mt, Hampton Park, Mangere Mt, McLaughlins Mt, Mclennan Hillls, Mt Victoria and Otara) samples had already been taken and major element concentrations reported in Miller (1996). The whole rock samples were re-crushed and analysed for both major and trace elements. Major elements were analysed by (XRF) at the Open University (OU), England, and trace elements were analysed by solution-ICP-MS at VUW. This study adds 99 individual whole rock major and trace element analyses to the existing AVF database.

- For the isotope work, the most primitive samples from Mt Wellington, Purchas Hill, Three Kings, Wiri Mt, Puketutu, Pupuke and Rangitoto were chosen for analysis. These centres were specifically chosen because they have previously published Sr-Nd-Pb isotope data available (McGee *et al.,* 2013). Sample preparation, crushing, powdering, and trace element analysis by solution ICP-MS was undertaken at VUW and major element analysis was undertaken at the OU by XRF analysis. Re and Os chemistry and analysis of Os and Re concentrations and Os isotopes took place at the University of Quebec in Montreal (UQAM) in their geochemical and radiogenic isotope laboratory (GEOTOP). The Pb isotope analysis by multi-collector (MC)-ICP-MS was undertaken at Durham University, UK (DU).

Section A – Tephra sampling and analysis

2.2. Auckland Volcanic Field Drill Cores

The maar craters formed by wet style phreatomagmatic eruptions provide excellent depocentres for a well-preserved sediment record. In the AVF, maar craters have long been exploited for their tephra (rhyolitic, andesitic, and basaltic) deposits (e.g., Molloy *et al.,* 2009). A collaborative group from GNS Science and the University of Auckland has created a collection of drill cores over the last 10 years. To date, there are 10 cores, 6 of which are suitable for analysis. These 6 cores include varying lengths from Hopua, Orakei Basin, Pupuke, Glover Park (St Heliers volcano), Pukaki, and Onepoto centres (highlighted in **Fig.1.2**.). The most recent core is from Onepoto, drilled in May 2011. The most extensive tephra record spanning depths of 16-80 m with a predicted age range of 7-83 ka is preserved in the Orakei Basin core (Molloy *et al.,* 2009). Details of the cores are outlined in **Table 2.1**. Collectively the cores preserve an extensive tephra record; however, the degree of preservation is patchy and prior to this research correlation of basaltic tephra horizons across *all* cores remained speculative.

As outlined in **Table 2.1** major element compositions of basaltic tephra-derived glass from within the AVF were published in some previous studies: Orakei, Pupuke, Onepoto (old core), and Hopua - Molloy et al. (2009); Pukaki Core – Sandiford et al. (2001); Onepoto (old core) – Shane and Hoverd (2002); Panmure, Hopua, Pukaki – Shane and Zawalna-Geer (2011). Andesitic to rhyolitic tephra from sources outside the AVF have also been analysed, including from the Taupo Volcanic Centre (TVC), Tongariro Volcanic Centre (TgVC), Okataina Volcanic Centre (OVC), Mount Tarankai (Tk) and Mayor Island (MI). These data have been used to infer a broad picture of the temporal evolution of AVF and central North Island volcanism. Molloy et al. (2009) correlated some AVF horizons between cores (outlined in **Section 1.5**.) using major element compositions and stratigraphic positions. However, no studies have looked into the trace element geochemistry. As a result, correlations of the tephra to their respective centres in the AVF remained less well constrained.

Table 2.1. *Overview of maar cores used in previous studies and this study, their location, the depth section of interest and the number of identified basaltic horizons,, the geochemical analyses obtained on the tephra and the references for the analyses. Note that all trace element data were analysed in this thesis, although for the Pupuke core, trace element data could not be obtained as samples were not available for re-analysis by this study. Ages are outlined as in previous studies where 'ca. 45.1' relates to the age of the Rotoehu tephra (see* ***Sect. 3.3.2*** *for discussion), and the centre name indicates that the core reached the base of the maar, however the centre's age is poorly defined.*

			Previous Studies				This Study		
Core (centre) Name	Grid Reference	Section of interest (m)	Proposed age range (ka) prior to this study	No. of basaltic horizons	Geochemical data	References	No. of basaltic horizons	Status of core and samples	Geochemical data obtained
Pupuke	36°46'49.83"S 174°45'57.67"E	57 to 70	0.4 to 38	7	Major	Molloy et al., (2009)	7	Mounts re-analysed	Major and trace
Onepoto	36°48'27.09"S 174°45'0.39"E	38 to 69	25 to Onepoto	6	Major	Shane and Hoverd, (2002)	9	Core sampled	Major and trace
Glover Park (St. Heliers)	36°50'49.68"S, 174°52'2.60"E	4 to 27	ca. 45.1 to St Heliers	13	Major	Hoverd *et al., (*2005)	4	Core Sampled	Major and trace
Orakei	36°52'4.14"S, 174°48'46.11"E	44 to 87	24 to 86	14	Major	Molloy et al., (2009)	16	Core sampled	Major and trace
Hopua	36°55'46.68"S, 174°47'3.82"E	38 to 49	7 to Hopua	5	Major	Molloy et al., (2009)	5	Mounts re-analysed	Major and trace
Pukaki	36°58'57.63"S, 174°48'37.74"E	45 to 62	7 to ca. 45.1	12	Major	to 52m Sandiford *et al., (*2001), 52m to base Shane, (2005)	12	Core nor mounts available for analysis	

2.2.1. Orakei Basin

The Orakei Basin (or Rakeiora) is a 0.8 km diameter maar crater in the central north-eastern section of the AVF. Ejected ash built the tuff ring that surrounds three sides of the crater, with the north-eastern side composed mostly of unconsolidated ash. On filling with fresh water from rainfall the crater became a freshwater lake for ~75,000 years and more recently rising sea level following the Last Glacial Maximum (LGM) transformed it into a tidal basin. It now contains intertidal brackish salt flats whose nutrient intake is controlled by floodgates beneath the railway line, which borders the north-eastern bank. The oldest lake sediment recovered with the Orakei Basin core was calculated to be 85 ka (81 m depth) (Molloy *et al.,* 2009) based on tephrochronology and sedimentation rates.

2.2.2. Onepoto Basin

Onepoto Basin (or Te Kopua o Matakerepo) is a 0.7 km diameter maar crater surrounded by a tuff ring formed from basaltic surge and fall deposits. This maar is located on the north-north western most part of the field. Similarly to the Orakei basin, Onepoto existed as a freshwater lake until ~9000 years ago when the south-eastern rim of the crater was breached as a result of sea level rise (Shane and Hoverd, 2002). The Onepoto core is ca. 69 m long, and the base of the core is characterised as a thick deposit of basaltic tephra and lapilli, which is considered to represent the crater floor (Shane and Sandiford, 2003).

2.2.3. Hopua

Te Hopua a Rangi (or Hopua, or Gloucester Park) is one of the smaller volcanic maars in the AVF at just 0.5 km in diameter. It is located in the centre of the AVF, but no longer has any outcrop. The eruption that formed the Hopua maar expelled a mixture of poorly sorted fine ash to lava bombs (Allen and Smith, 1994), and shows morphostratigraphic evidence of erupting through the lava of One Tree Hill (Searle, 1961b), showing it must be younger than One Tree Hill. The Hopua tuff ring was high sided to the north and low sided to the south, possibly as a consequence of the prevailing wind direction. After the LGM when sea levels rose the crater rim was breached and a tidal basin was created. The extracted Hopua core is 49 m long, of which the top 37.5 m were composed of estuarine sediments. The lower 11.5 m show lacustrine varves punctuated with tephra deposits of rhyolitic, andesitic, and basaltic composition. The core ended in a thick scoria unit proposed to represent the crater floor of the maar (G. Leonard *pers. comm.* 2015)

2.2.4. Lake Pupuke

Pupuke Moana (the ‘over flowing lake’) is one of the oldest volcanoes of the AVF, thought to have erupted around a similar time to Tank Farm and Onepoto (Lindsay *et al.,* 2011). New Ar-Ar dating has yielded an age for Pupuke of ca. 190 ka (Leonard *et al., in prep.* **Appendix D**), potentially younger than that proposed for Onepoto. The eruptions from Pupuke are thought to have occurred twice from two different vent sources, with eruptive products of slightly differing compositions

(Spargo, 2007). The initial eruptions did not interact with ground water and were therefore 'dry', with lava flows from two different vents building up a low, thin shield. These initial eruptions were followed by large explosive wet eruptions from two vents forming the maar lakes that are seen today (Spargo, 2007). The tuff ring resulting from these eruptions created a natural barrier and the lake has remained fresh water since it was originally filled (Hayward *et al.,* 2011). The core extracted from Lake Pupuke was 16.5 m long extending back to roughly 38 ka, and includes tephra from the eruptions of Rangitoto (Molloy *et al.,* 2009).

2.2.5. Pukaki Lagoon

Pukaki lagoon is located in the south of the AVF and is considered one of the best-preserved explosion craters in the AVF. The crater was formed by multiple pulsating wet eruptions resulting from rising magma interacting with ground water (Sandiford *et al.,* 2001). The current crater is 0.5 km across and 100 m deep with a 20-40 m high tuff ring that extends out, in places, a further 0.5 km (Hayward *et al.,* 2011). The age of the crater is poorly defined with estimates based on sedimentation rates suggesting a minimum age of 52 ka (Molloy *et al.,* 2009). Multiple cores have been extracted from this centre, and can be used to show the complexity of deposition for this environment. For example, **Figure 2.1** shows the published observations from cores retrieved in 2001 (Sandiford *et al.,* 2001), 2002 (Shane 2005 and Shane *pers. comm.* 2013) and 2008 (Zawalna-Geer, 2012), comparing the basaltic tephra horizons that were found by these authors. In this figure the complexity in identifying the basaltic horizons through visual observations alone is shown by the disparity in the correlations. For this thesis I have chosen to use the published details, (including the name (AVF#), thickness, position, and geochemical data; Sandiford *et al.,* 2001 and Shane 2005), rather than the most recent details from Zawalna-Geer (2012), which are not published and do not have geochemical data available.

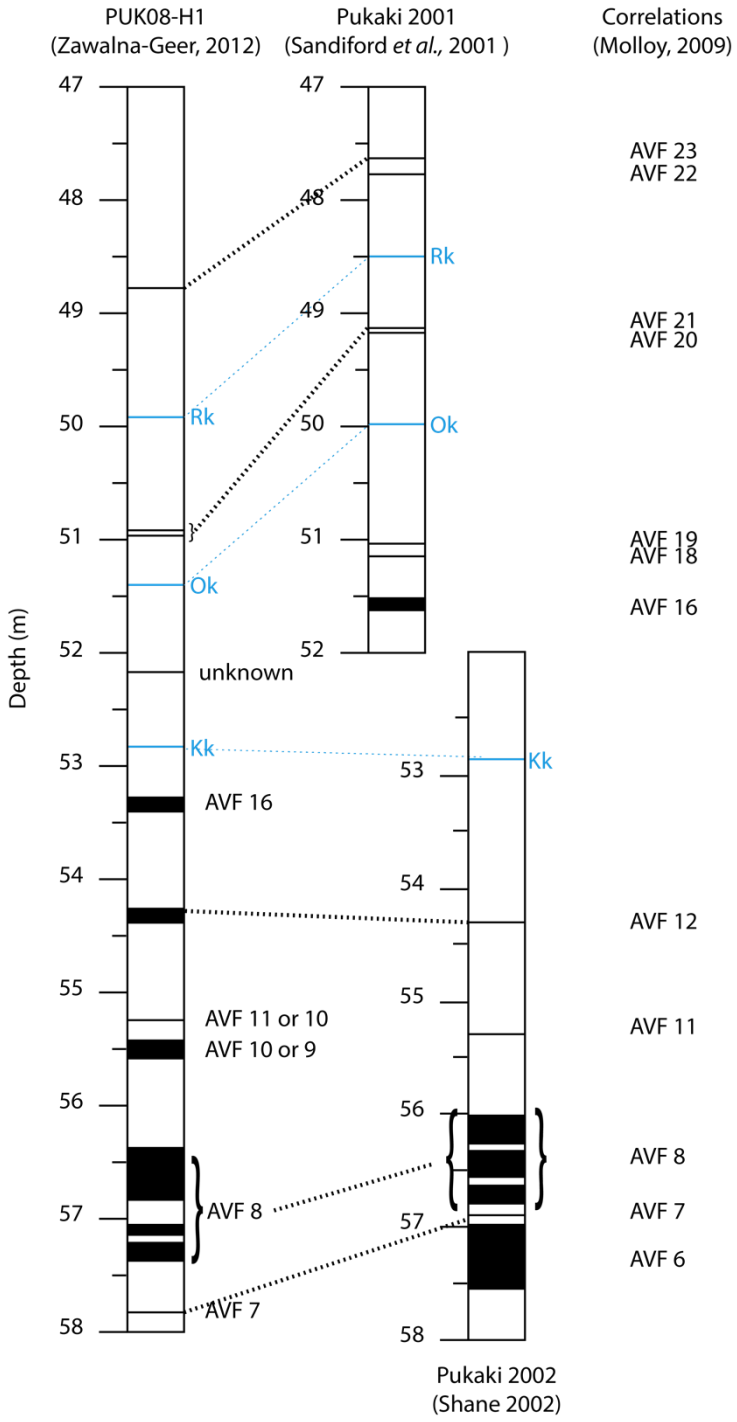

Figure 2.1. *Schematic diagram to show correlation of Pukaki cores from 2001, 2002 and 2008. Sandiford et al. (2001) and Shane (2005) are used for this thesis as Zawalna-Geer (2012) remains unpublished and inconsistencies remain with the correlations proposed by Zawalna-Geer (back dashed lines). Also shown are the proposed AVF# from Molloy et al. (2009) for the horizons in the 2001 and 2002 cores. Blue horizons are key rhyolitic deposits. Rk (Rerewhakaaitu), Ok (Okareka), Kk (Kawakawa).*

2.2.6. Glover Park (St Heliers)

St Heliers volcano is located beneath the modern day Glover Park. It was a classic phreatomagmatic eruptive centre forming a simple tuff ring structure. However, unlike most of the AVF maars, its base is 20 m above modern sea level and was therefore not breached by the post-LGM sea level rise. The crater was filled with fresh water that in geologically recent times had become in filled with sediment resulting in a swampy environment. Sixty years ago, the swamp was drained and turned into the Glover Park playing fields. In December 2004 two cores were drilled into the centre of Glover Park (GP1 and GP2), both of which terminated in hard vesicular basalt and consisted of ca. 2.7 m of backfilled topsoil, ca. 2.0 m of swamp deposits, ca. 11.4 m of fine grained massive, finely laminated freshwater sediments with interbedded tephra and finally below ca. 16.1 m intermittent coarse-grained horizons with distorted lacustrine sediments. This core is recorded in detail in Hoverd et al. (2005), with major element analyses on glass reported for 31 macroscopic tephra deposits including 8 rhyolitic horizons linked to Taupo Volcanic Zone (TVZ) and Mayor Island (MI), 10 trachytic-andesitic horizons linked to Mt. Taranaki (Tk) and Tongariro volcanic centre (TgVC), and 13 basaltic horizons linked to the AVF. These tephra horizons were re-sampled and re-analysed for this study.

2.3. Core Analysis and Sampling

All the cores used in this study were previously drilled, logged and analysed, but with the focus of research being palaeoclimate or silicic tephrochronology. In this study, Orakei was re-logged and sampled, and a new core from Onepoto was used from the same site as the old core. Samples from Hopua and Pupuke were re-analysed for trace elements using the same samples used by the Molloy et al. (2009), and Glover Park was totally resampled and analysed. Major element data from Pukaki used in this study are from published (Sandiford *et al.,* 2001) and unpublished work (P. Shane, *pers. comms,* 2013).

Cores from Orakei Basin and Onepoto were scanned using an Ultra EPX-F2800 portable veterinary radiological device (NIWA, Wellington, NZ). For the Onepoto core magnetic susceptibility analysis was undertaken using a Barington-MS2 Magnetic susceptibility meter connected to a MS2F probe (data from UoA for

the Orakei Core). Analysis was done every 2 cm down the centre of the core (1 cm in regions of interest) and recorded in 10^{-5} SI units with a sensitivity of 1.0 x 10^{-5} SI. The X-ray images were compared to composite photographs of each section, and magnetic susceptibility data was combined to pin point the location of each tephra layer/layer. Sampling was undertaken in the core lab at NIWA and multiple samples were taken from tephra that were thick enough to permit sub-sampling of single horizons. Samples were also taken from Glover Park core, previously only major element analysis was undertaken (Hoverd et al. (2005), and the samples were no longer available for trace element analysis.

A small amount of deposit was removed from the core surface to expose a fresh surface from which to sample tephra. Sections of tephra from the centre of the core shaft were removed in order to reduce contamination potentially caused by core suck at the tubing edges. Three types of basaltic tephra deposit were identified from their morphostratigraphy including:

i) deposits which were a homogenous thickness and shape with distinct upper and lower boundaries,
ii) deposits which tended to be larger in thickness and have an obvious grading and sorting within them from large clasts at the base to finer clasts towards the top (multiple samples were taken from these to confirm all one event),
iii) and very obviously deformed deposits which had irregular, non-horizontal boundaries, with some appearance of rafting events.

Approximately 2/3 of the bulk horizon sample was retained for archive purposes and 1/3 was processed for analysis. Samples were individually washed with ultrapure Milli-Q water in an ultra sonic bath to remove organic debris. If the shards were < 30 µm, excess water was allowed to evaporate (oven overnight at 50°C) and the sample was set aside. This is a bulk (B) sample, which includes both tephra shards and accidental ejecta (e.g. quartz, glauconite, shell fragments and sedimentary lithics). If the shards were larger than 30 µm, glass shards (G) were removed and separated into a vial and juvenile crystals (C) were also separated into a vial. Excess water was then evaporated from these to yield glass, crystal and bulk shard aliquots from each sample.

2.4. In-situ Major Element Analysis by EMPA

2.4.1. Sample preparation

Deep epoxy mounts were created using a 4:1 ratio of resin to hardener. The mounts were cut into 7 mm depths using a bandsaw, and then 6 individual holes were drilled through the mounts at 3.5 mm diameters. The holes were then filled with sample, then epoxy, and left to set on the hot plate at 50-55°C overnight. The analysis face was polished using a sequence of silicon carbide papers starting with a coarseness of 400, followed by 600, 1000 and 2500, finally being finished using a diamond lap polisher at 3 µm and 1 µm. This process exposed the sample faces and removed as much scratching from the surface as possible. Finally, a 25 nm carbon coat was applied to the mount prior to major element analysis.

2.4.2. Measurements

The major element or oxide proportions (SiO_2, TiO_2, Al_2O_3, FeO_t, MnO, MgO, CaO, Na_2O, K_2O, Cl, SO_3, and P_2O_5) were analysed using Wavelength Dispersive Spectrometry (WDS) on the JEOL JXA 8320 Superprobe at VUW. **Table 2.2** shows the analytical conditions for EMPA. To produce the analyses, an accelerating voltage of 15 kV under a static electron beam at 10 µm and 8 nA was used. 10-15 analyses were undertaken per sample on individual glass shards, with specific care taken not to hit any microcrysts or bubbles within the shards. Na_2O and K_2O were analysed first with shorter count times to reduce the loss of volatiles (**Table 2.2.**). Major element concentrations were determined using the ZAF correction method, and back-scattered electron images of each sample, and sample point, were taken to allow individual shard characterisation for later LA-ICP-MS analysis.

2.4.3. Standards

For quality control, the following standards were run along with our samples: 1) Basaltic Glass A99 (for SiO_2, TiO_2, Al_2O_3, FeO_t, MnO, MgO, CaO), 2) Rhyolitic Glass VG-568 (Na_2O and K_2O), 3) Scapolite PSU63-1805 (for Cl), 4) Celestine (for SO_3) and 5) Beesons Apatite (for P_2O_5). All standards were run at the beginning and end of each mount analysis, with A99 run 3 times between every 10-15 samples to monitor spectrometer drift. The data for all these standards can be found in **Appendix B**.

Table 2.2. *Instrumental operating conditions for electron microprobe analysis of in-situ major elements, analyser crystals are shortened to the acronyms, PETL/PETJ – pentaerythritol, TAP – thallium acid pthalate, and LIF – lithium fluoride, these are varied during analysis to cover the entire X-ray spectrum.*

EMPA	
Electron Microprobe Analysis	
Instrument	JEOL JXA 8320 superprobe
Analysis mode	Wavelength dispersive spectrometry (WDS)
Accelerating voltage	15 kV
Spot size	10 µm
Probe current	8 nA
Standards	
Calibration standards	Basaltic Glass A99 (SiO_2, TiO_2, Al_2O_3, FeO, MgO, CaO)
	Rhyolitic glass VG-568 (Na_2O and K_2O)
	Scapolite PSU63-1805 (Cl)
	Celestine (SO_3)
	Beesons Apatite (P_2O_5)
Secondary standard	Basaltic Glass A99

Method Parameters				
Channel 1	**Channel 2**	**Channel 3**	**Channel 4**	**Channel 5**
K (20 sec) PETL	Na (10 sec) TAP	Si (30 sec) TAP	Ca (30 sec) PETJ	P (30 sec) PETL
S (30 sec) PETL	Mg (50 sec) TAP	Al (30 sec) TAP	Fe (30 sec) LIF	Cl (30 sec) PETL
Ti (30 sec) PETL			Mn (30 sec) LIF	

2.5. In-situ Trace Element Analysis by LA-ICP-MS

2.5.1. Sample preparation

The carbon coat was removed from the pre-prepared mounts using AR grade methanol, and for VUW analyses the mounts were cut in half using a diamond edge saw and three samples on a ½ mount were loaded along with the standard BHVO2G into the sample chamber for analysis (**Fig. 2.2.A**). For UoO analyses, mounts were kept whole and two mounts (12 samples) were loaded along with standard BHVO2G, BCR2G, NIST612, and NIST610 (**Fig. 2.2.B**).

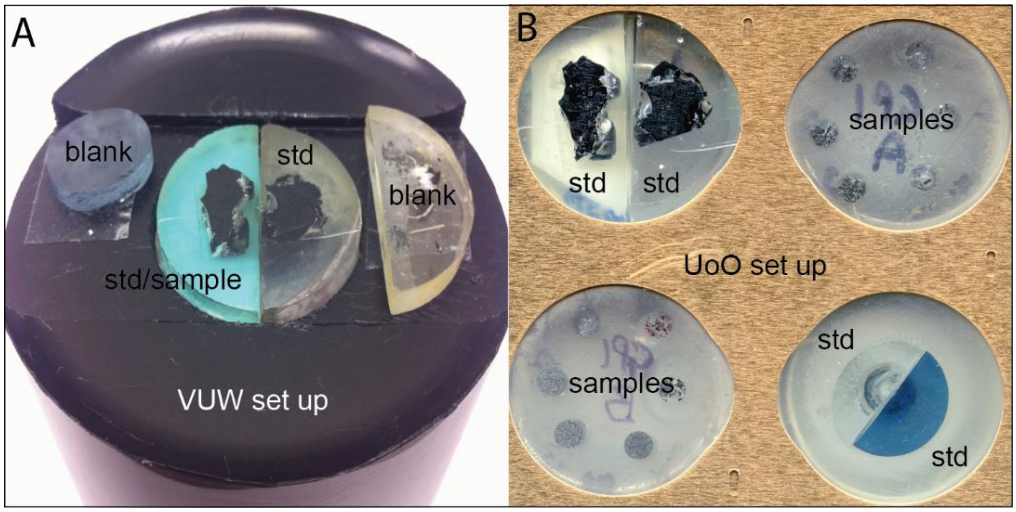

Figure 2.2. *(A) Photograph to demonstrate mount set up (VUW) for laser ablation chamber. 'Blank' blocks have been shown (Allan et al., 2008) to increase signal stability. Photograph shows set up for standard (std) analysis, for sample analysis left hand half moon mount would be replaced with sample half moon for 3 individual sample analyses. (B) Mount set up for UoO analysis for laser ablation chamber. Samples from Glover Park core shown in situ for 12 individual analyses, all standards remain in position with sample mounts swapped for analysis.*

2.5.2. Measurements

Trace element analysis was undertaken using an Agilent 7500cs Inductively Coupled Mass Spectrometer (ICP-MS) coupled with (at VUW) a New Wave UP 193nm Solid State laser, or (at UoO) a Resonetics RESOLution M-50-LR, using the methods developed by Allan et al. (2008). Analytical conditions for LA-ICP-MS analysis are detailed in **Table 2.3**. Prior to analysis the ICP-MS was tuned by rastering across BHVO-2G (or NIST612 at UoO) standard. The instrument conditions, predominantly the carrier gas (Ar) or optional gas (He) flow rates, were adjusted to optimise the machine sensitivity, but minimise the production of oxides. Oxide production was monitored using measured values of ThO^+/Th^+ (masses 248/232) and maintained to a value of ≤1.5 %. Pulse/Analogue (P/A) factors were measured on relevant elements (e.g. Si, Ca, Mg, V, Zr, Ti, Cr, Ni, Sr, Ba, Ce) to

allow the ICP-MS to perform the right correction when switching between pulse and analogue mode, which is required when the count rate is > 1million CPS. Multiple isotopes of selected elements were measured (e.g. ^{90}Zr and ^{91}Zr) to assess the quality of the data, usually producing concentrations of ± 0.5% variability between the isotopes. 41 elements were analysed: Si, Li, B, Mg, Ca, Sc, Ti, V, Cr, Mn, Ni, Cu, Zn, Ga, Rb, Sr, Y, Zr, Nb, Cs, Ba, La, Ce, Pr, Nd, Sm, Eu, Gd, Tb, Dy, Ho, Er, Tm, Yb, Lu, Hf, Ta, W, Pb, Th, and U. All the data were acquired from static spot analysis with a spot size of 25-35 µm pulsed at 5Hz.

Table 2.3. *Instrumental operating conditions for LA-ICP-MS analysis of in-situ trace elements at both Victoria University of Wellington and University of Otago.*

LA-ICP-MS		
Laser Ablation	**VUW**	**UoO**
Instrument	New wave 193nm (deep UV) solid state	New Wave UP 213 nm (deep UV) solid state
Ablation mode	static spot analysis	static spot analysis
Spot size	25 or 35um (predominantly 35um)	25 or 35 µm (predominantly 35µm)
Repetition rate	5Hz	5 Hz
Laser power	85-100%	100%
ICP-MS		
Instrument	Agilent 7500CS octopole	Agilent 7500CS octopole
Aquisition mode	Peak hopping	Peak hopping
Detection mode	Pulse and analogue counting (mostly pulse)	Pulse and analogue counting (mostly pulse)
Standards		
Calibration standard	BHVO-2G	NIST 612, BHVO-2G
Secondary standard	BHVO-2G, BCR-2G	BHVO-2G, BCR-2G
Internal standard value from EMPA	^{29}Si	^{29}Si
Method Parameters - same for both VUW and UoO		
Background acquisition	20 s	
Standard aquisition	60 s	
Sample aquisition	60 s	
Measured isotopes and integration times	10 ms:	^{25}Mg, ^{29}Si, ^{43}Ca, ^{47}Ti, ^{53}Cr, ^{55}Mn
	20 ms:	^{7}Li, ^{45}Sc, ^{51}V, ^{59}Co, ^{60}Ni, ^{63}Cu, ^{66}Zn, ^{71}Ga, ^{85}Rb, ^{86}Sr, ^{89}Y, ^{90}Zr, ^{91}Zr, ^{93}Nb, ^{95}Mo, ^{133}Cs, ^{138}Ba, ^{139}La ^{140}Ce, ^{141}Pr, ^{146}Nd, ^{147}Sm, ^{151}Eu ^{153}Eu, ^{157}Gd, ^{159}Tb, ^{163}Dy, ^{165}Ho, ^{166}Er, ^{169}Tm, ^{172}Yb, ^{175}Lu, ^{178}Hf, ^{181}Ta, ^{182}W, ^{208}Pb, ^{232}Th, ^{238}U,
Tuning		
Tuning standard	BCR-2G	
Ablation mode	Rastering (2um/s) beneath a 35um spot	
Monitored isotopes	^{7}Li, ^{24}Ca, ^{29}Si, ^{43}Ca, ^{55}Mn, ^{88}Sr, ^{140}Ce, ^{232}Th,	
Oxides	ThO^+/Th^+ typically <1.5%	
Carrier Gas (Ar)	0.83 - 0.87 L/min	
Ablation gas (He)	80 - 90%	
RF power	1500 W	
RF matching	1.77 V	
Sample depth	4 mm	
Extract 1 ion lense	3.2 - 5 V	
Extract 2 ion lense	-172 to -117 V	

2.5.3. Processing of raw LA-ICP-MS data

The raw data was reduced in the programme 'Iolite' (Paton *et al.,* 2011) using the SiO_2 values measured by EMPA as an internal standard for specific sample spot sites. The SiO_2 concentration for each site was converted into Si concentration and input as an internal calibration value for each shard. The .csv files output from the Agilent software was directly loaded in to iolite. The individual time-stamp for each analysis allowed multiple analyses to be loaded at once to allow calibration standard drift to be measured and corrected for over the course of a run ('Spline' process) (**Fig. 2.3.A**). During data processing care was taken to identify and remove any data that were compromised by accidental ablation of crystal inclusions (**Fig. 2.3.B**) or ablation through the glass shard itself (**Fig. 2.3.C**). This process is of critical importance to ensure the data for a given analysis are purely for the glass. Allan et al. (2008) detail some specific elements that show contamination by certain mineral phases, and these are detailed in **Table 2.4**. They were monitored during data reduction.

Table 2.4. *Elements that cause contamination in glass shards (from Allan et al. 2008) and their related mineral phase.*

Contaminant	Increased concentration	Decreased concentration
Olivine	Mg, Si, Ni, Co	
Plagioclase	Sr, Al, Ca	
Orthopyroxene	Mg, Mn, Zn	
Magnetite	Fe, Ti, Cr,	Si

Figure 2.3. *Annotated screen shot of iolite data reduction programme. (A) Set up for a standard data acquisition of calibration standards and 'unknowns'. (B) The identification of accidental ablation of a microcrystal shown by Mg concentrations plotted as secondary peak, (C) identification of accidental ablation through a glass shard.*

2.5.4. Accuracy and Precision of LA-ICP-MS

An initial standard test was run to check tuning using BHVO-2G as a bracketing standard and BCR-2G used as a secondary standard (e.g. run as an unknown but with known values for reference). The standard BHVO-2G was then run once every 5 samples for calibration. Values used for the reference materials were the preferred values from the GeoReM database (http://georem.mpch-mainz.gwdg.de; Jochum et al. (2005), **Table 2.5.**). Comparisons of the precision and accuracy of the measurements for VUW vs. UoO are discussed in **Section 2.11.4.**

Table 2.5 shows a summary of the analyses made by LA-ICP-MS. External precision of analysis (measured as 2sd% variability from the standard reference value) for BHVO-2G of elements at both UoO and VUW are poor for Li, Cr, Cu, Cs, Pb, for VUW specifically Lu is poor, and for UoO specifically Tm and Eu are poor. For BCR-2G both VUW and UoO have consistently poor precision for Li, Cr, Ni, Cu and Cs, however, all other elements have a precision of <3%. For BHVO-2G the accuracy at VUW (17 elements were measured at <1% offset (from the standard value), and 13 with 1-3% offset) is slightly better than at UoO (14 elements were measured at <1% offset, and 15 with 1-3% offset), including previously mentioned elements forming the outliers (>3% offset; Li, Cr, Cu, Cs, Pb, Eu, Tm, Lu). For BCR-2G the accuracy is better at UoO (9 elements were measured at <1% offset, and 22 with 1-5% offset) in comparison to VUW (8 elements were measured at <1% offset, and 17 with 1-5% offset), outliers (>5% offset) here include Ti, Cr, Zr, Tm, Ta for UoO, and Li, Cr, Ni, Cu, Zn, Y, Zr, Cs, Hf, Ta for VUW. In many cases the analysis is very accurate, with a small % offset from the reference value, but not very precise (e.g., VUW Ba on BCR-2G, % offset = 0.5, 2sd% = 7), suggesting multiple analyses are necessary to gain accurate concentration values.

***Table 2.5**. Summary of the standard data gained throughout the analysis sessions for 2011-2014 for standards BHVO-2G and BCR-2G analysed by LA-ICP-MS at VUW and UoO. All values are reported in ppm, accuracy of analyses shown by offset from reference values (GeoREM; Jochum et al., 2005) for n=264 number of analyses, for standard deviation of results see **Appendix Bii.** Elements are reported with their measured isotope numbers, and red highlights values discussed in the text as outliers.*

BHVO-2G values		VUW		UoO	
Element	Reference value	Average	% offset from std	Average	% offset from std
Li7	4.8	4.43	-7.78	4.61	-3.93
Sc45	32	32.9	2.69	32.3	0.90
Ti47	16300	16708	2.51	16709	2.51
V51	317	309	2.62	309	2.51
Cr53	280	294	5.14	315	12.6
Mn55	1317	1317	0.04	1311	-0.44
Ni60	119	116	2.57	120	1.15
Cu63	127	103	-19.0	137	8.07
Zn66	103	102	1.13	101	2.28
Ga71	22	22.0	0.03	22.1	0.25
Rb85	9.08	9.33	2.78	9.19	1.26
Sr88	396	396	0.11	397	0.25
Y89	26	25.9	0.30	25.6	1.47
Zr90	172	169	1.53	168	2.10
Nb93	18.1	18.3	0.88	18.1	0.08
Cs133	0.1	0.11	14.5	-0.14	-245
Ba137	131	133	1.52	131	0.13
La139	15.2	15.2	0.02	15.1	0.85
Ce140	37.5	37.6	0.32	37.5	0.10
Pr141	5.29	5.34	0.97	5.26	0.64
Nd146	24.5	24.5	0.01	24.4	0.21
Sm147	6.07	6.09	0.29	6.10	0.44
Eu153	2.07	2.07	0.03	2.17	4.66
Gd157	6.24	6.16	1.29	6.03	3.39
Tb159	0.936	0.92	1.98	0.91	2.93
Dy163	5.31	5.28	0.60	5.21	1.97
Ho165	0.972	0.98	0.93	0.99	1.72
Er166	2.54	2.56	0.82	2.46	3.17
Tm169	0.341	0.34	0.36	0.41	19.8
Yb172	2	2.02	0.77	2.01	0.55
Lu175	0.274	0.29	5.20	0.27	0.72
Hf178	4.36	4.31	1.25	4.23	2.98
Ta181	1.14	1.15	0.57	1.16	1.41
Pb208	1.6	1.80	12.6	1.81	13.1
Th232	1.22	1.23	1.22	1.20	1.79
U238	0.403	0.41	1.88	0.40	0.14

BCR-2G values		VUW		UoO	
Element	Reference value	Average	% offset from std	Average	% offset from std
Li7	9	9.49	5.48	9.01	0.08
Sc45	33	33.8	2.52	34.1	3.38
Ti47	13500	14027	3.90	14291	5.86
V51	416	416	-0.06	427	2.68
Cr53	13	15.7	20.8	17.1	31.2
Mn55	1550	1510	-2.55	1571	1.35
Ni60	12	10.6	-12.1	12.3	2.87
Cu63	21	5.69	-72.9	20.0	-4.94
Zn66	127	137	7.81	129	1.59
Ga71	23	23.7	2.95	23.0	0.14
Rb85	46.9	49.2	4.88	47.6	1.58
Sr88	340	346	1.75	345	1.56
Y89	37	34.7	-6.19	36.0	-2.84
Zr90	201	181	-10.2	188	-6.40
Nb93	12.6	12.8	1.69	12.7	0.85
Cs133	1.1	1.23	12.1	1.11	1.30
Ba137	677	680	0.50	691	2.11
La139	24.9	24.5	-1.70	25.3	1.74
Ce140	52.9	53.6	1.41	54.1	2.28
Pr141	6.7	6.72	0.36	6.83	1.88
Nd146	28.7	28.0	-2.33	29.6	3.24
Sm147	6.58	6.42	-2.49	6.57	-0.09
Eu153	1.96	1.95	-0.45	1.98	1.21
Gd157	6.75	6.58	-2.55	6.68	-0.97
Tb159	1.07	1.02	-4.62	1.04	-2.82
Dy163	6.41	6.24	-2.58	6.57	2.51
Ho165	1.28	1.25	-2.16	1.29	0.92
Er166	3.66	3.64	-0.52	3.72	1.62
Tm169	0.54	0.52	-4.05	0.50	-7.10
Yb172	3.38	3.38	-0.09	3.41	1.01
Lu175	0.503	0.51	0.89	0.51	1.00
Hf178	4.9	4.62	-5.62	4.93	0.57
Ta181	0.74	0.78	5.59	0.81	8.86
Pb208	11	10.80	-1.79	10.81	-1.72
Th232	6.03	5.99	-0.65	6.09	1.00
U238	1.69	1.71	1.40	1.71	1.07

Section B – Whole Rock Analysis

2.6. Sample Selection and Preparation

2.6.1. Sample selection

In order to make the most informed correlations between tephra deposits and whole rock, it was necessary to obtain whole rock data from as many centres as possible. In this thesis (**Chapter 4**) we present a minimum of 5 analyses for all centres of the Auckland Volcanic Field (AVF), excluding those with no surface exposure, to test correlation potential. These data are obtained from literature values, and from new data presented in this thesis where gaps were found in the literature values.

Additional rock samples for centres with less than 5 analyses were collected from the field or pre-existing rock collections. For samples collected in a field campaign, sites were chosen to sample a range of deposits including lava flows, scoria deposits, and tuff ring deposits. For lava flows, samples were selected from a number of different sites; they were broken with a sledgehammer to obtain fresh surfaces with limited weathering or oxidation. Scoria samples were taken by hand or with a sledgehammer, with the large scoriaceous bombs being preferable. Welded and imbedded bombs were also the preferred material for sampling from the tuff rings. The samples were taken, where possible, from a variety of sites around an individual centre and samples were chosen for their unweathered and juvenile appearance.

2.6.2. Sample preparation

Fresh samples were then crushed using a Rocklabs Boyd crusher to chips <15 mm in size. The crusher was cleaned with ethanol and dried using compressed air repeatedly between samples. The crushed material was then powdered using a TEMA tungsten-carbide swing mill at VUW.

2.7. Whole Rock Major Element Analysis by XRF

2.7.1. Sample preparation

Samples were made into fused lithium metaborate glass discs and analysed for major oxide concentrations following methods of Ramsey et al. (1995). Approximately 0.7g (1 part by weight) of powdered sample was dried at 110°C before being mixed with ca. 3.5g (5 parts by weight) of dried lithium metaborate flux. This mix was then placed in 95% Pt - 5% Au crucibles and fused in a muffle furnace at 1100°C for 15 minutes. Loss-on-ignition (LOI) measurements were calculated by heating dried powdered samples in pre-ignited crucibles to 1000°C for 1 hr and recording the weight loss.

2.7.2. Measurements

Glass discs were then measured for major elements (SiO_2, TiO_2, Al_2O_3, $Fe_2O_3^{tot}$, MnO, MgO, CaO, Na_2O, K_2O, P_2O_5) on an ARL® 8420+ dual goniometer wavelength dispersive X-ray fluorescence (XRF) spectrometer at the Open University. Analytical conditions are detailed in **Table 2.6**.

Table 2.6. *Analytical conditions for XRF analysis of major elements at the Open University, UK; fpc flow portional counter, and x-ray tube operated at 40kV/60mA, from Ramsey et al., 1995.*

Element Data				Analytical Conditions		
Element	X-ray line	Wavelength (Å)	Count time (s)	Crystal	Detector	Collimator
Na	K_α	11.910	40	AX06	fpc	coarse
Mg	K_α	9.890	25	AX06	fpc	coarse
Al	K_α	8.340	20	PET	fpc	coarse
Si	K_α	7.126	30	PET	fpc	coarse
P	K_α	6.158	30	Ge111	fpc	fine
S	K_α	5.373	20	Ge111	fpc	fine
K	K_α	3.742	15	LiF200	fpc	fine
Ca	K_α	3.359	15	LiF200	fpc	fine
Ti	K_α	2.750	20	LiF200	fpc	fine
Mn	K_α	2.130	15	LiF200	fpc	fine
Fe	K_α	1.937	15	LiF200	fpc	fine

2.7.3. Accuracy and precision of XRF

A bivariate regression line of multiple reference materials was used as calibration standard (c.f. Ramsey et al., 1995) for XRF analysis. Secondary standards Whin Sill Dolerite (WS-E) and Nanhoron Microgranite (OU-3) were run at the beginning and end of each batch of samples to monitor accuracy and precision of results. **Table 2.7** reports the average standard values over 4 batches, and **Appendix B** reports all the values measured for the standard analyses. For WS-E all elements agree closely with the reference value (<1% offset), except for Na_2O (-2.37%) and P_2O_5 (-1.59%), and exhibit precision of <1.5% for all except P_2O_5 (2.7%). For OU-3 all elements show <2% offset from the reference value, except CaO (3.08%) and all exhibit a precision value of <2%, indicating that the XRF technique shows a high level of both precision and accuracy. Blind duplicate analyses were run for selected samples and for BHVO (reported in **Appendix B)** and show excellent reproducibility. With blind BHVO analyses all within <2% offset of the reference value, and all with precision of <3%.

***Table 2.7**. Summary of the standard data gained through XRF analysis techniques for major element concentrations of whole rock. Reference values for WS-E from Govindaraju, 1994 with the exception of SiO_2, TiO_2, and Fe_2O_3 from Thompson et al., 2000 and for OU-3 reference values are accepted from long-term running averages from the Open University XRF lab.*

	Whin Sill Dolerite (WS-E)				Nanhoron Microgranite (OU-3)			
	Reference value	average (wt%) (n=8)	% offset from std	2sd%	Reference value	average (wt%) (n=8)	% offset from std	2sd%
SiO_2	51.10	51.03	0.15	0.12	74.09	74.13	0.05	0.21
TiO_2	2.43	2.43	0.33	0.35	0.22	0.22	0.11	2.50
Al_2O_3	13.78	13.89	0.80	0.24	11.11	11.08	0.28	0.47
$Fe_2O_3^{tot}$	13.15	13.16	0.05	0.28	3.83	3.87	0.92	0.51
MnO	0.17	0.17	0.50	1.14	0.09	0.09	1.78	1.35
MgO	5.55	5.55	0.07	0.60	-	0.03	-	-
CaO	8.95	8.94	0.14	0.32	0.20	0.21	3.08	1.82
Na_2O	2.47	2.41	2.37	0.72	3.68	3.71	0.68	0.99
K_2O	1.00	1.00	0.25	1.17	4.55	4.56	0.20	1.08
P_2O_5	0.30	0.30	1.59	2.70	-	0.02	-	-
LOI	0.85	0.85	0.00	0.00	1.82	1.82	0.00	0.00
Total	99.75	99.72	0.03	0.07	99.59	99.72	0.13	0.25

2.8. Trace Element Analysis by Solution-ICP-MS

2.8.1. Laboratory Protocol at VUW

Sample preparation was undertaken in an ultraclean laboratory facility using Class 10 laminar flow workstations. The air within the laboratory is positively pressured and filtered to Class 100, in order to minimise the risk of sample contamination.

2.8.2. Reagents

All the water used for any lab work in this study was filtered Millipore H_2O (MQ) with measured resistivity of ~18.2 MΩ. For sample preparation Seastar (SS) grade ultra-pure acids were used. For sample dissolution SS grade HNO_3 and HF were used. For trace element analysis, analytical reagent (AR) grade HNO_3 was distilled twice to produce a 2xsub-boiled (SB) acid. The acid dilutions were made with MQ water and their molarities checked using a density meter.

2.8.3. Beaker preparation

Prior to chemical procedures, 23 mL Savillex screw top beakers were cleaned to remove any potential contaminants. Dirty beakers were thoroughly rinsed with MQ and wiped down with methanol. The beakers were then soaked in AR grade 6M HCl for a minimum of 24 hours on a hotplate at 120°C. They were then removed and rinsed three times with MQ water. This process was then repeated but with 7M HNO_3. Finally, the beakers were filled with 4-5 mL of 6-7M SB HNO_3 sealed and refluxed for 24 hours. This acid was then removed and the beakers were rinsed three times with MQ water. This process was then repeated with 4-5 mL of 6-7M SS HNO_3. Once rinsed with MQ beakers were then dried down and ready for use. For Pb isotopes this step is repeated with 6M SS HCl, then rinsed and stored in SB HNO_3 until ready for use.

2.8.4. Trace element chemistry

For trace element analyses a split of the same sample powders previously used for XRF and isotope analysis from this and studies by McGee et al (2012 and 2013) was used. 50 mg of rock powder was weighed on a high precision balance to ±0.0001g in a pre-cleaned (outlined above) 23 mL Savillex screw top beaker. Samples and international reference standards BHVO-2G and BCR-2 were digested using conventional methods (**Fig. 2.4.**); ca. 1 mL concentrated (conc.) hydrofluoric acid (29M SS HF) was combined with ca. 0.5 mL conc. nitric acid (16M SS HNO_3), the beaker was sealed and this was refluxed at 120°C for 3-4 days to ensure complete digestion. Once digested, the solution was dried to incipient dryness (to reduce sample loss by the production of insoluble fluoride), and taken up with ca. 2 mL conc. HNO_3 and again dried to incipient dryness. This step is repeated to allow the removal of any fluorides that may have formed. Following this the samples were refluxed with 5 mL 6M HCl (2xSB) overnight. After complete dissolution of sample the HCl was evaporated and then taken up with ca. 2 mL conc. HNO_3. To allow the chlorides formed to turn back into nitrides the sample was then evaporated to incipient dryness, taken up again with 9 mL 1M HNO_3 (SS) and finally left to reflux for 2-3 days to form the analytical solution. Prior to analysis the samples were centrifuged at 2000 rpm for 5 minutes. The final solutions were then transferred to pre-cleaned 10 mL centrifuge tubes (c-tubes), ensuring all drops were removed from the beakers, and weighed on a high precision balance (±0.0001 g). To analyse the sample solutions dilutions of the stock solution are made by removing a 60 µL aliquot into another c-tube, the aliquot was again precisely weighed and it then topped up with 5.94 mL of 1% HNO_3 and weighed again, this procedure ensures the final dilution of the sample could be accurately calculated. The process is outlined in **Figure 2.4** using **equations 2.8.6.1** and **2.8.6.2** for dilution calculations, where sample weight is recorded in grams (g).

2.8.5. Analysis of elements on ICP-MS

The sample dilutions prepared as described above were analysed on an Agilent 7500CS ICP-MS (the same instrument as used for the in situ tephra-derived glass analysis) at the VUW. Analysis conditions are shown in **Table 2.8**. Prior to analysis the ICP-MS was tuned using an Agilent 10 ppb multi-element standard tuning solution diluted to 1 ppb. Instrumental conditions, torch conditions and gas flow rates, were optimised to maximise the machine sensitivity but minimise the production of oxides. This process was monitored using measured values of CeO^+/Ce^+ (masses 156/140) and maintained to a value of ≤1.5 %. Pulse/Analogue (P/A) factors were measured on relevant elements (e.g., Ca, V, Cr, Ni, Sr, Ba, Ce, Mo, and Zr), and multiple isotopes of selected elements were measured, as detailed in **Section 2.5.2**. Samples were introduced into the ICP-MS using a wet spray chamber and peripump. The individual analysis of a sample is 120 seconds (s) in duration, preceded by a 30 s water wash, 180 s 1% HNO_3 wash out, 60 s 1% HNO_3 background analysis. Each analysis session included 3 bracketing standards, 7 samples, and one internal standard (BCR-2).

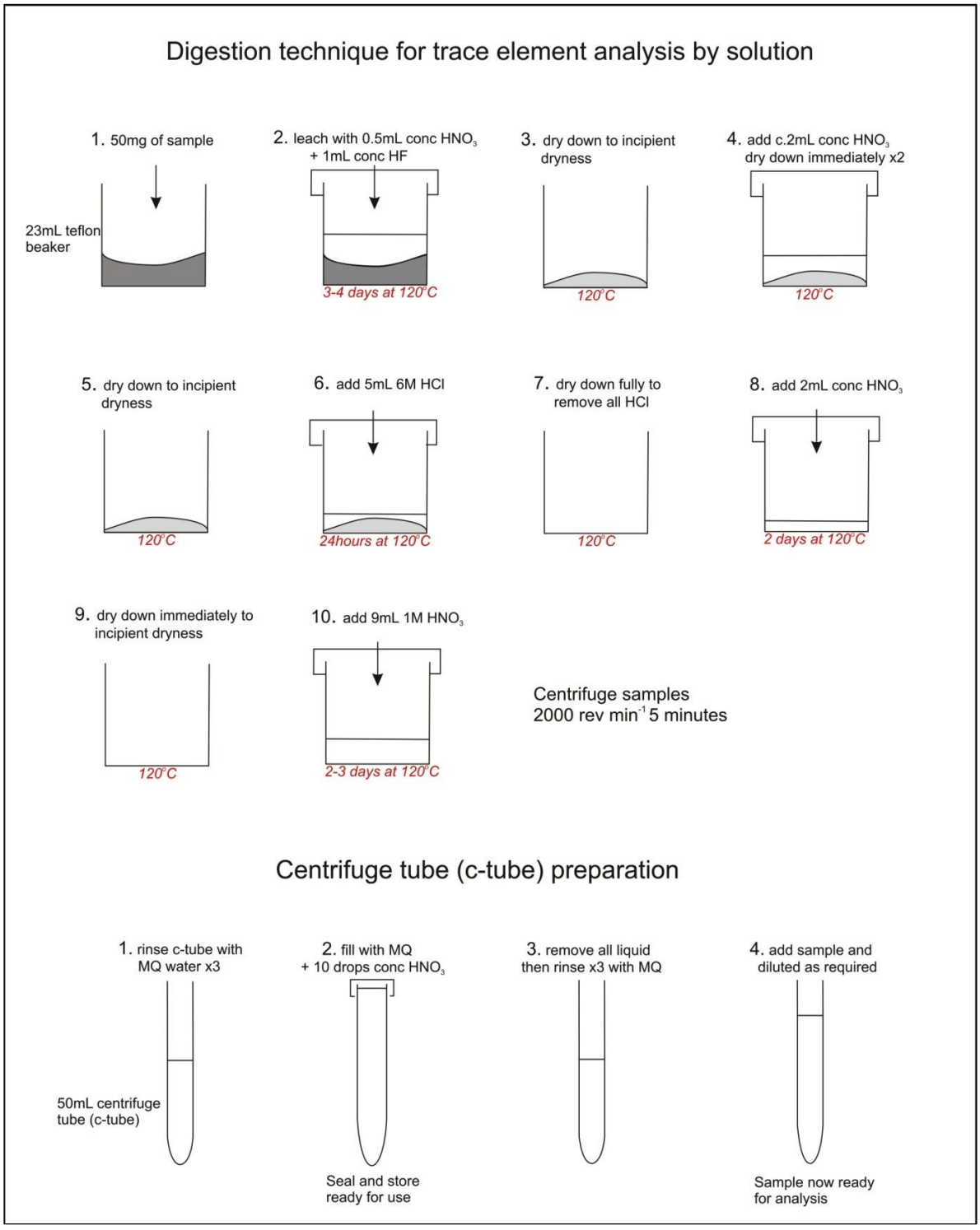

Figure 2.4. *Schematic diagram of the procedure for trace element digestion prior to analysis by solution-ICP-MS and centrifuge tube preparation (after McGee et al., 2013).*

Table 2.8. *Analysis conditions for solution ICP-MS analysis*

Solution-ICP-MS	
Instrument	Agilent 7500CS octopole
Aquisition mode	Peak hopping
Detection mode	Pulse and analogue counting (mostly pulse)
Standards	
Calibration standard	BHVO2
Secondary standard	BHVO2, BCR2
Blank standard	Procedural blank (1% HNO_3)
Internal standard	^{43}Ca
Method Parameters	
Background acquisition	60 s
Standard aquisition	60 s
Sample aquisition	120 s
Washout time	125 s (5 secs water, 120 secs 1% HNO3)
Measured isotopes and integration times	10 ms: ^{7}Li, ^{25}Mg, ^{43}Ca, ^{45}Sc, ^{53}Cr, ^{51}V, ^{60}Ni, ^{63}Cu, ^{66}Zn, ^{69}Ga, ^{71}Ga, ^{86}Sr, ^{89}Y, ^{90}Zr, ^{91}Zr, ^{93}Nb ^{137}Ba, ^{139}La, ^{140}Ce, ^{146}Nd 20 ms: ^{85}Rb, ^{141}Pr, ^{147}Sm, ^{157}Gd, ^{163}Dy 50 ms: ^{95}Mo, ^{133}Cs, ^{151}Eu, ^{153}Eu, ^{159}Tb, ^{165}Ho, ^{166}Er, ^{169}Tm, ^{172}Yb, ^{175}Lu, ^{178}Hf, ^{181}Ta, ^{205}Tl, ^{208}Pb, ^{232}Th, ^{238}U,
Tuning	
Tuning standard	Agilent 1ppb solution (Li, Co, Y, Ce, Tl)
Monitored isotopes during tuning	^{7}Li, ^{59}Co ^{89}Y, ^{140}Ce, ^{205}Tl, (RSD for each isotope <2%)
Calibration standard	BHVO2
Monitored isotopes during tuning	^{7}Li, ^{59}Co, ^{88}Sr, ^{89}Y, ^{139}La, ^{140}Ce, ^{157}Gd, ^{172}Yb, ^{205}Tl,
Oxides	CeO^{+}/Ce^{+} 1ppb solution <1.5%
Isotope P/A factors calculated on BHVO-2	^{7}Li, ^{24}Mg, ^{27}Al, ^{59}Co, ^{88}Sr, ^{89}Y, ^{140}Ce, ^{205}Tl, ^{238}U
Carrier Gas (Ar)	0.89 - 0.97 L/min
Makeup gas (Ar)	0.23-0.26 L/min
RF power	1500 W
RF matching	1.77 V
Sample depth	7 mm
Extract 1 ion lense	5.9 - 6.0 V
Extract 2 ion lense	-153.5 to -143.5 V

2.8.6. Data reduction and concentration calculations

Trace element abundances were calculated relative to a matrix-matched bracketing standard (BHVO-2), which was run every 4 samples, three times within an analysis session, under identical conditions. ^{43}Ca was used as the internal standard for secondary data normalisation and this value was taken from the XRF results from the same samples.

The background count rates were measured for 60s prior to analysis and the mean value was subtracted from the samples using the reduction programme Iolite. Once this is removed the trace element concentrations were calculated using the following equations;

$$C_{sample}^{CaO,ICP-MS} = C_{std}^{CaO} \times \left(\frac{CPS_{sample}^{Ca}}{CPS_{std}^{Ca}}\right) \quad \textbf{(Eq.2.8.6.1)}$$

Where;

$C_{sample}^{CaO,ICP-MS}, C_{sample}^{CaO,XRF}$ = concentration of CaO measured by ICP-MS or XRF

C_{std}^{CaO} = GeoREM CaO concentration for BHVO-2 standard

$CPS_{sample}^{Ca}, CPS_{std}^{Ca}$ = counts per second obtained on ^{43}Ca during analysis of whole rock dilution (sample) or BHVO-2 (std)

$$C_{sample}^{x,ICP-MS} = C_{std}^{x} \times \left(\frac{C_{sample}^{CaO,XRF}}{C_{sample}^{CaO,ICP-MS}}\right) \times \left(\frac{CPS_{sample}^{x}}{CPS_{std}^{x}}\right) \quad \textbf{(Eq.2.8.6.2)}$$

Where;

$C_{sample}^{x,ICP-MS}$ = concentration of element x determined by ICP-MS analysis

$C_{sample}^{CaO,XRF}$ = concentration of CaO measured by ICP-MS or XRF

C_{std}^{x} = GeoREM concentration of element x in std BHVO-2

$CPS_{sample}^{x}. CPS_{std}^{x}$ = counts per second obtained for element x during analysis of whole rock dilution (sample) or BHVO-2 (std)

2.8.7. Accuracy and precision of solution-ICP-MS

Two secondary standards were run throughout an analysis session to monitor the accuracy and precision of the solution ICP-MS analysis. International rock standards BCR-2 and BHVO-2 were chosen based on their well-documented compositions recorded from a number of laboratories using modern analytical conditions, and their similarity to the composition of the samples used for this study. All the trace element data obtained by solution-ICP-MS for these standards is recorded in **Appendix B**. **Table 2.9** records the average values of all the analyses and shows the accuracy (by % offset) and precision (by 2sd%) of the measurements made. Analytical precision based on 15 replicate analyses of BCR-2 is <6.5% for most trace elements. The exceptions to this include Cr ± 8.2%, Nb ± 16.5%, Cs ±6.8%, Ba ± 8%, Ta ± 19% and Pb ± 21%. For the majority of BCR-2 trace elements are accurate to ≤6% apart from Li, Cr, Cu, Nb, Cs, Eu and Ta. For 11 replicates of BHVO-2 precision is <5% for all trace elements except Nb (8.7%), Cs (6%) and Ta (8%), and all values are within <1.5% of the reference value, except for Ta with an offset of ± 6.4%.

Table 2.9. *Summary table of standard data gained whilst analysing whole rock for trace element concentrations using solution-ICP-MS. Reference values are taken from GeoREM preferred values; Jochum and Nerling, 2006. All values are reported in ppm, with meausred isotopes of elements detailed. Red highlights show those figures discussed in the text as outliers.*

BHVO values				
Element	Reference value	Average (wt%)	% offset from std	2sd%
Ca43	11.4	11.4	0.00	0.00
Li7	4.8	4.77	-0.71	2.69
Sc45	32.0	31.9	-0.38	3.29
Ti47	16300	16248	-0.32	3.40
Ti49	16300	16267	-0.20	1.99
V51	317	318	0.17	3.15
Cr53	280	279	-0.28	2.15
Mn55	0.2	0.17	-0.62	3.16
Co59	45.0	44.7	-0.65	2.01
Ni60	119	118	-0.43	3.17
Cu63	127	127	-0.15	2.99
Zn66	103	103	-0.23	2.41
Ga71	22.0	22.0	-0.22	2.68
Rb85	9.1	9.03	-0.53	3.16
Sr88	396	394	-0.43	1.76
Y89	26.0	25.9	-0.30	2.98
Zr90	172	171	-0.60	2.52
Zr91	172	171	-0.62	2.79
Nb93	18.1	18.3	1.22	8.68
Cs133	0.1	0.10	-0.95	6.00
Ba137	131	130	-0.72	2.21
La139	15.2	15.1	-0.48	2.53
Ce140	37.5	37.3	-0.51	2.81
Pr141	5.3	5.25	-0.84	2.38
Nd146	24.5	24.3	-0.69	2.38
Sm147	6.1	6.01	-0.95	3.41
Eu151	2.1	2.06	-0.47	3.17
Eu153	2.1	2.06	-0.46	2.26
Gd157	6.2	6.21	-0.51	2.96
Tb159	0.9	0.93	-1.04	2.67
Dy163	5.3	5.28	-0.51	3.46
Ho165	1.0	0.97	-0.16	2.80
Er166	2.5	2.53	-0.53	3.72
Tm169	0.3	0.34	-1.06	3.20
Yb172	2.0	1.98	-1.19	1.89
Lu175	0.3	0.27	-0.30	4.01
Hf178	4.4	4.34	-0.35	2.26
Ta181	1.1	1.21	6.39	7.97
Pb208	1.6	1.60	0.04	4.56
Th232	1.2	1.21	-1.18	1.89
U238	0.4	0.40	-1.01	3.52

BCR2 (internal standard) values				
Element	Reference value	Average (wt%)	% offset from std	2sd%
Ca43	7.1	7.12	0.00	0.03
Li7	9.0	10.2	13.01	5.59
Sc45	33.0	34.6	4.84	6.45
Ti47	13500	13847	2.57	4.87
Ti49	13500	13858	2.65	5.93
V51	416	429	3.10	4.98
Cr53	13.0	14.1	8.19	8.22
Mn55	0.2	0.20	2.30	4.99
Co59	37.0	38.8	4.99	5.52
Ni60	12.0	12.6	5.12	6.93
Cu63	21.0	3.50	-83.33	1983.15
Zn66	127	134	5.67	5.97
Ga71	23.0	23.6	2.71	6.00
Rb85	46.9	48.5	3.49	6.02
Sr88	340.0	352	3.58	6.05
Y89	37.0	37.2	0.62	6.08
Zr90	201	194	-3.46	5.43
Zr91	201	194	-3.38	6.01
Nb93	12.6	13.2	4.73	16.50
Cs133	1.1	1.24	12.49	6.79
Ba137	677	689	1.82	7.96
La139	24.9	25.9	4.16	6.19
Ce140	52.9	55.0	4.06	5.57
Pr141	6.7	7.03	4.92	5.64
Nd146	28.7	29.9	4.16	6.37
Sm147	6.6	6.80	3.35	6.35
Eu151	2.0	2.10	7.22	5.87
Eu153	2.0	2.15	9.59	6.18
Gd157	6.8	7.15	5.94	5.97
Tb159	1.1	1.10	2.45	5.84
Dy163	6.4	6.68	4.15	6.30
Ho165	1.3	1.33	4.17	5.71
Er166	3.7	3.79	3.60	5.81
Tm169	0.5	0.56	3.04	6.54
Yb172	3.4	3.51	3.96	6.00
Lu175	0.5	0.51	1.56	6.73
Hf178	4.9	5.03	2.55	6.10
Ta181	0.7	0.97	31.14	18.63
Pb208	11.0	10.9	-0.96	20.52
Th232	6.0	6.18	2.52	5.19
U238	1.7	1.70	0.73	5.85

Section C – Re, Os and Pb Analysis

2.8. Sample Selection and Preparation

Bulk rock samples were chosen to follow on from the work undertaken by McGee et al. (2013). Selected samples were chosen from the pre-existing sample set to satisfy two criteria

(1) be a primitive chemical composition (e.g., Mg# >60)
[caluculation Mg#=([Mg]/([Mg]+[Fe]))*100)]

(2) be representative for the range of AVF rock Pb isotopic composition.

By analysing this sample set it is possible to make a direct comparison with previous work and provide more robust conclusions as to the source characteristics below the AVF. 15 samples of both lava and scoria from Rangitoto, Mt. Wellington, Puketutu, Three Kings, Pupuke, Purchas Hill and Wiri were chosen. These samples were crushed using a Rocklabs Boyd crusher and powdered using an agate ring mill (to avoid contamination in Re) at VUW. Re-Os chemistry and analysis was undertaken in the GEOTOP facilities at UQAM.

2.9. Os isotopes, Os and Re Analysis

2.9.1. HPA-S digestion

1 g of sample powder was spiked with a known enriched tracer solution of $^{190}Os/^{185}Re$. This was then digested in Teflon sealed quartz tubes with 3 mL 6M HCl and 3 mL HNO_3 at 300°C and 100 bars in a high-pressure asher unit (HPA-S, Anton-Parr-Perkin Elmer Instruments) for 12 hours (Meisel *et al*., 2003). This equilibrates the powdered sample and liquid spike by oxidation to OsO_4 and acts to digest the sample.

2.9.2. Paris Br_2 Extraction

After digestion Os was extracted using the Paris Br_2 technique (after Birck *et al.,* 1997). 2 mL chilled Br_2 was added to sample and left on a hot plate at 90°C for 2 hours. This acts to scavenge the already oxidised Os from the aqueous solution into

the liquid Br_2, leaving Re and PGEs within the aqueous solution. Isolated liquid Br_2 (inc Os) was then removed to a large Teflon beaker (120 ml) and 20 drops of HBr was added to reduce the Os from volatile Os^{8+} (OsO_4) to non-volatile Os^{4+} ($OsBr_6^{2-}$). This was then left at <90°C for 12 hrs to allow the Br_2 to evaporate leaving the Os within the HBr. At this stage the Os is reasonably pure but requires a further micro-distillation step to achieve sufficient sample purity for analysis.

2.9.3. Micro-distillation of Os

The Os and HBr was then transferred into the lid of the teflon beaker and left on the hot plate for 12 hrs at 110°C to evaporate the HBr. The Re and PGE's were left to one side in the large Teflon beaker. One drop of Cr_2O_3 in H_2SO_4 was then added to the remaining residue. ½ drop of HBr was added to the tip of a conical tub, which was carefully inverted over the residue and secured tightly. This was then wrapped in Al-foil and left on a hot plate at <90°C for no longer than 3 hrs. This process acts as a micro-distillation to remove any remaining Re from the sample (**Fig. 2.5**.). The Cr_2O_3 works to oxidise the osmium complex $OsBr_6^{2-}$ and thereby causes it to re-volatilise as OsO_4. This then evaporates in its gas phase to the tip on the conical tub where it is reduced and stabilised by the HBr back to $OsBr_6^{2-}$ (Birck *et al.,* 1997). The Al-foil was carefully removed, the tub is opened discarding the lid and the conical tub reverted to the correct way up. This was then left to dry down further to 0.5-1.5 μL on a hot plate at 110°C for 20 minutes. The osmium is then ready for analysis by N-TIMS.

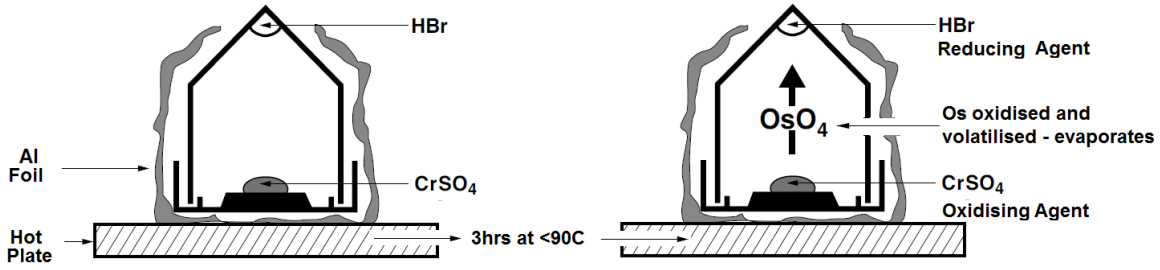

Figure 2.5. *Schematic diagram to show micro-distillation technique after Birck et al. (1997) used to remove remaining Re from sample.*

2.9.4. Analysis of Os by N-TIMS

Osmium isotopic measurements were carried out on a Triton TIMS in negative ion mode (Creaser *et al.,* 1991). High purity Pt filaments were de-gassed in air to white hot temperatures for 2 minutes (Birck *et al.,* 1997). Samples were then loaded onto the filaments in HBr, as $OsBr_6^{2-}$, and coated with a saturated solution of $Ba(OH)_2$ and NaOH, to act as an electron emitter (Birck *et al.,* 1997). The filaments were then quickly flash heated, to reduce the organic interference from masses 233-235. Samples were loaded into the mass spec and O_2 saturated with water vapour was leaked into the chamber (Walczyk *et al.,* 1991). Filaments were then heated slowly to a temperature of 705°C.

2.9.5. Re column chemistry

3 mL conc. HF was added to the large Teflon beaker containing the Re and PGEs in aqueous solution, and left, sealed on a hot plate for 1hr at 110°C. This was then uncapped and the HF evaporated off for 12 hrs at 110°C, to allow the removal of any remaining silicates. Pipette columns were prepared by the addition of ca. 0.6 mL AG1X8 200-400 resin. Whilst this was settling, 2 mL 0.8 M HNO_3 was added to the dried down samples, the beakers were then sealed and placed in a sonic bath to allow the Re to be fully dissolved. The columns were then cleaned by three washes through of 5 mL 8M HNO_3, conditioned with 2 mL 0.8M HNO_3, and the sample is then introduced. Two lots of 5 mL 0.8M HNO_3 were added to wash out the unwanted elements, followed by collection of Re in 1 mL 8M HNO_3 and 4 mL 8M HNO_3. The solution was then dried down for 24 hrs at 120°C and was then ready for analysis on Sector Field (SF) ICP-MS (**Fig. 2.6**.).

2.9.6. Analysis of Re by SF-ICP-MS

After evaporation, samples were taken back up in 1 mL of 2% HNO_3 and this solution was then transferred into 5 mL c-tubes, and centrifuged. Solutions were then transferred into miniature shot glasses (3 mL) ready for analysis. Analysis was undertaken on a NU instruments ATTO-M Sector Field (SF)-ICP-MS. Wash out with

MQ H_2O, 4% HNO_3 and 2% HNO_3, was run between each sample and every two samples a blank (2% HNO_3) and the standard NIST SRM 3141 was run.

2.9.7. Determination of Os and Re concentrations

Os and Re concentrations were determined by isotope dilution techniques using ^{185}Re and ^{190}Os spiked samples. Blanks for the total procedure were 0.3 pg for Os, and 7 pg for Re. These values were subtracted from the sample totals in data processing, along with an oxygen interference and sample-spike unmixing correction (c.f. Luguent *et al.,* 2000). Calculations for isotope dilution are after Albarède (1995).

2.9.8. Accuracy and precision of N-TIMS and SF-ICP-MS

Os isotope measurements were corrected for instrumental drift using the internal standard DROsS. Internal precisions (2 SE) for $^{187}Os/^{188}Os < \pm 0.00012$. All values are recorded in **Appendix B**. For Re, instrumental drift for SF-ICP-MS analysis was corrected for using the standard NIST SRM 3143 (values from Gramlich *et al.,* 1973). Internal precision (2SE) for $^{187}Re/^{185}Re$ were $< \pm 0.05$, and all valuesare recorded in **Appendix B.** Unfortunately, no natural rock standards wih low enough concentrations are currently available to act as appropriate secondary standards for basaltic Os or Re analysis. Currently existing standards contain high levels (ppb) of Os and Re, and their use would risk causing significant cross contamination. In addition, they also represent a poor matrix match to basaltic rocks and would not behave comparably to the samples during analysis.

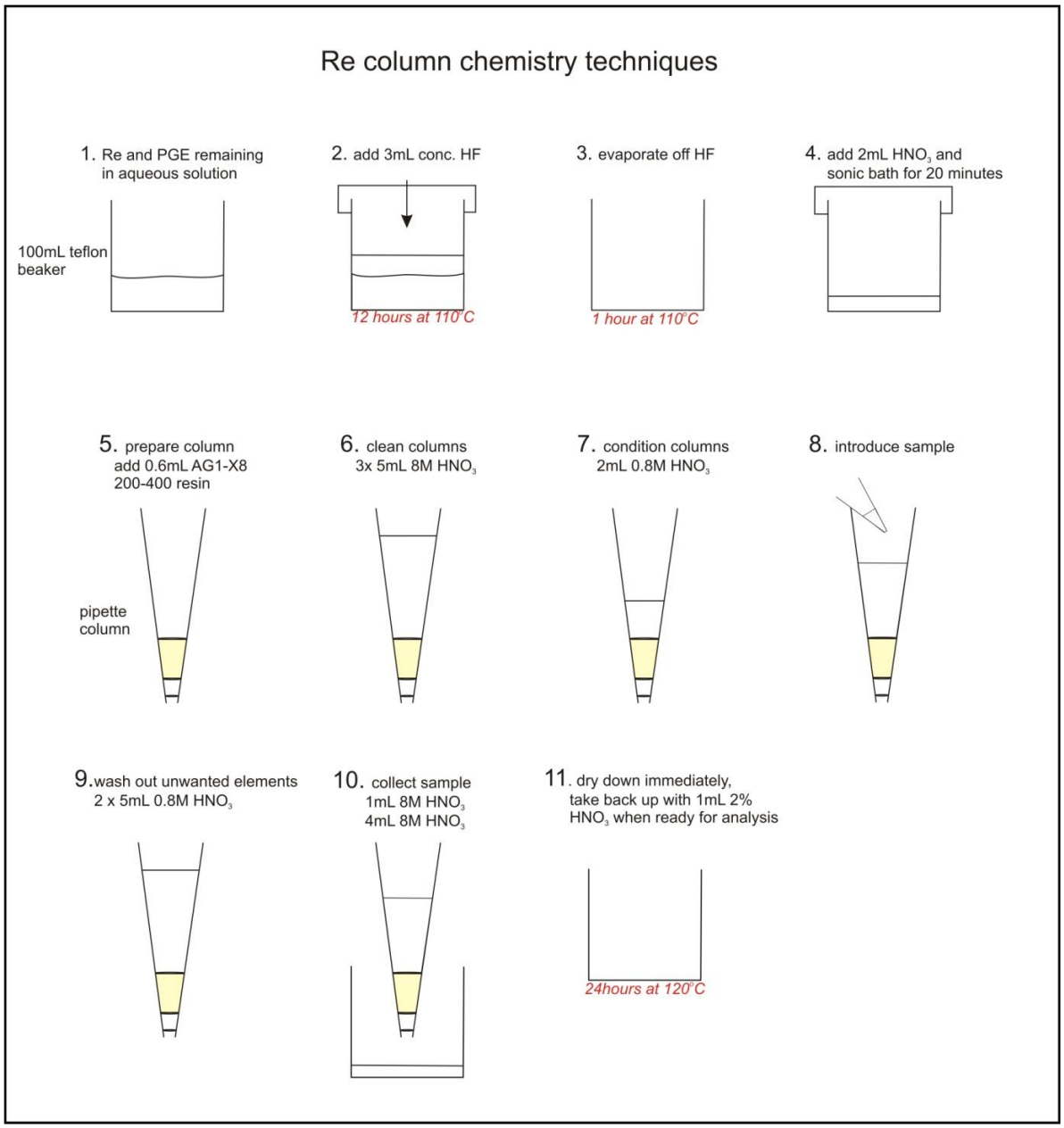

Figure 2.6. *Schematic diagram of the procedure for sample digestion and extraction of Re and column chemistry.*

2.10. Pb Isotope Analysis by MC-ICP-MS

Pb isotope analysis was required for all samples that were run for Os-Re isotope work. Selected samples included those that were not analysed by McGee et al. (2013), and some duplicates of previously analysed samples. In total 9, whole rock samples were prepared and purified at VUW for analysis at Durham University, UK.

2.10.1. Pb separation

Figure 2.7 shows a schematic diagram of the digestion and separation procedure following after Baker et al. *(*2004). All beakers were pre-cleaned 23 mL Savillex beakers as outlined in 2.5.3.3, and Seastar (SS) grade acids (HNO_3, HF, HCl and HBr) were used throughout the procedure. The rock powder is the same used in all stages of chemistry and in some cases the same as that prepared for the McGee study. 200 mg of rock powder (same as used for trace elements and in McGee et al., 2013) was weighed on a high precision balance to ±0.0001g and added to a pre-cleaned beaker. 4 mL of 6M HCL was added, the beaker was sealed and allowed to boil for 1 hour at 120°C. The supernatant formed was removed and the sample was rinsed 3 times with MQ water. The sample was then digested using conventional methods; 30 drops of conc. HF and 15 drops of conc. HNO_3 was allowed to reflux for 24 hours, followed by the sample being dried down to incipient dryness. 20 drops of conc. HNO_3 was added and allowed to dry down fully. This process was repeated twice. Following this 1.5 mL 0.8M HBr was added then evaporated immediately. 1.5 mL 0.8M HBr was added again and left to reflux at 120°C with the beaker sealed for 3 hours. The solution was centrifuged for 8 minutes at 2000 rpm and was ready to pass through the separation columns.

The columns for Pb separation were made from 1 mL disposable pipette tips, their ends were cut off and frits, made out of polypropylene soaked for a minimum of 5 minutes in 6M HCL (SS), were firmly inserted into the base of the column. Approximately 5 mm depth of Biorad anion exchange resin (AG1-X8) was inserted into the column within a small amount of MQ water. It was critical to ensure no bubbles were formed during emplacement that would affect the rate of flow through the column. The column and resin were then washed three times using 1 vol. of 6M HCl followed by 1 vol. of MQ.

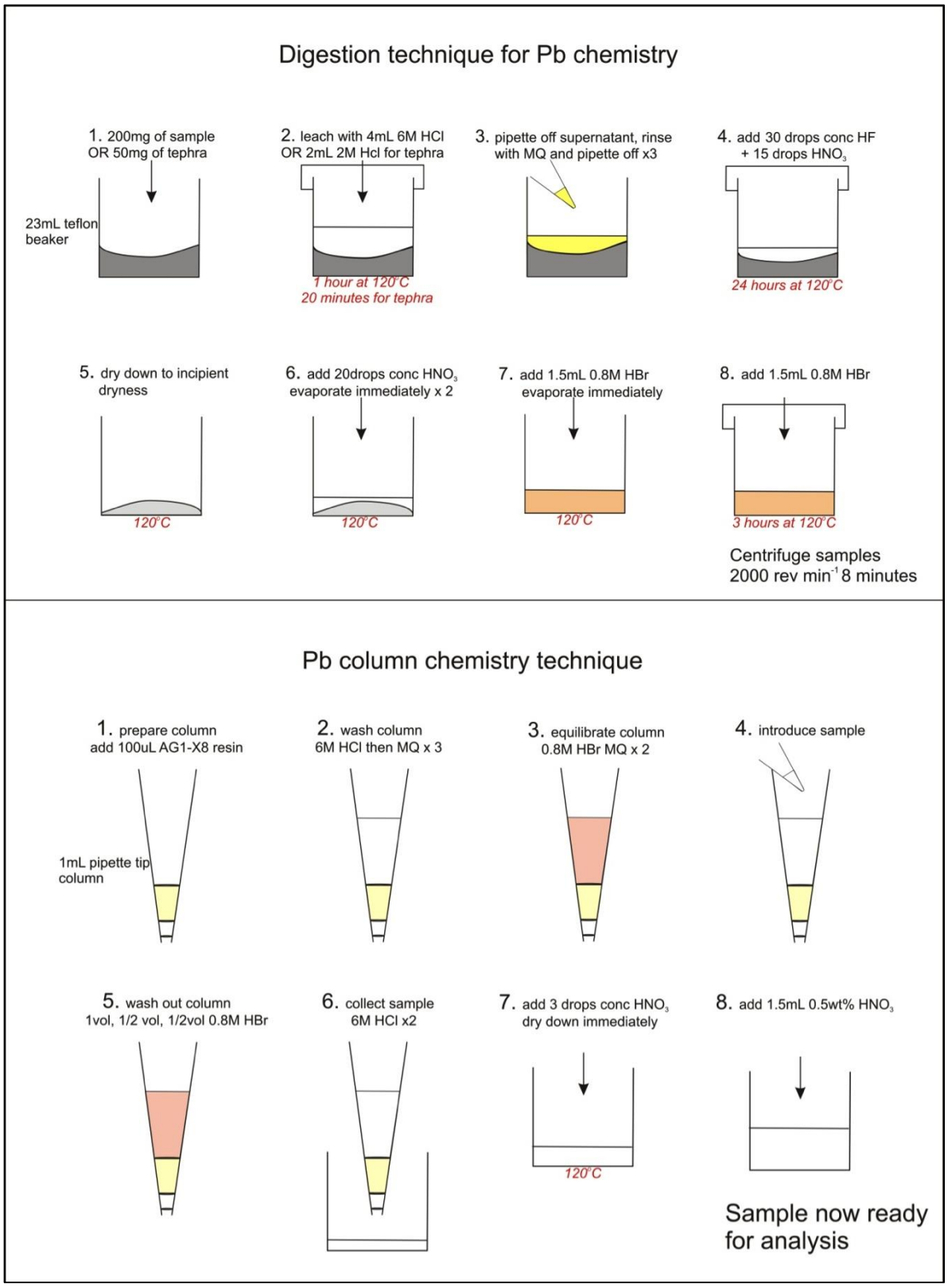

Figure 2.7. *Schematic diagram of the procedure for sample digestion and extraction of Pb and column chemistry.*

The resin was then equilibrated using 2 vol. 0.8M HBr. The sample was introduced and unwanted elements were washed out using 1, 0.5, 0.5 vol. of 0.8M HBr. The Pb isotope cut was collected by passing 2vol. 6M HCl through the column. This was immediately dried down and the column separation repeated. The process was repeated to ensure as pure as possible sample of Pb. The final solution was dried down and three drops of conc. HNO_3 was added and then dried down immediately. Samples were left in this dried down state until immediately before analysis where they were then taken up with 1.5 mL 0.5% HNO_3 (SS) and left on a hot plate at 120°C for at least 1 hour to ensure the full Pb cut goes into solution. The samples were then ready for analysis.

2.10.2. Pb isotope analysis

Samples were analysed for Pb isotope compositions using a Neptune MC-ICP-MS at Durham University, UK. Samples were introduced with the machine in wet plasma mode using a small volume cinnabar™ spray chamber. The machine was tuned using ca. 30 ppb of Pb standard solution NBS-981. Adjustments were made to instrument conditions including torch position, nebuliser gas flow and voltage across each lens to optimise analytical sensitivity to ca. 8V for ^{208}Pb. Samples were diluted to 8 ± 2V for ^{208}Pb using 3 wt.% HNO_3 in pre-prepared acid-cleaned c-tubes. Isotope measurements were recorded for the samples in 5s intervals over 50 integrations (2 blocks of 25). Background was recorded by deflecting the ion beam for 2 minutes and this value was automatically deducted from the sample measurements. Procedural blanks for this study were typically <15 pg and therefore insignificant.

2.10.3. Accuracy and precision of MC-ICP-MS

Pb isotope measurements were corrected for instrumental mass bias and drift by standard bracketing using NBS-981, internal precisions (2 SE) for this were for $^{206}Pb/^{204}Pb < \pm 0.0012$, $^{207}Pb/^{204}Pb < \pm 0.0013$, $^{208}Pb/^{204}Pb < \pm 0.0044$ all values are recorded in **Appendix B**. Secondary standard JB-2 was analysed repeatedly from multiple digestions, the average measured values are $^{206}Pb/^{204}Pb$ 18.3707 ±11, for $^{207}Pb/^{204}Pb$ 15.5586 ± 16 and for $^{208}Pb/^{204}Pb$ 38.2784 ± 34 which are all within analytical error of the reference values from Baker et al. (2004), all values are reported in **Table 2.10.**

Table 2.10. *Internal standard values for JB-2 showing accuracy and precision for Pb isotope chemistry and analysis by MC-ICP-MS. Reference values for JB-2 from Baker et al. (2004).*

Secondary Standard JB2 Run#	$^{206}Pb/^{204}Pb$	2SE	$^{207}Pb/^{204}Pb$	2SE	$^{208}Pb/^{204}Pb$	2SE
B1	18.3422	0.00099	15.5628	0.00089	38.2754	0.00345
B2	18.3451	0.00112	15.5629	0.00105	38.2771	0.00285
Ref values	18.3435	0.00170	15.5619	0.00160	38.2784	0.00500
average (n=2)	18.3437	0.00106	15.5628	0.00097	38.2762	0.00315

Section D – Review of Data Accuracy and Precision

2.11. Review of in-situ analysis of tephra-derived glass shards

For samples from Orakei Basin, Onepoto and Glover Park, new samples were taken from the cores, picked, mounted and analysed. Some of these horizons have already been previously sampled and analysed for major element concentrations and therefore values obtained can be compared to check for comparability of analyses. For shards from Hopua and Pupuke a more direct comparison can be made as the exact same shards and original mounts were re-analysed for this study.

2.11.1. Major Element analysis comparison

Previous analysis for all shards was run using EDS techniques on a Jeol JXA-840 EMPA at the University of Auckland (UoA), however for our analysis we used WDS techniques at Victoria University of Wellington. The WDS technique is shown to produce a much smaller error for the major elements concentrations with typical errors associated with both methods shown in **Table 2.11.** The data for major element shard concentrations published by the UoA is normalised to 100% with the discrepancy attributed to loss of water on ignition of the sample (Shane 2005). To allow the comparison to previously published work we also apply this normalisation technique, however original and normalised values are both shown in **Appendix C**.

The previously published data and the new data on the whole were shown to be comparable. **Figure 2.8** shows two examples of comparisons. Example A shows re-analysis of the same samples within a pre-made mount, initially by Molloy (2008) and then repeated by this study. Example B shows two separate samples and

analyses (Molloy (2008) and this study) for the same horizon (AVF 5 from the Orakei Basin core). Although the errors are much larger for the EDS analysis (**Table 2.11.**) these comparisons show that the data obtained by both methods are comparable and therefore confirms the ability to use a combination of both current and previously published data to correlate the tephra horizons. Tephra-derived glass shards from the AVF used for this study have not previously been analysed for trace element concentrations, and therefore the same principle of comparison cannot be applied to the trace element analyses made by this study.

Table 2.11*. Comparison of average offset values for EDS vs. WDS analysis techniques.*

Element	EDS analysis error - average % offset (Molloy 2008)	WDS analysis error – average % offset (This study)
SiO_2	< ± 0.13	< ± 0.01
Al_2O_3	< ± 0.75	< ± 0.43
TiO_2	< ± 10	< ± 0.24
FeO	< ± 2.5	< ± 0.16
MnO	< ± 25	< ± 11
MgO	< ± 10	< ± 1.25
CaO	< ± 2.5	< ± 1.5
Na_2O	< ± 1.5	< ± 5.5
K_2O	< ± 2	< ± 0.64
P_2O_5	< ± 10	< ± 1.8

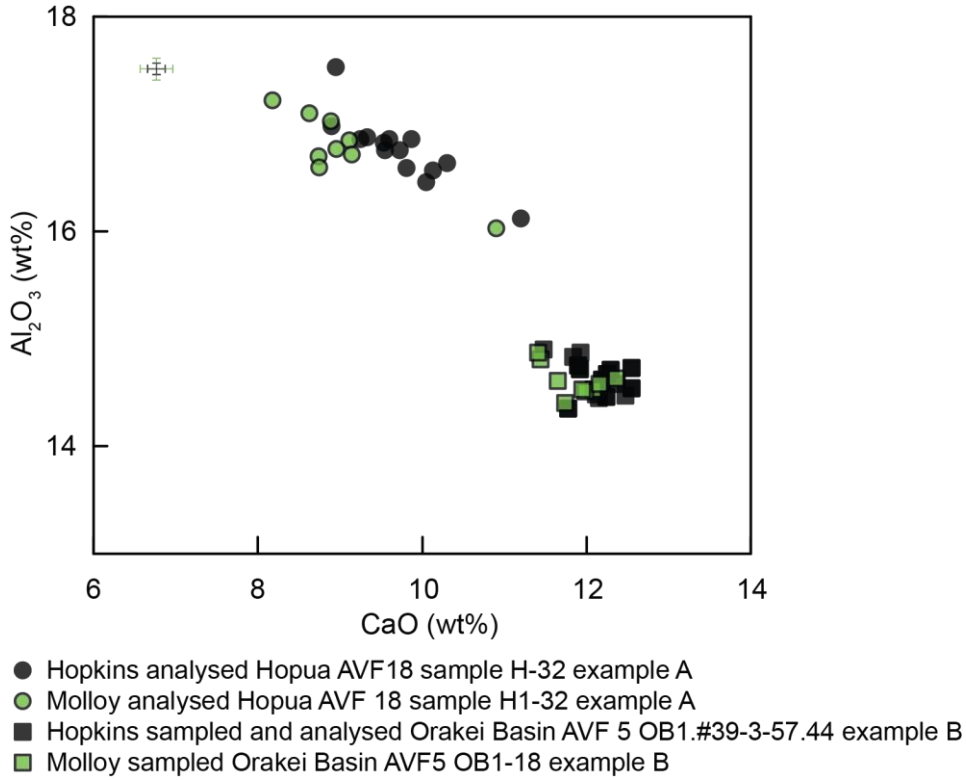

Figure 2.8. *Comparison of duplicate data for mounted samples from Hopua and Orakei Basin core, between Molloy (2008) and this study. Error bars are plotted as typical % offset outlined in Table 2.10, the green line indicates errors for Molloy (2008) and the black line for this study.*

2.11.3. Comparability of EMPA analysis with LA-ICP-MS analysis

To monitor the comparability of the results from the two methods MgO, CaO and TiO_2, concentrations were obtained by both analysis techniques. **Figure 2.9** shows the results obtained from a representative horizon with EMPA concentration (in wt.%) on the x-axis and LA-ICP-MS concentration (calculated in wt.%) on the y-axis. A 1:1 ratio line is also drawn to show where a perfect agreement between the two analyses would sit. For CaO and TiO_2 the results are very similar with points plotting very close to the 1:1 line, in comparison MgO values are slightly more variable with the LA-ICP-MS generally plotting at higher concentrations than the EMPA analysis. This range in variation in the laser data in comparison to the probe data is attributed to the slightly larger spot size that is analysed by the laser. It is therefore concluded that the CaO and TiO_2 analyses on the laser are more accurate and comparable to the probe data in comparison to MgO. CaO is therefore chosen to act as an internal standard for data manipulation.

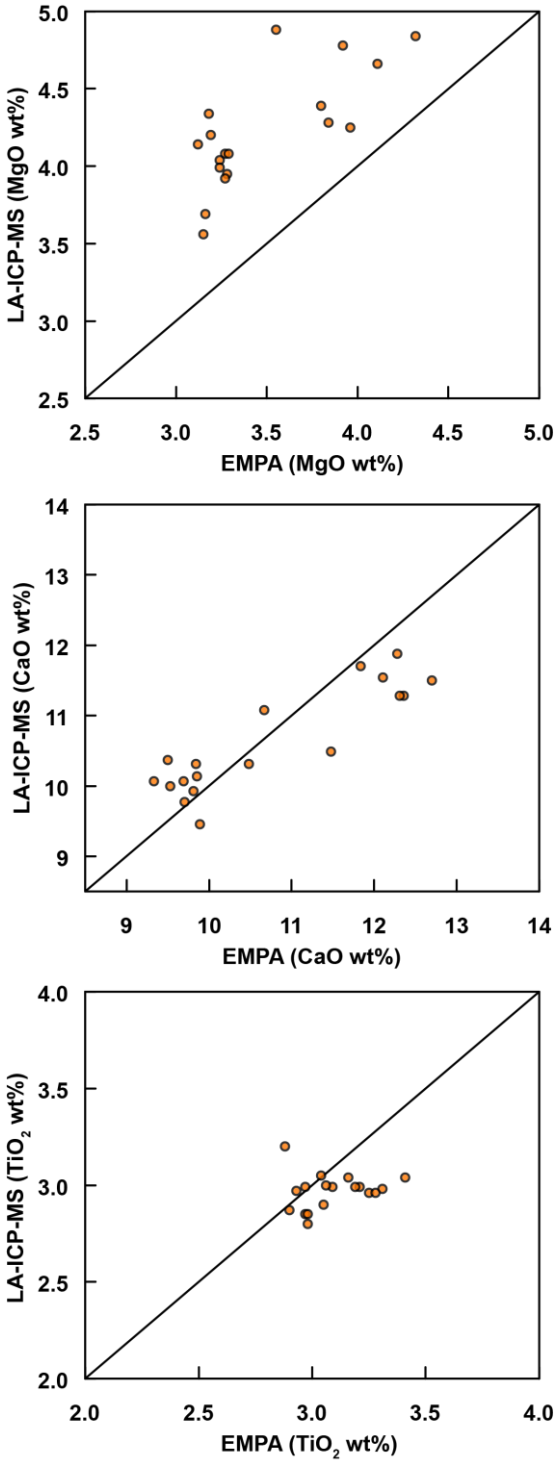

Figure 2.9. *Bivariate plots of MgO, CaO and TiO_2 for comparison of data obtained on duplicate analyses from EMPA and LA-ICP-MS techniques.*

2.11.4. LA-ICP-MS analysis at VUW vs. UoO

The majority of samples were analysed at VUW, however, some samples where analysed at the University of Otago, Dunedin, NZ (UoO). The location of sample analysis is outlined in **Appendix C**, and methodologies and machines used are outlined in **Section 2.5.** The same standards used at VUW for BHVO-2G and BCR-2G were used at UoO, with BHVO-2G used as a bracketing standard and BCR-2G as an internal standard. All analyses can be found in **Appendix B** with average values, accuracy and precision outlined in **Appendix B**. Based on the average values for all the analyses done at both VUW and UoO on the internal standard BCR-2G (run as an unknown), both methods are equally as accurate with % offset for the standard values variable with maximum errors on the same elements as outlined above. However, the UoO analyses are much more precise than the VUW values, with 2sd% values for UoO between 3.14% (V) to 32.06% (Cr) and for VUW between 5.69% (Ti) to 72.66% (Ni).

Preface to Chapter 3

The study region for this thesis, the Auckland Volcanic Field (AVF), was introduced in **Chapter 1**, and the limits of the current understanding outlined. One of the key outstanding issues for the AVF is the lack of knowledge relating to the relative eruptive history of the field. Outlined in **Chapter 1** are the benefits of tephrostratigraphy to build an eruptive history of a volcanically active region, and, due to the lack of sub-aerial tephra exposure in the AVF, tephrostratigraphy is considered the most appropriate way to reveal more details about the previous eruptions.

Extensive sediment cores have been retrieved out of the maar craters containing multiple basaltic tephra horizons sourced from the AVF centres, which can be used to over come the lack of surface exposures. In **Chapter 3** I outline the improved tools and techniques used in assessing and sampling the maar lake cores, and the methods used to allow cross core correlation of the tephra horizons.

This chapter is in the form of a multi-author published paper; *Hopkins, J.L., Millet, M.-A., Timm, C., Wilson, C.J.N., Leonard, G.S., Palin, J.M., Neil, H., 2015. Tools and techniques for developing tephra stratigraphies in lake cores: a case study from the basaltic Auckland Volcanic Field, New Zealand. Quaternary Science Reviews 123, 58-75.* Authorship contributions include; Millet – facilitated research and manuscript development; Timm, Wilson, and Leonard – manuscript edits; Palin – training of Hopkins on LA-ICP-MS; Neil – training of Hopkins on x-ray and magnetic susceptibility scanners.

The study shows that the combination of X-ray and magnetic susceptibility analysis provides much more information about the maar cores (both sediments and basaltic tephra) in comparison to simple visual observations. Coupling these two new techniques allows accurate identification of the basaltic tephra in the cores including some new horizons previously not observed and more detail as to the characteristics of the previously identified deposits (i.e. primary vs. reworked). These identification methods are coupled with major and trace element analysis of individual basaltic tephra-derived glass shards. In combining these techniques the cross core correlation of the tephra deposits is improved, and results in the construction of a more accurate and precise eruptive history of the AVF to be constructed.

Chapter 3

Tools and techniques for developing tephra stratigraphies in lake cores: A case study from the basaltic Auckland Volcanic Field, New Zealand

Jenni L. Hopkins*[a]

Marc-Alban Millet[b], Christian Timm[c], Colin J.N. Wilson[a], Graham S. Leonard[c], J. Michael Palin[d], Helen Neil[e].

[a]School of Geography, Environment and Earth Sciences, Victoria University, PO Box 600, Wellington, New Zealand

[b]Department of Earth Sciences, Durham University, Durham DH1 3LE, England

[c]GNS Science, PO Box 30368, Lower Hutt, Wellington, New Zealand

[d]Department of Geology, University of Otago, PO Box 56, Dunedin, New Zealand

[e]National Institute of Water and Atmospheric Research, PO Box 14-911, Wellington, New Zealand

Keywords

Tephrostratigraphy; basalt; tephra; lake cores; magnetic susceptibility; X-ray density scanning; geochemistry; Auckland Volcanic Field; tephra reworking

Abstract

Probabilistic hazard forecasting for a volcanic region relies on understanding and reconstructing the eruptive record (derived potentially from proximal as well as distal volcanoes). Tephrostratigraphy is commonly used as a reconstructive tool by cross-correlating tephra deposits to create a stratigraphic framework that can be used to assess magnitude-frequency relationships for eruptive histories. When applied to widespread rhyolitic deposits, tephra identifications and correlations have been successful; however, the identification and correlation of basaltic tephras are more problematic. Here, using tephras in drill cores from six maars in the Auckland Volcanic Field (AVF), New Zealand, we show how X-ray density scanning coupled with magnetic susceptibility analysis can be used to accurately and reliably identify basaltic glass shard-bearing horizons in lacustrine sediments and which, when combined with the major and trace element signatures of the tephras, can be used to distinguish primary from reworked layers. After reliably identifying primary vs. reworked basaltic horizons within the cores, we detail an improved method for cross-core correlation based on stratigraphy and geochemical fingerprinting. We present major and trace element data for individual glass shards from 57 separate basaltic horizons identified within the cores. Our results suggest that in cases where major element compositions (SiO_2, CaO, Al_2O_3, FeO, MgO) do not provide unambiguous correlations, trace elements (e.g. La, Gd, Yb, Zr, Nb, Nd) and trace element ratios (e.g. $[La/Yb]_N$, $[Gd/Yb]_N$, $[Zr/Yb]_N$) are successful in improving the compositional distinction between the AVF basaltic tephra horizons, thereby allowing an improved eruptive history of the AVF to be reconstructed.

3.1. Introduction

Tephrostratigraphy is an important tool in many research disciplines because it has the ability to create chronostratigraphic horizons, by which other geological, palaeoenvironmental or archaeological events can be constrained (Lowe, 2011). When such chronostratigraphies are coupled with geochemical analysis of the tephra horizons, a detailed record of the evolution of a volcanic region can be established (e.g. Shane, 2005; Óladóttir *et al.,* 2012; Kraus *et al.,* 2013). A key aspect of tephrostratigraphy is the correlation of tephra deposits across localities (e.g. Shane, 2000; Alloway *et al.,* 2004; Lowe *et al.,* 2008; Lowe, 2011). Multiple problems can arise in cross correlation of tephra, most commonly where deposits are one or more of: (1) sparse or poorly preserved -for example where subsequent eruptions or urbanisation have occurred (e.g. Alloway *et al.,* 1994; Dirksen *et al.,* 2011; Engwell *et al.,* 2014); (2) reworked (e.g. Payne and Gehrels, 2010; Bertrand *et al.,* 2014; Sorrentino *et al.,* 2014); or (3) where geochemical signatures are ambiguous, preventing unique characterisation of a deposit (e.g. Pearce *et al.,* 2004; Brendryen *et al.,* 2010; Bourne *et al.,* 2013; Davies *et al.,* 2014).

Preservation issues are often resolved by collecting samples in medial to distal environments rather than proximal locations (Lowe 2011). Tephra deposits in sediment cores are preferable, for example from lacustrine (e.g. Shane and Hoverd, 2002), peat lands (Payne and Gehrels, 2010) or marine environments (e.g. Allan *et al.,* 2008), because they represent stratigraphically constrained deposits (Lowe *et al.,* 2008; Lowe 2011). However, post-depositional reworking is sometimes observed in these environments (e.g. Payne and Gehrels, 2010), but a number of indicators can help identify areas where reworking has occurred. These include the geochemical signature of the shards (e.g. Allan *et al.,* 2008), mineral assemblages within the deposits (e.g. de Klerk *et al.,* 2008), palynostratigraphy (e.g. Newnham and Lowe, 1999), or the collection of multiple cores from a single area (e.g. Green and Lowe, 1985; Lowe, 1988a; Boygle, 1999). Where overlapping major element compositions preclude distinguishing between different eruptions (e.g. Icelandic tephra; Brendryen *et al.,* 2010), trace element concentrations can be used to provide further fingerprinting because of their increased sensitivity to

fractionation processes and mantle source heterogeneity (e.g. Westgate *et al.,* 1994; Shane *et al.,* 1998; Pearce *et al.,* 2004; Alloway *et al.,* 2004; Allan *et al.,* 2008). Such techniques have permitted the distinction between tephra horizons that may otherwise be interpreted to be the same (e.g. Allan *et al.,* 2008; Óladóttir *et al.,* 2011).

In this study we introduce a protocol to identify more accurately, and effectively correlate the basaltic tephra record in cores extracted from maar crater lakes in the Auckland Volcanic Field (AVF), New Zealand. We first use a combination of X-ray density and magnetic susceptibility scanning to reveal the detailed structure of tephra deposits and host sediments in order to provide new insights about reworking within the sediment cores. We then couple these results with in-situ major and trace element analysis of glass shards handpicked from tephra horizons to test the ability of major and trace elements as well as trace element ratios to distinguish and fingerprint horizons and thus aid cross-core correlations. Based on these correlations, the dispersal and frequency of the AVF eruptions can be developed to enable a more robust reconstruction of the eruptive history of the field.

3.2. The Auckland Volcanic Field

3.2.1. Geological Setting

New Zealand's largest city, Auckland, has a population of ca. 1.4 million and is superimposed on a collection of 53 Quaternary monogenetic basaltic centres, the Auckland Volcanic Field (AVF; **Fig. 3.1.A**). Individual centres typically show a range of eruption styles from explosive phreatomagmatic activity, caused by contact between upwelling magma and ground water, to magmatic activity coupled with synchronous or subsequent effusive activity after exhaustion or disconnection from local water sources (Allen and Smith, 1994; Németh *et al.,* 2012). The initial phreatomagmatic activity results in the formation of maars and associated tuff rings, whereas the magmatic stages build scoria cones. Pyroclastic material (tephra) is associated with all eruption styles but is more important in terms of its

dispersal in the initial phreatomagmatic phases that produce both tephra fall and surge deposits (Agustin-Flores *et al.,* 2014). The close proximity of the maar craters to other eruptive centres (e.g. Lake Pukaki and Orakei Basin; **Fig. 3.1.A**) creates an environment that is favourable to preserve pyroclastic deposits from the other AVF eruptions.

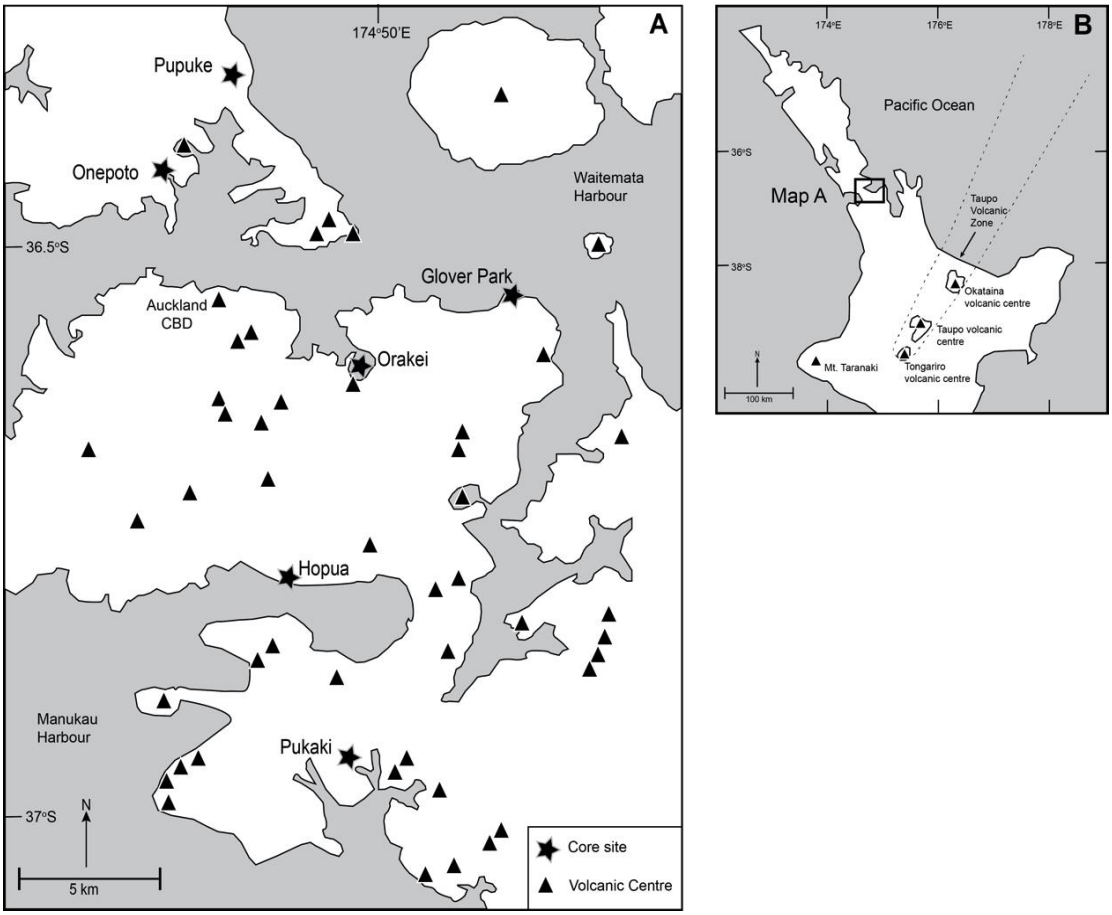

Figure 3.1. *A) Extent of the Auckland Volcanic Field (AVF), with volcanic centres marked by triangles and core sites marked with a star and named, derived from Hayward et al., 2011. B) Location of the AVF within the North Island, New Zealand, and location of other volcanic centres, from which tephras have been recorded in the Auckland maar cores.*

Recent investigations of lacustrine tephra preservation elsewhere have discussed depositional complexities where deposits are affected by fluvial input from streams, run off, or lake currents, which lead to ambiguities in primary horizon identification (e.g. Bertrand *et al.,* 2014; Shapley and Finney, 2015). The AVF maar craters are mostly closed systems; the surrounding tuff rings are outward dipping and composed of indurated, poorly sorted tuff, the surrounding topographic relief is very low, and the stream catchments that they intersect tend to be very small, resulting in minimal currents within the lakes (Striewski *et al.,* 2013). During the Holocene sea-level maximum some of the maar craters were breached, but currently only Orakei Basin remains open to the marine environment. As a result the top ca. 25 m of the Orakei Basin core records marine muds rather than lacustrine sediments. The apparent pre-breach quiescence and consistency of the deposition in the maars is reflected in the finely laminated lacustrine sediments within core sequences (Hayward *et al.,* 2008; Striewski *et al.,* 2013). The maar lakes are therefore considered to provide a more accurate and complete tephra deposition history in comparison to open lacustrine systems, because they do not produce as many re-worked or over-thickened deposits (Molloy *et al.,* 2009).

The superimposition of Auckland city, with its large population and complex infrastructure, over the area of the AVF, with the likelihood of future eruptive activity poses a significant volcanic hazard. Tephrochronology facilitates the reconstruction of the eruptive history of the area, in order to aid accurate hazard and risk forecasting (e.g. Shane and Zawalna-Geer 2011).

3.2.2. Previous Tephrostratigraphic Studies

To date, the highest resolution tephrostratigraphic study of the AVF maar lake cores have analysed shards from andesitic, rhyolitic (from distant sources) and basaltic (from the AVF) tephra horizons within multiple cores (Newnham et al., 1999; Molloy *et al.,* 2009). The horizons were visually identified, which, although adequate for fine-grained, light-coloured silicic deposits, proved difficult for dark-coloured basaltic tephra deposits. This

raises the possibility of errors in the identification of thin, very fine-grained basaltic tephra horizons or layers of a similar colour to the host lacustrine sediments. All glass shards in Molloy et al. (2009) were analysed for major element concentrations by electron microprobe analysis (EMPA), using energy dispersive X-ray spectroscopy (EDS) techniques, and sedimentation rates were estimated for each core based on reported ages of the rhyolitic tephras. These sedimentation rates were then used to estimate the age of the basaltic deposits, and thus constrain cross-core correlations.

In many cases where basaltic tephras were sparse and stratigraphically well constrained (by rhyolitic or andesitic marker horizons, and sedimentation rates), major element chemistries could uniquely fingerprint individual tephra horizons to allow correlations between cores (Molloy *et al.,* 2009). However, when horizons were poorly constrained by stratigraphy, major element compositions for the basaltic tephras were not distinctive enough to distinguish and fingerprint individual horizons and cross-core correlations were ambiguous and unreliable. Some studies have identified the use of trace elements as a way to more uniquely fingerprint tephra horizons. For example, Alloway et al. (2004) measured Th, Nd and Y to distinguish tephras deposited in the Auckland region from rhyolitic and andesitic centres in the North Island, but these techniques have only been applied to local AVF basaltic tephras for Rangitoto by Needham et al. (2011). In addition, trace element ratios have the ability to outline smaller geochemical heterogeneities that provide additional fingerprinting criteria in correlations, however few studies have investigated the full use of these as a tool for correlation (Allan *et al.,* 2008). Trace element ratios have the added advantage of being independent of the actual elemental concentrations and thus are also less affected by analytical issues (Pearce *et al.,* 2007; Allan *et al.,* 2008). They are therefore preferred where major and trace element compositions are largely indistinguishable or ambiguous for individual horizons.

3.3. Techniques and Samples

3.3.1. Techniques

3.3.1.1. Identification of tephra horizons

Visual observations were coupled with non-destructive X-ray density scanning and magnetic susceptibility analysis to initially identify which sections of the core hosted basaltic glass shards. The density of basaltic tephra and its abundance of heavy X-ray absorbing elements (e.g. FeO content in basalts ca. 5-14 wt % vs. rhyolites ca. 0-4 wt %) makes the basaltic horizons appear bright on X-ray imagery, and the abundance of Fe-rich magnetic minerals is responsible for the peaks in magnetic susceptibility.

X-ray density scanning was undertaken at the National Institute of Water and Atmospheric Research (NIWA), Wellington, using an Ultra EPX-F2800 portable veterinary radiological device. The voltage was optimized between 70-100 kV with analysis duration of 25–5 mAs. This analysis was coupled with magnetic susceptibility scanning using a Bartington-MS2 magnetic susceptibility meter connected to a MS2F probe (also at NIWA). Magnetic susceptibilities are dimensionless and are reported according to the 10^{-5} SI system with a sensitivity of 1.0 x 10^{-5} SI. These values represent the ratio between the magnetization of the sample material (amps/metre [Am^{-1}]) and the applied magnetic field strength (Am^{-1}). Data were obtained every 2 cm along the centre of the core and at 1 cm spacing across any regions of special interest. Together these analyses highlight the horizons of basaltic tephra within the lacustrine sediments (**Fig. 3.2.**): the horizons identified are then sampled for geochemical analysis.

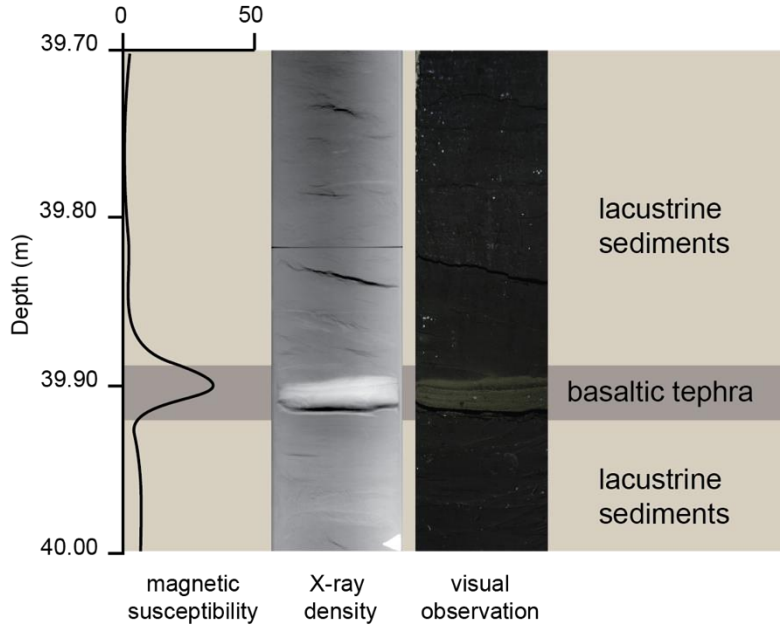

Figure 3.2. *An example of a typical basaltic horizon identified from within the Orakei Basin core, showing sharp peak in magnetic susceptibility (S.I. units) and the bright contrast of the horizons on the X-ray density scan, in comparison to the 'background' lacustrine sediments.*

3.3.1.2. Distinction of primary and reworked tephra horizons

To distinguish primary horizons we coupled results from the X-ray analysis and magnetic susceptibility scanning with the protocol outlined by Óladóttir et al. (2011), identifying (1) sharp contacts (including those in the X-ray imagery) indicating an undisturbed deposit, (2) overall heterogeneous grain sizes and shapes, indicating a lack of erosion-related abrasion, and (3) shard grading as horizons deposited through water most commonly show normal grading if undisturbed. Most of the horizons were of sufficient thickness (>10 mm) to take multiple sub-samples to constrain geochemical variations across each horizon. All samples were taken from the centre of the sediment core in order to minimize shard contamination through 'core suck' (where removal of the core drags sediments up, or penetration of coring device drags sediments down at the edges of the casing). Exposed surfaces of the deposit were removed prior to sampling to avoid any sample contamination caused during core splitting.

3.3.2. Samples

Amongst all the volcanic centres within the AVF, nine maar and tuff-ring formations have not been buried by subsequent eruptive phases. Six of these have core material available for analysis (see **Fig. 3.1**). The six maars are spread across the width of the AVF and provide an extensive record of the last ca. 200 ka (Lindsay *et al.,* 2011). For this study the Orakei Basin and Onepoto cores were available for full analysis and were used to test and develop the techniques discussed above. The other cores were used for correlation purposes: for the Glover Park core (St Heliers volcano) tephra horizons were re-sampled and analysed; for Pupuke and Hopua cores original mounts from Molloy et al. (2009) were analysed for major and trace elements; and data from Pukaki core were taken from the literature (Sandiford *et al.,* 2001) or from unpublished work (Phil Shane, *pers. comms,* 2015). The AVF tephra deposits are labelled with the prefix 'AVF' then a number from 1 at the base to 24 at the top. This nomenclature was based on the Orakei Basin core (Molloy *et al.,* 2009) and extended throughout the cores, aiding clarity in cross-core correlation. Where possible this study maintains the nomenclature assigned by previous studies for the AVF basalts. Previous studies (e.g. Lowe 1988b) have outlined the complexity associated with post-depositional compaction of tephra horizons. Here we report deposit thicknesses as actually observed, and take them to be minimum thicknesses. Detailed core information can be found in **Table 3.1**.

Sections of the cores, where applicable, have been split into five age groups, based on the well-established ages of rhyolitic and andesitic tephras originating from the Taupo Volcanic Zone (TVZ) and Mt Taranaki (Eg). These serve as key stratigraphic marker horizons and for this study include, Rerewhakaaitu (Rk) 17,496 ± 462 calendar (cal.) yr. BP; Okareka (Ok) 21,858 ± 290 cal. yr. BP; Kawakawa/Oruanui (Kk) 25,358 ± 162 cal. yr. BP (all ages from Lowe *et al*., 2013) and Rotoehu (Re), which currently has a less well defined age with estimates of between ca. 44.3 cal. ka (Shane and Sandiford, 2003) to ca. 61 ± 1.4 ka (Wilson *et al.,* 2007). For the purpose of this study we use the most recently published age estimate (45,100 ± 3,300 cal. yr BP; Danišík et al., 2014) to provide a minimum age constraint to basaltic tephras

found below this horizon. The cores, where applicable, have been split into five age groups, based on the minimum and maximum errors (2 s.d.) associated with the published values to give the maximum age ranges for the groupings These groups are: older than Re (> 41,800 ka cal. yr. BP); Kk to Re (25,196 – 61,000 cal. yr. BP); Ok to Kk (21,568 – 25,520 cal. yr. BP); Rk to Ok (17,034 – 22,148 cal. yr BP) and younger than Rk (< 17,958 cal. yr. BP).

Table 3.1. *Overview of drill cores, their locations, the section of the core that has been used for this study (in metres below the drill hole top), and the proposed age that the core section covers, based on the ages proposed for bracketing rhyolitic tephra. Also included are the number of basaltic horizons found within the cores by this study, and previous studies, and the geochemical data that are available for the glass shards.*

				Previous studies			This study		
Core (centre) name	Grid reference	Section of interest (m)	Proposed age range (cal. ka)	No. of basaltic horizons	Geochemical data	References	No. of basaltic horizons	Status	Geochemical data
Pupuke	36°46'49.83"S 174°45'57.67"E	57 to 70	0.4 to 38	7	Major	Molloy et al., 2009	7	Mounts re-analysed	Major and trace
Onepoto	36°48'27.09"S 174°45'0.39"E	38 to 69	25 to >150	6	Major	Shane and Hoverd 2002	9	Core sampled	Major and trace
Glover Park (St. Heliers)	36°50'49.68"S, 174°52'2.60"E	4 to 27	Rotoehu to St Heliers	13	Major	Hoverd *et al.,* 2005	4	Core Sampled	Major and trace
Orakei	36°52'4.14"S, 174°48'46.11"E	44 to 87	24 to 86	14	Major	Molloy et al., 2009	16	Core sampled	Major and trace
Hopua	36°55'46.68"S, 174°47'3.82"E	38 to 49	7 to 31	5	Major	Molloy *et al.,* 2009	5	Mounts re-analysed	Major and trace
Pukaki	36°58'57.63"S, 174°48'37.74"E	45 to 62	7 to Rotoehu	12	Major	to 52 m Sandiford *et al.,* 2001, 52 m to base Shane, 2005	12	Core nor mounts available for analysis	

3.3.3. Tephra Geochemical Analysis

The bulk tephra samples were washed and cleaned using an ultrasonic bath to remove organic debris. The glass shards were then mounted as bulk samples if shards were <30 µm across, and larger shards were hand-picked and mounted individually. Epoxy mounts 10 mm deep were created using a 4:1 ratio of resin to hardener. Once solidified, six holes were drilled through the mounts, the mounts were placed on adhesive tape and individual samples were then positioned into each hole, back-filled with epoxy, and left to harden. To expose the samples, mounts were polished using a sequence of SiC papers starting at 400 grade, followed by 600, 1000 and 2500, and finally finished using a diamond lap polisher at 3 µm and 1 µm.

3.3.3.1. Major-Element Analysis

In-situ major element analyses as oxides (SiO_2, TiO_2, Al_2O_3, FeO_t, MnO, MgO, CaO, Na_2O, K_2O and P_2O_5) were undertaken on carbon coated sample mounts at Victoria University of Wellington (VUW) using WDS on a JEOL JXA 8230 Superprobe (EMPA) with a static beam at 10 µm and 8 nA. For each horizon, back-scattered electron images of the shards were taken to locate the sampling spots for subsequent LA-ICP-MS analysis. Matrix-matched standard A99 basaltic glass was used as a bracketing standard and run three times every 10 samples to monitor instrument drift. Accuracy of the analyses was within 2 % of the recommended values for the internal standards and analytical precision (2 s.d.) is 1 % relative or better for all elements. Major element concentrations were determined using the ZAF correction method, and analytical totals for unknown glass were 97-100 % with deviations from 100 % attributed to variable degrees of post-eruption hydration (Shane, 2000). To account for this secondary process, all major element data were normalised to 100 %.

3.3.3.2. Trace element analysis

After the carbon coat was removed, trace element concentrations were analysed by in-situ LA-ICP-MS using an Agilent 7500cs ICP-MS coupled with either a New Wave UP 193 nm solid state laser ablation system at VUW or a Resonetics RESOlution M-50-LR 193nm excimer laser ablation system at the University of Otago (UoO). Backscatter electron images obtained from probe analysis were used to allow re-location of individual analysis sites. All the data were acquired using static spot analysis with spot sizes of either 25 or 35 µm with an ablation time of 60 seconds, with fluence varied between 2-4 J/cm^2. Ablated material was carried by He gas (0.75- 0.77 L/min [VUW], 0.65-0.75 L/min [UoO]), and mixed with Ar (0.83-0.87 L/min [VUW], 0.65-0.750 L/min [UoO]). Gas flows were adjusted after each sample exchange to achieve maximum sensitivity and stability, and during analysis care was taken to avoid any visible microcrysts or thin bubble walls on the shards. BHVO-2G and NIST612 standards were run every 5 analyses and at the beginning and end of each session, with BCR-2G run as an internal standard at the beginning of

each session. All data were reduced off-line using the Iolite software (Paton *et al.,* 2011), using ^{29}Si analysis as the internal standard and BHVO-2G as the calibration standard. Analytical precision based on 15 replicate analyses of BCR-2 for both VUW and UoO is <6.5%. Exceptions to this include Cr ± 10%, Nb ± 22%, Cs ± 12%, Ba ± 11.8%, Ta ± 21% and Pb ±31%, and the accuracy for all elements is ≤6% apart from Li, Cr, Nb, Cs, Eu and Ta, with duplicate sample analyses yielding results within error between VUW and UoO.

When analysing the glass shards, every care was taken to analyse pure glass only, rather than any microcrystals (e.g. olivine, plagioclase or Fe-Ti oxides; **Fig. 3.3.B**). On occasion, accidental ablation of microcrysts did occur and was identified by extreme spikes in major element concentration (e.g. Mg for olivine; **Fig. 3.3.A**). Such analyses were rejected from the data set.

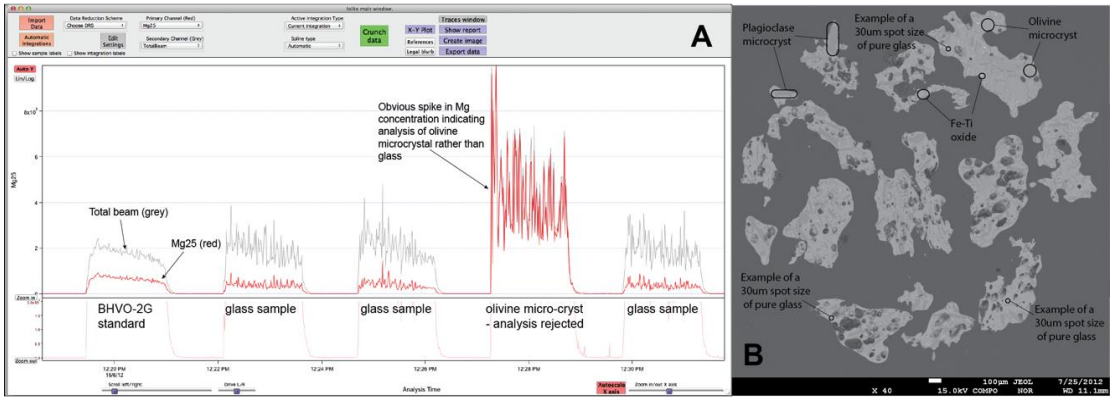

Figure 3.3. *A) Example of identification of accidental microcryst analysis detected in Iolite data reduction software (Paton et al., 2011) with obvious concentration spike in Mg in comparison to pure glass analyses. B) Back Scatter Electron image from EMPA analysis, identifying clearly microcrystal types and locations, and examples of a 30μm spot size, where pure glass analyses could be taken.*

3.4. Results

3.4.1. Tephra horizon identification and classification

Visual observations show the basaltic tephra horizons are light grey to black in colour with shard size ranging from very fine ash (<20 µm) to lapilli (2 mm to 2 cm). Tephra horizons in the Orakei and Onepoto cores range from 1-2 mm to ca. 750 mm in thickness. Horizons <20 mm thick show relatively small but well-defined magnetic peaks of ≥50 (10^{-5} SI) combined with bright appearance on X-ray scan. In comparison, >20 mm thick horizons exhibit more complex X-ray and magnetic susceptibility results. All horizons have sharp lower contacts, however, often only the thinner horizons (<20 mm) have well defined sharp upper contacts as well. The primary deposits are mostly (ca. 80%) non-graded, or have normal grading. Some deposits contain visible minerals (commonly olivine or pyroxene) and/or a high proportion (30-60%) of accidental ejecta (quartz crystals, shell fragments and sedimentary lithic fragments derived from the underlying Tertiary Waitemata beds). Thirty-eight tephra horizons are identified in the Orakei Basin, Onepoto and Glover Park cores collectively. These are combined with nineteen other horizons previously identified and sampled from within the Hopua, Pukaki and Pupuke cores.

The lacustrine sediments comprising most of the thickness in the maar cores show little to no increase in magnetic susceptibility from baseline values of 0 to a maximum of 10 S.I. This lack of susceptibility change is coupled with homogeneous grey tones in the X-ray scans, punctuated with black lines. These black lines represent cavities within the cores that are most likely caused by the coring process, or drying out and contraction during storage (**Fig. 3.2**.). Rare small peaks (<10 S.I.) were detected in magnetic susceptibility within the lacustrine sediments but no coincident glass shards were identified during subsequent X-ray scanning or sampling. These magnetic peaks are likely to represent variations of the magnetic properties in the lacustrine sediments. Conversely the deposits formed during marine incursions are more homogeneous than lacustrine deposits, showing no bedding, consistently low magnetic-susceptibility, and less frequent cavities in

the core on the X-ray scan. Within the marine muds, the X-ray scans pick up small discontinuous spots of high-density reflecting the presence of small shells (**Fig. 3.7.A**).

3.4.2. Tephra-derived glass shard Geochemistry

We analysed 10-20 shards for major and trace elements from each of 57 basaltic tephra horizons from the six cores. In addition, where possible, subsamples of some of the thicker deposits were taken to monitor re-working or primary geochemical variation through an eruption sequence. For within-core tephra horizons, MgO content variations are minimal, and consistent, with all varying from 2.1 to 7.5 wt.% (**Fig. 3.4.**). Compositional ranges in CaO, FeO, K_2O, and TiO_2 are consistent throughout all cores, but the ranges for Al_2O_3 and SiO_2 are less consistent between the cores. Onepoto and Orakei Basin core shards in general have consistently lower Al_2O_3 values for a given MgO value making the concentrations different to those of tephra in Pukaki, Glover Park, Hopua, or Pupuke cores. Onepoto core contains tephra with glass that has consistently higher SiO_2 values at a given MgO value in comparison to the glass in the Hopua and Pukaki cores, but similar to values for glass shards from Pupuke, Orakei and Glover Park cores.

Most of the tephra horizons (50 out 57) show a unimodal signature with limited variability in major element concentrations with MgO, SiO_2, FeO, and TiO_2 all with a variation of <1 wt.% and CaO, Al_2O_3, Na_2O and K_2O with a variation of <3 wt.%. Bivariate plots of a combination of SiO_2, MgO, Al_2O_3, CaO and FeO show the most distinction between the horizons (e.g. **Fig. 3.5.A**). Three of the 57 horizons show a bimodal distribution in major element/oxide concentrations. Differences between the two modes for SiO_2, Al_2O_3 and FeO concentrations can be up to 5 wt.%, but are <2 wt.% for MgO, CaO, TiO_2. For another small proportion of horizons (n=4), a systematic range is observed - for example, SiO_2 ranges from 44-49 wt.%, FeO from 12-14 wt.% and CaO from 8-10 wt.%.

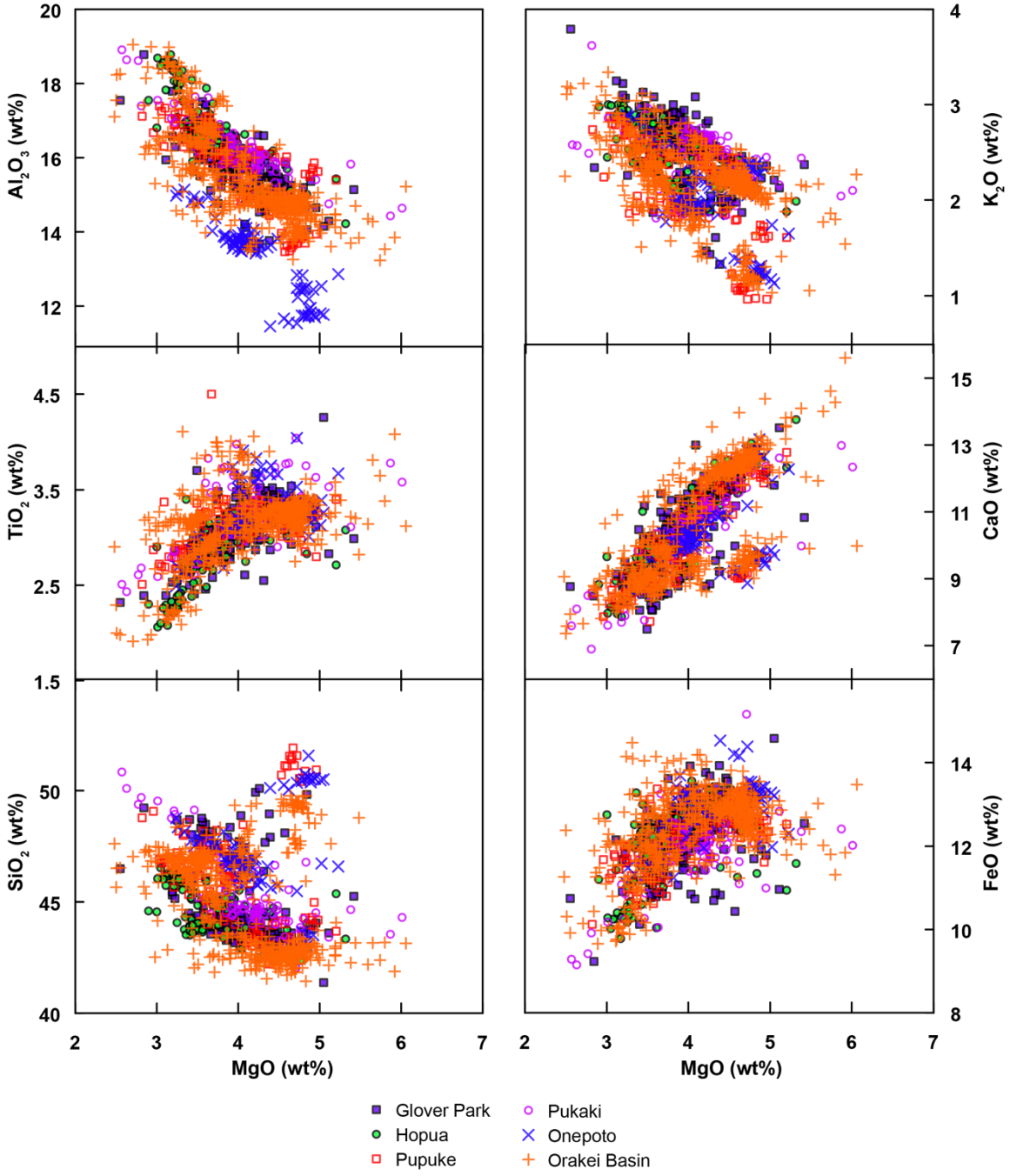

Figure 3.4. *Selected major elements as oxides vs. MgO for all shards from all tephra horizons found within all six cores studied for this paper.*

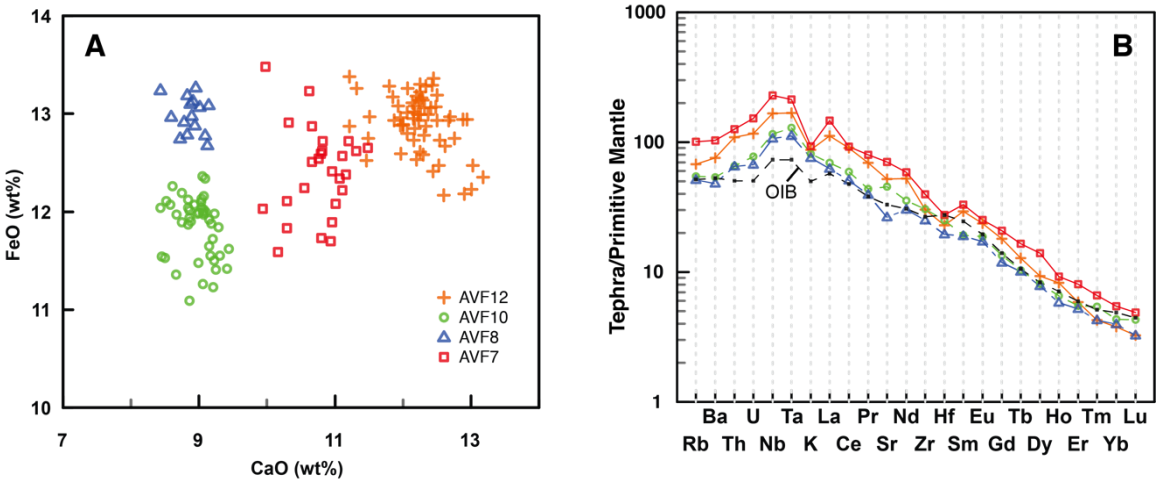

Figure 3.5. *Data from selected successive horizons from Orakei Basin (AVF 12, 10, 8, and 7) to show major and trace element variability from shards in tephras within a single core. (A) CaO vs. FeO (wt.%). (B) Primitive mantle-normalized trace element patterns, with OIB values and normalisation values from Sun and McDonough (1989).*

Forty-nine tephra horizons from five of the cores (Pukaki had no trace element data available) had shards large enough (>30 μm) to be analysed for trace elements. Overall, all shards show a wide range in concentrations. For example La ranges from ca. 5 to 100 ppm, Nb from ca. 20 to 175 ppm, and Rb from ca. 5 to 75 ppm (**Fig. 3.6.**). All glass samples show trace element distributions similar to those of ocean island basalts (OIB-type) on a primitive mantle-normalised multi-element plot (after Sun and McDonough, 1989). Pupuke and Onepoto samples have a much more limited range in variability in some trace elements in comparison to the ranges of glasses from the other cores. For example, in Pupuke and Glover Park cores, glass La values range between ca. 50-75 ppm. Glover Park glasses show a very high variation in trace elements that are coupled with high (>4 wt.%) MgO. This is not seen within the glasses in the tephras from the other cores.

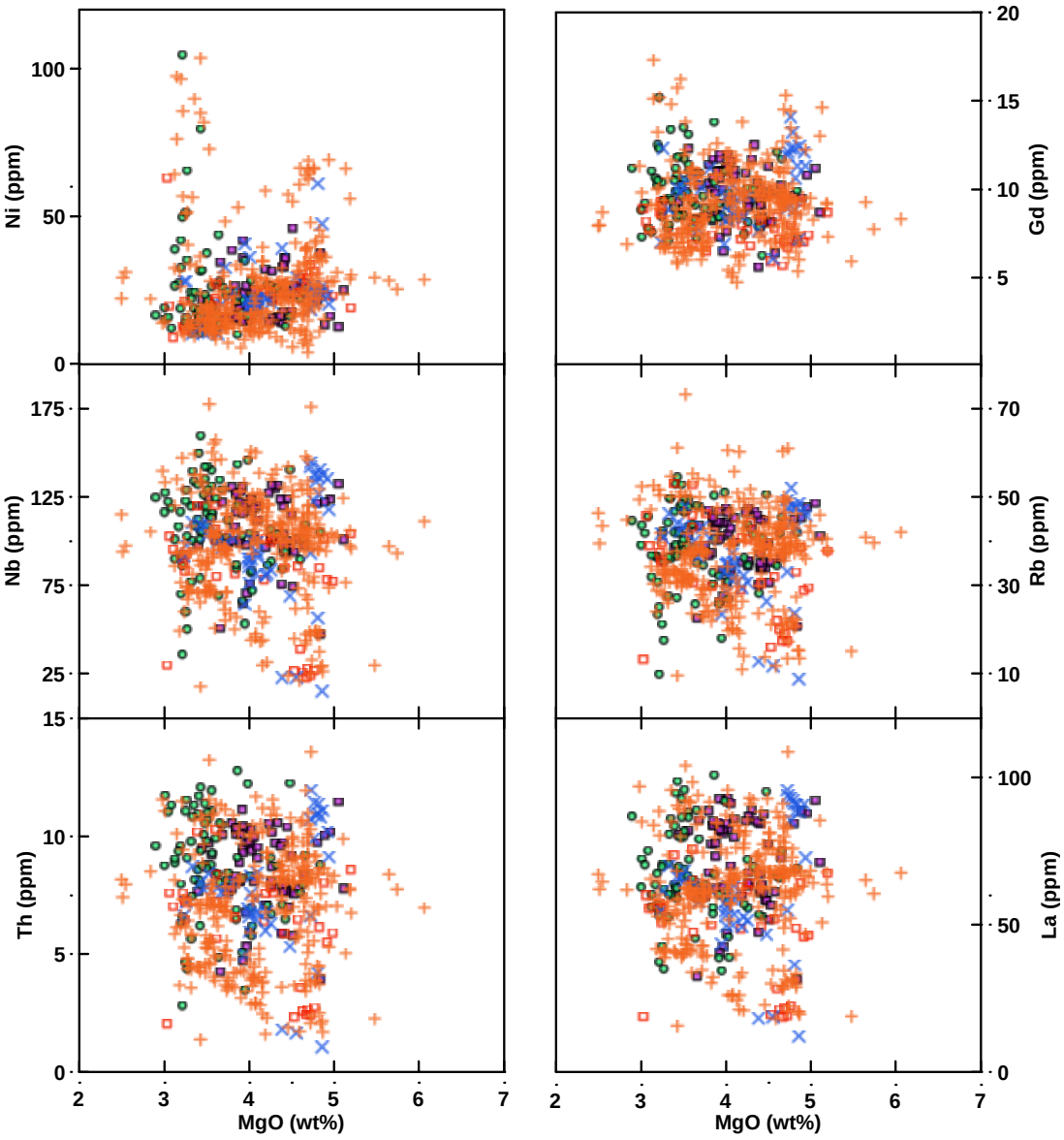

Figure 3.6. *Concentrations of selected trace elements vs. MgO for shards from all tephra horizons from within five of the six cores (no trace element data available for Pukaki). Symbols are the same as* ***Figure 3.4****.*

For Orakei Basin, Hopua, and to a lesser extent Glover Park, the trace element variations in the glass shards in the core are much greater, with La varying from ca. 5-100 ppm, 40-100 ppm and 35-95 ppm, respectively. For the individual horizons, the glass trace element variations are a lot less than those within all the tephra in the cores as whole. In general, the glass La values vary by ca. <30 ppm, with Nb values a little more variable at ca. <50 ppm and Rb values a little less at <10 ppm.

Figure 3.5.B shows trace element values for glass of the Orakei Basin horizons AVF12, 10, 8, and 7 that indicate the average concentration for each horizon has a relatively distinct geochemical signature, and that this distinction is similar for all horizons. Although distinct, all analyses share the same general OIB-type pattern when normalised, with enrichment in LREE compared to HREE (e.g. $(La/Yb)_N$ = 21 to 41). Given that major and trace element concentration variations within glass pertaining to a single horizon are often small, and in most cases within error, the observed range in geochemistry of glass shards within, and between cores, is attributed to differences between individual horizons.

3.5. Discussion

3.5.1. Identification of primary tephra horizons

Observations (visual, magnetic susceptibility and X-ray) and geochemical composition are important for the identification and definition of primary tephra horizons. For the thin (<20 mm) deposits there is little ambiguity: the horizons are always constrained by sharp upper and lower contacts, seen by contrasting bright sections on the X-ray images and by a clear peak in magnetic susceptibility (**Fig. 3.7.B**). In some cases the thin deposits can be visually obscured because of their minimal thickness or similarity in colour to the lacustrine sediments. However, the X-ray imaging and magnetic susceptibility analyses overcome this difficulty. In comparison, thicker deposits (>20 mm) often appear more complex in both the X-ray images and magnetic susceptibility scans. **Figure 3.7.C** shows two contrasting thicker deposits. At the top of the core an apparently homogeneous deposit shows consistently high magnetic susceptibility and consistently bright X-ray imagery. In comparison the lower deposit shows an apparently heterogeneous horizon with changes in grain size displayed by variations in grey-scale of the X-ray images as well as multiple peaks in magnetic susceptibility. Both of these horizons are horizontally bedded, consistent with constant deposition, suggesting that they are both primary horizons. In addition, the similar geochemical composition of glasses from multiple tephra subsamples from each horizon supports the interpretation that

both horizons are primary deposits. However, the slight variation in geochemical composition of glass from the lower horizon, coupled with the variation in shard size but lack of depositional hiatus, suggests this horizon has formed from multiple deposition events from one eruption episode.

A less clear example (**Fig. 3.7.D**) is evident where a section showing lower contrasting X-ray imagery and a gradual incline to an inconsistent peak in magnetic susceptibility follows the initial primary horizon. This subsequent section has blurred basal and upper contacts, with an X-ray transmissivity that is gradational, rather than sharply contrasting, from that shown by the lacustrine sediments. There are no obvious horizontal beds and some deformation can be picked out in the X-radiograph within the section. There is also a clear hiatus between the two sections shown by the magnetic susceptibility trough. If these features are combined with indistinguishable glass geochemistries from each section, then the deposits can be interpreted as being reworked.

We considered that re-mobilisation of a tephra horizon could also cause a sharp basal contact, here ascribed as a primary feature. However, it is likely that this feature would be coupled with 1) within-horizon deformation (e.g. overturning or convolute bedding), and 2) a mixture of sediment and glass shards, both of which would distinguish the deposit as reworked. Alternatively a diffuse contact, here taken as an indication of reworking, has the potential to form through density settling of a primary deposit (Manville and Wilson, 2004). However, if this were the case Stokes Law would dictate a fining upwards of the shards, which is not observed for those horizons classed as reworked. In addition, nearly all the AVF eruptions are volumetrically very small, and considered to only last for a number of weeks to months (Hayward et al., 2011). If the diffuse contacts observed within these cores were to be formed through gradual influx of material, sedimentation rates would suggest time periods of tens of years of constant eruption in most cases, which is wholly improbable for the AVF eruptions. Further clarification of these distinctions could be gained through the use of multiple cores to compare the individual deposit characteristics (e.g. Green and Lowe, 1985; Lowe, 1988a); however, multiple cores were not available for this study.

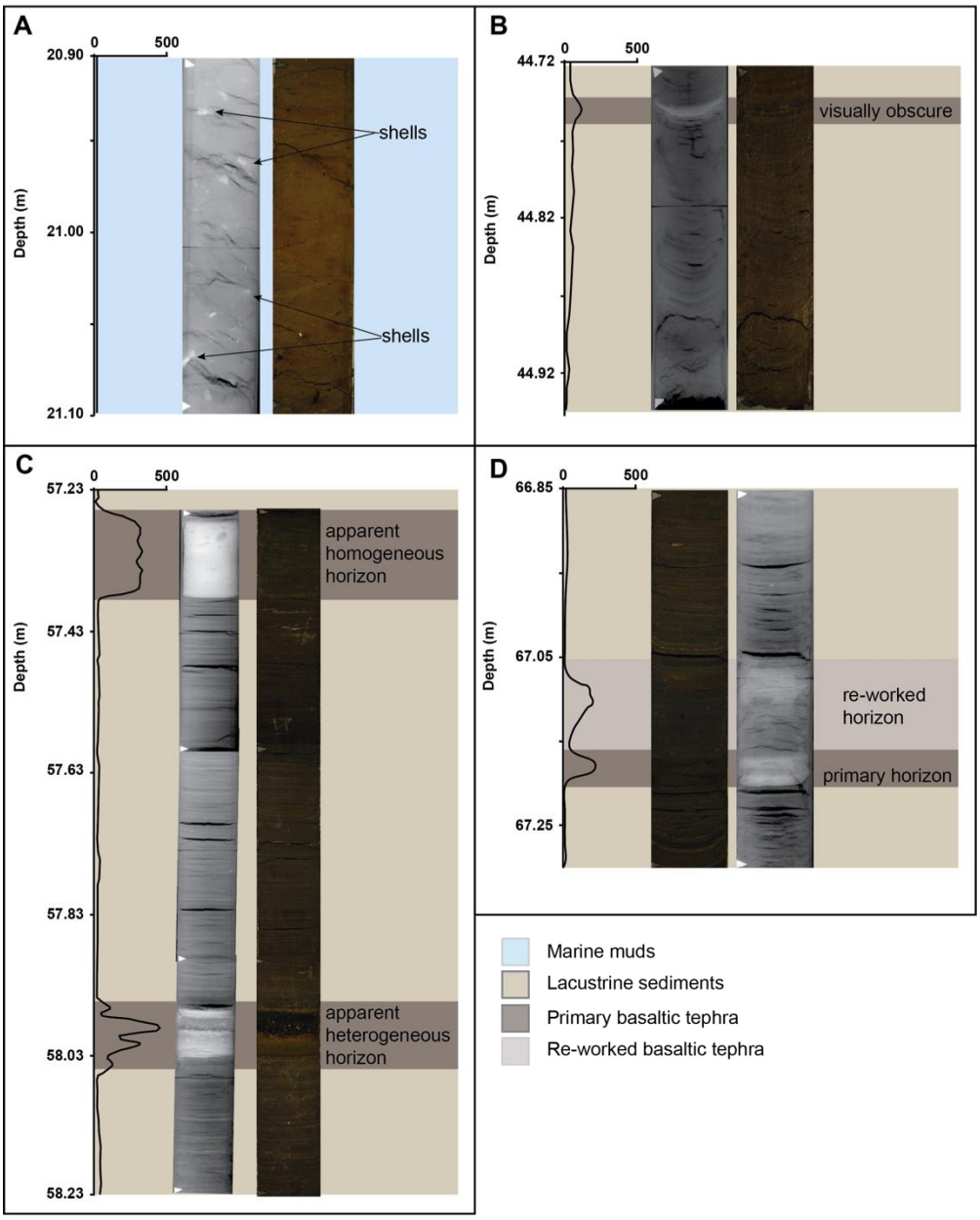

Figure 3.7. *Examples of features seen within the Orakei Basin core. A) Intermittent bright signals on the X-ray image picking up shells within marine muds. B) A thin basaltic deposit showing sharp upper and basal contacts in X-ray and magnetic susceptibility but ambiguity in visual observation. C) Two contrasting primary deposits. The upper deposit appears mostly homogeneous, as indicated by uniform X-ray contrast and corresponding magnetic susceptibility peak. In comparison, the lower deposit is more heterogeneous in shard size, as indicated by peaks and troughs in magnetic susceptibility and variable grey-tones in the X-ray imagery. D) Primary and re-worked deposit. The lower labelled band is a primary deposit with a sharp basal contact with a marked sharp contrast in grey scale on X-ray image and a sharp peak in magnetic susceptibility. The upper-labelled band has a blurred upper and basal contact, a lower contrast in grey scale on X-ray imagery, and more variable magnetic susceptibility levels.*

In summary, homogeneous glass-based trace element geochemistry, a sharp basal and upper contact between the tephra deposit and the lacustrine sediments, coupled with a sharp peak in magnetic susceptibility, and a highly contrasting section on the X-ray imagery are interpreted by us to indicate a primary deposit. A re-worked deposit is characterised typically by heterogeneous glass trace element geochemistry, blurred upper and lower contact boundaries, lower grey scale contrast in the X-ray imagery and sometimes upward grading of grey scale intensity (darker, lower density towards the top). A lack of horizontal bedding is usually observed, and deformation or a hiatus within the deposits can also be seen. The magnetic susceptibility is usually more variable in reworked deposits and often shows a more gradual peak in comparison to the sharp peak that is seen for a primary deposit.

It is important to note that the X-ray density scanning and magnetic susceptibility analysis rely on the contrasting characteristics of basaltic material versus and lacustrine sediments. As outlined in the methods, in comparison with lacustrine sediments, basaltic tephra has a higher proportion x-ray absorbing elements (e.g. FeO) coupled with a higher abundance of magnetic minerals. It is this contrast that allows the basaltic tephra to be identified by these methods. However, rhyolitic and to a lesser extent andesitic tephra have lower proportions of these elements and minerals implying that tephras of such composition may not be easily detected by these methods. Nevertheless, rhyolitic and andesitic tephra are usually light in colour, and (if sufficiently concentrated or thick enough) are thus more easily detected by careful visual observation.

Methods used in previous studies often may have led to inaccurate identification of primary vs. re-worked sections of deposits (Hoverd *et al.,* 2005; Molloy *et al.,* 2009) and left fine-grained and thin horizons unidentified, which led to misinterpretation of the thicknesses of some of the deposits. This misassociation has important implications for the establishment of sedimentation rates and past eruptive frequency (discussed in **sect. 3.5.6**.). Using our combined methodology, all basaltic tephra horizons from Orakei

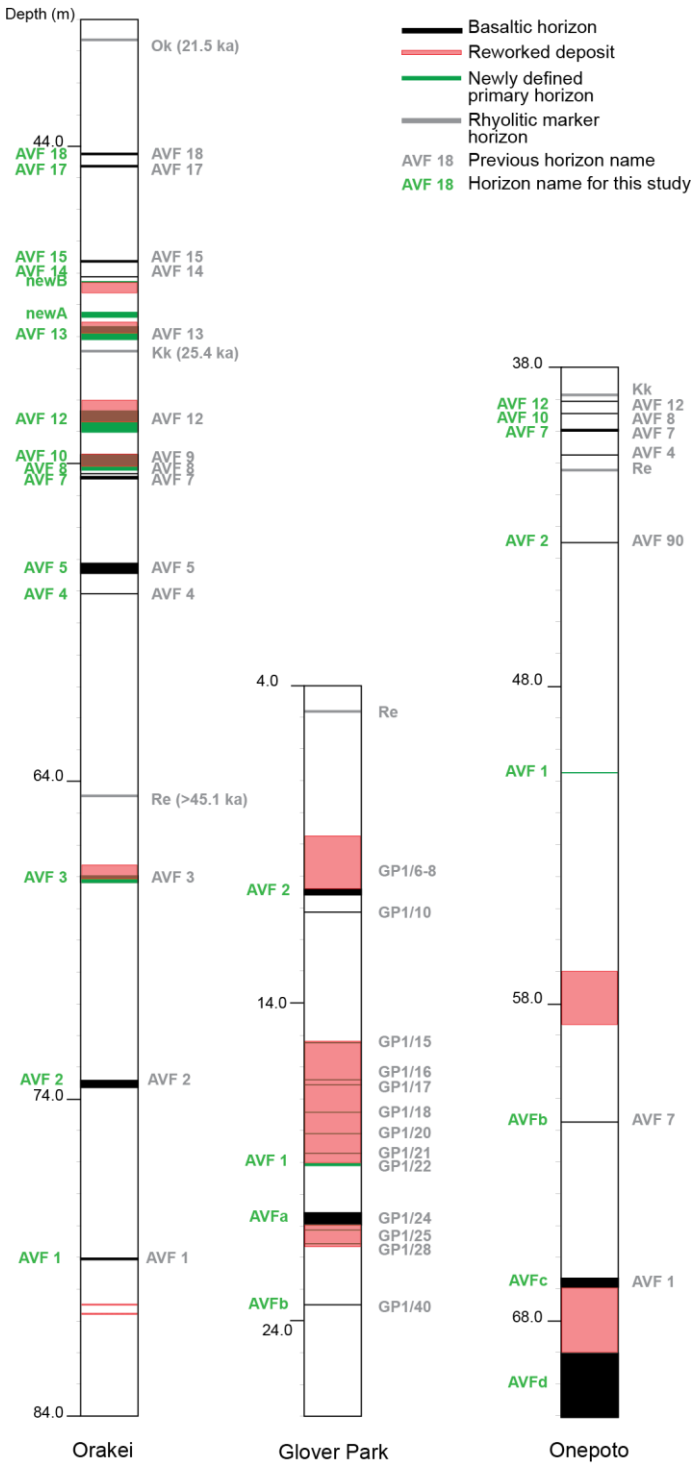

Figure 3.8. *Schematic stratigraphic columns for the cores that were available for re-assessment: Orakei Basin (Molloy et al., 2009), Glover Park (Hoverd et al., 2005), and Onepoto (Shane and Hoverd, 2002). Basaltic horizons are marked within the cores in black, sections identified as re-worked by this study are outlined in red dotted lines and green lines show the newly defined horizons. Grey text defines previous horizon name and green text shows previous and new names for all horizons given by this study. Key rhyolitic marker horizons are shown by grey lines (Ok – Okareka; Kk - Kawakawa/Oruanui; Re – Rotoehu).*

Basin, Onepoto and Glover Park were re-assessed as being primary or reworked deposits.

Figure 3.8 shows all individual horizons found within these cores. We have identified eight new horizons and redefined seven as reworked, these previously being considered as primary. Thin horizons (<20 mm) previously identified (Orakei Basin by Molloy *et al.,* 2009; Onepoto by Shane and Hoverd, 2002; and Glover Park by Hoverd *et al.,* 2005) were confirmed and, as previously discussed, their nomenclature maintained. Two of the horizons, AVF 4 in Onepoto, and GP1/10 in Glover Park, were not found by this study, potentially because of poor or discontinuous preservation. All relatively thick horizons (>100 mm) previously identified have been split using the techniques adopted in this study into 'primary' and 'reworked' categories, reducing the thickness of the primary deposit when compared to previous interpretations (Molloy *et al.,* 2009). Examples of these (for the Orakei Basin core) include AVF14 with a combined thickness of 31 mm of intermittent primary deposits (previously 340 mm), AVF13 with a primary deposit thickness of 160 mm (previously 740 mm), and AVF3 with a primary thickness of 41 mm (previously 120 mm). In summary, we identified two new tephra horizons within the Orakei Basin core (giving sixteen primary tephras in total) and one fewer than previously identified in the Onepoto core (giving nine in total). Finally, eight of the tephra horizons in the Glover Park core, previously interpreted as primary deposits, are now classified as re-worked, and one was not found, thereby reducing the number of primary horizons within the Glover Park core from thirteen to four.

3.5.2. Tephra deposit re-working

The geochemical signatures of tephras from each horizon are also essential to identify reworking relationships highlighted by the X-ray and magnetic susceptibility analyses. We classify the different types of reworked horizons observed into three groups (A-C) as discussed in the following sections.

3.5.2.1. Evidence for immediate re-working of deposits ('type-A')

Type-A deposits show evidence of immediate re-working, with no evidence of a time break. This type encompasses horizons that have previously been interpreted as single thick primary deposits because of their apparent homogeneity in visual observations. Through coupling the X-ray imagery and magnetic susceptibility data, a more detailed stratigraphy is revealed (**Fig. 3.9.A**). Each basaltic horizon has a sharp basal contact with the laminated lacustrine deposits. These sharp contacts are clearly seen as magnetic susceptibility peaks and as bright sections within the X-ray images, contrasting with the grey background. The contacts are considered to be the base of a primary deposit from which the thickness of the deposit is measured.

Within some of the thick tephra deposits disturbances are identified in the form of cavities in the core, or angled or convolute bedding within the deposit. If these features coincide with dark patches on the X-ray image and low magnetic susceptibility (indicative of cavities within the core), or with grey scale-graded X-ray portions and declining magnetic susceptibility (indicative of a decreasing proportion of tephra in the lacustrine host sediment), the section is interpreted as reworked. Often in the case of immediate re-working, the top of the re-worked section is clearly seen by a very steep decline in magnetic susceptibility and a change to darker grey background colour in the X-ray images. In addition, a deposit is classified 'type-A' if the shards in a reworked material show the same geochemical composition (within error) as those of the primary tephra below, implying that the tephra is derived from a single geochemically homogeneous source. 'Type-A' reworking is considered to occur as a result of density flows from sub-lacustrine bank destabilisation due to loading from very thick tephra deposits (Bertrand *et al.,* 2014). In these cases the primary deposit thickness is reduced in comparison to those reported in previous studies and is measured up to the point where reworking is first identified.

Figure 3.9.A shows a section from the Orakei Basin core that exemplifies a type-A reworked deposit. Here, our new results suggest that the primary deposit (AVF13) is only ca. 160 mm thick, compared to previous

visual observations which classified the entire 710 mm thick deposit, from 50.19 to 49.48 m depth, as a single primary tephra horizon (Molloy *et al.,* 2009).

3.5.2.2. Evidence for periodic re-working ('type-B')

Type-B deposits were found only within the Orakei Basin core, and are found in parts of the core that have multiple, closely spaced, visually similar horizons, interbedded with sections of laminated lacustrine deposits (<10 cm thick) (**Fig. 3.9.A**). The tephra horizons have sharp basal contacts and are normally graded, similar to a primary horizon, and are therefore assumed to be representing individual depositional events. However, their upper contacts are blurred and show grey-tone grading on the X-ray imagery and a gradational decline in their magnetic susceptibility. These observations are interpreted to reflect upwards-decreasing shard concentrations, which we have earlier linked to re-working. We therefore propose that these repeated deposits are formed either as a result of episodic eruptions from a single centre, or periodic re-working of a single proximal deposit from a single eruption event.

Evidence for episodic eruptions exists for a number of AVF eruptive centres, including Rangitoto, and Motukorea. Needham et al. (2011) proposed two Rangitoto eruptions with a ca. 40-year period of quiescence based on ^{14}C dating of two individual tephra deposits (at 533 ± 7 and 504 ± 5 cal. yr. BP). The tephra horizons were separated by ca. 10-50 cm of peat, and have been shown to geochemically match the contrasting composition of lavas from two different eruption phases of Rangitoto. Studies of other AVF eruptions have also highlighted multiple explosive episodes from single centres (e.g. Crater Hill, Houghton *et al.,* 1996; Motukorea, McGee *et al.,* 2012). However, these other eruptive episodes, unlike Rangitoto, are defined from proximal pyroclastic successions, and are interpreted to reflect on-going eruptive activity as no hiatuses are reported. The changing styles of explosive volcanism are attributed to intermittent water-magma interaction, changes in magma supply rate and degassing, and shifting vent positions (Houghton *et al.,* 1999). The aforementioned studies all monitored the geochemistry of the eruptive products and indicated that there were minor changes in

geochemical composition throughout the eruption indicative of a gradational change between two source melts. Therefore if the 'type-B' deposits identified were related to episodic eruptions we would expect to see chemical evolution reflected in the tephra composition (e.g. Needham *et al.,* 2011).

An example of the type-B reworked horizon is given here from the Orakei Basin core (**Fig. 3.9.A**). The section of interest includes three tephra units with their basal contacts at 49.14 m, 49.33 m and 49.46 m. Based on calculated sedimentation rates (e.g. 1.96 mm/yr; Molloy, 2008, as discussed in the introduction), this section was proposed to span ca. 100 years, with ca. 50 years quiescence between each deposit. The glass geochemical signature of these horizons is different from that of the previous primary horizon, hence ruling out re-working of a previous deposit. However, the geochemical signatures of the three units are indistinguishable from one another (**Fig. 3.9.B**), and the lack of geochemical variation is taken to indicate that the three layers do not reflect episodic eruptions from one centre, but instead two periods of reworking, possible derived from influx from south eastern stream catchments, following deposition of the earliest, single primary deposit (Pickrill *et al.,* 1991; Bertrand *et al.,* 2014).

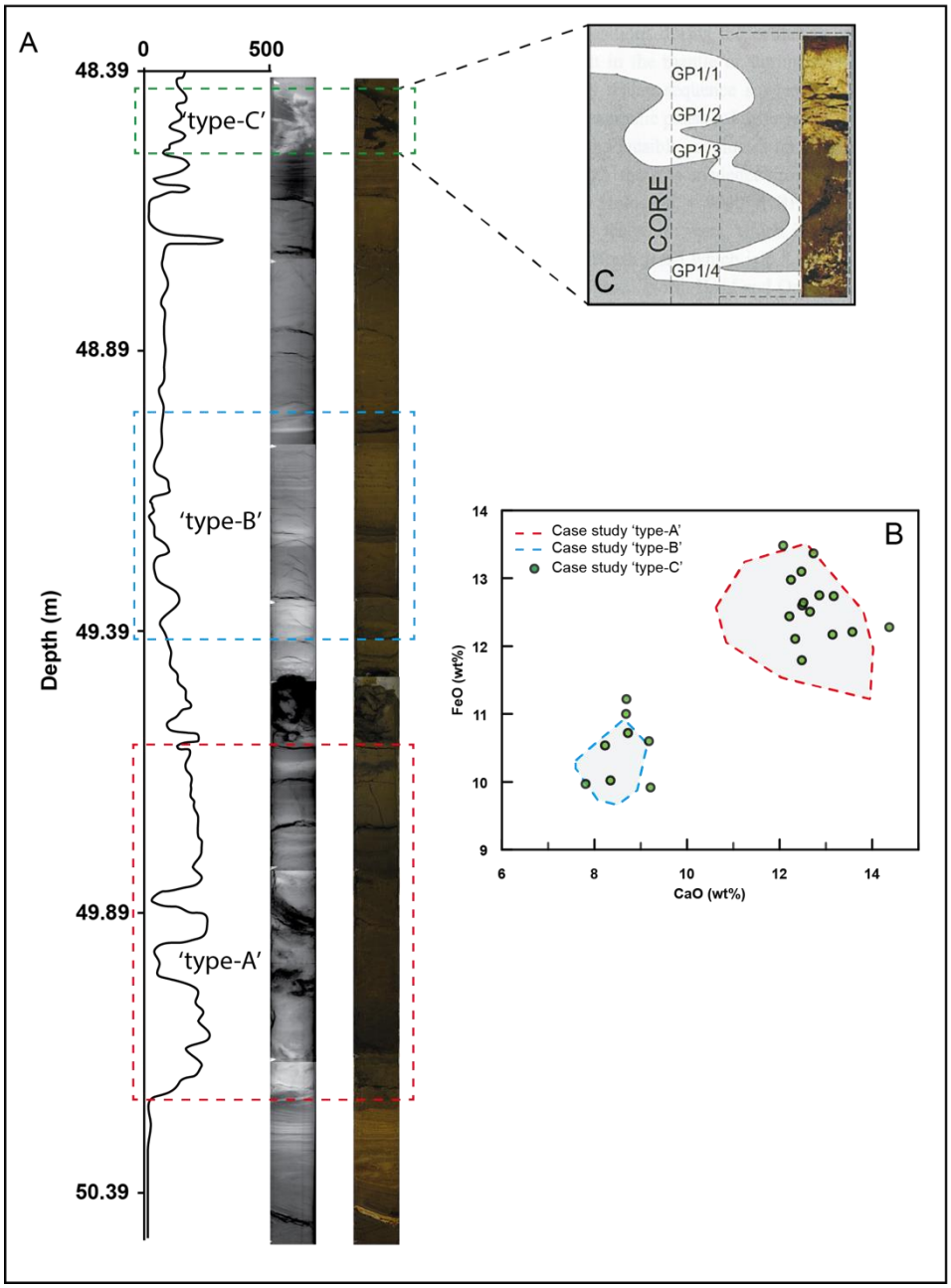

Figure 3.9. *Case study from the Orakei Basin core from 50.39-48.39 m depth to show examples of re-working within the tephra sequence. (A) Magnetic susceptibility, X-ray image, and photograph of core section. From base to top immediate reworking of deposits ('type-A'); periodic re-working of deposits ('type-B'); delayed reworking of deposits ('type-C'). See text for descriptions. In addition a bivariate plot (B) of CaO vs. FeO measured in shards from each of the three units is given to show the geochemical variability of the horizons: 'Type-A' is shown by the dashed outline in red, 'type-B' by the dashed outline in blue, and 'type-C' by the green circles. (C) Shows the proposed slumping seen in a 'type-C' horizon, adapted from Hoverd et al. (2005) from the Glover Park core for the Rotoehu tephra deposit.*

3.5.2.3. Evidence for slumped re-working of deposits ('type-C')

Type-C deposits occur infrequently (one deposit in the Orakei Basin core, one in the Onepoto core, four in the Glover Park core), but their identification is essential to avoid the misinterpretation of such deposits as representing multiple primary deposits. The termed 'slumped' (cf. Pickrill *et al.,* 1991) is used here because the horizons are typically highly deformed with convolute bedding, and poorly sorted shard sizes. These characteristics show up as 'mottled' bright and dark colours in the X-ray scans and as an oscillatory result on the magnetic susceptibility analyses (**Fig. 3.9.A**). These results, together with a tephra geochemistry that is indistinguishable from the compositions of materials in the preceding (underlying) tephra(s) within the core, are here attributed to remobilisation of previously deposited tephra horizon(s).

Figure 3.9.A shows a typical 'type-C' deposit, where horizon disturbance is obvious, and magnetic susceptibility values are variable. The geochemistry for this horizon shows a mixture of shard compositions that match those of the two preceding deposits' signatures (**Fig. 3.9.B**), proposed to reflect sub-lacustrine mass flow re-working of both tephra layers together at some stage (centuries) after the eruptions (Pickrill *et al.,* 1991). In contrast, **Figure 3.9.C** shows another example (Rotoehu rhyolitic tephra) of slumping, identified previously by Hoverd et al. (2005) within the Glover Park core that has formed a type C deposit. This deposit (Re) was inferred to reflect post depositional deformation of a single tephra unit (Hoverd *et al.,* 2005).

3.5.3. Geochemical variations within an individual tephra horizon

For individual primary tephra horizons, major element concentrations may show three patterns: 1) unimodal, 2) bimodal, and 3) gradational variations. Because of the improved identification of primary tephra horizons (outlined in **sect. 3.5.1**), any variability in tephra geochemical composition represents a natural variation in the sample itself, and is not considered to be a result of reworking. Samples of glass from 50 primary horizons show a unimodal distribution of major element contents (e.g., **Fig. 3.10.B**), with

variations of <1 wt. % attributed to natural variation within the glass shards or the EMPA process. Three horizons show a bimodal distribution of major element concentrations (e.g., **Fig. 3.10.A**), which had previously been attributed (Smith *et al.,* 2008) to the rapid ascent of magma from two sources. Rapid magma ascent is likely to prevent homogenization resulting in the eruption of geochemically heterogeneous melt batches. Molloy et al. (2009) and Needham et al. (2011) also noted this bimodality within some tephra horizons, and McGee et al. (2012) further confirmed evidence of multiple magma sources based on whole rock analysis. Gradational variations, seen within four of the tephra horizons, are defined here from analyses of multiple shards in a single primary tephra horizon that lie on an increasing or decreasing trend for certain major element combination plots (e.g., **Fig. 3.10.C**). These variations are more indicative of the effects of microscopic-scale fractional crystallisation of the tephra rather than the glass geochemical signature of the primary magma.

The major element (as oxide) concentrations of glass from some primary tephra horizons show considerable overlap and thus can yield ambiguities in fingerprinting and correlation. This limitation is overcome by the use of trace elements whose concentrations are much more strongly affected by processes pertaining to the genesis and evolution of magmas (partial melting, fractional crystallisation and magma mixing/mingling). Selected trace element combinations are therefore used to: 1) distinguish between two tephra horizons with similar major element geochemistry within a single core (**Fig. 3.10.B**), and 2) constrain better the geochemical composition of a tephra horizon (**Fig. 3.10.A and C**). Incompatible trace elements and trace element ratios (e.g. La, Gd, Nb, and La/Yb, Gd/Yb, Zr/Gd) are used here for two key reasons: 1) they are the least susceptible to the effects of fractional crystallisation; and 2) they are most sensitive to mantle source processes. Some elements, especially most major elements (e.g. Mg, Si, Al, Ca) are affected by fractional crystallisation, and therefore their concentrations are controlled by the growth of microcrysts, rather than the magma batch's residual melt. These elements are therefore not useful in fingerprinting individual tephra deposits and are avoided.

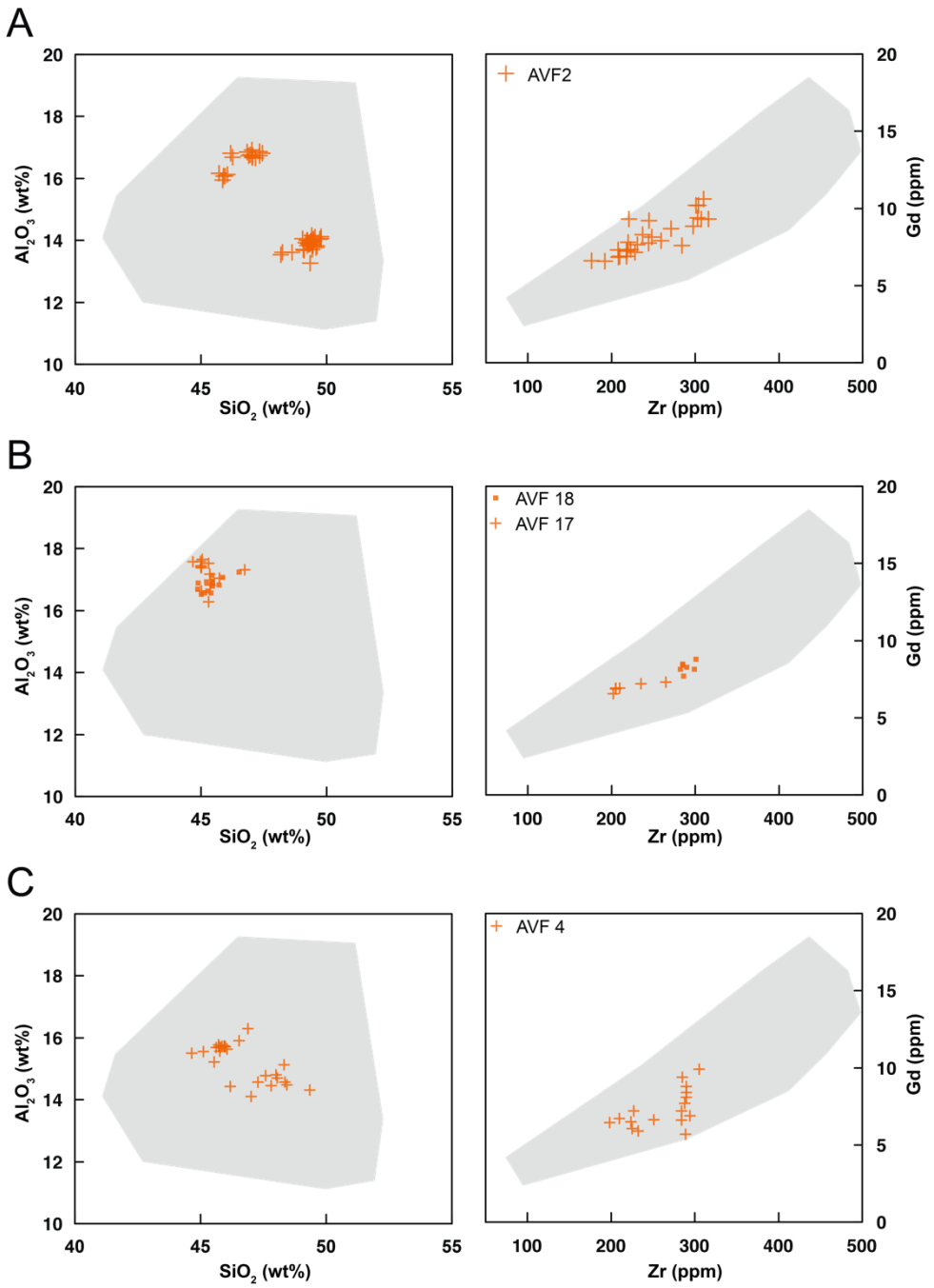

Figure 3.10. *Examples of the resolution of some major element (as oxides) ambiguities using trace element concentrations in glass shards extracted from the AVF tephra horizons. The shaded region indicates the total ranges for SiO_2 vs. Al_2O_3 (wt. %) and Zr vs. Gd (ppm) for shards from selected primary tephra horizons from the Orakei Basin core sequence. (A) A bimodal distribution in major element signature for a single horizon (AVF 2) narrows to a more homogeneous signature in trace element concentrations. B) Two contiguous primary tephra horizons (AVF 17 and 18) are indistinguishable on the basis of selected major elements (as oxides), but are distinguished by trace element concentrations. C) Gradational variation in major element signature for a single primary tephra horizon, attributed to effects of crystal removal, narrowed to a more homogeneous signature by trace elements.*

The trace elements chosen (e.g. La, Gd, Nb, Zr, Nd, Yb) are incompatible, and therefore will have similar concentrations in both pure glass and glass that includes microcrysts. In turn, ratios of these elements will be identical because any enrichment in the glass will be the same for both elements. These elements and ratios are also the most sensitive to mantle source processes and are therefore the most likely to be unique for individual magma batches and hence eruption centres. **Figure 3.10** demonstrate that, for example, Zr vs. Gd better constrains the horizon's chemical fingerprint than do major element concentrations. This improved trace element fingerprinting is essential when attempting to correlate the horizons between cores to help ensure an accurate match. For example, **Fig. 3.10.B**, shows horizons AVF18 and AVF17, which are indistinguishable with major elements but can be distinguished by their trace element composition.

3.5.4. Cross-core correlation of individual tephra horizons

The basaltic tephra horizons found within the cores from across the AVF display a wide range of compositional diversity (**sect. 3.4.2.**), some of which show indistinguishable major element compositions. Here, trace elements are invaluable for providing a geochemically more distinct fingerprint for the individual horizons as noted above. Trace element compositions are not only useful to resolve both the relationship of complex deposits within the cores (e.g. primary vs. reworked deposits), but also provide the ability to more uniquely fingerprint individual horizons.

Cross-core correlations of AVF basaltic tephras for six cores are shown in **Figure 3.11** and details are outlined in **Table 3.2**. For the first time, horizons from Pukaki, Onepoto, and Glover Park cores are inter-correlated with pre-existing 'AVF#' classification originally proposed by Molloy et al. (2009) resulting in 14 well constrained cross correlated chronostratigraphic marker tephras, and another 15 tephras that were only found within one core. Previous correlations are enhanced and the ambiguity is reduced through trace element fingerprinting. For example, the newly assigned AVF10 in the Orakei Basin core was previously assigned to AVF9. The geochemistry (and

location of the tephra) suggests it is more appropriately correlated to AVF10 within Onepoto and Pupuke cores. The addition of the Glover Park and Onepoto cores into the correlation suite extends the stratigraphy back from AVF1 (Molloy *et al.,* 2009), with the new horizons here named AVFa, AVFb, and AVFc down core. Although much of the Glover Park core is affected by soft sediment deformation and reworking, our glass-based geochemical analyses have allowed recognition of these stratigraphic interrelationships, and helped to resolve of the complex relationships of the tephra deposits. Through our geochemical analysis AVF1 is now correlated from the Orakei Basin core into Onepoto and Glover Park cores as well: AVFa is only found in Glover Park, AVFb is correlated between Onepoto and Glover Park, and AVFc is only found in Onepoto.

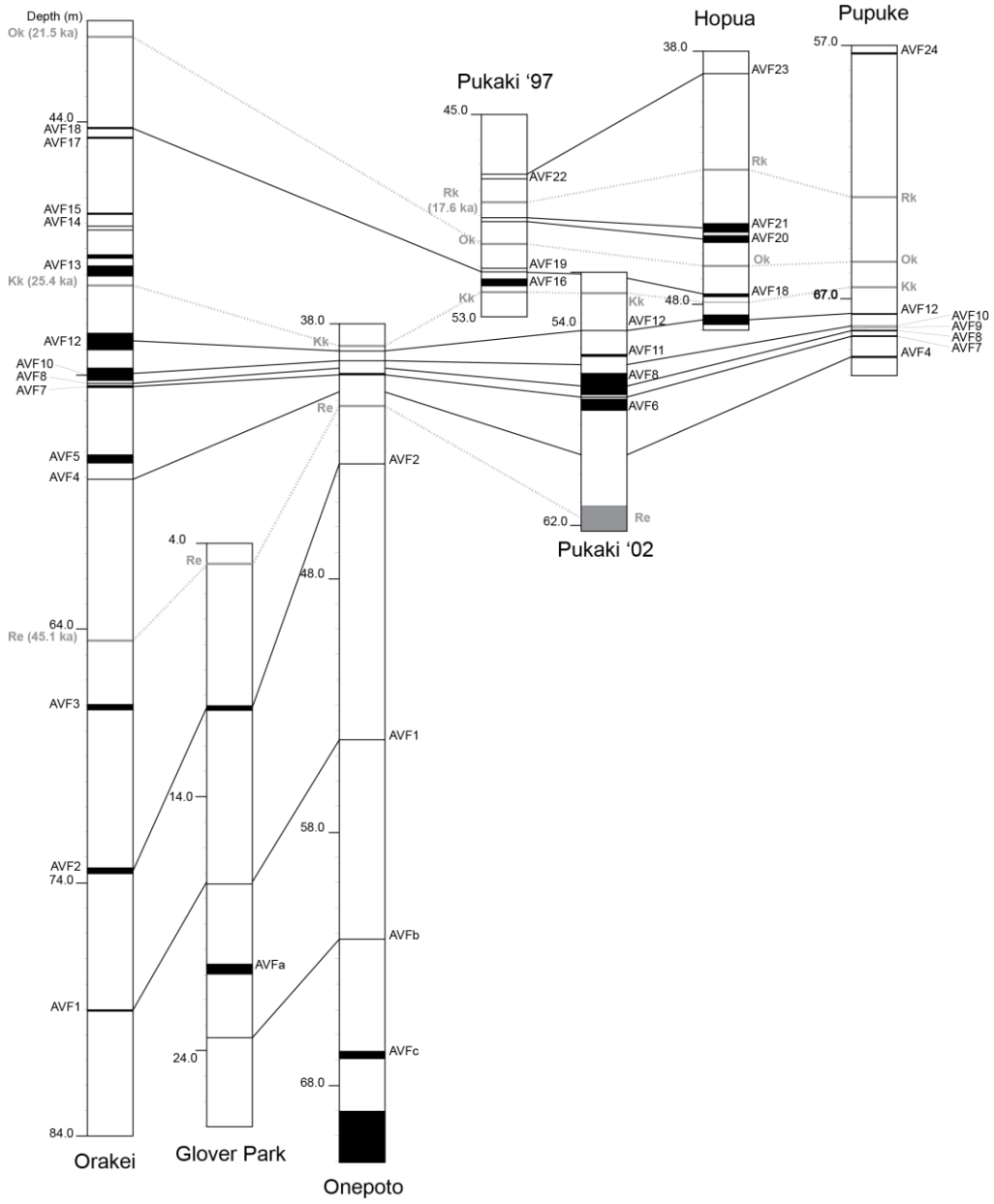

Figure 3.11. *Stratigraphic columns depicting the new correlations of tephra horizons for the six maar cores. Basaltic tephras are in black and rhyolitic marker horizons shown in grey (Rk-Rerewhakaaitu, Ok-Okareka, Kk-Kawakawa/Oranui, Re-Rotoehu)*

Table 3.2 (below). *Summary of the tephra horizons identified and analysed, with newly defined primary tephra horizon thickness and new tephra horizon names. Also included are previous horizon names and references where applicable. Samples from Orakei Basin, Glover Park, and Onepoto were collected for this study. For Pupuke and Hopua, the original samples mounted and picked by Molloy et al. (2009) were re-analysed with sample depth, thickness and sample name maintained, and for Pukaki, post-Rotoehu data were obtained from Sandiford et al. (2001), and pre-Rotoehu data were obtained from P. Shane (pers. comms, 2014). Horizon depths stated in the table are reported to the nearest centimetre and define the base of the primary horizon.*

Core	Sample name	New horizon#	Depth (m)	Thickness (mm)	Previous horizon#	Ref for previous horizon #
Post Rerewhakaaitu (< 17.5 ka)						
Pupuke	T21-1-48/58929	24	57.895	22	24	Molloy *et al.*, 2009
Hopua	T4-2-H1-2/58839	23	38.945	3	23	Molloy *et al.*, 2009
Pukaki	T14 47.72m	22	47.72	1.0	T14	Sandiford *et al.*, 2001
Rerewhakaaitu to Okareka (17.5-21.5 ka)						
Pukaki	AT209 49.15m	21	49.15	3.0	AT209	Sandiford *et al.*, 2001
Hopua	T5-2-H1-18/58855(-58856)	21	45.17	290	20	Molloy *et al.*, 2009
Pukaki	AT210 49.17m	20	49.17	2.0	AT210	Sandiford *et al.*, 2001
Hopua	T6-5-H1-20/58857(-58858)	20	45.505	235	21	Molloy *et al.*, 2009
Okareka to Kawakawa/Oruanui (21.5-25.4 ka)						
Pukaki	T43 51.05	19	51.05	1.0	T43	Sandiford *et al.*, 2001
Orakei Basin	OB1.#30-4-44.22	18	44.22	8	18	Molloy *et al.*, 2009
Hopua	T5-6-H1-32-58869	18	47.81	40	18	Molloy *et al.*, 2009
Pukaki	T45 51.19	18	51.19	0.5	T45	Sandiford *et al.*, 2001
Orakei Basin	OB1.#30-6-44.652(-44.654)	17	44.654	5	17	Molloy *et al.*, 2009
Pukaki	T42/45 51.52	16	51.52	50.0	T42	Sandiford *et al.*, 2001
Orakei Basin	OB1.#30-6-47.715	15	47.715	12	15	Molloy *et al.*, 2009
Orakei Basin	OB1.#33-2-48.12(-48.128)	14	48.128	12	14	Molloy *et al.*, 2009
Orakei Basin	OB1.#33-2-48.19(-48.276)	newB	48.276	10	-	
Orakei Basin	OB1.#33-4-49.14(-49.46)	newA	49.46	45	-	
Orakei Basin	OB1.#34-3-50.089(-49.554)	13	50.089	160	13	Molloy *et al.*, 2009
Oruanui to Rotoehu (25.4-45.1 ka)						
Orakei Basin	OB1.#36-2-52.817(-53.029)	12	53.029	410	12	Molloy *et al.*, 2009
Onepoto	On2.#4-39.06	12	36.1	12	121	Shane and Hoverd 2002
Pukaki	54.355m	12	54.355	-	12	Shane Unpublished
Pupuke	P23/58947	12	67.59	7	12	Molloy *et al.*, 2009
Hopua	T6-3-H1-39/58876	12	48.8	460	12	Molloy *et al.*, 2009
Pukaki	c. 55.355m	11	55.335	-	11	Shane Unpublished
Orakei Basin	OB1.#37-2-54.119(-54.213)	10	54.213	407	9	Molloy *et al.*, 2009
Onepoto	On2.#4-39.47	10	39.5	15	116/115	Shane and Hoverd 2002
Pupuke	T18-7-P26/58951	10	68.09	3	10	Molloy *et al.*, 2009
Pupuke	P27/58952	9	68.15	6	9	Molloy *et al.*, 2009
Orakei Basin	OB1.#37-2-54.27	8	54.27	45	8	Molloy *et al.*, 2009
Pupuke	P28/58953	8	68.24	20	8	Molloy *et al.*, 2009
Pukaki	ca. 56.87	8	56.4	ca. 720	8	Shane Unpublished
Orakei Basin	OB1.#37-2-54.324 (AVF7)	7	54.34	20	7	Molloy et al., 2009
Onepoto	On2.#4-39.905(-39.914)	7	39.9	20	114	Shane and Hoverd 2002
Pukaki	c. 56.8	7	56.9	-	7	Shane Unpublished
Pupuke	T19-3-P29/58954	7	68.485	2	7	Molloy *et al.*, 2009
Pukaki	c.57.0	6	57.1	c.a. 500	6	Shane Unpublished
Orakei Basin	OB1.#39-3-57.342(-57.44)	5	57.342	110	5	Molloy et al., 2009
Orakei Basin	OB1.#39-5-58.11(-58.07)	4	58.11	41	4	Molloy et al., 2009
Pupuke	P33/58960	4	69.315	15	4	Molloy *et al.*, 2009
Pre Rotoehu 45.1 ka						
Orakei Basin	OB1.#45-5-67.039(-61.17)	3	67.039	41	3	Molloy et al., 2009
Orakei Basin	OB1.#50-2-73.555	2	73.555	510	2	Molloy et al., 2009
Glover Park	GP6-8-10.38(-10.6)	2	10.6	60	GP1/6-8	Hoverd *et al.*, 2005
Onepoto	On2.#6-2-43.66	2	43.7	4	90	Shane and Hoverd 2002
Orakei Basin	OB1.#54-3-80.047	1	80.047	100	1	Molloy et al., 2009
Onepoto	AB1-On2-#11-51.30	1	51.3	15	-	Shane and Hoverd 2002
Glover Park	GP16-17.52(&18.15)	1	18.15	12	GP1/20-18	Hoverd *et al.*, 2005
Glover Park	GP1/24 - 20.78-21.0	a	21.0	40	GP1/24	Hoverd *et al.*, 2005
Onepoto	On2.#18-62.36	b	62.0	45	7	Shane and Hoverd 2002
Glover Park	GP1/40 - 23.67	b	23.67	10	GP1/40	Hoverd *et al.*, 2005
Onepoto	On2.#21-66.68	c	66.7	270	1	Shane and Hoverd 2002

3.5.5. Tephra dispersal and thickness

As a result of correlations of the AVF tephra horizons between the maar cores, revised thicknesses and radii of tephra dispersions patterns can be inferred. Lacustrine tephra deposits will have a higher compaction rate than their on-land counterparts (e.g. on-land the tephra are a factor of about 1.75 thicker; Lowe, 1988a). Therefore the newly identified primary tephra horizon thicknesses represent minimum values (e.g. Óladóttir *et al.,* 2012), which may be significant for on-land isopach mapping, or hazard assessment.

For correlated horizons, relative tephra thicknesses are variable. For example, tephra horizons found in the maar cores at the outer limits of the field (e.g. Onepoto, Pukaki and Pupuke) were consistently thinner than those found in the central cores (e.g. Orakei and Hopua). The thicker deposits (>100 mm) are more common within the central cores, which likely reflects the higher density of eruptive centres in close proximity. However, thick deposits are not found exclusively in the central maars; for example, Pukaki core has multiple thick deposits (e.g. AVF6 ca. 500 mm thick) that are linked to eruptions from nearby sources (Sandiford *et al.,* 2001).

The preservation potential of tephra horizons, and thus the completeness of the tephra record, can be assessed based on a number of factors, including the total number of individual tephra horizons found in relation to the number of eruptions within the time period covered by the maars, and the number of deposits found along a dispersal pathway. Although currently the age ranges of the maar cores are quite poorly chronologically constrained, they have been estimated to range from >150 ka (Onepoto; Lindsay *et al.,* 2011) to present (Pupuke). Based on the modelled values from Bebbington and Cronin (2011) there is estimated to have been ca. 42 eruptions within this time period, with a “flare up” noted at 40-20 ka (Molloy *et al.,* 2009; Bebbington and Cronin, 2011). The tephra deposits within the cores do reflect this period of increased activity, although the total number of individual horizons found within the cores only total 28. One or more of the following factors can explain the absence of individual tephra horizons in some cores: (1) the eruption was not dispersed widely enough; (2) poor preservation at the specific maar site linked with smaller quantities of tephra;

(3) dispersal direction of tephra did not coincide with a maar. Fifteen of the primary tephra deposits identified are only found in one core and very few (n=5) of the correlated deposits appear in all of the cores studied, indicating that, for a single eruptive event, the pyroclastic material does not necessarily cover the entire field area. A number of correlations link tephra horizons to restricted areas of the field, and a number of field observations show tephra dispersal away from the directions of the maar sites (e.g. Green Mt; Hayward e*t al.,* 2011), suggesting field scale limits to the tephra dispersal. These limitations are attributed to the small eruptive volumes and eruption ash column heights, and the impact of wind direction of the AVF centres (e.g. Lowe, 1988a, b; Shane, 2005).

In some cases deposits are not necessarily found in all maars along a dispersal pathway. For example, two tephra horizons are linked to Orakei and Pupuke but are not found in Onepoto, which is located geographically between the two. These dispersal patterns are most likely indicative of either discontinuous preservation and/or complex diffuse distal fall out (Molloy *et al.,* 2009). For more distal sites, where tephra thicknesses are minimal (1-2 mm), preservation potential through water columns is highly reduced, resulting in differential settling of tephra and thus in many cases discontinuous deposition (Beierle and Bond, 2002).

3.5.6. Sedimentation rates

As tephras are considered to represent instantaneous events (Shane, 2000), to calculate sedimentation rates their thicknesses are subtracted from the core thickness constrained by marker horizons with accurately documented ages. The thicknesses of the remaining lacustrine sediments, assumed to have accumulated at constant sedimentation rates between data points, are then divided by the number of years between the rhyolitic marker horizons to yield the sedimentation rate for the maar (e.g. in Orakei Basin, the sediment between Okareka and Kawakawa has a mean sedimentation rate of 1.96 mm/yr; Molloy *et al.,* 2009). The reduction of thickness of primary deposits – now identified as being reworked - not only has implications for

primary deposits, but also may affect calculated sedimentation rates and thus modelling for estimated eruption ages, frequency rates and source centre correlations. Bebbington and Cronin (2011) and Green et al. (2014) use previously published (Molloy *et al.,* 2009) horizon thicknesses and correlations as inputs into horizon age, source centre modelling and thus source centre age estimates. Our study will allow more accurate data input into the models, with improved horizon correlation and horizon thickness estimates, thus supporting and improving future statistical modelling for the AVF eruption frequencies and centre ages. Future statistical analysis will also help to corroborate the tephra correlation and identification made in our study.

3.6. Conclusions

The use of multiple analytical techniques is critical to produce a high-resolution correlation of basaltic tephras within sediment cores. X-ray density scanning not only reveals the areas of high-density material (e.g. basaltic shards) within a core, but also is sensitive enough to indicate inherent intra-stratigraphic details that can be interpreted to reflect primary vs. re-worked deposits, grain shapes, grain sizes, and bedding features. Gradational grey scaling of the X-ray imagery is indicative of the proportions of shards within background sediment and in many cases shows the upward of basaltic shards that is also reflected in a decline in magnetic susceptibility. Provided that the background sediment is low in magnetic minerals, the magnetic susceptibility analysis is highly responsive to sub-millimetre scale basaltic tephra horizons, providing support to the inferences made from the X-ray imagery.

Reworking of tephra can occur through various means such as repetition of sedimentary processes or slumping of tephra-rich material. Evidence for this, shown by the X-ray and magnetic susceptibility analysis, is supported and enhanced by the complementary (for reworking) or contrasting (for primary deposition) glass-based geochemical signatures of the units. The combination of these methods allows a more detailed tephrostratigraphy to be constructed and resolution of ambiguities that arise from simple visual observations regarding the reworking and duplication of deposits.

Complexities observed with re-working have important implications for sedimentation rate calculations and therefore the evaluation of eruption spacing.

For the AVF tephras, the major element (as oxides) relationships of Al_2O_3 vs. SiO_2, MgO vs. CaO, and CaO vs. FeO are useful for correlation purposes, because they are the least variable for individual horizons but most variable for the field as a whole. In the cases where major element signatures are inadequate, incompatible trace elements (mainly REE) and trace element ratios (e.g. REE/Yb) from glass analyses are valuable for providing more distinctive signatures that can allow individual tephras to be distinguished. It is important to note that for the ca. 53 centres in the AVF, geochemistry is not diverse enough to be used alone as a definitive correlation tool, and the use of stratigraphy and well dated marker horizons provides important additional constraints in cross core correlations. When using these methodological improvements, 52 individual basaltic tephra deposits were identified from six cores from the AVF maars. Of these, fourteen horizons have been cross-correlated and another thirteen individual horizons identified, to provide a more robust tephrostratigraphic framework for the eruption evolution of the Auckland volcanic field.

Acknowledgements from published paper
JH is funded by the DEVORA (Determining VOlcanic Risk in Auckland) project, led by Jan Lindsay and Graham Leonard. We thank David Lowe and an anonymous reviewer for their constructive comments that helped to improve this manuscript. We also thank Richard Wysoczanski (NIWA) for helpful discussion on X-ray and probe analysis, Phil Shane for supplying unpublished tephra data from Pukaki core and helpful discussion, and University of Auckland Collections for supplying tephra mounts from Catherine Molloy's MSc thesis study. JH would also like to thank Elaine Smid and Shaun Eaves for aiding and assisting in transporting cores, Alan Orpin (NIWA) for discussion and assistance with core analysis and Malcolm Reid (UoO) for assistance with LA-ICP-MS analysis.

Preface to Chapter 4

In **Chapter 3** an eruptive history was constructed for the Auckland Volcanic Field by cross correlating tephra deposits between 6 lacustrine maar cores. Detailed geochemical analysis was undertaken on individual glass shards in order to fingerprint the chemical signature of individual horizons for correlation purposes. In building this tephrostratigraphic framework, the tephra dispersal and eruption frequency of the AVF was assessed. However, due to the high density of volcanic centres in the AVF, the source vent of each horizon remains unaddressed. Establishing a link between specific tephra horizons and their centre of origin is important as it allows consideration of the combined geochemical, spatial and temporal relationship within the AVF. It is therefore essential to develop a method that allows tracing tephra deposits back to their centre of origin.

Standard tephrostratigraphic protocols link distal tephra deposits to source using well-characterised proximal tephras (Lowe, 2011). However, due to the maritime climate and high urbanisation in the Auckland region, there are very few sub-aerial tephra deposits available that are exposed, and in fresh enough condition, for characterisation (c.f. **Chapter 1; sect. 1.5.2.**). In addition, the high spatial density of the centres in some cases prevents even proximal tephra deposits from being unambiguously matched to a given source centre.

It is potentially possible to use the geochemical signature of distal tephras to fingerprint their source centre. However, a prerequisite for this is to establish a comprehensive major- and trace-element tephra and whole rock database for all AVF centres. In order to allow comparisons and correlations to be made, in this chapter,I evaluate previous geochemical data for the Auckland centres, and present new major and trace element data for those centres that were un- or under-sampled prior to this research.

Chapter 4

An overview of the geochemistry of the AVF from new and existing major and trace element, and isotope data; foundation for the tephra-whole rock correlation principles

'Te Riri a Mataaho - Tāmaki Makaurau'

Inspired by Maori legend, the formation of the Auckland volcanoes through the wrath of Mataaho (image by Hopkins, J.L.).

4.1. Introduction

The Auckland Volcanic Field (AVF) is a world-renowned example of a small-scale basaltic monogenetic field, and as such the geochemistry has been extensively studied over the past thirty years. Previous studies have often focused on exploring the geochemical composition of a single centre, (e.g. Crater Hill; Smith *et al.,* 2008, Motukorea; McGee *et al.,* 2011, Rangitoto; Needham *et al.,* 2011) (**Table 4.1**.) or a selection of centres (e.g., n = 12; McGee *et al.,* 2013). To provide the most complete basis for tephra-source correlations (**Chapter 5**), a critical requirement is the existence of an extensive major and trace element database for *all* volcanic centres in the field, to which tephra-derived glass geochemical data can be compared. This chapter therefore present a major- and trace-element geochemical database including all existing whole-rock data from the AVF, complemented by new whole rock data from 24 centres which were previously un- (no analyses) or under-sampled (<3 trace element analyses).

Early studies by Heming and Barnet (1986) provided the first whole rock major element geochemical data. More recent studies have, however, provided more reliable and reproducible data, and therefore where possible the best quality data has been collated for this research. The most recent work of McGee (2012) significantly increased the amount of data in the geochemical database, through generating new major and trace element data for some previously under- or un-sampled centres, including Albert Park, Motukorea, Mt Eden, Mt Richmond, Mt Roskill, Mt Smart, Mt Wellington, Otara, Puketutu, Purchas Hill, Taylor's Hill, Waitomokia, and Wiri Mt. In addition, I couple this existing data set with multiple unpublished data sets (see Bryner (1991), Miller (1996), Franklin (1999), Hookway (2000), Spargo (2007), and Eade (2009)), and unpublished data from Ian Smith and co-workers (UoA and DEVORA). **Table 4.1** outlines the existing geochemical database, and the additional 99 samples for 24 centres added in this study. Prior to this study, 28 centres had three or more pre-existing major and trace element analyses, 15 centres had less than three, and ten had no data at all. Now, 46 of the 53 centres have three or more major and trace element whole rock analyses available.

4.2. Methods

4.2.1. Sample selection for geochemical analysis

Volcanic centres with less than three existing whole rock analyses were targeted for field sampling (field locations are listed in **Appendix A**). The seventeen new centres sampled for this study are Boggust Park, Little Rangitoto, Mt Albert, Mt Cambria, Mt Hobson, Mt Roskill, Mt Smart, Onepoto, Otuataua, Pigeon Mt, Pukaki, Pukeiti, Pupuke, Mt Robertson, St Heliers, Taylors Hill and Te Pou Hawaiki (highlighted orange on **Fig. 4.1**.). For an additional seven centres major element data exist (Miller, 1996), but no trace element data are reported. Thus, for these seven centres (highlighted yellow **Fig. 4.1**; Green Mt, Hampton Park, Mangere Mt, McLaughlins Mt, Mclennan Hills, Mt Victoria, and Otara) the samples collected by Miller (1996) were re-analysed for both major and trace elements. For six centres (Ash Hill, Kohuora, Mangere Lagoon, Styaks Swamp, Cemetery Hill, and Tank Farm; red on **Fig. 4.1.**) there are no longer exposures available (due to urbanisation and erosion) for sampling and therefore these centres have no available geochemical data.

4.2.2. Major element analysis

Whole rock samples were crushed to <15 mm in a Rocklabs Boyd crusher, then powdered using a Rocklabs tungsten-carbide TEMA swing mill at Victoria University of Wellington, Wellington, NZ (VUW). Powders were made into fused lithium metaborate glass discs and analysed for major element oxide concentrations at the Open University, Milton Keynes, UK using X-ray Fluorescence (XRF) analysis following the methods of Ramsey et al. (1995). Internal standards WS-E (Whin Sill Dolerite) and OU-3 (Nanhoron microgranite) were analysed to monitor precision and accuracy. Major element oxides were accurate to within 2.0% of the recommended values for the internal standards and analytical precision (2σ) was 1.5% or better for all elements (**Appendix B**).

Table 4.1. *Summary of geochemical data (pre-existing and additions from this study) ordered by the number of analyses, including those centres without any current data; of 50 centres 3 or more data points were achieved for 44 volcanoes.*

	Pre-existing data (≤ 2013)				This thesis		
Centre	Major	Trace	Isotope	References	Major	Trace	Isotope
CRATER HILL	61	61	0	Smith *et al.,* 2008			
RANGITOTO	55	55	7	Hookway, 2000; Needham *et al.,* 2011	2	2	3 (Os, Pb)
MOTUKOREA	53	53	16	Bryner, 1991; McGee, 2012, McGee *et al.,* 2012			
PUPUKE	51	51	4	Spargo, 2007	1	1	2 (Os, Pb)
ORAKEI	41	21	0	Franklin, 1999; Smith unpub data			
THREE KINGS	36	35	2	Eade, 2009; Smith unpub data			
MT WELLINGTON	34	34	8	McGee, 2012, McGee *et al.,* 2013		2	2 (Os, Pb)
MT EDEN	29	17	1	Eade, 2009; McGee, 2012			
PURCHAS HILL	27	27	6	McGee 2012; McGee *et al.,* 2013			2 (Os, Pb)
MAUNGATAKETAKE	23	23	0	Smith unpub data			
PUKETUTU	23	13	3	Miller, 1996; McGee, 2012		2	
LITTLE RANGITOTO	17	1	0	Franklin, 1999; Smith unpub data	6	6	
MT ST JOHN	22	13	0	Franklin, 1999; Eade, 2009			
PANMURE BASIN	22	21	0	Smith unpub data			
DOMAIN	19	7	0	Smith unpub data			
TE POU HAWAIKI	13	0	0	Franklin, 1999	5	5	
MT HOBSON	10	2	0	Smith unpub data	5	5	
OTARA	12	0	2	Miller, 1996; McGee, 2012		5	
WIRI	12	12	2	McGee, 2012; McGee *et al.,* 2013			2 (Os, Pb)
GRAFTON PARK	10	10	0	DEVORA group unpub data			
WAITOMOKIA	9	9	0	McGee, 2012			
MT ROSKILL	3	2	0	McGee, 2012	6	6	
TAYLOR'S HILL	3	3	2	McGee, 2012; Smith unpub data	6	6	
ONE TREE HILL	8	4	0	Eade, 2009; Smith unpub data			
MT SMART	2	2	0	McGee, 2012; Smith unpub data	6	6	
MANGERE MT	7	2	0	Miller, 1996		3	
MCLENNAN HILLS	6	3	0	Miller, 1996		3	
MT RICHMOND	6	3	2	Eade, 2009; McGee, 2012; Smith unpub data			
NORTH HEAD	6	5	0	Smith unpub data			
PUKAKI	2	2	0	Zawalna-Geer, 2012	4	4	
MCLAUGHLINS HILL	1	0	0	Heming unpub data	5	5	
MT CAMBRIA	1	1	0	Smith unpub data	5	5	
OTUATAUA	1	1	0	Heming unpub data	5	5	
PIGEON MT	1	1	0	Smith unpub data	5	5	
PUKEITI	1	1	0	Smith unpub data	4	4	
ALBERT PARK	4	4	0	McGee, 2012; Smith unpub data			
HAMPTON PARK	4	0	0	Miller, 1996		4	
MT VICTORIA	4	2	0	Smith unpub data		1	
PUKEKIWIRIKI	4	3	0	Smith unpub data			
ROBERTSON HILL	0	0	0		4	4	
GREEN HILL	3	1	0	Miller, 1996		2	
MT ALBERT	2	4	0	Smith unpub data	1	1	
ST HELIERS	1	1	0	Smith unpub data	2	2	
BOGGUST PARK	0	0	0		3	3	
ONEPOTO	0	0	0		2	2	
HOPUA	1	1	0	Smith unpub data	Surface exposure no longer in existence		
ASH HILL	0	0	0		Surface exposure no longer in existence		
CEMETERY HILL	0	0	0		newly identified centre		
KOHUORA	0	0	0		Surface exposure no longer in existence		
MANGERE LAGOON	0	0	0				
PUHINUI CRATERS	0	0	0		newly identified centre		
STYAKS SWAMP	0	0	0		Surface exposure no longer in existence		
TANK FARM	0	0	0		Surface exposure no longer in existence		
TOTALS	**650**	**511**	**55**		**72**	**99**	**11**

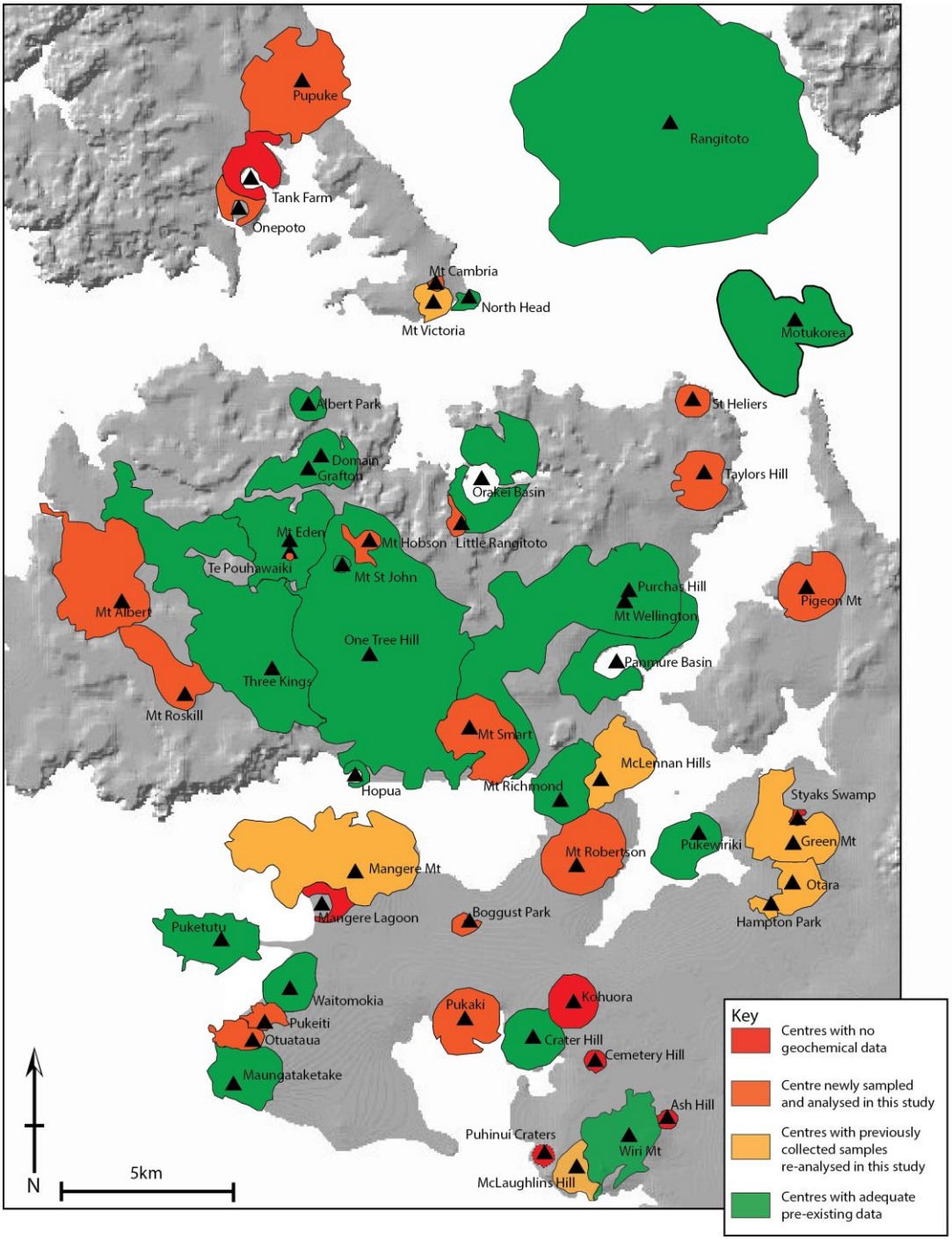

***Figure 4.1**. Location map for the centres of the AVF outlining the amount of geochemical data available for each centre. Prior to this study those in green (n=23) had an adequate number (>3) analyses. Those in orange did not have an adequate number of analyses and so were analysed for major and trace element by this study; the dark orange show centres sampled in the field by this study (n=17, field sites detailed in **Appendix A**), the light orange show centres with existing whole rocks with only major element analysis (n=7, Miller, 1996) that were re-analysed for major and trace elements for this study. Those in red (n=6), have no available data and currently no exposure available to sample, Puhinui Craters has a dashed outline because the extent of this centre is currently undefined (B. Hayward pers. comm. 2014).*

4.2.3. Trace element analysis

For trace element analysis, 50mg of whole rock powder was treated using conventional methods (details in **Chapter 2**) of HF-HNO_3 digestion and analysed on an Agilent 7500CS ICP-MS (VUW) in solution mode. Trace element abundances were calculated using the reduction program Iolite (Paton *et al.,* 2011), using BHVO-2 as a bracketing standard, and BCR-2 as a normalisation standard. ^{43}Ca was used as an internal standard using CaO contents measured by XRF. Trace element analyses were accurate to within <6% of the recommended values for the secondary standard (BCR-2) and precision (2 σ) was <6.5 % with the exceptions of Cr ±10.4 %, Nb ±22 %, Cs ±12.2 %, Ba ±11.8 %, Ta ±20.9 % and Pb ±31 % (**Appendix B**).

4.3. Results

This study adds 99 individual whole rock major and trace element analyses for 24 centres (previously under or un-sample) to the AVF database, increasing the number of centres with major and trace element data available from 28 to 46 out of 53. Representative values for each of the new centres are shown in **Table 4.2**, with all new data given in **Appendix C**.

4.3.1. Major Elements

All analysed samples range from basanitic/nephelenitic to basaltic in composition (based on the rock classification of LeMaitre, 2002) with SiO_2 values ranging from 39 - 49 wt.% and MgO contents ranging from 6 - 16 wt.% (Mg# = 50-72) (**Fig. 4.2**.).

Overall, the new data show a positive relationship between MgO vs. CaO, and a negative relationship between MgO vs. Al_2O_3. There are less distinct, but generally negative trends, for MgO vs. SiO_2, TiO_2, $Fe_2O_3^{tot}$, and P_2O_5, and for these elements, a higher range in compositional variation is recorded within a single centre's data, than observed for MgO vs. CaO and Al_2O_3. For example for MgO vs. TiO_2, the Taylors Hill data show a flat trend where MgO variations but no TiO_2 variation, but in comparison the Pukaki samples show minimal variation in MgO content but have a larger variation in TiO_2. In general, data plotted from individual centres (**Fig. 4.3**.) show clustered signatures that mimic the general trend but often show their own

specific, separate trend lines, consistent with the findings of McGee et al. (2013). Representative values from this study for the newley sampled centres, and extreme values representing the AVF endmember compositions from McGee et al. (2013) (Rangitoto, Purchas Hill, and Motukorea) are outlined in **Table 4.2**, for comparison all pre-existing values are also plotted on all figures.

Table 4.2. *Selected representative results for new whole rock data suite. Major elements are reported as oxides in wt.%, trace elements in ppm. Additional representative data for the AVF geochemical endmembers, Rangitoto, Purchas Hill and Motukorea are taken from McGee et al. (2013) for comparison.*

Centre name	Boggust Park	Little Rangitoto	McLaughlins Hill	Mt Cambria	Mt Hobson	Mt Roskill	Mt Smart	Onepoto	Otuataua
Field Number	BgPk003	LilRa002	McLaH003	MtCam004	MtHob001	MtRos006	MtSm001	On002	Otua002
SiO_2	47.63	44.03	42.26	41.48	41.14	43.23	43.65	44.10	45.98
TiO_2	3.06	2.78	2.86	2.78	2.80	2.72	2.69	2.44	2.34
Al_2O_3	13.57	13.42	12.98	12.07	12.10	12.46	12.65	11.51	13.74
$Fe_2O_{3\ (total)}$	13.83	14.39	14.56	14.75	14.71	13.92	14.08	13.60	13.22
MnO	0.15	0.19	0.19	0.21	0.20	0.19	0.19	0.19	0.18
MgO	6.36	9.43	11.64	11.28	12.20	11.99	11.62	15.82	10.15
CaO	7.95	8.73	9.56	10.25	10.64	10.18	10.39	8.55	10.60
Na_2O	2.52	3.60	2.42	3.81	2.38	2.50	3.30	3.06	2.88
K_2O	1.13	1.67	0.99	1.32	0.67	1.25	1.34	1.12	0.89
P_2O_5	0.79	0.69	0.61	0.88	0.71	0.56	0.63	0.52	0.37
LOI	2.97	0.72	1.55	0.95	2.08	0.67	-0.17	-0.39	-0.10
Total	99.95	99.67	99.63	99.79	99.62	99.66	100.38	100.50	100.25
Sc	13.9	17.2	20.9	19.1	21.5	21.5	21.0	23.3	25.2
V	195	190	237	223	218	256	231	198	243
Cr	151	236	307	273	338	398	336	466	356
Ni	100	186	263	237	267	272	239	545	191
Rb	18.5	23.3	28.9	27.5	18.2	17.0	20.8	16.8	12.2
Sr	766	740	609	831	663	611	638	510	433
Y	21.5	21.7	20.4	25.1	22.7	20.0	21.3	20.8	20.2
Zr	322	274	214	269	236	212	206	184	145
Nb	69.7	60.9	44.9	65.5	56.9	44.5	53.3	35.3	33.4
Cs	0.38	0.22	1.03	0.48	0.69	0.24	0.33	0.23	0.25
Ba	422	273	267	378	357	233	274	216	170
La	45.5	38.8	35.1	59.7	49.3	33.7	37.2	29.1	21.0
Ce	99.0	81.9	69.4	114	93.9	68.1	73.6	57.0	43.4
Pr	11.2	9.29	8.38	12.6	10.64	8.10	8.59	6.73	5.29
Nd	44.2	37.1	33.8	49.5	41.9	32.4	34.4	27.2	22.7
Sm	8.59	7.34	6.83	9.47	8.15	6.61	6.99	5.55	5.09
Eu	2.76	2.42	2.27	3.04	2.63	2.16	2.26	1.86	1.74
Gd	7.97	7.02	6.62	8.89	7.72	6.46	6.82	5.61	5.13
Tb	0.98	0.92	0.87	1.13	0.99	0.85	0.89	0.77	0.75
Dy	4.92	4.68	4.47	5.56	5.03	4.47	4.68	4.15	4.19
Ho	0.81	0.79	0.76	0.93	0.83	0.77	0.81	0.77	0.75
Er	1.99	1.99	1.89	2.29	2.09	1.87	2.02	2.00	1.96
Tm	0.26	0.26	0.24	0.27	0.25	0.24	0.25	0.27	0.26
Yb	1.37	1.50	1.34	1.55	1.48	1.32	1.41	1.57	1.54
Lu	0.18	0.20	0.17	0.20	0.19	0.18	0.19	0.23	0.21
Hf	6.97	5.81	4.60	5.69	5.18	4.74	4.66	4.07	3.45
Ta	4.50	3.50	2.34	3.51	3.14	2.62	3.01	1.96	2.03
Pb	3.58	3.32	1.44	1.26	2.00	2.33	3.24	1.97	1.37
Th	5.42	4.14	3.98	6.97	5.46	3.77	4.41	3.39	2.52
U	1.23	1.37	1.20	1.94	1.45	1.10	1.28	1.00	0.69

Table 4.2 *continued.*

Centre name	Pigeon Mt	Pukeiti	Robertson Hill	St Heliers	Taylors Hill	Te Pou Hawaiki	Rangitoto	Purchas Hill	Motukorea
Field Number	PgMt004	Pkit004	RoHl003	StHel003	TaHi001	TePou005	Ra-AN-79	AVF-917	AVF-560
SiO_2	42.30	44.56	42.98	43.81	44.76	47.38	48.97	40.06	43.41
TiO_2	2.75	2.44	3.08	2.58	2.69	1.91	1.86	3.00	2.71
Al_2O_3	12.25	13.55	13.08	12.78	14.05	13.68	14.06	11.46	12.48
$Fe_2O_{3\ (total)}$	14.01	13.52	15.40	14.10	14.14	12.54	12.22	16.38	14.01
MnO	0.19	0.19	0.20	0.20	0.18	0.17	0.17	0.24	0.22
MgO	12.08	10.63	9.25	11.09	9.11	10.54	9.68	9.60	11.63
CaO	10.37	10.77	9.85	10.74	9.39	9.48	9.31	11.38	11.33
Na_2O	3.27	2.60	3.61	3.41	2.75	2.96	3.10	4.87	3.15
K_2O	1.41	0.79	1.63	1.32	1.04	0.73	0.62	1.88	1.50
P_2O_5	0.60	0.49	0.89	0.75	0.76	0.31	0.24	1.34	0.75
LOI	-0.18	0.56	0.51	-0.04	1.23	0.15	-0.42	0.10	0.97
Total	99.04	100.09	100.47	100.74	100.11	99.84	99.91	99.88	102.16
Sc	21.5	25.3	17.9	22.9	20.6	24.3	27.6	20.0	25.7
V	253	252	223	247	211	202	208	217	271
Cr	345	398	211	299	260	378	319	202	469
Ni	275	204	165	233	170	243	225	195	248
Rb	22.0	11.3	27.0	22.2	13.9	10.7	10.2	32.6	24.3
Sr	630	468	870	721	555	371	322	1213	784
Y	21.0	21.0	24.5	24.5	20.1	18.7	19.8	34.8	24.7
Zr	201	152	304	218	208	130	123	371	246
Nb	55.7	33.3	73.5	60.5	44.1	21.9	13.2	114	77.2
Cs	0.28	0.17	0.41	0.32	0.20	0.26	0.34	0.43	0.37
Ba	277	190	340	300	235	125	101	431	356
La	36.0	23.7	51.5	44.3	27.9	14.6	12.5	90	54.5
Ce	71.9	48.6	107	87.4	56.5	31.9	26.5	166	101
Pr	8.46	5.87	12.0	10.3	6.85	4.07	3.52	19.4	11.7
Nd	34.1	24.7	47.3	41.0	27.9	17.7	16.9	76.2	46.5
Sm	6.81	5.60	9.30	8.10	6.06	4.18	4.18	14.0	8.90
Eu	2.22	1.87	2.99	2.64	2.03	1.48	1.45	4.14	2.66
Gd	6.51	5.48	8.61	7.74	5.84	4.50	4.49	11.76	7.55
Tb	0.88	0.79	1.11	1.01	0.82	0.67	0.66	1.48	1.07
Dy	4.58	4.31	5.58	5.29	4.35	3.77	4.26	7.88	5.54
Ho	0.79	0.78	0.91	0.91	0.76	0.69	0.78	1.27	0.97
Er	1.91	1.99	2.17	2.22	1.90	1.83	2.09	2.87	2.45
Tm	0.24	0.26	0.28	0.29	0.25	0.25	0.31	0.35	0.30
Yb	1.36	1.55	1.45	1.63	1.42	1.50	1.87	1.91	1.82
Lu	0.18	0.21	0.19	0.22	0.18	0.21	0.26	0.23	0.24
Hf	4.57	3.61	6.42	4.83	4.62	3.11	3.18	8.5	5.13
Ta	3.08	1.96	3.98	3.17	2.49	1.30	0.94	7.63	5.40
Pb	2.02	1.56	3.69	3.16	2.07	1.78	2.40	5.95	6.23
Th	4.18	2.85	5.94	5.01	3.26	1.63	1.62	10.6	6.84
U	1.22	0.81	1.84	1.43	0.95	0.48	0.42	2.84	1.76

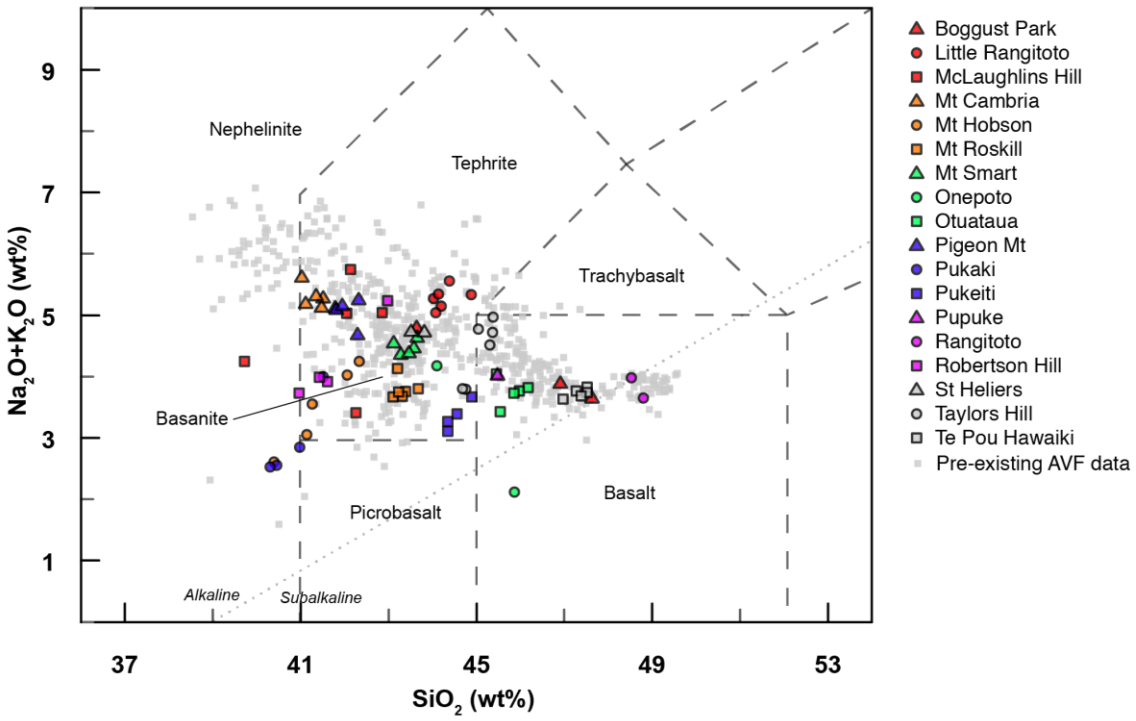

Figure 4.2.*Total-alkali vs. silica (TAS) diagram (after LeMaitre, 2002) to show the comparison between the existing database and the samples added by this study. Previous data plotted as grey outline (see references in text* ***sect. 4.1****.); new values plotted by colour for each centre (full data in* ***Appendix C****).*

For most major element concentrations the new data plot within the limits previously documented by McGee et al. (2013). However, a number of samples, from Boggust Park, Onepoto, and Pupuke, plot outside of the main field of AVF major element data (**Fig. 4.3**.). Samples from Onepoto and Pupuke have higher MgO (>14 wt.%), and lower CaO (<8 wt.%) and Al_2O_3 (<10 wt.%) contents compared to samples from other AVF centres. For the Boggust park samples, the element signatures are different to Onepoto and Pupuke, with low CaO concentrations (<8%), but coupled with very low MgO content (<8%) (**Fig. 4.3**.).

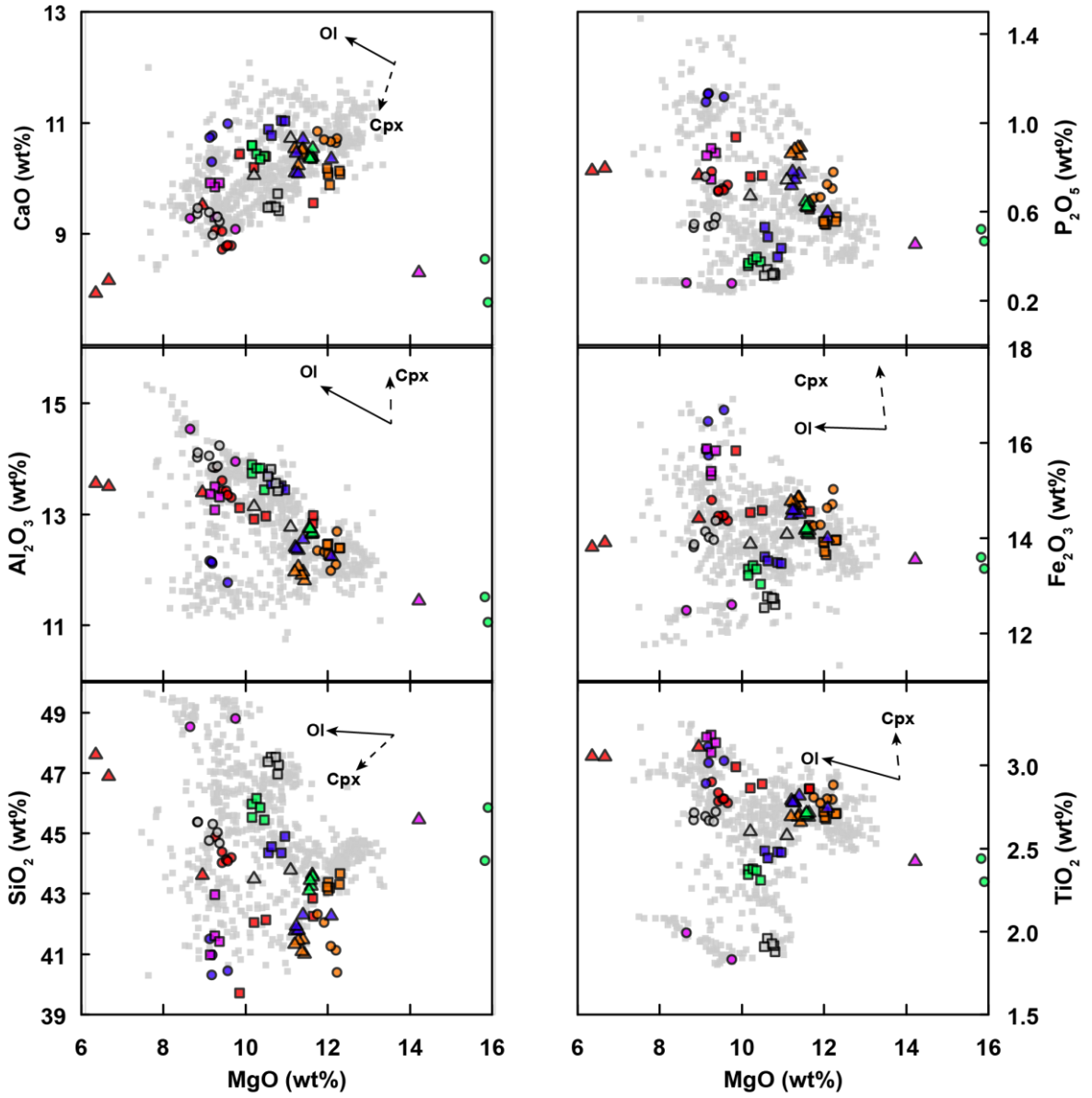

Figure 4.3. Multi-element variation diagrams (wt.%) for AVF volcanic rocks. New data plotted as coloured symbols and existing data plotted as grey symbols, see Figure 4.2 for key. Trajectory values from Needham et al., 2010 from individual mineral analysis on Rangitoto samples.

4.3.2. Trace Elements

The new analytical data in general exhibit large ranges for trace element concentrations, for example, La 10-90 ppm, Nb 10-80 ppm and Sr 300-1000 ppm. Similar to the major element relationships, the trace elements again show general trends for the field overall, as well as trends specific to each centre. There is a strong positive trend for MgO vs. Cr, and Sc, and for MgO vs. Th, Nb, Sr, and La there is a general negative trend of variable slope. Again no new extremes are observed, with all the new data sitting within the pre-existing data fields (**Fig. 4.4**.).

Primitive mantle-normalized trace element patterns are plotted for each centre (**Fig. 4.5**.), with all showing broadly similar patterns characterized by a peak at Nb and a negative slope to less incompatible elements, similar to Ocean Island Basalt (OIB). Some centres are less enriched in trace elements, and are characterised by a shallower REE pattern gradient. In contrast, other samples from more trace element-enriched centres have a relatively steep REE pattern gradient, and show a small trough at Zr-Hf. A positive Sr anomaly (>1; calculated as ($Sr_N/\sqrt{(Pr_N*Nd_N)}$), where elements are normalised ($_N$) to primitive mantle values after McDonough and Sun, 1995) is present in centres that are less enriched in trace elements, but absent in those that are more enriched (0.94-1.27). There is no significant Eu anomaly (calculated in the same manner as the Sr anomaly, in this case using Sm and Gd) for any centres (1.0-1.05), and for those centres without an Sr anomaly typically there is a negative K anomaly (0.93-0.19; calculated as previously outlined for Sr and Eu anomaly, but using Ta and La). There is a strong negative correlation exhibited between Sr anomaly vs. $(La/Sm)_N$ and Th/Yb, with values for $(La/Sm)_N$ ranging from 1.86 to 4.16 and Th/Yb values ranging from 0.87 to 5.61 (**Fig. 4.7**.).

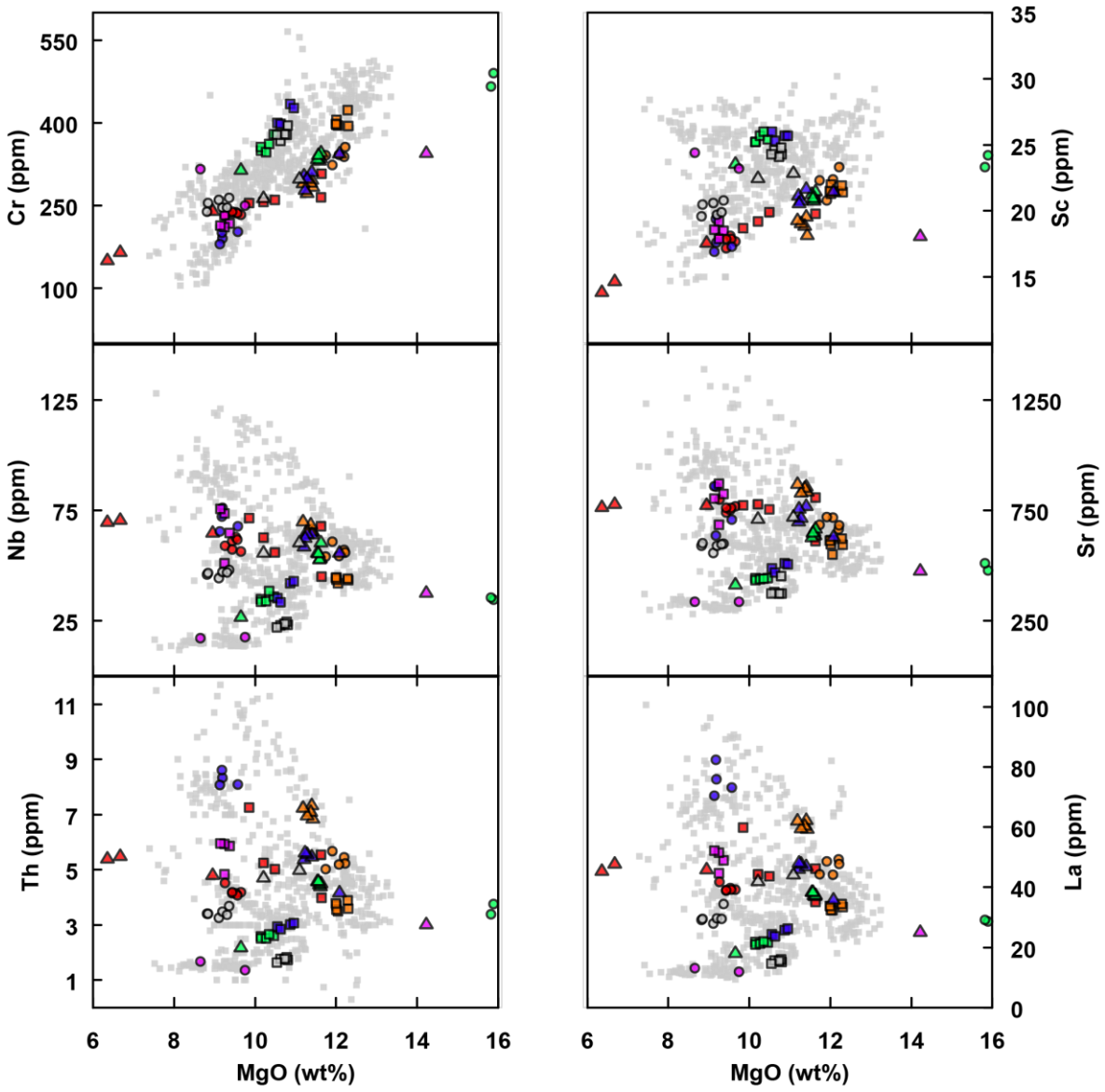

Figure 4.4. *Trace element multi-variation diagrams for AVF volcanic rocks. New data plotted as coloured symbols, outlined in the key for* ***Figure 4.2.*** *Existing data is plotted as grey symbols.*

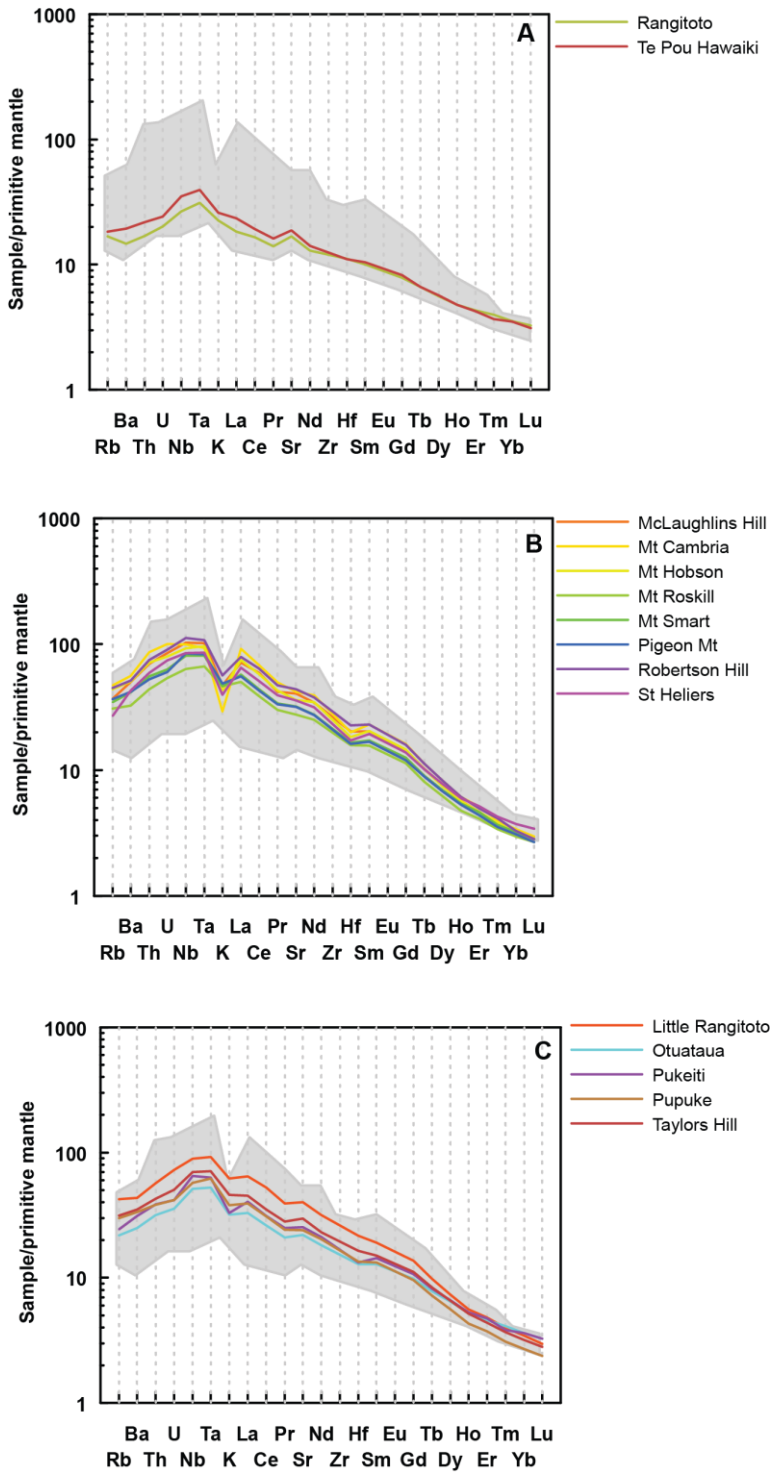

Figure 4.5. *Primitive mantle-normalised multi-element plots for newly analysed samples from the AVF. Pale grey field shows the total AVF database range with pre-existing Purchas Hill sample defining the upper limit, and Rangitoto sample defining the lower limit (from McGee et al., 2013). Normalisation values are from McDonough and Sun (1995). (A) Samples that exhibit a large Sr anomaly coupled with no K anomaly and a shallow REE pattern gradient. (B) Samples that exhibit no Sr anomaly, a large K anomaly, and a steep REE pattern gradient. (C) Samples with a small K anomaly and a small Sr anomaly.*

4.4. Discussion

4.4.1. Evaluation and comparison to previously obtained analyses

The database constructed for whole rock analysis contains data from multiple sources (McGee, 2012; Bryner, 1991; Miller, 1996; Franklin, 1999; Hookway, 2000; Spargo, 2007; Eade, 2009; Needham, 2009) and unpublished data from Ian Smith and co-workers (UoA and DEVORA)). All the previous major element analyses were run at University of Auckland using XRF analysis, and most trace elements were analysed by LA-ICP-MS at the Australian National University (ANU) using the mounts prepared for XRF analysis. Analyses of some trace elements from McGee et al. (2013) were run at Victoria University of Wellington using the same digestion methods and instruments that were used by this study (**section 4.2.3**). The only samples that have been discounted are those analysed by Heming and Barnet in the 1980s because they show a systematic offset in all elements suggesting an incompatibility of the data sets. In addition, the vast majority of these samples now have superseding analyses with much higher precision and accuracy (based on analyses of appropriate standards). A number of individual analyses (in Hookway, 2000; Spargo, 2007; and I.E.M. Smith *unpub.*) are obvious outliers affected by fractional crystallisation or olivine accumulation. This modification is also observed in the new samples: the signature of the Boggust Park samples (CaO and MgO <8 wt.%) is indicative of fractional crystallisation of olivine. However, this cannot explain the low CaO content seen in the Pupuke and Onepoto samples, which is here ascribed to olivine accumulation causing a dilution effect on the CaO content. The concentrations of these samples, and therefore the signatures that they give the centres, are not reflecting mantle source, but ascent processes, therefore these samples will not be used in the correlation process.

To maintain consistency with the previous data GEOReM values were used as reference values (**Appendix B**), and primitive mantle values from (McDonough and Sun 1995) were used for normalisation. To identify potential differences between the existing and our new datasets, ten samples from different centres previously analysed by McGee et al. (2013) and Eade (2009) were compared to new analyses of the same samples. **Figure 4.6** shows a representative selection of trace element comparisons for these data where previous analyses are plotted against the

corresponding samples analysed by this study. For most elements there is very little discrepancy between the two data sets. Concentration variations between the two data sets are observed in Cr, Ni, and Cs, and also for some of the HREE with very low concentrations Er, Tm, Yb and Lu. These differences are not significant (they overlap at 2sd% error) and confirm that the new data are comparable with the previously obtained analyses.

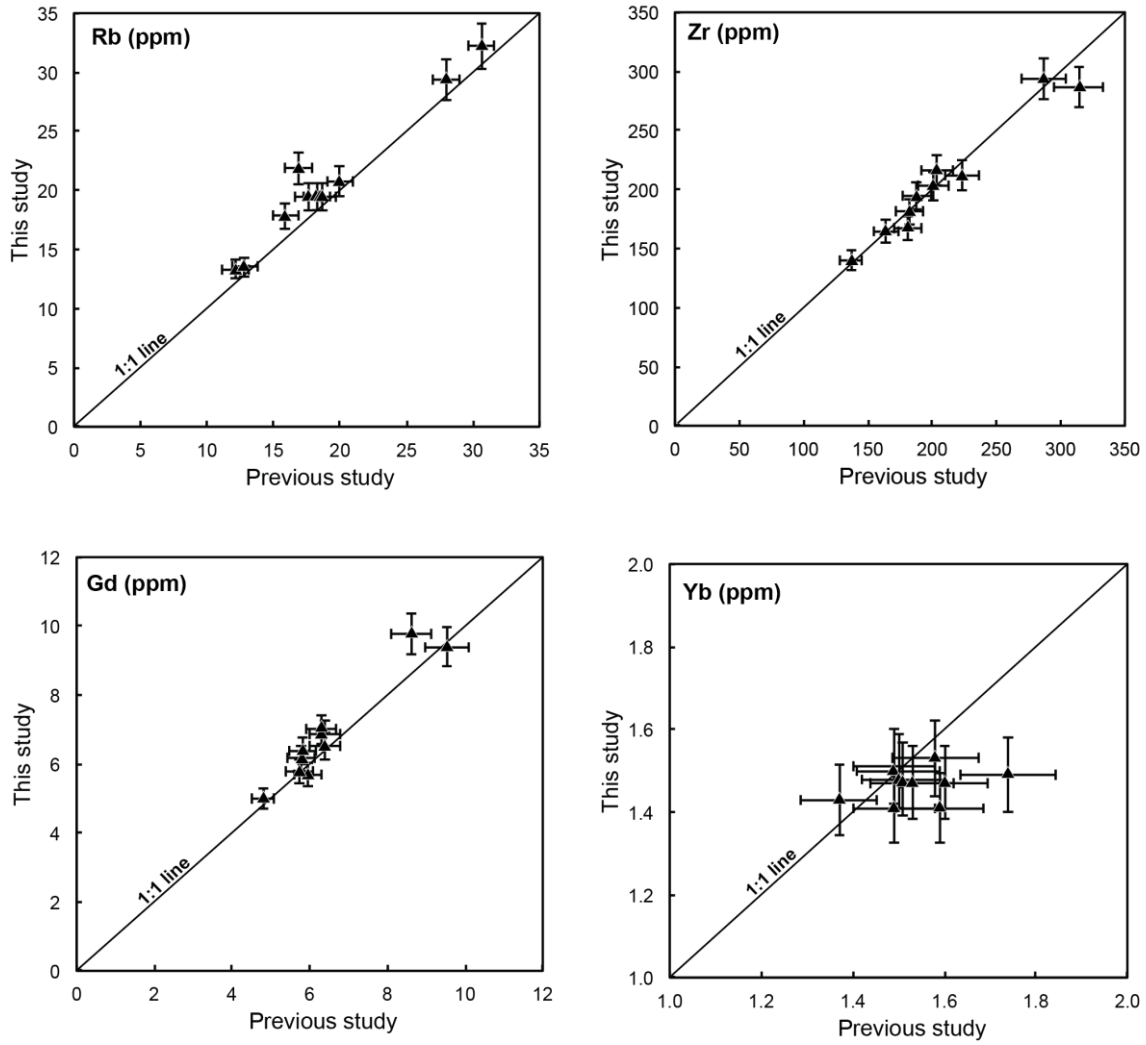

Figure 4.6. *Selected trace element duplicate analyses to compare whole rock sample analyses from this study to those presented in previous studies. The 1:1 relationship line is shown with most samples overlapping this line within 2sd% error.*

4.4.2. Geochemical variability intra-centre and field-wide

For the new data gathered, the intra-centre variability in geochemical signatures is much smaller than the field-wide variability. For example intra-centre variation for SiO_2 is <3 wt.%, for MgO <2 wt.%, and for all other major elements (TiO_2, Al_2O_3, $Fe_2O_3^{tot}$, P_2O_5, and CaO) <1.5 wt.%. In comparison the range for the field for SiO_2 is ≤10 wt.%, for MgO <8 wt.%, for Al_2O_3, $Fe_2O_3^{tot}$ <5 wt.%, for CaO <4 wt.% and for TiO_2 and P_2O_5 <2 wt.% (e.g. **Fig. 4.3.**). A number of intra-centre geochemical trends are noted: 1) minimal variation (e.g. <0.5 wt.%) across multiple samples, 2) ≤ 2 data points and therefore no trends can be identified and, 3) minor systematic variations in composition, which can be explained by fractional crystallisation.

Figure 4.3 shows the trajectories for fractional crystallisation of olivine (ol), clinopyroxene (cpx), and high-pressure clinopyroxene (cpx^{hiP}) (c.f. Deer *et al.,* 1992). Influences from Ti-augite and amphibole were discounted as their crystallisation trajectories fail to recreate any of the trends observed in the data. Although plagioclase is known to occur in very small proportions in the groundmass phases of the AVF lavas (e.g., Needham *et al.,* 2011), the general lack of an Eu anomaly or any large plagioclase phenocrysts, and the inability of plagioclase trajectories to recreate any of the trends observed, suggest that plagioclase does not play a major role (McGee *et al.,* 2013). Previous authors (Smith *et al.,* 2008; McGee *et al.,* 2013) have also suggested that high-pressure clinopyroxene can be used to explain a decreasing Al_2O_3 with decreasing MgO trend seen in other centres (e.g., Crater Hill, Mt Eden, Mt Wellington). This trend however, is not observed in the new data presented here (**Fig. 4.3**.).

The trends in geochemical data (**Fig. 4.3**.) exhibited for Little Rangitoto, Otuataua, Pigeon Mt, Mt Cambria, and Te Pou Hawaiki, can be explained by varying fractional crystallisation of olivine, with decreasing MgO and $Fe_2O_3^{tot}$ coupled with increasing SiO_2, Al_2O_3, and TiO_2. For McLaughlins Hill, these trends are also seen, but require minor amounts of clinopyroxene crystallisation also to form the decreasing SiO_2 and increasing $Fe_2O_3^{tot}$ with MgO. The trends in erupted material from Mt Hobson can be explained by clinopyroxene crystallisation, showing increasing Al_2O_3 and $Fe_2O_3^{tot}$ at consistent MgO content. This is also seen at Pukaki, coupled with a minor decrease in MgO suggesting that a minor amount of olivine

crystallisation is also present. Fractional crystallisation is not needed to explain the variations in centres that have tightly clustered data. These results are consistent with the conclusions in Smith et al. (2008) and McGee et al. (2013).

The within-field geochemical variability is much greater than the within-centre variability, and is responsible for the individual geochemical signatures associated with each centre. The within-field variation cannot be explained simply by modification of the magma from a single source by fractional crystallisation or crystal accumulation, and therefore multiple sources are inferred to be present.

The primitive mantle-normalised multi-element plots for the new data show that the new AVF samples have a range of trends between two end-members. At one end-member (e.g., Mt Cambria; **Fig. 4.5.B**.) there is a steep HREE trend showing a trough at Zr-Hf, and large negative K anomaly which becomes increasingly less pronounced to the other end-member, which exhibits a positive Sr anomaly, no K anomaly, a shallower HREE trend and no trough at Zr-Hf (e.g., Rangitoto; **Fig.4.5.A**).

Most centres show a relatively flat relationship between Sr anomaly and Zr/Nb, with a larger range in Sr anomaly values (0.47 to 1.15) in comparison to Zr/Nb (5 to 8) (**Fig. 4.7.**).Interestingly, Rangitoto and Te Pou Hawaiki show highly variable Zr/Nb values (5 to 8) for more restricted Sr anomaly values (1.22-1.28) in comparison to all other centres. Zr/Nb and $(La/Sm)_N$ ratios can be used to show depleted or enriched mantle sources (e.g., Haase and Devey, 1996; Kamber and Collerson, 2000), the signatures of these ratios are here attributed to mixing of melts generated from mantle sources that have seen variable amounts of melt extraction. Depleted sources show higher Zr/Nb, and higher positive Sr anomaly, and lower $(La/Sm)_N$ than fertile sources (Haase and Devey, 1996; Kamber and Collerson, 2000), indicating that samples that show a positive Sr anomaly originate from a mantle source with a history of previous melt depletion. In addition, the relationship between the Sr anomaly and $^{207}Pb/^{204}Pb$ and $^{87}Sr/^{86}Sr$ in the AVF rocks (c.f. McGee *et al.,* 2013) is consistent with a relationship between Sr anomaly and mantle source, rather than it being due to crystal fractionation or crustal contamination (McGee *et al.,* 2013).

The negative K anomaly observed in most samples is typical of OIB-type basalts (e.g., Sun and McDonough, 1989). The negative K anomaly and positive Sr anomaly have a positive correlation (**Fig. 4.7**.). A negative K anomaly (<1) is seen in a higher proportion of the samples than a positive Sr anomaly (>1). These anomalies are only mutually exclusive in the end-member samples, with most samples exhibiting evidence of both signatures (**Fig. 4.5**.). This is indicative of variable mixing between multiple mantle sources, with the dominant input from the source of the negative K anomaly. As previously outlined, the samples with a negative K anomaly also exhibit steeper HREE trend and lower Zr-Hf contents. The HREE and Zr-Hf are more compatible in garnet in comparison to the LREE and therefore they are preferentially retained in a garnet-bearing source, creating a relative depletion in these elements in melts that have garnet in their source.

The samples with a high positive Sr anomaly (and a small or no negative K anomaly) show a trough at Zr-Hf and have a shallower HREE trend, indicating their signature is not depleted in HREE or Zr-Hf, and therefore come from a source that does not contain garnet. Due to the stability of garnet in peridotite at depths of ≥80 km (e.g., McKenzie and O'Nions, 1991), it is possible to conclude that the geochemical variations exhibited by the AVF melts are linked to the source depth of the melt and the presence or absence of garnet. Based on the stability field of garnet, a garnet-bearing mantle must be found at depths of ≥80 km, and spinel bearing mantle found ≤80 km depth (McKenzie and O'Nions, 1991). McGee et al. (2013) split these zones into deeper garnet bearing 'asthenosphere' and overlying spinel-bearing 'lithosphere'.

These data are further and more extensively discussed in **Chapter 5 section 5.5.5,** with regards to the geochemical evolution of the field and source, and the relationship between chemistry and eruptive centre characteristics.

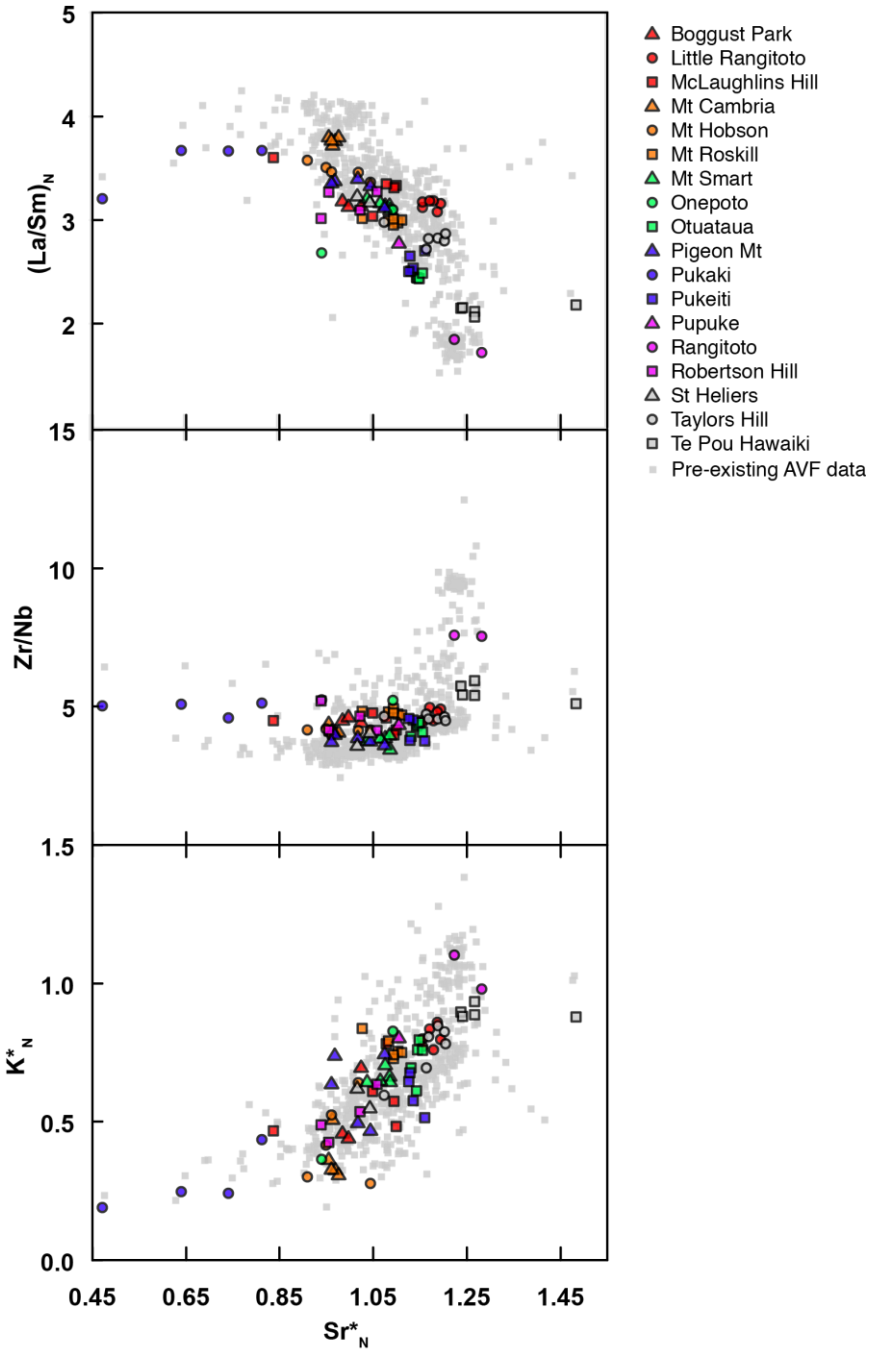

Figure 4.7. *Sr anomaly (Sr^*_N) vs. elements suggestive of varying source fertility and composition. The Sr anomaly is calculated as $Sr_N\sqrt{(Pr_N*Nd_N)}$, K anomaly is calculated as $K_N\sqrt{(Ta_N*La_N)}$, where $_N$ indicates normalisation to primitive mantle values after McDonough and Sun (1995).*

4.5. Conclusions

This study provides 99 new whole rock major and trace element analyses to the AVF database for previously un- or under-sampled centres (**Appendix C**). In doing this, the study gains more detailed insight into the whole rock signatures of the AVF as a whole. The results of this study support conclusions made by previous studies (McGee *et al.,* 2011; McGee *et al.,* 2012; McGee *et al.,* 2013; McGee *et al.,* 2015); minor intra-centre geochemical variability is related to the fractional crystallisation of olivine, coupled with minor amounts of clinopyroxene and potentially some high pressure clinopyroxene; the major intra-field geochemical variability relates to the mixing of three mantle sources, in varying proportions for each magma batch, to produce unique geochemical signatures for each centre. The individuality of each magma batch, coupled with the minor fractional crystallisation, facilitates the ability to geochemically fingerprint each centre. Thus further highlighting the potential to fingerprint each centre's products, and therefore correlate distal deposits back to source.

Preface to Chapter 5

Chapter 5 presents new methods developed to correlate distal tephra deposits to their source volcano. In order to achieve these correlations, the tephra-derived glass geochemistry and cross-core horizon correlations from **Chapter 3** are compared with previous and newly obtained whole rock geochemistry for the entire field (**Chapter 4**). These data are analysed to ascertain which geochemical signatures can be used to correlate between tephra and whole rock.

The results suggest that incompatible trace element ratios are the most variable in volcanic rocks from the Auckland Volcanic Field. These ratios are also the least affected by fractional crystallisation, and crystal removal, and are therefore considered to be the most appropriate tools for correlation. However, the volcanic rocks from all individual centres do not have a unique geochemistry in the field as a whole, to be successfully correlated purely based on these signatures. I therefore combine a number of criteria to further constrain the source centres for the horizons, resulting in proposed sourced centres for most of the tephra horizons identified.

Once the tephra horizons are correlated to their proposed source, and therefore stratigraphically constrained, I combine this tephrostratigraphic framework with Ar-Ar dated centres, and calculated sedimentation rate ages for the tephra horizons, to resolve the chronostratigraphy for 45 of the 53 centres in the field. I then use this newly constructed age order to comment on the spatial, temporal, and geochemical evolution of the AVF.

Chapter 5

The correlation of basaltic tephras to source volcanoes: Method development and implications for spatial, temporal and geochemical eruptive sequencing in the Auckland Volcanic Field, New Zealand

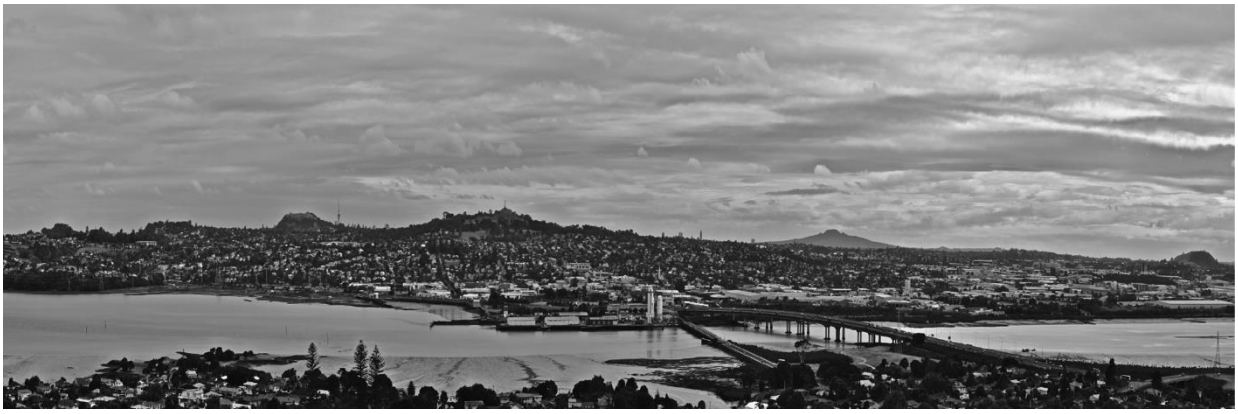

'Auckland - A city on volcanoes'

View from Mangere Mt to the north across the city, with volcanic scoria cones from left; Mt. Roskill, Three Kings, Mt. Eden, (Sky Tower), One Tree Hill, Rangitoto, Mt. Wellington, Hopua maar is located at the northern end of the bridge, and Mangere lava flows can be identified in the foreground to the left (image by Hopkins, J.L.).

5.1. Introduction

5.1.1. Tephrochronology and provenance

Tephrochronology is the process of linking, dating, and synchronizing a sequence of geological, palaeoenvironmental or archaeological events using tephra deposits (Lowe, 2011). Tephra correlation is used on a number of levels from simply correlating tephra deposit across cores or outcrops, defining stratigraphic marker horizons (e.g. Molloy *et al.,* 2009), or matching horizons to volcanic source or provenance to yield information about the eruptive history of a region (e.g. Alloway *et al.,* 2004; Allan *et al.,* 2008). Linking tephra horizons (or deposits) back to their source volcanic centre can be a relatively simple exercise when potential sources are limited, the eruptive episodes (and horizons) are precisely dated, stratigraphic succession is established in proximal tephra layering, and/or the volcanic products have highly distinctive geochemical signatures (Lowe, 2011). However, where these criteria are not met, difficulties arise in accurately linking the tephra deposit to their source. In cases of multiple potential sources, with multiple poorly characterised proximal eruption products, there currently is no established method to resolve the origin of distal tephra horizons.

5.1.2. Reconstructing eruptive history using tephra deposits

The eruptive history of a region can often be reconstructed by dating of lava and scoria deposits. In monogenetic fields however, often the errors associated with the age dating are greater than the eruption spacing, and thus do not allow a definitive stratigraphic age order of the centres to be created (e.g., Leonard *et al., in prep.* **Appendix D**). Similarly, due to the restricted distribution of scoria and lavas from small monogenetic centres, stratigraphic relationships and laws of superposition often cannot be relied on alone to resolve the ambiguities that arise from the dating techniques. In these circumstances distal fall deposits can often be more successful at resolving the chronological uncertainties due to their higher preservation potential, and often stratigraphically restricted relationships.

Fortunately maar craters that form in monogenetic fields from phreatomagmatic eruption styles can provide ideal, within-field, depocentres for any subsequent eruptions. Meteoric water retained by the tuff ring often creates a lacustrine environment for capturing and preserving the palaeoenvironmental history of the surrounding region. Tephra deposits within cores retrieved from these maar lakes, therefore have the potential to accurately preserve the stratigraphic sequence of eruptions from the field that is otherwise lost through surface erosion and weathering (**Chapter 3**). If these distal deposits can be linked to their source centre the chronology of a region can be resolved.

5.1.3. Auckland Volcanic Field

The AVF is one such case where climate and urbanization has resulted in a loss, or obscuration, of proximal tephra deposit outcrops. The spatial density of centres (53 centres distributed over 360 km^2) adds further complexity; if a proximal tephra deposit is found, often it has the potential to have come from one of a number of possible centres. In addition, because of the rapid thinning of basaltic tephra away from each source, evidence of stratigraphic succession is often limited in subaerial outcrops. Proximal lava and scoria deposits in the AVF have a higher preservation potential, and their sources are more easily defined. Therefore it is necessary to develop a methodology to reliably correlate distal tephra to their source centre, allowing us establish the provenance of the tephra. With its several maars (**Fig.5.1.**) the AVF is an ideal location to develop and test this methodology. Although previous studies have undertaken a significant effort to date a number of the centres using a range of techniques (e.g. Lindsay *et al.,* 2011; Leonard *et al., in prep.* **Appendix D**), the complete eruption sequence of the AVF remains unknown. Consequently the spatial and geochemical evolution of the field also remains uncertain. Here we combine new developments in tephrochronology (**Chapter 3**), with geochemical analysis of whole rock samples (**Chapter 4**), to develop a new tephra correlation method.

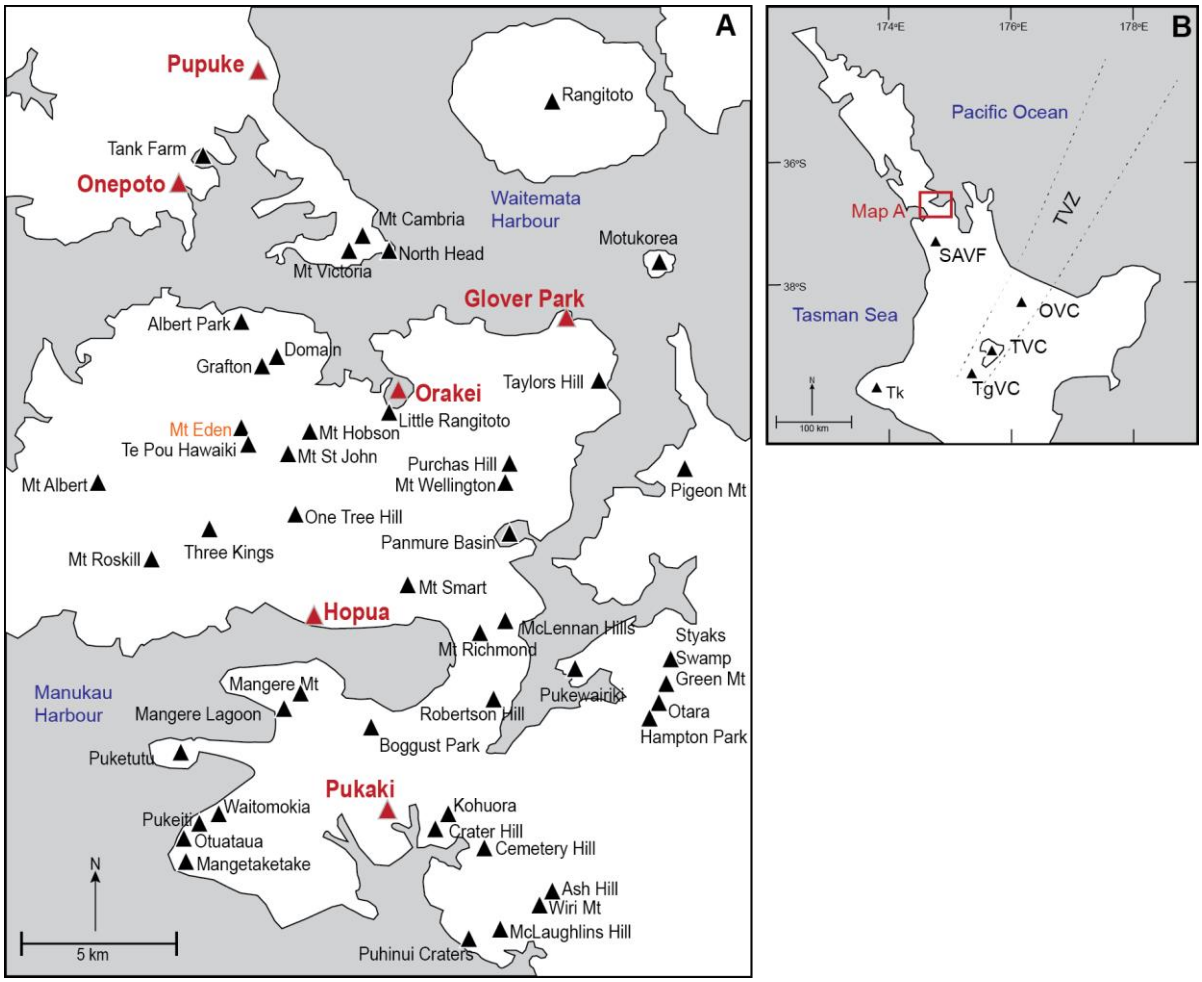

Figure 5.1. *(A) Map of the Auckland Volcanic Field and its eruptive centres (from Hayward et al., 2011). The locations of maar craters from which cores documented in this chapter were collected are highlighted by red symbols and red font: Pupuke, Onepoto, Glover Park, Orakei, Hopua and Pukaki. Although the Glover Park core is from St Heliers Volcano, to avoid confusion within this chapter the core location will continue to be called Glover Park. (B) General location of the AVF within the North Island, New Zealand. Highlighted are other key volcanic centres including the South Auckland Volcanic Field, and the key rhyolitic (Taupo Volcanic Centre (TVC), Okataina Volcanic Centre (OVC)) and andesitic (Tongariro Volcanic Centre (TgVC), Mt. Taranaki (Tk)) sources of tephra found in Auckland maar cores.*

Table 5.1. *Details of all 53 centres in the AVF, their eruption type; relative age relationships where known including, current age estimates and the methods by which they are calculated and the morphological features which give age constraints (*Hayward et al., 2011; å Allen and Smith 1992; Ω Affleck et al., 2001); the estimated eruptive size of the centres (Kereszturi et al., 2013); the geochemical data available for each centre including data added by this study (**Chapter 4**). For the eruption types, A) phreatomagmatic wet explosive eruption which produces maar craters and tuff rings, B) dry magmatic eruptions including fire fountaining creating scoria cones, and C) effusive eruptions resulting in lava flows, and shield building (* details from Hayward et al., 2011).*

Centre name	Eruption types*	Age estimate (ka) 2sd			Method and reference	Relative ages and relationships based on morphology	Minimum total DRE km^3		Geochemical analyses (2013)			Geochemical reference
		min 2sd	mean	max 2sd			Kereszturi et al., 2013	Allen and Smith, 1992	major	trace	isotope	
ALBERT PARK	A,B,C	138.8	144.4	150.0	Ar-Ar; Leonard et al., Appendix D		0.028	0.002	4	4	0	Smith unpub data; McGee, 2012, PhD thesis
ASH HILL	A	31.6	31.8	32.0	14C; Lindsay et al., 2001	older than Wiri Mt å	0.000076	0.00008	0	0	0	
BOGGUST PARK	A? (new)						0.00032		3	3	0	This thesis
CEMETERY HILL	(new)						0.00024		0	0	0	
CRATER HILL	A,B,C	26.7	32.1	37.5	Ar-Ar; Cassata et al., 2008	paleomag excursion (32.4±0.3ka), younger than Kohuora*	0.024	0.01	61	61	0	Smith *et al.,* 2008
DOMAIN	A,B	45.0			Rotoehu Tephra in drill core	younger than Grafton Park*	0.011	0.01	19	7	0	Smith unpub data
GRAFTON PARK	A,B	45.0			morphostratigrpahy ->	older than Domain*	0.011		10	10	0	DEVORA
GREEN MT	A,B,C	12.7	19.1	25.5	Ar-Ar; Leonard et al., Appendix D	older than Styaks Swamp*	0.012	0.02	3	3	0	Miller, 1996; This thesis
HAMPTON PARK	A,B,C	19.0	27.0	35.0	Ar-Ar; Cassata et al., 2008	just older than Otara*	0.0024	0.002	4	4	0	Miller, 1996; This thesis
HOPUA	A	44.4	50.4	56.4	Ar-Ar; Leonard et al., Appendix D	younger than One Tree Hill*	0.00086	0.004	1	1	0	Smith unpub data
KOHUORA	A	30.0	31.0	32.0	Ar-Ar; Leonard et al., Appendix D	older than Crater Hill*	0.0072	0.001	0	0	0	
LITTLE RANGITOTO	B,C	15.9	20.3	24.7	Ar-Ar; Leonard et al., Appendix D	younger than Orakei*	0.0017	0.0003	23	7	0	Franklin, 1999; Smith unpub data: This thesis
MANGERE LAGOON	A,B				morphostratigrpahy ->	older than Mangere Mt*	0.0020	0.002	0	0	0	
MANGERE MT	B,C	64.7	71.7	78.7	Ar-Ar; Leonard et al., Appendix D		0.046	0.2	7	5	0	Miller, 1996; This thesis
MAUNGATAKETAKE	A,B,C	82.6	87.4	92.2	Ar-Ar; Leonard et al., Appendix D		0.034	0.008	23	23	0	Smith unpub data
MCLAUGHLINS HILL	A,B,C	41.7	48.3	54.9	Ar-Ar; Leonard et al., Appendix D		0.0076	0.007	6	5	0	Heming and Barnet, 1986; This thesis
MCLENNAN HILLS	A,B,C	29.3	34.1	38.9	Ar-Ar; Leonard et al., Appendix D	paleomag excursion (40.4±1.1ka), older than Mt Richmond*	0.022	0.01	6	6	0	Miller, 1996; This thesis
MOTUKOREA	A,B,C	3.3	14.3	25.3	Ar-Ar; Leonard et al., Appendix D		0.0046	0.02	53	53	16	Bryner, 1991; McGee, 2012,

Table 5.1. *continued.*

Centre name	Eruption types*	Age estimate (ka) 2sd			Method and reference	Relative ages and relationships based on morphology	Minimum total DRE km^3		Geochemical analyses (2013)			Geochemical reference
		min 2sd	mean	max 2sd			Kereszturi et al., 2013	Allen and Smith, 1992	major	trace	isotope	
MT ALBERT	A,B,C	112.4	117.6	122.8	Ar-Ar; Leonard et al., Appendix D	older than Mt Eden and Mt Roskill*	0.023	0.03	4	5	0	Smith unpub data; This thesis
MT CAMBRIA	B,C	23.9	44.5	65.1	Ar-Ar; Leonard et al., Appendix D		0.00029	0.0002	6	6	0	Smith unpub data; This thesis
MT EDEN	B,C	13.3	19.3	25.3	Ar-Ar; Leonard et al., Appendix D	much younger than Mt St John, younger than Three Kings*	0.090	0.2	29	17	1	Eade, 2009; DEVORA; McGee, 2012
MT HOBSON	B,C	44.9	55.9	66.9	Ar-Ar; Leonard et al., Appendix D	older than Three Kings*	0.0067	0.005	15	7	0	Smith unpub data; This thesis
MT RICHMOND	A,B	18.4	23.8	29.2	Ar-Ar; Leonard et al., Appendix D	paleomag excursion (32.4±0.3ka), younger than McLennan Hills*	0.0057	0.004	6	3	2	Eade, 2009; Smith unpub data; DEVORA; McGee, 2012
MT ROBERTSON	A,B						0.0027	0.002	4	4	0	This thesis
MT ROSKILL	A,B,C	98.6	104.8	111.0	Ar-Ar; Leonard et al., Appendix D	younger than Mt Albert*	0.014	0.007	9	8	0	McGee, 2012; This thesis
MT SMART	A,B,C	11.9	16.1	20.3	Ar-Ar; Leonard et al., Appendix D	younger than One Tree Hill*	0.013	0.09	8	8	0	Smith unpub data; McGee, 2012; This thesis
MT ST JOHN	B,C	71.1	74.3	77.5	Ar-Ar; Leonard et al., Appendix D	much older than Mt Eden and Three Kings*	0.028	0.003	22	13	0	Franklin, 1999; Eade, 2009
MT VICTORIA	B,C	46.1	54.5	62.9	Ar-Ar; Leonard et al., Appendix D		0.0048	0.002	4	3	0	Smith unpub data; This thesis
MT WELLINGTON	B,C	10.0	10.5	11.0	14C; Lindsay et al., 2001	just younger than Purchas Hill*	0.082	0.2	34	36	10	DEVORA; McGee, 2012; This thesis
NORTH HEAD	A,B	70.8	86.0	101.2	Ar-Ar; Leonard et al., Appendix D		0.0026	0.003	6	5	0	Smith unpub data
ONE TREE HILL	B,C	44.3	51.9	59.5	Ar-Ar; Leonard et al., Appendix D	older than Hopua, Mt Hobson, Mt Eden, Mt Smart, Three Kings*	0.26	0.3	8	4	0	Eade, 2009; Smith unpub data
ONEPOTO	A	45.0			Rotoehu Tephra in drill core	younger than Pupuke*	0.0026	0.004	2	2	0	This thesis
ORAKEI	A	85.0		130.0	sed. rate ages of tephra horizons; Molloy et al., 2009	not breached in last interglacial, older than Little Rangitoto*	0.0067	0.010	41	21	0	Smith unpub data; Franklin, 1999
OTARA	A,B,C	0.0		35.0	morphostratigrpahy ->	just younger than Hampton Park*	0.0023	0.008	12	5	2	Miller, 1996; McGee, 2012; This thesis
OTUATAUA	A,B,C						0.0063	0.004	6	6	0	Heming unpub data; This thesis
PANMURE BASIN	A,B	17.5			Rerewhakaaitu tephra in drill core		0.0074	0.009	22	21	0	Smith unpub data
PIGEON MT	A,B,C						0.0033	0.003	6	6	0	Smith unpub data; This thesis
PUHINUI CRATERS	(new)								0	0	0	

Table 5.1. *continued.*

Centre name	Eruption types*	Age estimate (ka) 2sd			Method and reference	Relative ages and relationships based on morphology	Minimum total DRE km^3		Geochemical analyses (2013)			Geochemical reference
		min 2sd	mean	max 2sd			Kereszturi et al., 2013	Allen and Smith, 1992	major	trace	isotope	
PUKAKI	A	52.0			Core extent		0.0092	0.006	6	6	0	Zawalna-Greer, 2012; This thesis
PUKEITI	B,C	3.2	10.6	18.0	Ar-Ar; Leonard et al., Appendix D		0.0037	0.004	5	5	0	Smith unpub data; This thesis
PUKEWAIRIKI	A,C	130.0			morphostratigrpahy ->	sea cut platform from last interglacial*	0.011	0.005	4	3	0	Smith unpub data
PUKETUTU	B,C	29.8	33.6	37.4	Ar-Ar; Cassata et al., 2008	paleomag excursion (32.4±0.3ka)	0.018	0.03	23	15	3	Miller, 1996; McGee, 2012; This thesis
PUPUKE	C,B,A	184.7	190.3	195.9	Ar-Ar; Leonard et al., Appendix D	Older than Tank Farm and Onepoto*	0.047	0.05	52	52	6	Spargo, 2007; This thesis
PURCHAS HILL	A,B	11.0	11.0	11.0	14C; Lindsay et al., 2001	just older than Mt Wellington*	0.0017	0.000	27	27	6	McGee, 2012
RANGITOTO	A,B,C	0.5	0.6	0.6	14C; Lindsay et al., 2001	youngest in the field*	0.70	2.0	57	57	10	Hookway, 2000; Needham et al., 2011; McGee 2012; This thesis
ST HELIERS	A,	45.0			Rotoehu Tephra in drill core		0.0022	0.002	3	3	0	Smith unpub data; This thesis
STYAKS SWAMP	A,	0.0		25.5	morphostratigrpahy ->	younger than Green Mt*	0.00037	0.0004	0	0	0	
TANK FARM	A	45.0			morphostratigrpahy ->	younger than Onepoto*	0.0059	0.003	0	0	0	
TAYLORS HILL	A,B,C	23.8	26.8	29.8	Ar-Ar; Leonard et al., Appendix D	palaeomag excursion (32.4±0.3ka)	0.0051	0.003	9	9	2	Smith unpub data; McGee, 2012; This thesis
TE POU HAWAIKI	B	13.3			morphostratigrpahy ->	older than Mt Eden $^{\Omega}$	0.028	0.0003	18	5	0	Franklin, 1999; This thesis
THREE KINGS	A,B,C	28.4	28.6	28.8	14C; Lindsay et al., 2001	younger than OTH, Mt St John, Mt Hobson, older than Mt Eden*	0.069	0.1	36	35	2	Eade, 2009; Smith unpub data
WAITOMOKIA	A,B	18.0			morphostratigrpahy ->	older than Pukeiti*	0.0098	0.003	9	9	0	McGee, 2012
WIRI	A,B,C	25.7	30.1	34.5	Ar-Ar; Cassata et al., 2008	paleomag excursion (32.4±0.3ka), younger than Ash Hill$^{\delta}$	0.016	0.03	12	12	4	DEVORA; McGee, 2012; This thesis

5.2. Source correlation method and sequencing data

The key aspects of this method are to accurately link the cross-core correlated tephra horizons to their source centre. In order to test a method by which tephra can be correlated to the whole rock composition of a candidate source, detailed information about each individual centre, and distal tephra deposit has been collated. An assessment of all the current data, including tephrochronology and tephra horizon ages (**Chapter 3**), source volcano geochemistries and ages (**Chapter 4**), and a number of other additional criteria, is discussed below. This selection process was used to determine the input data for the development of the tephra-to-source correlation method.

5.2.1. Tephrochronology

Tephrochronology has been applied to, and utilized extensively, for the deposits from the AVF maar cores. Relevant studies used the correlation of multiple distally derived rhyolitic and andesitic tephras for different reasons, from volcanology (Shane, 2000) to archaeology (Lowe and Newham 2004). Multiple well-dated rhyolitic marker horizons found across the Auckland region, in multiple lacustrine maar cores, have helped to establish the construction of a well-constrained chronostratigraphic history. The basaltic horizons within the cores have been cross-correlated by a number of different techniques, most recently through geochemistry and stratigraphy (see **Chapter 3**), and through statistical modelling (Green *et al.,* 2014). Green et al. (2014) used basaltic horizon details (geochemistry, stratigraphy, mineralogy) from Molloy et al. (2009), together with age data from statistical models (Bebbington and Cronin 2011), to produce the cross core correlations. All the input data used by Green et al. (2014) have now been superseded, and therefore here I used the geochemistry, AVF nomenclature, correlations, and tephra horizon thicknesses from **Chapter 3** (**Figure 3.11 and Table 3.2)**.

5.2.2. Basaltic tephra horizon ages

The most recently published ages of key rhyolitic marker horizons (RMHs) are used as a comparative framework to constrain the basaltic horizons with age ranges across the cores. The cores are constrained by four chosen key horizons, which denote five age brackets (see **Chapter 3**):

(1) Younger than the Rerewhakaaitu (<17.5 ka) including tephra numbers AVF 24 to 22;

(2) Rerewhakaaitu to the Okareka (17.5 to 21.5 ka) including AVF 21 and 22;

(3) Okareka to Kawakawa/Oruanui (21.5 to 25.4 ka) including AVF 19 to 13;

(4) Kawakawa/Oruanui to Rotoehu (25.4 to ≤45.1 ka) including AVF 12 to 4;

(5) Older than the Rotoehu (>45.1ka) including AVF 3 to 1 (and AVF a-c)

The ages for Rerewhakaaitu (Rk), Okareka (Ok), and Kawakawa/Oruanui (Kk) RMHs are reviewed in Lowe et al. (2013). The age of the Rotoehu RMH is, however, relatively controversial. Regardless, this tephra is found in four of the six cores studied, and is thus a useful horizon to correlate older core sections. Therefore here the Rotoehu RMH is used for correlation purposes, in contrast to some previous AVF tephra studies (e.g., Shane and Hoverd, 2002; Molloy *et al.,* 2009). For the purpose of this study we use the most recently published age estimate of 45.1 ka (Danišík *et al.,* 2014) to provide a minimum age constraint to basaltic tephras found beneath this horizon.

The numerical ages of the basaltic tephra horizons within all the cores have previously been estimated using two methods: 1) through sedimentation rates relative to the rhyolitic marker horizons (Molloy, 2008) and 2) through statistical modelling (Green *et al.,* 2014). However, both these studies used sources that have been recently superseded for both rhyolitic horizon ages, and basaltic tephra deposit thicknesses. For the purpose of this study, the sedimentation rates, and ages have therefore been recalculated using the more recent data for basaltic horizon thicknesses in Orakei and Glover Park cores (**Chapter 3**) and RMH ages (Lowe *et al.,* 2013; Danišík *et al.,* 2014).

The new basaltic tephra horizon thicknesses for the Onepoto core were not used here, as these data comes from a new core in which the rhyolite and andesite marker horizons have not been assessed yet. For the Onepoto core all tephra thicknesses and depths were adapted from Shane and Hoverd (2002). Marker rhyolite and andesite tephra thicknesses in Orakei Basin, Hopua, Pupuke and lower Pukaki cores (below the Kk) are from Molloy (2008) and from Sandiford et al. (2001) in upper Pukaki core (above Kk). Tephra deposits preserve effectively instantaneous events (Shane, 2005), and therefore are removed from the total sediment thickness for a section bound by key rhyolitic marker horizons. The total sediment thickness is then divided by the age range for the given section, calculated from the mean ages for the rhyolitic horizons (**Table 5.2**).

The sedimentation rate recorded in the Onepoto core was consistent from the top to the Rotoehu tephra horizon (**Fig. 5.2**.). Therefore the overall sedimentation rate value was taken from the best-fit line (r^2=0.99) as 0.136 mm/yr (**Fig. 5.2.**). For the sedimentation rate between the Rotoehu and the base of the core, the basaltic deposit AVFd (c.f **Chapter 3**), was used as a lower constraint. AVFd, although not a tephra fall deposit (nor a rhyolitic marker horizon), was labelled thus in **Chapter 3** to allow for unambiguous identification. This deposit comprises of lava and scoriaceous blocks interpreted to represent the Onepoto maar crater floor (Shane and Hoverd, 2002). Although no age dates exists from the Onepoto eruption, morphostratigraphy shows that it is younger than Pupuke, and we therefore use the mean age measured for Pupuke (190.3 ± 5.6 ka; Ar-Ar dating Leonard *et al., in prep.* ***Appendix D***) as a maximum age for Onepoto. The respective calculated sedimentation rate of 0.19 mm/yr is comparable to those recorded previously (0.18 mm/yr; Shane and Hoverd, 2002). In addition, the calculated ages are comparable to those calculated for the correlated horizons AVF2 and AVF1 in the Orakei Basin core (**Table 5.3.**), suggesting that these assumptions are realistic.

The thickness estimates for the basaltic and rhyolitic horizons below the Kawakawa/Oruanui marker horizon in the Pukaki core are ambiguous (andesite horizon details are outlined in Shane, 2005). Therefore the sedimentation rates for these sections (Kawakawa/Oruanui (Kk) to Okaia (O), and Okaia to Maketu (Mk)), are also calculated from best-fit lines (**Fig. 5.2.**).

***Table 5.2**. Calculated sedimentation rates for all cores assessed from the Auckland Volcanic Field maars. The rhyolitic marker horizons used to constrain sections include Rotoma (Ro), Opepe (Op), Waiohau (Wh), Rotorua (Rr), Rerewhakaaitu (Rk), Okareka (Ok), Te Rere (Tr), Kawakawa/Oruanui (Kk), Okaia (O), Maketu (Mk), and Rotoehu (Re). * Indicates sedimentation rates calculated from best-fit line equations as discussed in the text. ** See discussion in the text for calculation of this rate. [1] Indicates where sedimentation rates are assumed constant below the Rotoehu, and [2] indicates where Glover Park sedimentation rate is calculated from the ages of the correlated basaltic horizons found in Onepoto core.*

	Total rhyolite thickness (mm)	Total basalt thickness (mm)	Total andesite thickness (mm)	Total tephra thickness (mm)	Sediment thickness (mm)	Age range of section (ka)	Sedimentation rate (mm/yr)
ORAKEI BASIN							
Ok to KK	10	197	17	224	9876	3.5	2.81
KK to Mk	45	626	10	681	7859	11.0	0.72
Mk to Re[1]	75	0	3.5	78.5	5432	8.8	0.62
ONEPOTO							
Ro to Re[1]							0.14*
Re to base**	-	217	-	217	27580	145.2	0.19
GLOVER PARK							
AVF1 to AVFb[2]	-	50	-	50	5520	82.9	0.07
HOPUA							
Ro to Op	2	3	0	5	120	0.6	0.21
Rk to Ok	23	525	9	557	2793	4.4	0.64
Ok to Kk	61	40	5	106	1679	3.5	0.48
PUKAKI							
Wh to Ro	20	1	0	21	229	1.6	0.14
Rk to Ok	4	2	9	15	1755	4.4	0.40
Ok to Tr	0.5	2	4	6.5	1363.5	3.3	0.41
Tr to Kk	22	50	1	73	137	0.2	0.72
Kk to O							0.93*
O to Mk							0.55*
PUPUKE							
Kk to O	7.5	7	4	18.5	486.5	3.3	0.15
O to Mk	73	46	6.5	125.5	2190	7.7	0.28

In the Glover Park core, only the Rotoehu RMH has been identified but no other well-dated deposits are found below precluding the calculation of a sedimentation rate. Therefore, for the horizons correlated to other cores (AVF2 and AVF1) the ages are assigned from an average of the values calculated from these cores. For horizon AVFa, which is only found within Glover Park, an age estimate was obtained through calculating the sedimentation rate between the bounding basaltic horizons, AVF1 and AVFb. The ages for these horizons were assigned based on the ages calculated for these deposits in Orakei Basin (AVF1) and Onepoto cores (AVF1 and AVFb).

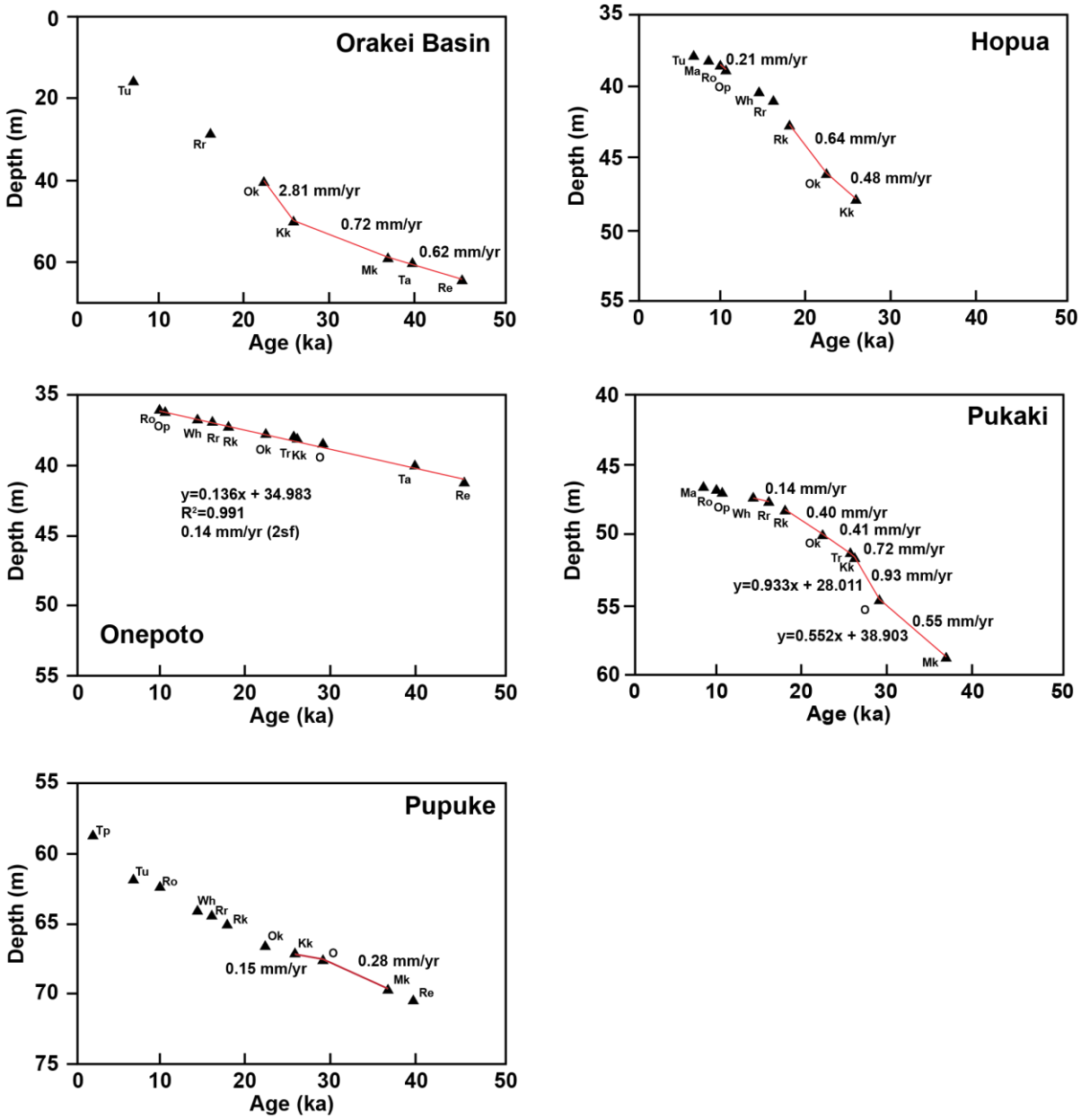

Figure 5.2. *Sedimentation rate plots for all cores with multiple rhyolitic marker horizons. Abbreviations are defined in* ***Table 5.2.*** *Lines in red define sections where basaltic horizons have had their ages estimated with the corresponding sedimentation rates shown (in mm/yr.). Where sedimentation rates have been taken from best-fit lines (discussed in the text), the equation of the line is also shown.*

These results produce an up-to-date estimation for the ages of all the tephra horizons used in this study. Overall the ages produced show a good agreement where multiple deposits are correlated across core (for all horizons post Re, a maximum error of ± 1.7 ka from the calculated mean value for deposits in horizon AVF7, and a maximum error of ± 15.2 ka for deposits in AVF1 horizon pre Rotoehu). There are however two discrepancies (highlighted in **Table 5.3.**): 1) The calculated age for AVF 17 (Orakei Basin core) is too young for the horizon order, and 2) the calculated age of AVF16 is older than the nomenclature order dictates.

The age for AVF 17 (23.4 ka) within only the Orakei Basin core is not out of place (AVF18 is 23.2 ka and AVF15 is 24.5 ka). However, the average age for AVF18 is calculated from a range of ages (Hopua 25.2 ka, Pukaki 24.6 ka and Orakei) that are slightly older than the Orakei Basin core estimates. Therefore the average age for this horizon is calculated to be higher than that of the preceding horizon, which is only found in Orakei Basin.

AVF 16 (Pukaki core only) has also been repositioned within the overall core sequence. Not only does the age estimate imply it is older than suggested by the original position in the AVF nomenclature sequence, but also there are limited constraints on this horizon's relationship with the other deposits from other cores. The Te Rere and the Kawakawa/Oruanui rhyolitic horizons stratigraphically constrain horizon AVF16, but there are no other basaltic tephra restricted to this (Te Rere tephra is not found in the Orakei Basin core). Therefore based on the age estimates and the flexibility of the positioning, AVF16 is repositioned between AVF14 and AVF13 (**Table 5.3.**).

For this study, the numerical ages of the rhyolitic marker horizons are taken as boundaries and the calculated sedimentation rate ages taken as guide to estimate the basaltic tephra ages. A caveat is that there are still errors (±5-5000 yrs.) associated with the ages of these rhyolitic markers, and although smaller than those associated with the Ar-Ar age dates for the AVF centres, they still need to be taken into account (see discussion in **Sect. 5.3.4**.).

Table 5.3. *The ages calculated for each basaltic horizon (in ka) using the sedimentation rates from* ***Table 5.2.*** *References: a. Needham et al. (2011), b. Lowe et al. (2013), c. Molloy (2008), d. Danišík et al. (2014), and e. Leonard et al. (in prep.). AVF24 is split into Rangitoto1 and 2 identified and dated (^{14}C in cal. yr. BP) by Needham et al. (2011), the upper and basal units nomenclature from *Molloy et al. (2009), see text for details. The ages for the rhyolitic marker horizons (grey text) are outlined in cal. yr. BP. The age of AVF17 is highlighted as an outlier as discussed in the text, and the position of AVF16 is highlighted as out of sequence, also discussed in the text. The age of deposit AVFd in the base of the Onepoto core is taken from the minimum Ar-Ar age estimation for Pupuke centre, see text for details. All errors are reported as 1 sd.*

		Calculated age of horizon (ka)							
Source	**abv.**	**Orakei**	**Onepoto**	**Glover Park**	**Hopua**	**Pukaki**	**Pupuke**	**ref.**	**Average (ka)**
AVF24 [P48]*				504 ± 5				a	0.5
AVF24 [P49]*				553 ± 7				a	0.5
Taupo	Tp			1,718 ± 30				b	1.7
Tuhua	Tu			6,577 ± 547				b	6.6
Mamaku	Ma			7,940 ± 257				b	7.9
Rotoma	Ro			9,423 ± 120				b	9.4
AVF23					10.0				10.0
Opepe	Op			9,991 ± 160				b	10.0
Waiohau	Wh			14,009 ± 155				b	14.0
AVF22						15.4			15.4
Rotorua	Rr			15,635 ±412				b	15.6
Rerewhakaaitu	Rk			17,496 ± 462				b	17.5
AVF21					20.3	19.6			19.9
AVF20					21.6	19.6			20.6
Okareka	Ok			21,858 ± 290				b	21.9
AVF19						24.2			24.2
AVF18		23.2			25.2	24.6			24.3
AVF17		23.4							23.4
AVF15		24.5							24.5
AVF14		24.6							24.6
Te Rere	Tr			25,171 ± 964				b	25.2
AVF16						25.3			25.3
AVF13		25.3							25.3
Kawakawa/Oruanui	Kk			25,358 ± 162				b	25.4
AVF12		26.3	26.4		27.0	28.3	27.9		27.2
Okaia	O			28,621 ± 1428				b	28.6
AVF11						29.3			29.3
AVF10		30.6	29.1				30.0		29.9
AVF9							30.2		30.2
AVF8		30.7				31.7	30.5		31.3
AVF7		30.8	34.2			32.6	31.4		32.5
AVF6						33.7			33.7
AVF5		35.0							35.0
AVF4		36.0					34.3		35.2
Maketu	Mk			36,320 ± 575				c	36.3
Tahuna	Ta			39,268 ± 1193				c	39.3
Rotoehu	Re			45,100 ± 3300				d	45.1
AVF3		49.3							49.3
AVF2		59.9	60.7						60.3
AVF1		70.4	100.8						85.6
AVFa				*129.2*					*129.2*
AVFb			140.6						140.6
AVFc			173.1						173.1
AVFd				<190,300 ± 5600				e	190.3

5.2.3. Volcanic centre geochemistry

In order to develop a method to geochemically correlate tephra horizons to source centres it was imperative to create a comprehensive source centre geochemical database to maintained a thorough and holistic approach. The whole rock database as collated in **Chapter 4** (**Appendix C**) is the most complete compilation of geochemical data from the AVF centres. I report that 46 of 53 centres now have >3 major and trace element analyses available (**Appendix C**). For the newly discovered centres Puhinui Craters and Cemetery Hill (Hayward *pers. comms,* 2012), no geochemical or age data exist and therefore these centres are not included in this study. Furthermore, due to evidence of extreme fractional crystallisation or olivine accumulation (common in Pupuke samples) as **Chapter 4** details, measurements made by Heming and Barnet (1986) are all excluded, as are a number of single data points from previous authors (Hookway, 2000; Spargo, 2007; and Smith unpublished).

5.2.4. Volcanic centre ages

To maximise the data available for the ages of the individual eruptive centres, data from three methods have been collated. These methods include morphostratigraphic evidence (e.g. Hayward *et al.,* 2011), $^{40}Ar/^{39}Ar$ dating of groundmass (Leonard *et al., in prep,* **Appendix D**; Cassata *et al.,* 2008) , and ^{14}C dating of organic debris (compiled in Lindsay *et al.,* 2011). The centre ages, and their sources are outlined in **Table 5.1**.

Modelled ages for the AVF centres given by Bebbington and Cronin (2011) are excluded from this study, as they are considered to form a circular argument with our proposed method:

(1) Tephra horizons details (from Molloy *et al.,* 2009) were input into the model to get the age outputs.
(2) The tephra horizons details are now superseded by work presented in **Chapter 3**.

Morphostratigraphy is here defined as the interrelationships exhibited by the surface landforms (see examples below). Due to the proximity of the centres to one another within the field, 35 of 53 centres have morphostratigraphic constraints associated with them. Based on the laws of superposition a number of examples can be identified:

(1) Tephra or lava deposits that are found on top of other deposits must be from a younger eruption: e.g., Mt. Eden tephra on top of Three Kings lava flows.
(2) Lava that has flowed around or into another centre must be from a younger source: e.g., Little Rangitoto lava flowing around Orakei Basin tuff ring.
(3) A volcano that has erupted through an older lava flow must be younger than the lava's source: e.g., Hopua through One Tree Hill lava.
(4) Erosional features from sea level changes provide additional constraints: e.g., Pukewiriki has a wave cut platform, arguably from the last interglacial, and is therefore > ca. 130 ka yrs old.
(5) For three of the centres (Domain, St Heliers and Onepoto) the morphostratigraphic constraint is based on tephrochronology, with the presence of the Rotoehu tephra within crater drill cores showing a minimum age for the centre of 45.1 ka.

These morphostratigraphic constraints give optimum relative ages, which need to be combined with the numerical ages derived from Ar-Ar dating. In all cases the Ar-Ar age ranges are consistent with the morphostratigraphic constraints.

The Ar-Ar ages presented in Leonard et al. (*in prep.* **Appendix D**) are stated through the following text as age ranges with a 2sd error (the mean ages are reported in **Table 5.1.**), although any age within the range is considered appropriate with no extra emphasis given to the mean ages. The Ar-Ar data suite produced by Leonard et al. (*in prep.* **Appendix D**) triples the number of centres with measured age dates from 11 to 33 (Lindsay *et al.,* 2011). From the remaining twenty centres with no Ar-Ar or ^{14}C ages, relative ages of fourteen centres were derived by morphostratigraphy (or tephrochronology; see **Table 5.1.**). With the age of six

(Otuataua, Pigeon Mt., Robertson Hill, Boggust Park, Cemetery Hill, and the Puhinui Craters) from the 53 AVF centres remaining unknown. As previously mentioned Cemetery Hill and Puhinui Craters are not considered for this study, and therefore the centres Otuataua, Pigeon Mt., Robertson Hill, and Boggust Park will be included as possible correlatives for any dated horizon during the correlation process.

5.2.5. Additional criteria

To complement the geochemical and age data, a number of other assumptions are made to constrain the correlations further. These include the scale and style of eruptions, the location of the relevant centre(s), and locality(ies) of the relevant core(s). These criteria are discussed below.

The volcanoes of the AVF erupt with a range of styles and scales that need to be considered when approaching the problem of tephra correlation. Strombolian and Hawaiian styles produce only minor ash plumes that deposit tephra to only a few kilometres from source and are thus less likely to deposit large quantities of distal tephra (Valentine and Gregg, 2008). To form cm-thick tephra deposits a few kilometers from the vent, eruptions must either be 'violent-Strombolian' or phreatomagmatic in style (Houghton *et al.,* 1999). However, for the AVF the designation between Hawaiian, Strombolian, and violent-Strombolian styles are not defined (Kerezturi *et al.,* 2014; Allen and Smith, 1994) and therefore for correlation purposes the differences between phreatomagmatic vs. magmatic styles are considered. It is assumed that during a phreatomagmatic eruption the potential of a centre to disperse more tephra to greater distances is higher, in comparison to a similar sized centre with only magmatic (explosive or effusive) eruption phases.

For this study, the total erupted volume (total dense rock equivalent, DRE^{tot}; Kereszturi *et al.,* 2013, **Table 5.1.**) is assumed to be equivalent to the scale of an eruption, which correlates to dispersal distance. Here we take the most recently published DRE^{tot} values from Kereszturi et al. (2013) rather than the original estimates from Allen and Smith (1994) (both of which are reported in **Table 5.1.).** The values from Kereszturi et al. (2013) are preferred as they take into account multiple additional factors (e.g., diatreme volume, crater infil volume) that were not

considered by Allen and Smith (1994), and also include all the currently identified volcanoes.

In addition tephra deposits are assumed to thin away from source (Pyle, 1989; Lowe, 2011). Therefore an eruption that produces a large DRE^{tot} volume will be assumed to produce a volumetrically large tephra output and hence, a thick proximal deposit, and a thin, but greater dispersed distal deposit. For thick tephra deposits (>100 mm) in a core, the source centre is therefore constrained to either 1) being close to the deposition site (≤ few kilometres, Brand *et al.,* 2014), and/or 2) having a predominantly phreatomagmatic eruption style.

Due to the relatively volumetrically small size of the AVF volcanoes, the tephra dispersal area from single eruptions usually does not cover the entire field (Kermonde, 1992). Therefore the distribution and thickness of the tephra deposits in cores can be indicative of the source centre. For example, tephra deposits that are only found in the northern maar sites (Onepoto, Pupuke, Orakei and Glover Park) are assumed to indicate sources in the north or central AVF (based on the dominant wind direction, discussed below). Conversely a deposit only found in the southern maar site (Pukaki) is suggestive of sources in the south of the field. Tephra deposits found in both northern and southern maar sites are likely derived from the central part of the field, and/or reflect a large enough eruption widely dispersing tephra over the AVF area.

Wind direction is also a factor taken into consideration when making source correlations due to its controlling influence on volcanic plume direction and tephra dispersal. For the Auckland region evidence of prevailing past wind directions can be inferred from the morphology of the volcanic centres. Two examples include:

(1) The build up of a higher tuff ring on Motukorea's north-eastern side (McGee *et al.,* 2012) and One Tree Hill's asymmetrical scoria cone built up on the north-eastern side of the vent (Hayward *et al.,* 2011).

(2) Some of the eastern centres, e.g. Green Mt., Otara Hill, Styaks Swamp and Hampton Park, show evidence for a dominant westerly wind, creating high tuff rings to the east of the vents (Hayward *et al.,* 2011).

These historic wind patterns in the Auckland region are still the dominant patterns for today (Houghton *et al.,* 2006), resulting in more common tephra deposition to the northeast and east of the field (confirmed by the high number of deposits found within the Orakei Basin core, situated north-east of most centres; **Fig. 5.1.**). Tephra deposits are therefore more readily traced back to sources to the west and southwest. Accordingly centres found to the east or north east of the maar sites (e.g. Pigeon Mt., Hampton Park, Otara, Green Mt., and Styaks Swamp; **Fig. 5.1.**) are less likely to be represented in the maar tephra record.

When the correlation technique is applied, each horizon is taken as an individual case, and all potential sources are accounted for and discussed. In some cases potential sources will have been correlated to an alternative horizon, however, because each correlation is not definitive, correlated sources are not discounted for other tephra horizons. In these instances, those centres correlated to a horizon are identified in italic font, with their correlated horizon detailed. They do however, become a less likely potential source for another horizon if they are already a best fit for an alternative deposit.

The factors discussed here are all taken into account when making correlations, and a 'confidence value' is assigned for each correlation based on the number of criteria that are satisfied. In general, if all four criteria (geochemistry, age, scale, location) are satisfied a confidence level of 1 is given, when three are satisfied a confidence level of 2 is give, and if only two are satisfied a confidence level of 3 is given. Each of these criteria is variably weighted in importance with age ≥ geochemistry >> locality ≥ scale and style, and therefore in some cases the confidence values are skewed to show this. For example if geochemistry, locality and scale are all appropriate, but age is not, the confidence value will be 3 rather than 2 because age is a more important and restricting factor.

By collating the maximum amount of information about the tephrostratigraphic framework, and the known eruptive scales, styles, ages and geochemistries, this study presents the method developed to correlate of AVF tephra horizons to their source centre. I initially discuss the method developed to correlate tephra to whole rock samples, followed by detailing the correlations made, and the resultant implications of the outcomes.

5.3. Discussion

5.3.1. Geochemical compositions of whole rock and tephra-derived glass

5.3.1.1. Discriminating elements

The (generally) monogenetic nature of the AVF results in the potential for each centre to have a discrete geochemical signature. Previous studies on the petrogenesis of the AVF eruptives (Huang *et al.,* 1997; McGee *et al.,* 2013) have shown that each batch of magma is generated by differing degrees of partial melting of multiple mantle sources located at different depths within the mantle. This includes a deep source (≥80km, more cpx + more garnet) and a shallower source (≤80km, less cpx + less garnet) (McGee *et al.,* 2012). The involvement of multiple mantle sources is the cause of the large trace element variability observed in the AVF lavas (discussed in **Chapter 4**).

The geochemical results show that although there is overlap for many elements for the field, some specific element concentrations and their trends can be more discriminatory for individual centres (**Fig. 5.3.**). Combinations of major (SiO_2, MgO, CaO, FeO, P_2O_5) and trace (Zr, Gd, La, Sm, Nd, Nb, Ce) elements, and trace element ratios (e.g., La/Yb or La/Y) are particularly useful for this purpose. The selected elements not only show the widest range in concentrations in eruptive products from the AVF, but are most representative in eruptive products from individual centres.

The rare earth elements (REEs) are especially useful as they can be used to discriminate between melts from a deep or shallow source. (e.g., McKenzie and O'Nions, 1991; Robinson and Wood, 1998; **Table 5.4.**). The light REE (LREE) are incompatible in garnet (e.g. K_D [La] = 0.001; Winter, 2010) compared to the heavy REE (HREE) which are compatible in garnet (e.g. K_D [Yb] = 3.1; Winter 2010). As a result melts from a deep garnet-bearing mantle source have lower LREE/HREE ratios. Y and Yb are used here as the HREE denominators. If a sample has a high LREE/Y or LREE/Yb ratio it is indicative of a deeper, more garnet rich source, in comparison to a low LREE/Y or LREE/Yb ratio, which will be indicative of more of an input from a shallower source. In addition, during low pressure differentiation, for example fractional crystallisation of magmas on ascent, the effects on these ratios is

minor in comparison to the effects of partial melting in the source in the presence of garnet or spinel stability fields. Therefore there is very minor alteration of these source signatures on ascent.

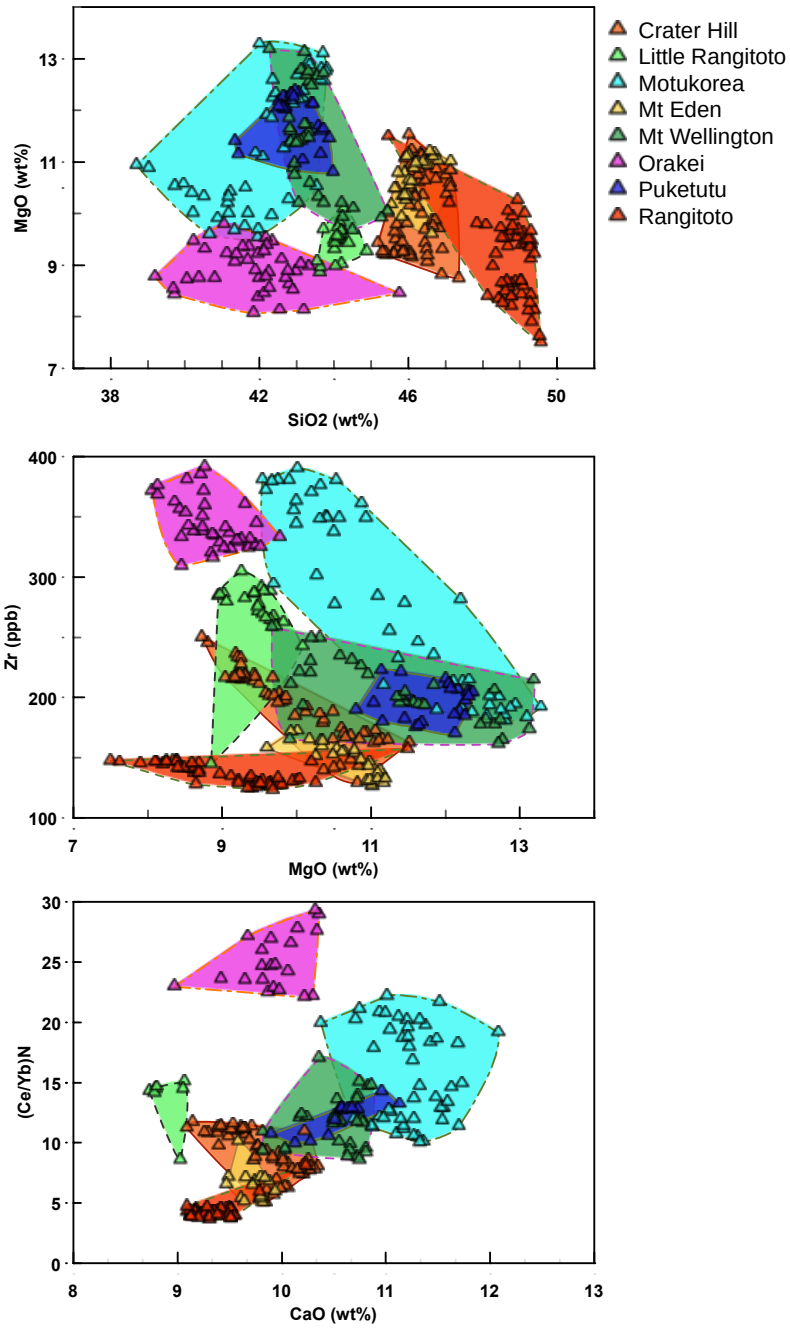

Figure 5.3. *Collection of whole rock element/oxide plots (data in* ***Appendix C****) to show an example of a selection of those elements that are discriminatory for the AVF. I include examples of elements that have the widest range in the field and the least overlap for each centre, and are therefore the most individual for each centre. (N = normalised to primitive mantle values after McDonough and Sun, 1995).*

Table 5.4. *Distribution co-efficient values for selected trace elements into selected minerals. Of note are the compatibility (K_D >1) of Yb and Y in garnet, and the incompatibility (K_D <<1) of all REE into olivine. From Winter (2010, p 165, and references therein.)*

	Distribution Co-efficients (K_D)				
Element	**Olivine**	**Opx**	**Cpx**	**Plag**	**Garnet**
Ni	14	5	7	0.01	0.955
Cr	0.7	10	34	0.01	1.345
La	0.007	0.030	0.056	0.148	0.001
Ce	0.006	0.020	0.092	0.082	0.007
Nd	0.006	0.030	0.230	0.055	0.026
Nb	0.004	0.004	0.006	0.024	0.010
Zr	0.003	0.030	0.130	0.090	0.900
Gd	0.004	0.034	0.400	0.040	0.500
Yb	0.049	0.340	0.542	0.023	5.500
Y	0.007	0.300	0.410	0.010	3.100

5.3.1.2. Comparison of whole rock to tephra-derived glass geochemistry

In general, when the entire whole rock and tephra-derived glass data suites are compared MgO, Cr, and Ni whole rocks all show distinctly higher concentrations than in the glasses (e.g. MgO in glass ca. 2-6 wt.%; in whole rock ca. 6-16 wt.%) (**Fig. 5.4.A**). Compared to whole rock analyses, all glasses have higher (but slightly overlapping) SiO_2, Al_2O_3, Na_2O, and K_2O contents (e.g. SiO_2 in tephra ca. 42-52 wt.%; whole rock ca. 38-50 wt.%). CaO, $Fe_2O_3^{tot}$, TiO_2, and P_2O_5 are comparable range between whole rock and glass, as are the trace elements, including REEs. The REEs in general do show a slightly wider range in the glass than the whole rock, although, this discrepancy is removed by the use of trace element ratios. For example Mg, Cr and Ni are highly compatible with olivine, pyroxene (cpx) and oxides, and are strongly partitioned and enriched in these minerals. Consequently, these elements are not useful for trying to correlate tephra to whole rock. The REE are generally incompatible with the major silicate mineral phases, and are therefore not preferentially enriched in crystals. They therefore have comparable REE contents and ratios in tephra-derived glass and whole rock (e.g. **Fig. 5.4.B**). The discrepancies seen between the tephra and whole rock compositions are therefore inferred to reflect the difference between whole rock, which includes both melt and crystals components, in comparison to tephra, which just reflects the melt.

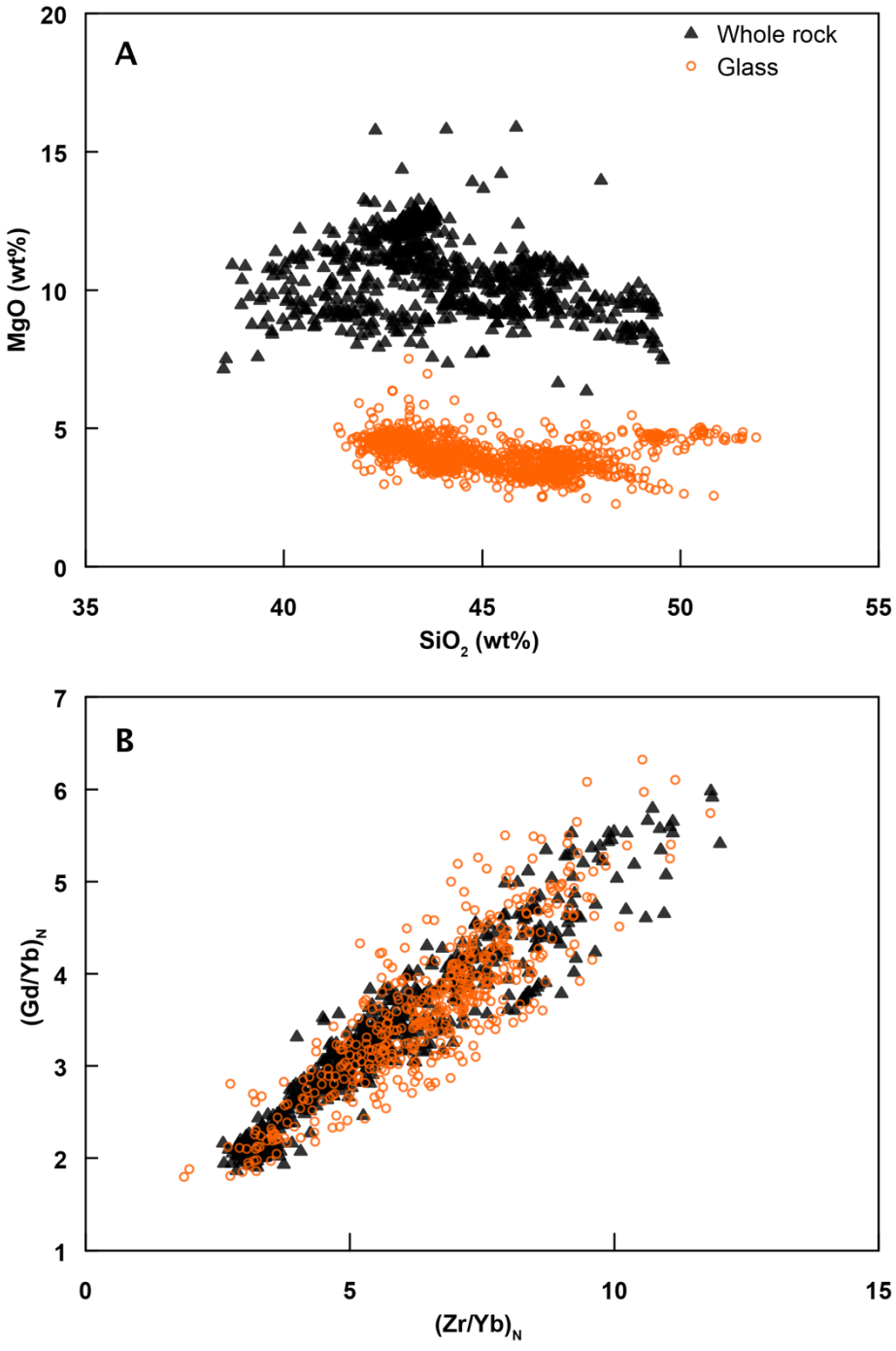

Figure 5.4. *Comparison plot for concentrations of major and trace elements for whole rock and glass for full sample suite (all data in* ***Appendix C****). (A) MgO vs. SiO_2 indicating an example of elements that do not correlate, and (B) $(Zr/Yb)_N$ vs. $(Gd/Yb)_N$ indicating an example of trace element ratios that do correlate.*

5.3.2. Correlation of tephra with interstitial glass in whole rock samples

Due to the discrepancies in the element concentrations between glass in tephra and crystal-bearing whole rock, it is hypothesised that interstitial glass contained in the whole rock samples will provide a more comparable signature to the tephra (**Fig.5.5. A and B**). To test this hypothesis, a sample from Mt. Wellington (AU62394) was chosen as a 'test sample' for two reasons, 1) it was a glassy whole rock sample (glass ground mass with phenocrysts) and, 2) because distal tephra from Mt. Wellington has been unambiguously identified within the Hopua core based on age, scale and stratigraphy (Molloy *et al.,* 2009; **Fig. 5.5**.). The whole rock sample (AU62394) was processed in two ways, first as a whole rock sample (as outlined in **Chapter 4**) and second as a 'simulated (tephra) glass' sample. This process involved roughly crushing the whole rock, and then picking shards of interstitial glass that were of comparable size (30-100 µm) to the glass shards in the cores. These simulated whole rock-derived-glass shards were then treated as tephra derived-glass shards and analysed by the methods outlined in **Chapter 3** (**Fig.5.5. C and D**).

Figure 5.6 shows the results of multi-element comparison of the simulated glass with the known glass samples (from Hopua core). A wide range of both major and trace element compositions (including, MgO vs. full major element suite plus trace elements Rb, Zr, Cs, Ni, Cr, Y, and Er; SiO_2 vs. Al_2O_3, Na_2O, K_2O, and CaO vs. Al_2O_3, Na_2O) are comparable in these two sample types. Limited variability exists between trace elements (e.g., Rb, Zr, Ni, Cr and Y, and the REE) when plotted against each other, or against Al_2O_3 or MgO. Regardless, these elements show a good overall agreement between the two glass types.

Some elements (**Figure 5.6.**) in the tephra derived-glass show a larger spread compared to the simulated glass, which we attribute to two potential reasons: 1) simulated glass was made from a single whole rock sample therefore there would be limited variability in element content, and 2) a natural tephra-derived glass sample will show some minor variability due to the effects of crystal removal and source heterogeneity in different tephra-derived shards. Because both the simulated whole rock-derived glass and known tephra-derived glass exclude the phenocrystic material, they can best be correlated using elements which are highly compatible and which are preferentially incorporated in key crystallising minerals within the

whole rock (e.g. olivine). These elements are therefore strongly partitioned into the crystal phases, and result in comparable glass chemistries. We therefore propose that interstitial glass of whole rock samples can be used, with caveats, for correlation purposes. This method, however, relies on the ability to sample and extract interstitial glass from whole rock samples, which is often not possible. For this reason we aimed to further develop the tephra-whole rock correlation method to correlate tephra deposits to their corresponding whole rock (if devitrified), and thus their centre of origin.

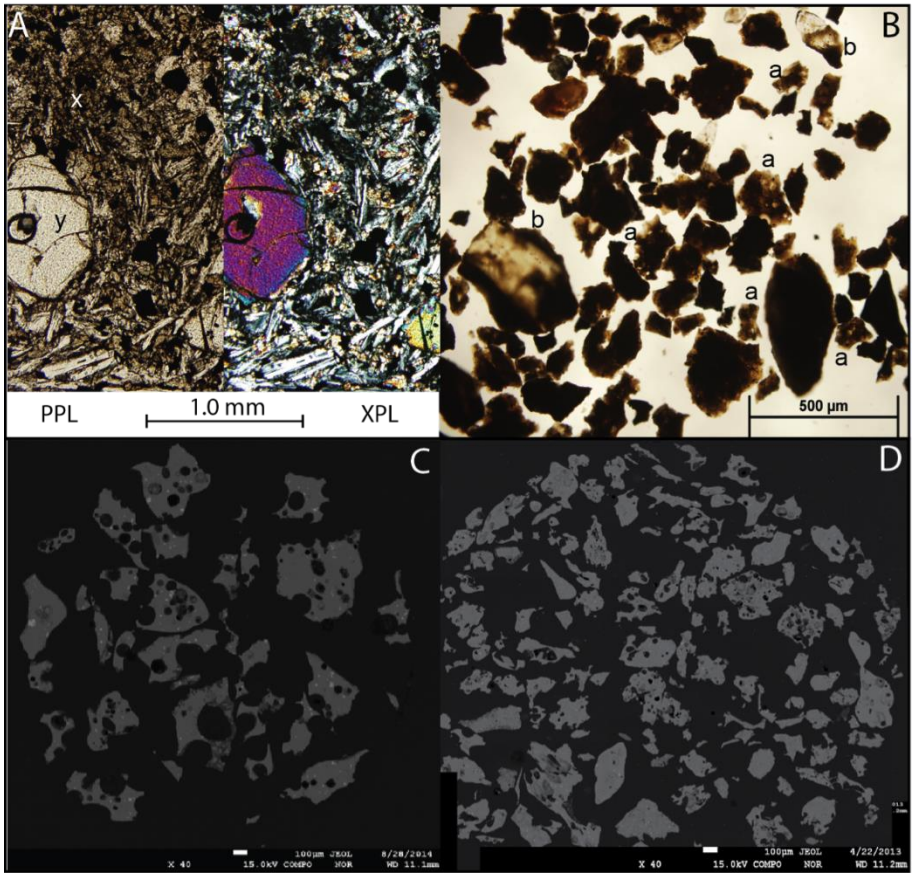

Figure 5.5. *Pictures to show simulated tephra created by crushing a glassy whole rock sample and separation of the interstitial glass component. (A) Shows a microscope image of a thin section of the whole rock sample AU62394 in plain polarised light (ppl) on the left and cross polarised light (xpl) on the right. Glassy groundmass (x) can be identified with a few large phenocrysts of predominantly olivine (y). (B) Crushed whole rock sample AU62394 including glass shards (a) that were hand picked and mounted for analysis and comparison, and phenocrysts (b) specifically large olivine crystals that were not analysed. (C) SEM backscattered electron image of handpicked, mounted, polished, 'simulated whole rock derived-glass' shards created from interstitial glass and, (D) a distal deposit of Mt. Wellington tephra from within Hopua maar core. Scales for images in panels C and D are the same.*

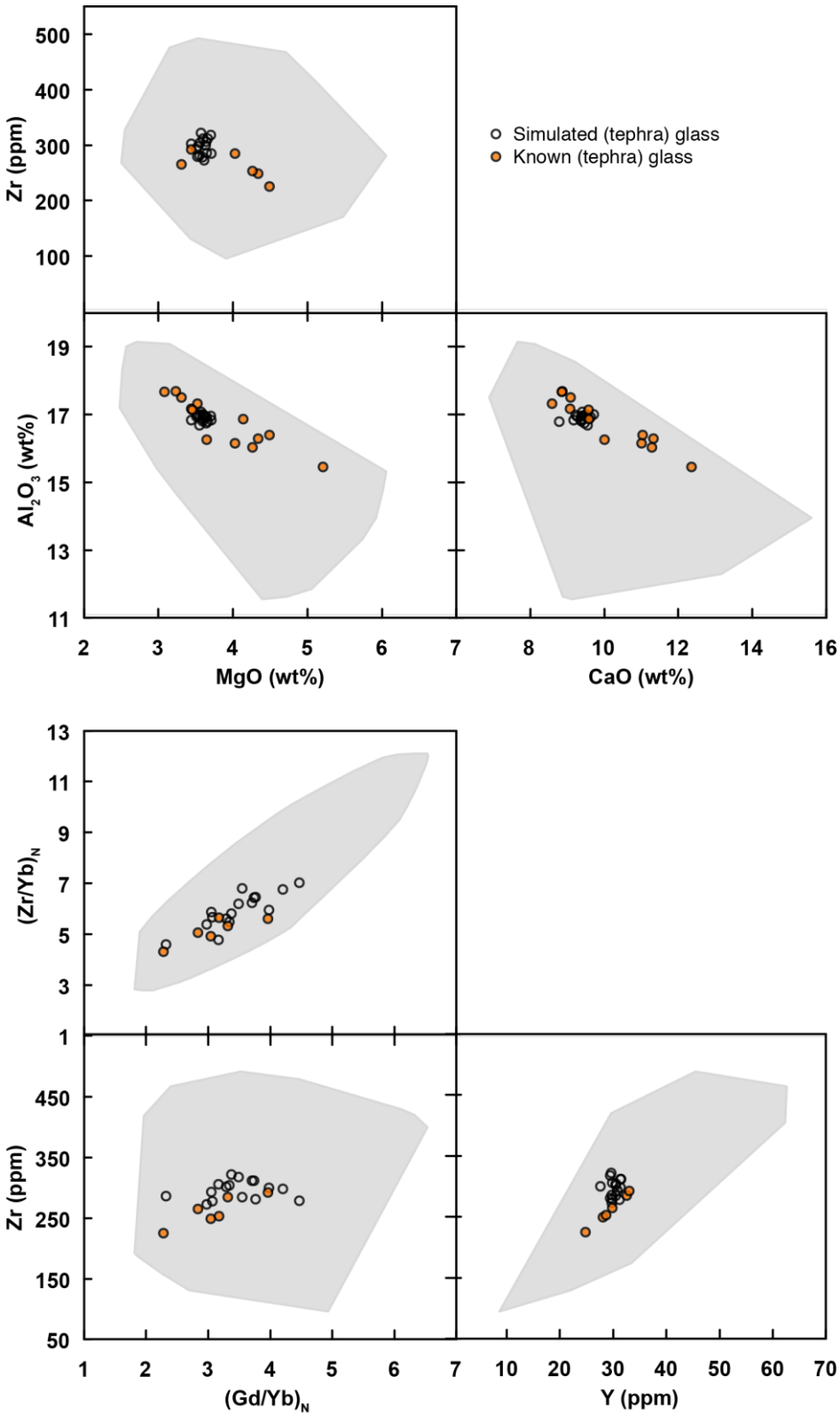

Figure 5.6. *Multi-element plot for comparison of a known Mt. Wellington tephra deposit from the Hopua maar core with simulated tephra (interstitial glass) made from Mt. Wellington whole rock sample AU62394. Grey areas show the range of values (for glass analysis) for the entire field.*

5.3.3. Correlation of tephra with bulk whole rock samples

5.3.3.1. Geochemical constraints

Correlating major element concentrations from whole rock to tephra (glass) samples has proved difficult due to the effect fractional crystallization has on the concentrations of some elements. Plotting element concentrations (for a whole rock from a single centre or tephra shard analyses from one horizon) against other elements that are compatible with certain crystals, (e.g. MgO for olivine, CaO and Al_2O_3 for pyroxene or plagioclase), can monitor the effect of crystal removal on these elements. If an element shows a positive or negative correlation with these key compatible major elements ($r^2 \geq 0.6$, where no single point is responsible for the trend), then it is significantly affected by crystal removal and therefore will not be useful for correlation purposes. Most major elements are affected, as are certain more compatible trace elements (e.g. Ni, Cr, Sc) with high partition coefficients for olivine and pyroxene (**Table 5.4**.). **Figure 5.7** shows that for MgO vs. Ni, whole rock ($r^2 = 0.75$) and tephra-derived glass ($r^2 = 0.61$) and, vs. La ($r^2 = 0.02$ for tephra, $r^2 = 0.11$ for whole rock). This exercise was repeated for all tephra horizons and all centres using MgO, CaO, Al_2O_3, Ni, Mn and Sr on the x-axis, and results suggested that the incompatible REE (and Nb, Zr) were the least affected by crystal removal.

The incompatible trace elements (such as La, Gd, Zr) are therefore well suited for geochemical fingerprinting because they have similar concentrations in whole rock and tephra, and are not affected by crystal removal. Incompatible trace element ratios of both Y and Yb were also tested. The results showed in a number of cases ratios with Y had minor correlations with MgO and Ni, suggesting a preferential enrichment in olivine. Conversely, the ratios with Yb showed no correlation with any of the x-axis elements. Therefore, in the AVF samples La/Yb, Gd/Yb, Zr/Yb, Ce/Yb, Nb/Yb and Nd/Yb are distinguished as the best ratios for correlation. Showing a broad range in the field as a whole, but relatively restricted ranges in samples from the same centre, and no relationship with fractional crystallisation.

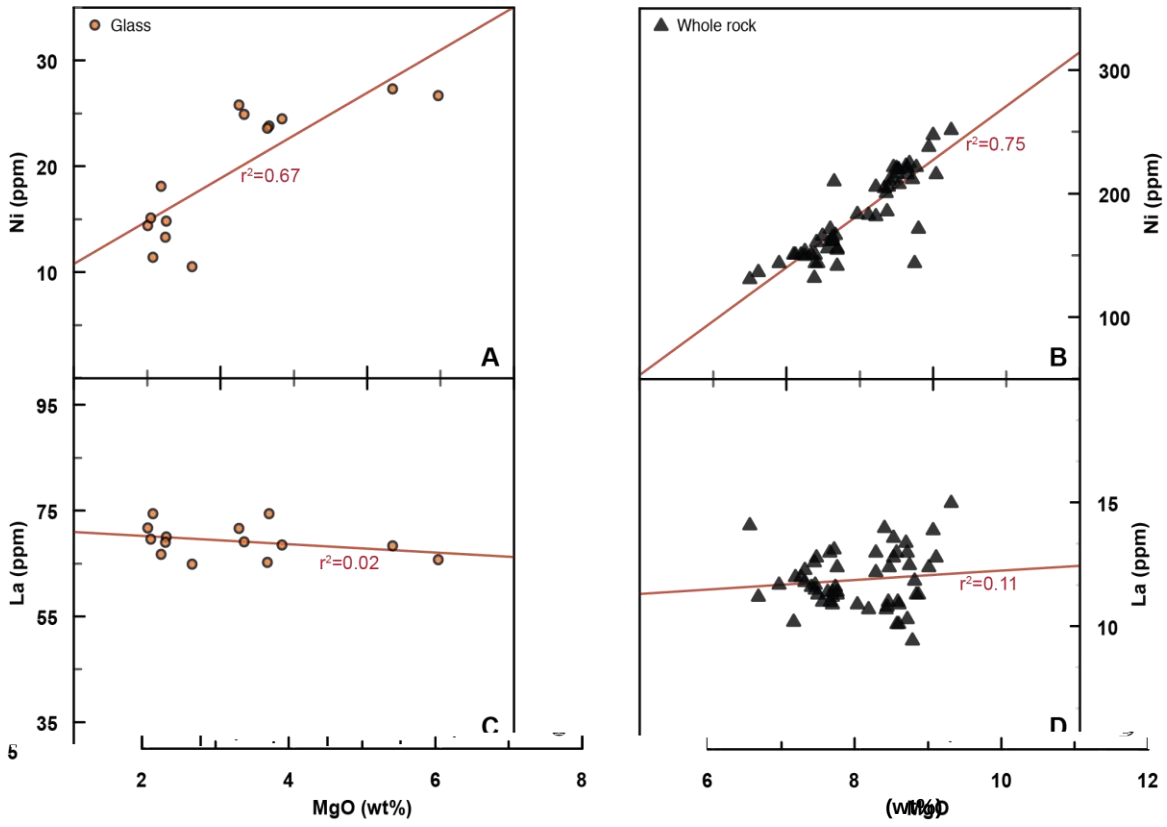

Figure 5.7. *Selected whole rock and tephra sample concentrations from Rangitoto, to show the effects of crystal removal. (A) MgO vs. Ni for tephra-derived glass and, (B) whole rock. Both show a high r^2 value suggesting a statistically significant relationship between the two elements. In comparison (C) MgO vs. La for glass and, (D) for whole rock. Both show r^2 values near zero, indicating no statistically significant relationships between the elements.*

5.3.3.2. Method testing using Mt. Wellington samples

The previous sections have highlighted some specific combinations of major, trace, and trace element ratios that are suitable for correlation between whole rock and tephra, and can therefore be tested. To test for this, we used Mt. Wellington simulated tephra from whole rock sample AU62394, and Mt Wellington derived tephra from the Hopua core.

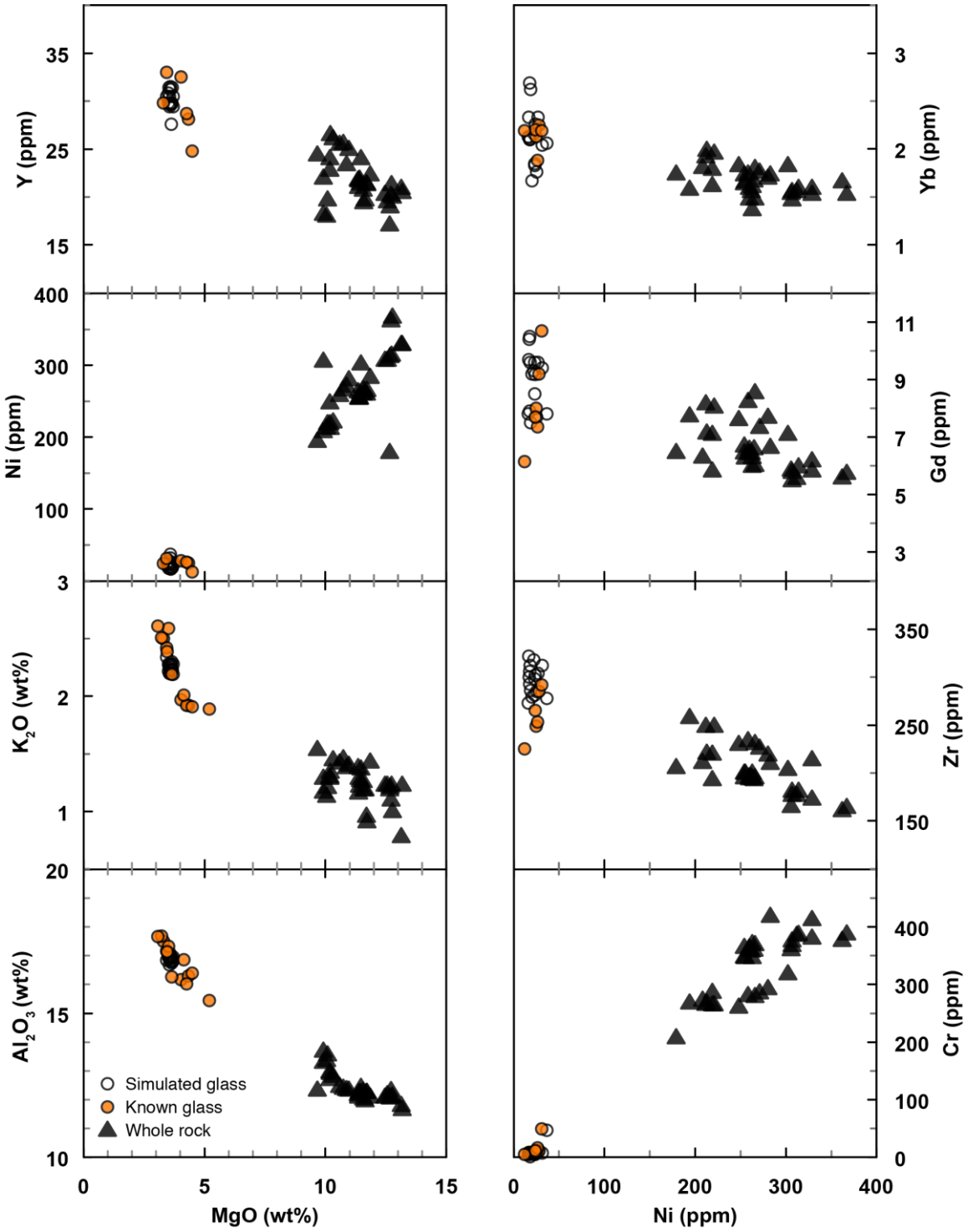

Figure 5.8. *Selected major and trace element combinations for Mt. Wellington that were shown to correlate tephra ('known glass') to interstitial glass ('simulated glass'), but do not correlate tephra (both types) to whole rock. See text for discussion.*

Figure 5.8 shows selected element combinations of MgO vs. Al_2O_3, K_2O, Ni, Cr, and the REE that work for glass-glass correlations but do not work for glass-whole rock correlations. Contrary to this, some major element combinations do appear to correlate the bulk whole rock with the tephra-derived glass (including SiO_2 vs. TiO_2 and FeO, and CaO vs. TiO_2, FeO and Al_2O_3; **Fig. 5.9.**). However, this is mainly due to the small variability observed in these Mt Wellington samples, and may not be applicable for the field as a whole. **Figure 5.10** shows some of the selected trace element and trace element ratio combinations that are sufficiently distinctive to allow independent correlation to be made between the field wide suite of whole rock and tephra-derived glass data. It is therefore concluded that from incompatible ratios LREE/HREE (La/Yb, Gd/Yb, Zr/Yb, Ce/Yb, Nd/Yb and Nb/Yb), correlation between tephra and whole rock *is* possible.

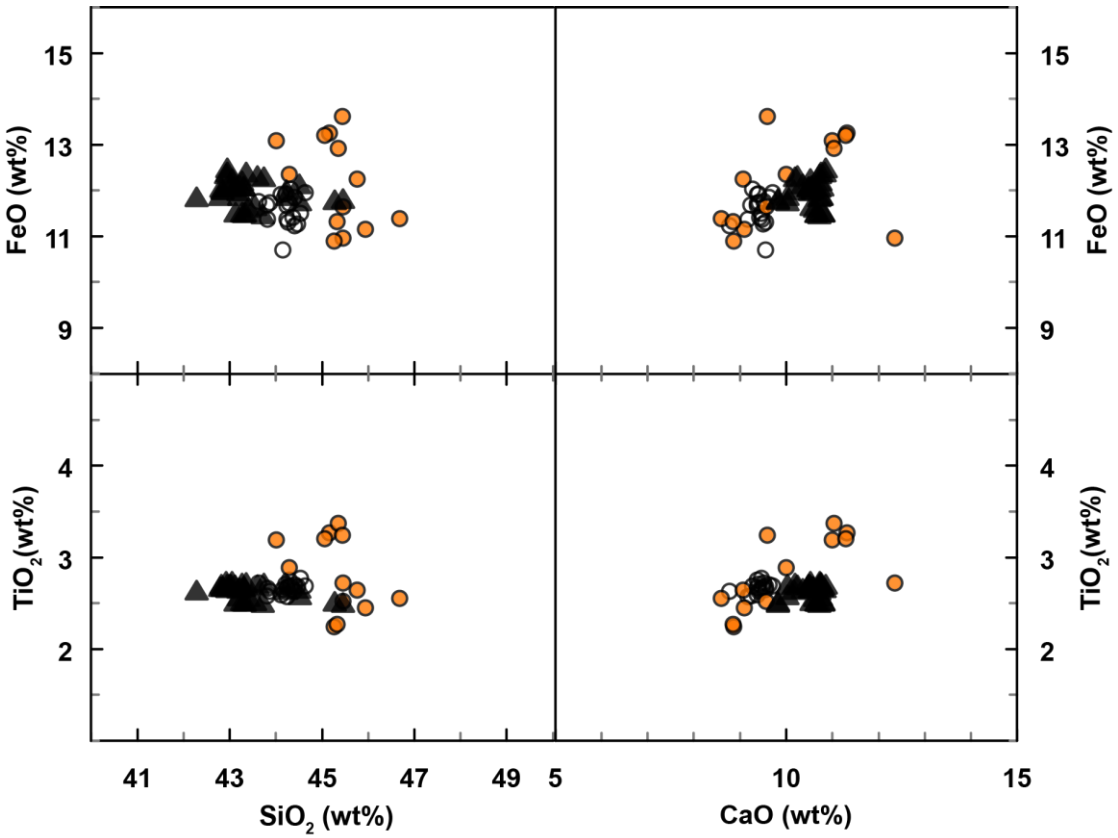

Figure 5.9. *Selected major element combinations for Mt. Wellington that were shown to be comparable for tephra-derived glass and interstitial glass, and are also comparable for whole rock vs. glass. Symbols as in* ***Figure 5.8****.*

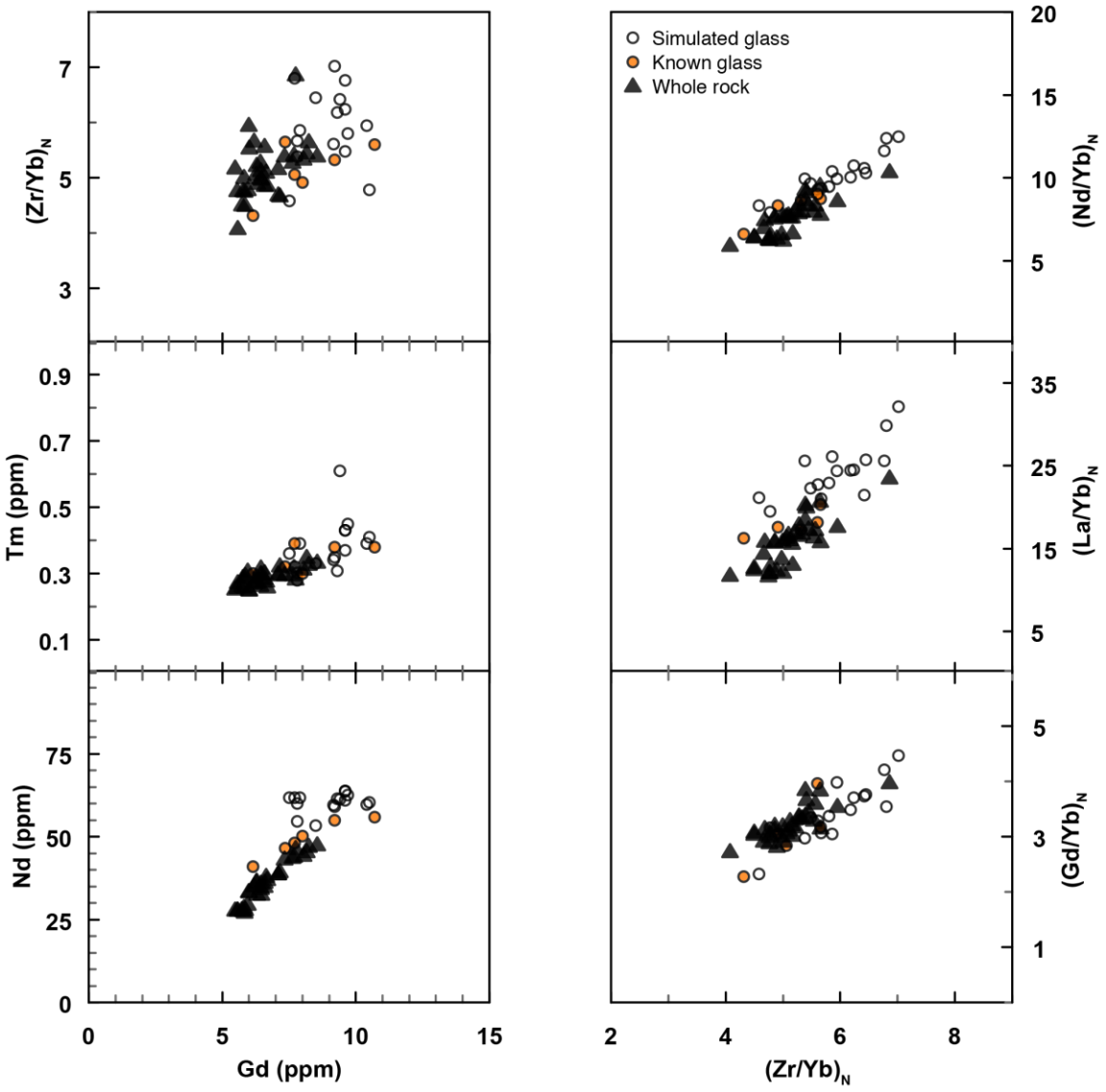

Figure 5.10. *Selected trace element combinations for Mt. Wellington that are comparable for tephra-derived glass and interstitial glass, and are also comparable for whole rock vs. glass. Symbols as in* ***Figure 5.9.***

5.3.3.3. Geochemical variations in single eruptions

Previous studies have shown a variation in the geochemistry throughout an eruption in samples from some of the AVF centres (e.g. Crater Hill; Smith *et al.,* 2008, and Motukorea; McGee *et al.,* 2012), primarily evolving in eruption style from phreatomagmatic to magmatic (**Table 5.1.**). These centres consistently show, for example, initially low SiO_2 and Mg/Fe ratios (Smith *et al.,* 2008) and higher incompatible elements that evolve to final products with higher SiO_2, Mg/Fe ratios and lower incompatible elements (**Fig. 5.11**. and **Fig. 5.12**.). It was therefore considered important to test whether the geochemical signature of the widely dispersed tephra reflects only one specific part of the eruption sequence.

Figure 5.12 shows the geochemical progression throughout the eruption of Motukorea (data from McGee *et al.,* 2012), compared with the correlated Motukorea tephra horizon found within the Orakei Basin Core for SiO_2 vs. Zr, and normalised (to primitive mantle values: McDonough and Sun, 1995) trace element ratios for $(Zr/Yb)_N$ vs. $(Gd/Yb)_N$ (similar relationships are also seen for $(La/Yb)_N$, $(Ce/Yb)_N$, $(Nb/Yb)_N$, and $(Nd/Yb)_N$). The tephra-derived glass shards appear to show slightly higher SiO_2 concentrations for the same Zr concentrations (as previously discussed due to fractional crystallisation) but show the signatures of the full evolutionary trend for the entire eruption. For the trace element ratios the glass shards appear to be geochemically comparable and again have signatures that are the same as all phases of the eruption including tuff, lava and scoria.

However, it is considered that for some of the eruptions where there are both explosive and effusive phases, distal tephra deposits may only preserve evidence for the explosive phases of the eruption. This is because the explosive phases are generally more violent, and produce more pyroclastic material, which is distributed further (discussed **sect. 5.2.5.**). For the AVF centres, most of the primary eruptive phases are explosive (**Table 5.1.**), and therefore, if all centres show a geochemical evolution throughout an eruption (e.g. Motukorea and Crater Hill), there is the potential for tephra deposits (from early phreatomagmatic phases) to have higher trace element ratios than their subsequent lava or scoria deposits (from later magmatic phases). This deposition bias may hinder the potential for some tephras to be matched to their source centre.

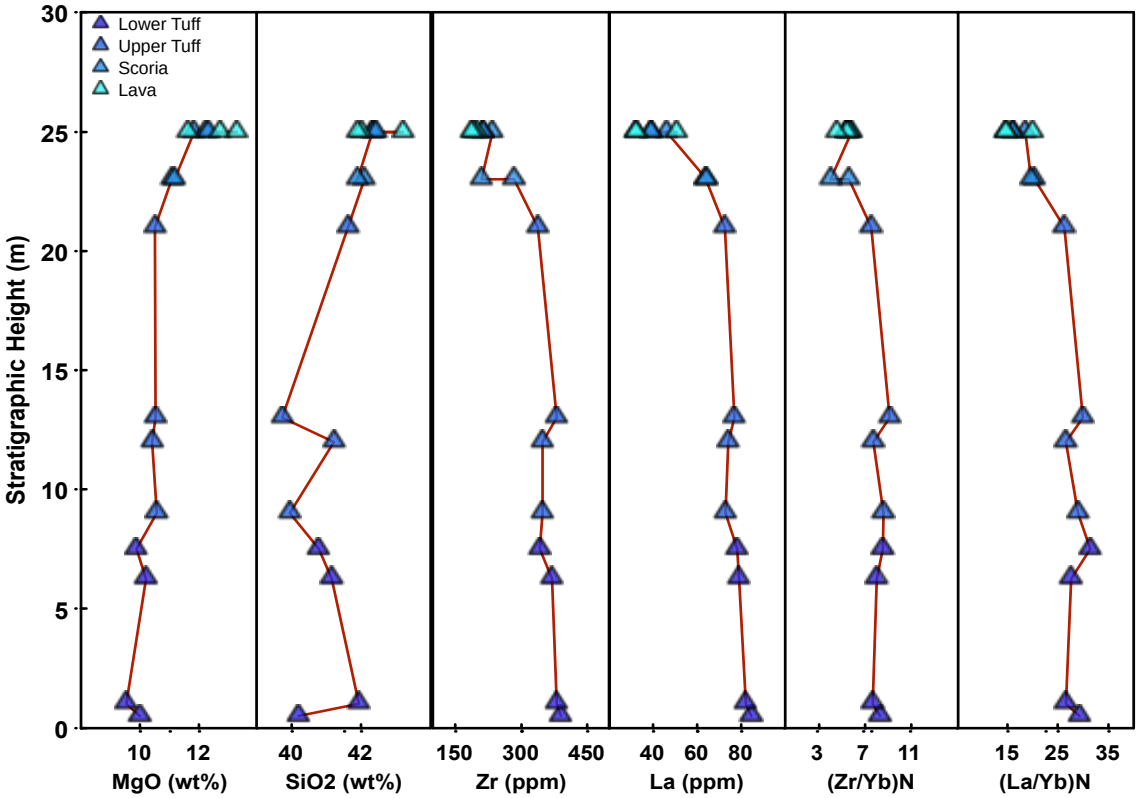

Figure 5.11. *Variations seen in selected elements for the Motukorea eruption products. Data and figure adapted from McGee et al. (2012).*

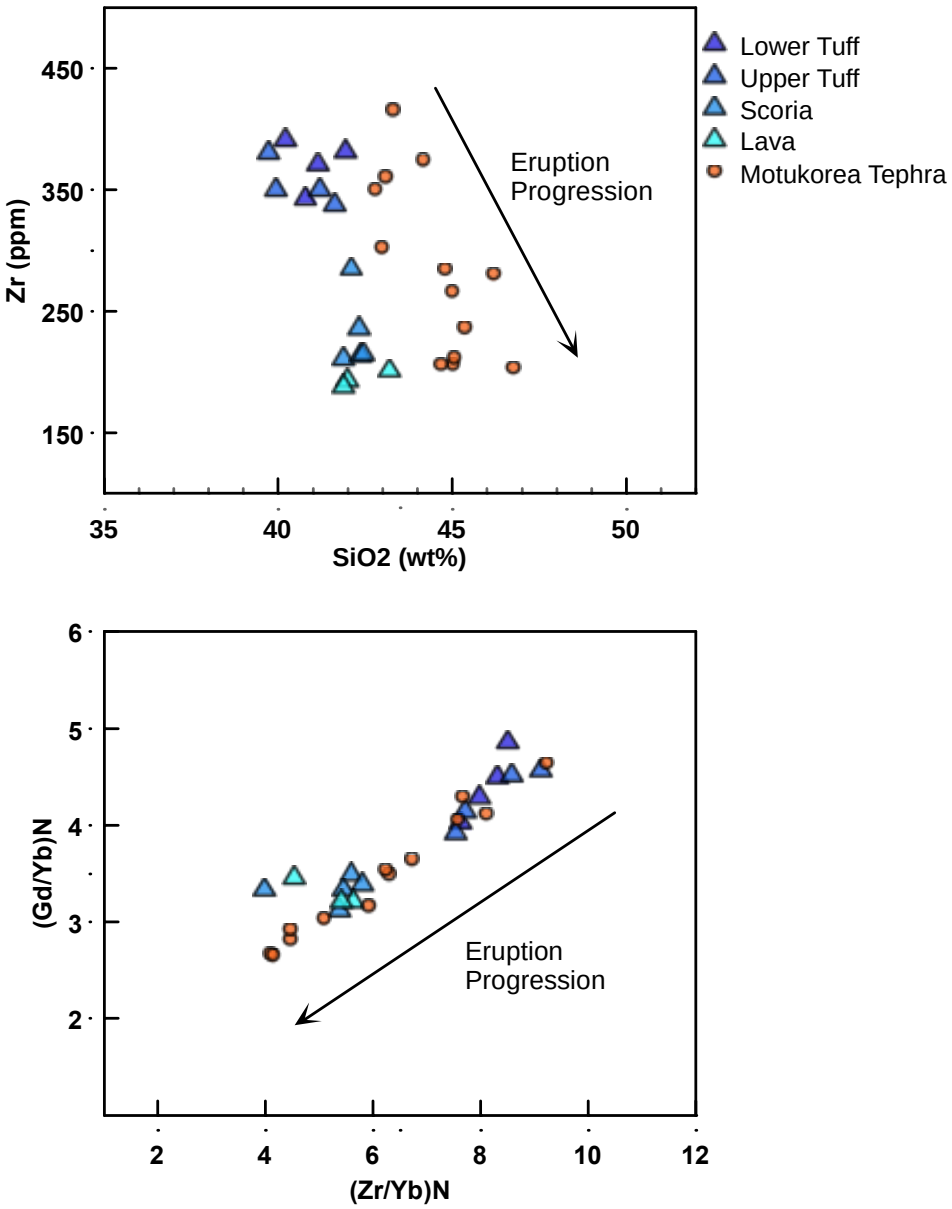

Figure 5.12. *Graphs showing the geochemical variations and comparability of the geochemical signatures observed through the eruptive products of Motukorea volcano (from McGee et al., 2012), and the distal tephra erupted from this volcano found within the Orakei Basin core (data from* ***Appendix C****).*

5.3.3.4. Limiting factors with geochemical correlation

Although the ability to correlate tephra to whole rock has been confirmed, there are a number of limiting factors. In addition to the previously outlined complexity of geochemical variability in some centres (**sect. 5.3.3.3.**), the geochemical composition of most lava from individual AVF volcanic centres overlap. Thus there are not 53 individual signatures that can be used to directly correlate the geochemical composition of the distal tephra deposits and whole rock samples. In the instances where the geochemical composition alone cannot unambiguously fingerprint the centre, this is due to either the large number of centres with relatively similar geochemical compositions, and/or due to a general lack of geochemical data (either whole rock or tephra). It is therefore necessary to introduce other criteria to allow the most confident correlations to be made. These criteria were discussed in **Section 5.2.5**, and are outlined where appropriate in relation to each of the correlations discussed below.

5.3.4. Tephra source correlations

Chapter 3 outlines the methodology of cross core tephra correlations. It details twenty-nine tephra horizons, twelve of which are cross-correlated linking two or more deposits, and seventeen of which are single deposits found within one core. Below I discuss each horizon in turn, and detail the process by which the source centre has been assigned. For twenty-nine horizons the proposed source centres are given in **Table 5.5** along with the alternatives that were considered. Each tephra to source correlation is given a confidence rating as discussed in **Section 5.2.5**, based on the criteria which are satisfied (cf. **Figure 5.13).** Of the twenty-nine horizons, eight have been given a correlation with confidence rating of 1, twelve have been given a confidence rating of 2, and seven have been given a confidence rating of 3, with two horizons remaining uncorrelated. An example of the geochemical signatures for a level 1 confidence rated correlation is given in **Figure 5.14**, all other geochemical correlation plots can be found in Appendix E.

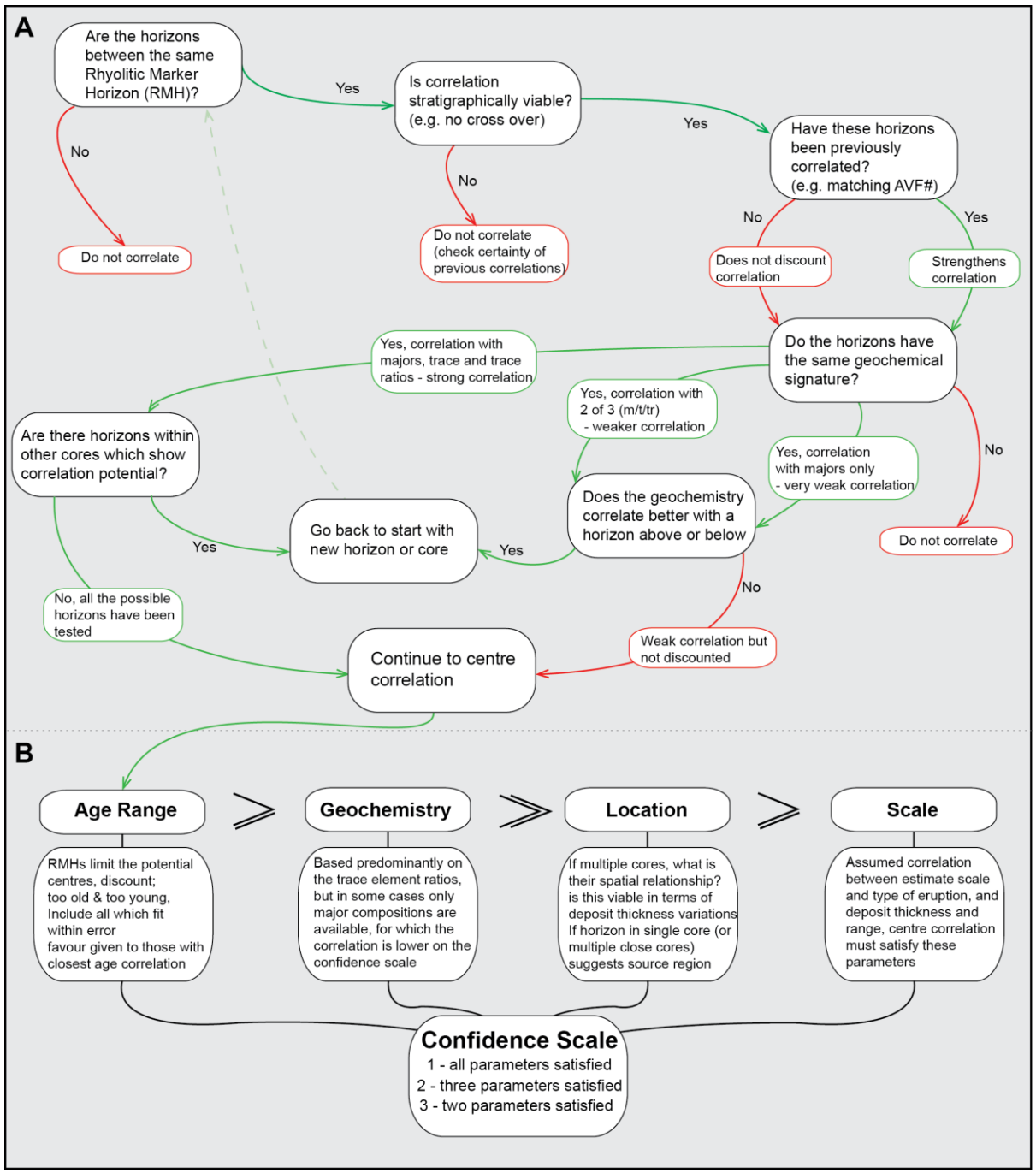

Figure 5.13. *(A) Flow chart outlining the step-by-step process in determining the correlation of tephra horizons across cores (used for* ***Chapter 3****). It is important to note that major elements alone are not enough to accurately determine a horizon match or not, and in all cases a multi-parameter approach is used to obtain the result with highest confidence value, 'm/t/tr' – major/trace/trace ratio. (B) Steps in determining the source centre for the previously linked horizons and the confidence scale as a result of satisfying the outlined parameters. Highlighted is a hierarchy of importance for the parameters.*

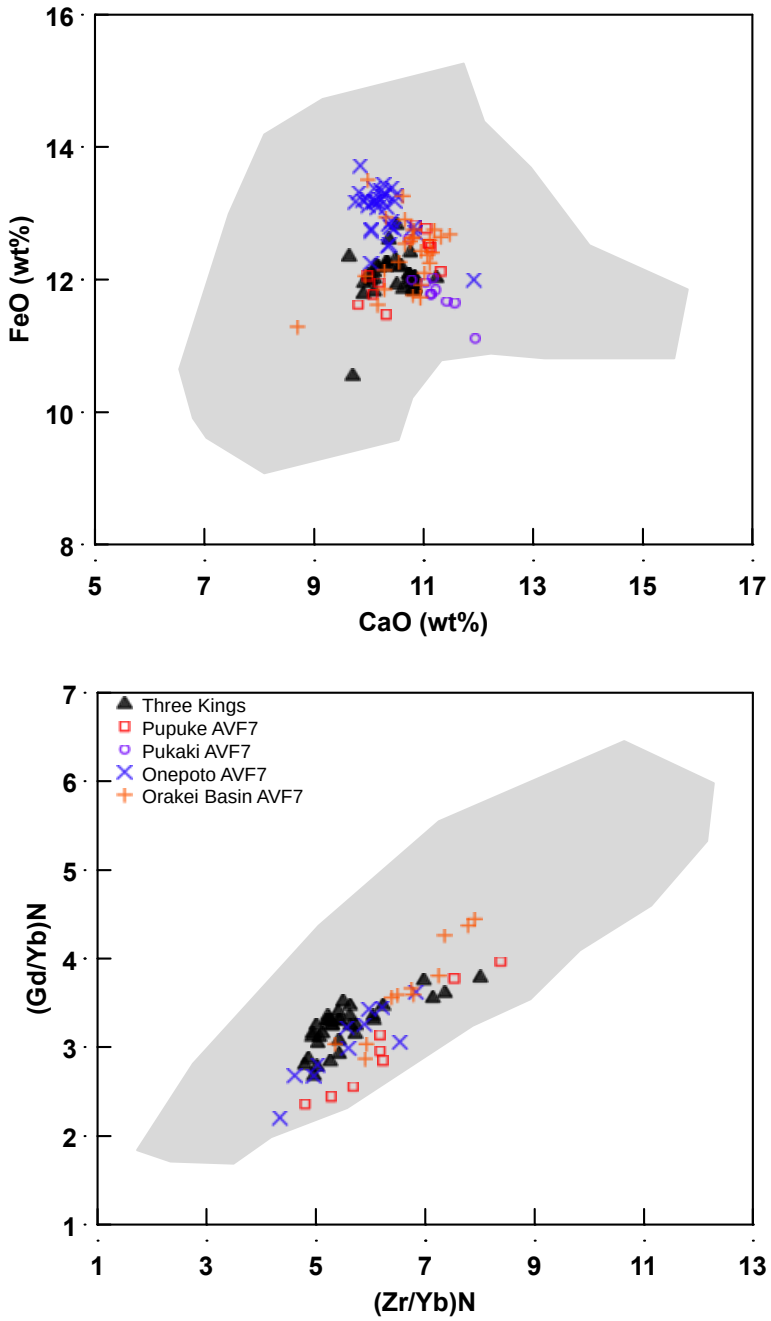

Figure 5.14. *Example of a confidence level 1 correlation for the Three Kings centre with tephra layer AVF7, showing selected major element and normalised trace element ratios (all data is outlined in* ***Appendix C****). Tephra shown in coloured symbols indicating each core, whole rock shown by black triangles, while the grey field shows the spread for the entire AVF. Age constraints are also well matched, as are centre location, tephra dispersal area and eruption scale*

Previously assigned AVF numbers by Molloy et al. (2009) have been maintained to ensure a consistent tephra horizon nomenclature in the literature. However, if the geochemical composition of tephras in some deposits were inconsistent with previously proposed correlations (e.g., AVF9 and AVF10, **Chapter 3**) new correlations across cores were established. For more detail the reader is referred to **Chapter 3**, where the respective horizons were re-assigned AVF numbers based on the new data from this study (**Table 3.2**). In **Chapter 3** horizon thickness is also discussed and re-evaluated in relation to primary vs. reworked horizons. For many of the thicker horizons new primary thicknesses are outlined (**Table 3.2.**), and these new values are used within this thesis chapter. The ages of tephra horizons were recalculated in this study and can be found in **Table 5.3**. Groundmass feldspar Ar-Ar ages from the AVF centres (quoted as ranges with a 2sd error) are adapted from Leonard et al. *(in prep;* **Appendix D**; for mean ages refer to **Table 5.1**). Eruptive scales used in this study are taken from Kereszturi et al. (2013) (discussion in **Sect. 5.2.5. Table 5.1.**), and relevant tephra-whole rock geochemical plots can be found in **Appendix E**.

Within each paragraph the AVF number of the horizon in discussion is in bold, and once the corresponding centre is assigned, its name is also bold. Each tephra horizon is assessed as an individual, and therefore all potential centres are discussed, even if they have been correlated to an alternative horizon (discussion in **Sect. 5.2.5.**). Correlations of tephra horizon to source centre are discussed below in order from youngest to oldest horizon:

AVF24 from the Pupuke core (samples P48 and P49, “separated by 15mm of slumpy unlaminated sediments”; Molloy, 2008) and **AVF23** (Hopua core) have previously been assigned centres with a high level of confidence due to their stratigraphy and major element geochemistry (Molloy *et al.,* 2009; Needham *et al.,* 2011; Shane and Zawalna-Geer, 2011). The addition of the trace element geochemistry from this study supports these correlations, with **AVF24** (upper [P48] and basal [P49]; Molloy, 2008) assigned to **Rangitoto 2 and 1** respectively and **AVF23** to **Mt. Wellington,** all with confidence level 1.

AVF22 is a fine (1mm thick) deposit at a depth of 47.72 m within the Pukaki core. The calculated age for this horizon is 15.4 cal. ka BP (**Table 5.3**.). Data from Sandiford et al. (2001) consists of one major element analysis and therefore correlation of this horizon based on geochemical composition is problematic. There is only one centre, however, which is appropriate in age, scale and location and that is **Pukeiti**, (DRE^{tot} 0.0037 km^3) in the south of the field (ca. 5 km from Pukaki) with Ar-Ar age range of 3.2-18.0 ka. It is therefore given a confidence level 2 correlation, taking into account the sparse geochemical information.

AVF21 and **20** are both similar deposits. They display similar geochemical signatures, are both thick within the Hopua core (290 mm and 235 mm, respectively) and much thinner within the Pukaki core (3 mm and 2 mm, respectively). The estimated ages for the horizons are 19.9 ka and 20.6 ka, respectively (**Table 5.3**.). The deposit thicknesses and distributions point to source centres within close proximity of Hopua core in the central-south of the field. Tephras from both horizons have similar geochemical compositions, leading to difficulty in assigning specific source centres. Potential source options for these tephra horizons, that fit the age and location criteria, therefore include Pukeiti, Mt. Richmond, Mt. Smart, Panmure Basin, Mt. Robertson, and Waitomokia. Mt. Robertson can be excluded as the geochemistry does not match and the age is not constrained. Pukeiti could also be included as the geochemistry is relatively well correlated; however, its small eruptive volume and the distance (ca. 6.5 km) from Hopua and Pukaki make Pukeiti an unlikely candidate. Waitomokia can also potentially be ruled out, because the centre is larger than Pukeiti, was predominantly a phreatomagmatic eruption, and therefore, the expected tephra deposit should be much thicker within the Pukaki core. This, together with a poorly constrained age, and lack of geochemical data makes it less likely than the alternatives. Panmure Basin, Mt. Richmond and Mt. Smart all have similar whole rock geochemical signatures (**Appendix E**) which match that of tephra horizons AVF20 and AVF21. Panmure Basin is, however, less likely due to its greater distance to the Hopua core than Mt. Smart and Mt. Richmond. In addition the Panmure Basin centre is located closer to the Orakei Basin core which shows no evidence of a ~20 ka old tephra deposit. Mt. Smart and Mt. Richmond are therefore the most likely source centres for **AVF21** and **AVF20**. The Ar-Ar ages of 11.9-20.3 ka (Mt Smart) and 21.1-30.7 ka (Mt Richmond) suggest that Mt. Smart is slightly

younger than Mt. Richmond and thus **AVF21** is assigned to **Mt. Smart** and **AVF20** to **Mt. Richmond.** However due to the ambiguity in age and inconclusive geochemistry, these correlations are given a confidence rating of 3.

AVF 19 is only found as a very thin deposit (1 mm) within the Pukaki core with only one published major element point (Sandiford *et al.,* 2001), precluding any conclusive correlation based on geochemistry. Potential source centres however need to satisfy the following criteria, a small-medium size eruption in the south of the field (as no deposits of this age span are present in any other cores), most likely less than 10 km away from Pukaki, with an age of 24.2 cal. ka BP (**Table 5.3**.). Centres with these characteristics include Green Mt. (12.7-25.5 ka), Hampton Park (11.0-65.0 ka), Otara (5.5-70.5 ka), Otuataua (no Ar-Ar age) and Wiri Mt. (22.0-38.0 ka). Of these, Green Mt., Hampton Park and Otara are the furthest away, all >8 km from Pukaki and are therefore considered as less likely eruption source. Wiri Mt. and Otuataua are both just over 5 km for Pukaki, and have DRE^{tot} volumes of 0.016 km^3 and 0.006 km^3 respectively. Therefore, due to the thinness of the deposit in the Pukaki core and its limited dispersal, a small eruption from Otuataua is considered as a more likely source than Wiri Mt. Due to the lack of geochemical data and age constraints on **Otuataua** centre the correlation is given a confidence rating of 3.

AVF 19 is separated from **AVF 18** within the Pukaki core by an andesitic deposit (Eg36) from the Taranaki Volcanic Centre (Molloy *et al.,* 2009), which therefore acts as a secondary constraint on the cross core correlation for the AVF18 deposit. AVF 18 occurs as an 8 mm deposit in the Orakei Basin core, a 40 mm deposit in the Hopua core, and a 0.5 mm deposit in the Pukaki core. This dispersal is indicative of a medium sized eruption from the central-southern part of the field, which must have occurred between 23.2 and 25.3 cal. ka BP (cf. **Table 5.3**.). Centres that satisfy these criteria include Mt. Richmond (AVF20), Otuataua (AVF19), Panmure Basin, Puketutu (slightly too old), and Waitomokia (undated). Panmure Basin and Otuataua are ruled out, as the geochemistry does not correlate (**Appendix E**). In comparison, Waitomokia, Puketutu, and Mt. Richmond all show good geochemical correlation (although there are minimal data for Mt. Richmond; **Appendix E**). The localities and scales of eruption for Puketutu (5 km to Hopua, and large DRE^{tot}=0.018 km^3) and Mt. Richmond (5 km to Hopua and DRE^{tot}=0.0057 km^3)

reduce their likelihood to be the source centre for AVF 18. Waitomokia is undated by Ar-Ar techniques, however, morphostratigraphy makes it older than Pukeiti and the other factors all correlate well. Therefore **Waitomokia** is given a correlation confidence level of 2 for horizon **AVF18**.

AVF17 is only found in Orakei Basin core with a thickness of 5 mm at a depth of 44.65 m. Based on sedimentation rates an age of 23.4 cal. ka BP was calculated for this horizon (see discussion in **section. 5.2**, and **Table 5.3**.). Potential sources therefore are most likely to be a small-medium sized eruption from within <10 km of Orakei Basin. As AVF17 was not identified in the Pupuke and Onepoto cores, the source eruption is more likely to be in the north or north-east of the field. Possible eruption sources therefore include Little Rangitoto, Motukorea, Mt. Cambria, Mt. Richmond (AVF20), Panmure Basin, Pigeon Mt., and Taylors Hill. Because geochemical composition of samples from Mt. Cambria, Mt. Richmond, Panmure Basin, and Taylors Hill are different to the AVF17 tephra these centres are initially discounted (**Appendix E**). Due to its very close proximity to Orakei Basin, an eruption from Little Rangitoto would have formed a thicker deposit with much larger shard sizes. Pigeon Mt. and Motukorea are both ca. 8 km from Orakei, and Motukorea is slightly larger (DRE^{tot} 0.0046 km^3) than Pigeon Mt. (DRE^{tot} 0.0033 km^3). Both have similar geochemical compositions (although Pigeon Mt. has less data) and Motukorea is dated (although with large error) to 3.3-25.3 ka (Ar-Ar, Leonard *et al*., *in prep*, **Appendix D**). Although difficult to split with similar geochemistry, based on the scale of the eruption coupled with the deposit thickness, **AVF17** is assigned to **Pigeon Mt.** with a confidence level 3**.**

AVF 16 is a relatively thick deposit (50 mm) only identified within the Pukaki core at a depth of 51.52 m, suggesting a source in the south of the field. It is located just slightly above the Kawakawa/Oruanui (Kk) rhyolitic marker horizon, and therefore has an age estimate of 25.3 cal. ka BP (**Table 5.3**.). There is limited geochemical data for this deposit (2 major element analyses) and therefore geochemical constraints are limited, and correlations are therefore based primarily on alternative criteria. Potential source centres that satisfy the age and locality criteria include Puketutu (29.8-37.4 ka), Otuataua (AVF19, undated), Crater Hill (26.7-37.5 ka), Kohuora (30.0-32.0 ka), Wiri Mt. (25.7-34.5 ka), Ash Hill (31.6-32.0

ka), Mt. Robertson (undated), or Mt. Richmond (AVF20, 18.4-29.2 ka). Crater Hill is immediately eliminated as the Kawakawa/Oruanui RMH has been identified overlying the centre in the field (Hayward *et al.,* 2011). Because Kohuora represents a relatively large eruption (DRE^{tot} 0.0076 km^3) and is located nearby (<3 km), this centre is likely to have produced a much thicker tephra deposit (also true for Crater Hill) and is therefore also discounted as the source. Ash Hill (no geochemical data) is also discounted, as the eruption was very small (DRE^{tot} 0.000076 km^3) and the centre is located ca. 6 km away, to the south-east of Pukaki, making it very unlikely to be the source. This leaves Puketutu, Otuataua, Wiri Mt., and Mt. Richmond: all of these are appropriately located, and only Puketutu is slightly too old. The larger volumes of Wiri Mt. (DRE^{tot} 0.016 km^3), Otuataua (DRE^{tot} 0.006 km^3), and Mt. Richmond (DRE^{tot} 0.0057 km^3), all of which are located 5-6 km away, make them an unlikely source to produce a 50 mm deposit in Pukaki. However the geochemistry for Wiri Mt. matches well with geochemistry of the tephra deposit (unlike for Otuataua and Mt. Richmond) (**Appendix E**). The geochemical composition of Puketutu samples is similar to the geochemical composition of the deposit and the centre is slightly larger (DRE^{tot} 0.017 km^3) than Wiri Mt. In addition Puketutu is located ~ 6 km to the west of Pukaki, which is a more favourable position based on the predominant south-westerly winds. Although the Ar-Ar age for Puketutu is slightly older than the stratigraphic position of the deposit, **AVF 16** is correlated to **Puketutu** with a confidence level 2.

AVF15 is only found within Orakei Basin with a thickness of 12 mm at a depth of 47.715 m. This deposit has an age estimate of 24.5 cal. ka BP (**Table 5.3**.). Many centres are an appropriate source within this age range, but the occurrence of this thin deposit only in the Orakei Basin core is indicative of an origin in the north or central-north of the field from a relatively small eruption. This narrows the potential source centres down to Motukorea (3.3-25.3 ka), Mt. Cambria (23.9-65.1 ka), or Pigeon Mt. (undated). The geochemistry of this deposit is similar to both Motukorea and Pigeon Mt., but not to Mt. Cambria, and therefore could be assigned to either Motokurea or Pigeon Mt. Motukorea was a slightly larger eruption (DRE^{tot} 0.0046 km^3) located ca. 8.5 km away, in comparison to Pigeon Mt. which was a slightly smaller eruption (DRE^{tot} 0.0033 km^3) but located a similar distance away. Therefore

based on the deposit thickness, **AVF15** is assigned to **Motukorea.** A confidence level of 2 is given although the age remains poorly constrained.

At depth of ca. 50-48 m the Orakei Basin core becomes extremely complex containing multiple deposits and a number of reworked sections. Details of this complex core sequence are given in **Chapter 3** (and **Appendix A**). In **Chapter 3** I confirmed AVF13 (50.089-49.554 m, including ca. 70 cm of reworking, **Chapter 3**) and below I correlate this deposit to its source centre. I also:

(1) define a new horizon '**newA**' which is represented by three layers at 49.14 m, 49.33 m and 49.46 m;

(2) discredit original **AVF14 (**cf. Molloy, 2008) as representing the reworking of the two underlying units (AVF13 and newA), and redefine to a continuous deposit with samples taken at 48.128 m and 48.120 m;

(3) define a new horizon '**newB**' which is represented by two layers at 48.19 m and 48.27 m.

Due to the limited age range for these new deposits (ca. 24.6-25.3 ka; sedimentation rates from this study, **Table 5.3**.), they all have a similar range of possibilities for centre correlations. These include (with Ar-Ar age ranges reported), Little Rangitoto (15.9-24.7 ka), Motukorea (AVF15, 3.3-25.3 ka), Mt. Cambria (23.9-65.1 ka), Panmure Basin (15.6-33.6 ka), Taylors Hill (23.8-29.8 ka), and McLennan Hills (23.9-65.1 ka). For horizons **newA** and **newB** the geochemistry does not correlate specifically well to any of these centres in particular and is therefore not a discerning feature. As a result these horizons cannot be confidently correlated and therefore are left as unknowns.

AVF14, although only a thin deposit only found in the Orakei Basin core, has very large shard sizes (>150 μm), suggesting the source is in close proximity to Orakei, but a small-scale eruption. The calculated age of this deposit is 24.6 cal. ka BP (**Table 5.3**.). The geochemical composition of this deposit matches the geochemical composition of **Little Rangitoto** (**Appendix E**), and therefore this correlation is given a confidence rating of 1, because all parameters (geochemistry, age, scale, location) are satisfied.

AVF13 is only found within the Orakei Core at a depth of 50.089 m (although reworked up to 49.554 m) with a primary deposit thickness of ca. 160 mm (**Chapter 3**), and an estimated age of 25.3 cal. ka BP (**Table 5.3**.). Due to the thickness of the deposits in Orakei, the source centre is proposed to be a relatively large eruption from nearto Orakei. Potential options which satisfy age, locality and scale for this include; Mt. Eden, Little Rangitoto (AVF14), Panmure Basin, Mt. Richmond (AVF20), and Taylors Hill. Of these centres only **Panmure Basin** has a matching geochemical composition (**Appendix E**) and because the correlation satisfies all the criteria, this is given a confidence rating of 1.

AVF12 is found in all analysed AVF cores of appropriate age (Pupuke, Onepoto, Orakei, Hopua, and Pukaki), the scale, distribution, and thickness of the tephra deposits suggest a very large eruption in the centre of the field just prior to the Kawakawa/Oruanui. The horizon has an estimated average age of 27.2 cal. ka BP, but a range throughout the cores of 26.3-28.3 ca. ka BP (**Table 5.3**.). The only centre that satisfies these criteria is **Mt Eden**, however the geochemical signature of horizon AVF12 is complex, and highly variable (**Appendix E**). The top two subsections of tephra within the Hopua core show very different geochemical composition to the basal section. This could be indicative of a separate eruption occurring at the same time with a different geochemical signature. There is, however, no mixing of shard signatures within the deposit (which would be expected from coeval deposition from two separate eruptions), or break in the deposition of the horizon. The horizon could therefore be interpreted in two ways, 1) to represent one continuous eruption, with the tephra showing a geochemical evolution from more- to less REE-rich, or 2) to represent two immediately successive eruptions, with products from the first eruption having higher REE contents and the second having

lower REE contents. Of note is that the centre Te Pou Hawaiki, is morphostratigraphically constrained to just older than Mt Eden, it is therefore conceivable that these two eruptions were successive, and would have produced tephra deposits without a hiatus. However, the geochemical signatures of Mt Eden and Te Pou Hawaiiki are indistinguishable, both of which correlate to the upper horizon in the Hopua core. As this geochemical complexity is unresolvable, **AVF12** is assigned here to **Mt Eden** with a confidence level 1, with Te Pou Hawaiki remaining slightly older in age. AVF12 also marks the base of the Hopua core, thus providing a minimum age constraint on the eruption of this centre.

AVF11 is a relatively thin unit (ca. <10 mm; *P. Shane pers. comms*, 2014), only found within the Pukaki core at a depth of ca. 55.35 m and with an estimated age of 29.3 cal. ka BP (**Table 5.3**.). The thickness and restricted dispersal of this layer indicates a relatively small eruption source in the south of the field, most likely within 5-10 km of Pukaki. Centres that satisfy these criteria include, Kohuora, Otuataua (AVF19), Mt. Robertson, Puketutu (AVF16,) and Wiri Mt. Although Otuataua and Mt. Robertson are appropriate in locality and scale, samples from these centres have somewhat different geochemical compositions to the AVF11 tephras and their ages are unknown. Kohuora has no geochemical data but is of similar age, although its scale and locality should have formed a much thicker deposit (>100 mm) in the Pukaki core. Puketutu has similar (major element) geochemistry to the horizon and is of similar age and well located as source centre. However, Puketutu has been assigned as source centre for AVF16. **Wiri Mt.** also satisfies all the criteria, including matching major element composition, but is given a confidence level of 2 as a source centre because only major element data are available and the difficulty in resolving the correlation between Wiri Mt. and Puketutu.

Within the Pupuke core Molloy (2008) recorded deposits labelled as AVF10, AVF9 and AVF8, with each one classified as an individual eruption. Shard sizes within AVF9 and AVF8 were too small (<25 μm) for trace element analysis for this study. However, AVF10 included large shards (>100 μm) which have a similar size and chemistry to shards found in a horizon at 39.47 m within the Onepoto core. Although previously unclassified in the Onepoto core, this horizon is geochemically, stratigraphically and locationally appropriate to be correlated with AVF10 within the

Pupuke core. Thicknesses within the cores for Onepoto and Pupuke are 15 mm and 3 mm respectively, with both deposits containing large (>100 μm) shards. Horizon AVF 9 was previously correlated with deposits in Orakei Basin (407 mm thick, **Chapter 3**) and Pupuke (6 mm thick). The major elements AVF9 and AVF10 are indistinguishable and because no trace element chemistry has been analysed for AVF 9, the cross core correlation remains ambiguous. However, based on the scale of the deposits and the shard sizes the deposit within the Orakei core it is more appropriately correlated to AVF10 (Onepoto and Pupuke). Therefore, I here consider the AVF10 horizon to consist of deposits in Orakei Basin (depth of 54.213 m), Onepoto (39.47 m) and the original AVF10 deposit from Pupuke at 68.09 m depth, and AVF9 remains as a single horizon found within in Pupuke core.

The thickness of **AVF10** in the Orakei core, and the presence of large shards of this deposit in the Onepoto and Pupuke cores require a source centre near Orakei with an age of ca. 29.9 cal. ka BP (**Table 5.3**.). Based on its proximity to Orakei and scale of eruption (DRE^{tot} 0.0067 km^3) Mt. Hobson was initially considered. However, the Ar-Ar age is 44.9-66.9 ka (Leonard *et al., in prep,* **Appendix D**), and morphostratigraphically it has to be older than Three Kings eruption (due to Three Kings tephra found mantling Mt Hobson; Hayward *et al.,* 2011). In addition the geochemical composition of this horizon does not match with those from Mt Hobson ruling out this possibility. Little Rangitoto (AVF14) is too young (Ar-Ar age range of 15.9 - 24.7 ka) and the geochemistry is poorly correlated. The remaining possible source centres that are relatively close and in the correct age range are Taylors Hill (23.8-29.8 ka) and Panmure Basin (AVF13, >17.5 ka). Panmure Basin was a slightly larger eruption (DRE^{tot} 0.0074 km^3) than Taylors Hill (DRE^{tot} 0.0051 km^3; Kereszturi *et al.,* 2013), with Panmure Basin ca. 14-16 km away from Pupuke and Onepoto, in comparison to Taylors Hill, which is ca. 12-13 km away. The geochemistry correlates better for Taylors Hill than Panmure Basin (**Appendix E**), and therefore all criteria considered, **AVF 10** is correlated to **Taylors Hill** with a confidence level of 2.

AVF9 consists of a 6 mm deposit in the Pupuke core at 68.15 m, with a sedimentation rate age estimate of 30.2 cal. ka BP (**Table 5.3**.). Due to the thickness of the deposit and its absence in other cores and thus limited dispersal the source is likely in the north of the field (close to Pupuke). The only eruption that fits these

criteria and age is Mt. Cambria (Ar-Ar age range of 23.9-65.1 ka, Leonard *et al*., *in prep,* **Appendix D**), however, the geochemistry (majors only) does not correlate (**Appendix E**). If the potential source area is widened (to the middle of the field), McLennan Hills (Ar-Ar age range 29.3-38.9 ka) is the only other centre with a similar age, however the geochemistry also does not correlate. With a DRE^{tot} = 0.022 km^3 and the location of the McLennan Hills 18 km to the south-east this centre is a less likely match than Mt. Cambria. Another potential alternative source centre is the ~10 ka older centre Hopua (44.4-56.4 ka; Leonard *et al., in prep,* **Appendix D**). The Hopua maar core, contains the Kawakawa/Oruanui rhyolitic tephra (at ca. 48 m), followed by AVF12 (Molloy *et al.,* 2009), followed by thick scoria, assumed to represent the maar floor of Hopua (Leonard *pers. comms,* 2015). If Kawakawa/Oruanui has an age of 25.4 ka, and AVF 12 has an estimated age of 27.2 ka, the deposit relating to the Hopua eruption has a similar age to AVF9 and does not seem impossible as the source centre. However Hopua is one of the smallest AVF centres (0.00086 km^3) located 17 km away from Pupuke. In addition the geochemical composition of AVF9 tephra is similar to the geochemical composition of Hopua samples although only based on a single set of major element whole rock data from Hopua. Although it is surprising that no deposit is found in Orakei Basin linked with this eruption, this deposit tentatively assigned to **Hopua**, but with a confidence level of 3 due to the insufficient geochemical evidence and the poor age constraint.

AVF 8 is correlated across the Pukaki, Orakei Basin and Pupuke cores (**Chapter 3**), with thicknesses of 720, 45 and 20 mm, respectively, and an average age of 31.3 cal. ka BP (**Table 5.3**.). The thick deposit in the Pukaki core, its widespread dispersal and thinning to the north suggests a large eruption in the (central) south of the field, taking into account potential impacts from wind. The shard sizes within the Pupuke deposit are not large enough to analyse for trace elements and therefore both cross-core correlation and centre correlation are of lower confidence levels. To produce such a thick deposit in Pukaki the source centre is considered to be very close in proximity, such as Kohuora and Crater Hill. Both centres have similar Ar-Ar ages to the AVF8 tephra horizon (22.0-42.0 ka for Crater Hill and 28.0-36.0 ka for Kohuora). There are no whole rock data available for Kohuora, and only limited major element data from the Pukaki core, therefore only

limited conclusions can be drawn based on geochemistry. In addition, Kohuora represents a small volume eruption (DRE^{tot} 0.0076 km^3), whereas Crater Hill, with DRE^{tot} 0.024 km^3 is one of the larger eruptions in the field (Kereszturi *et al.,* 2013). In addition morphostratigraphy shows Kohuora to be older than Crater Hill. Therefore, based primarily on the thickness of the deposit in the maar and the morphological constraints, **AVF8** is correlated to **Crater Hill** with a confidence of only 2 due to the minimal geochemical data from the Pukaki core tephra deposit.

AVF7 is a field-wide dispersed tephra found in Orakei Basin (20 mm), Pupuke (2 mm), Onepoto (12 mm), and Pukaki (≤ 10 mm; P. Shane *pers. comms,* 2014). Rather than concentrated in one core (like AVF8) the thickness of AVF7 is more homogeneous across the field, suggesting a potentially large eruption within the central field (e.g. not specifically close to any of the depocentres). One option is the centre Three Kings, which is located in the central part of the field, and represents one of the largest eruptions in the AVF (DRE^{tot} = 0.069 km^3). There is a slight discrepancy with the ages; **AVF7** has a modelled age of 32.5 cal. ka BP (**Table 5.3**.), however, the ^{14}C age measured for Three Kings centre is 28.6 ± 0.4 ka cal. yrs. BP (Lindsay *et al.,* 2011). In addition the geochemical signatures of the Three Kings whole rock and the tephra horizons are very similar (**Fig. 5.14**) and so, this horizon is correlated with a level 1 confidence to **Three Kings** volcano.

AVF6 is found only in the Pukaki core at a depth of ca. 57 m. There is only major element data available for this horizon, thereby precluding any conclusive correlation based on geochemistry. The deposit is 500 mm thick and is given a modelled age of 33.7 cal. ka BP (**Table 5.3**.). The source centre is therefore most likely to be in the south of the field very close to Pukaki. Crater Hill (AVF8), Kohuora, Puketutu (AVF16), Mt. Robertson, and Wiri Mt. (AVF11) all satisfy these criteria. For Wiri Mt. and Mt. Robertson, although only major elements are compared, the geochemistry does not show a convincing correlation (**Appendix E**). Crater Hill and Puketutu both show well-correlated geochemistry (**Appendix E**) and are within the correct age range, but both these centres have quite large eruptive scales (DRE^{tot} 0.024 km^3 and 0.018 km^3 respectively, Kereszturi *et al.,* 2013) and would therefore be assumed to produce distal tephra units. Kohuora eruption however is proposed to only have total DRE 0.0076 km^3 and is within <3 km of Pukaki centre. Ar-Ar dating

for Kohuora yields an age estimate of 28.0-36.0 ka (Leonard *et al.,* in prep, **Appendix D**), which is supported by morphostratigraphy (Kohuora is older than Crater Hill), and previous ^{14}C dating for a Kohuora core putting it at ca. 33 ka (c.f. Newnham et al., 2007). Therefore, although there is no whole rock geochemical data for **Kohuora** to allow full confirmation the other criteria are all satisfied and the correlation is given a confidence rating level 2.

AVF5 is a thick (110 mm) homogeneous deposit found only in the Orakei Basin core at a depth of ca. 57.44 m, with coarse shard sizes and abundant detritus included in the bulk sample. The source must therefore be relatively close to Orakei Basin in the north of the field. Sedimentation rates imply an age of 35.0 cal. ka BP for the horizon (**Table 5.3**.). Only Mt. Cambria (AVF9) has the appropriate age, however due to the thickness of the deposit and shard size, Mt Cambria is unlikely to be the source. It is one of the smallest centres in the field (DRE^{tot} 0.00029 km^3) and is located ca. 5 km away therefore it is highly improbable that this would have produced a 110 mm thick tephra deposit within Orakei Basin. Many other centres have appropriate locations but are older than 35 ka (Ar-Ar ages from Leonard *et al., in prep,* **Appendix D**): Mt. Hobson (44.9-66.9 ka), Mt. St John (71.1-77.5 ka), Mt. Victoria (46.1-62.9 ka), and North Head (70.8-101.2 ka), and conversely Little Rangitoto (AVF14) (15.9-24.7 ka), Taylors Hill (AVF10) (23.8-29.8 ka), and Panmure Basin (AVF13) (15.6-33.6 ka) are younger than required. Of these centres only Mt. Victoria and Mt. Hobson have a similar (but indiscriminate) geochemical signature to the tephras within the AVF5 horizon (Appendix E). Mt. Victoria has a DRE^{tot} = 0.0048 km^3 and is located ca. 4.7 km to the northwest of Orakei. In comparison Mt. Hobson has a DRE^{tot} = 0.0067 km^3 and is ca. 2.5 km down wind to the south west of Orakei basin. Based on this, Mt. Hobson is more likely than Mt. Victoria to have produced a thick deposit with large shard sizes. The Ar-Ar age for Mt. Hobson (44.9-66.9 ka) is older than the modelled horizon age (35.0 cal. ka BP), however, the only morphostratigraphic constraint is that **Mt. Hobson** is older than Three Kings (which this correlation does satisfy). As this correlation is predominantly based on the locality and scale of eruption, coupled with locality and scale of the deposit, with inconclusive geochemistry and age, it is given a confidence rating of 3.

AVF4 is found cross-correlated (**Chapter 3**) within Orakei Basin and Pupuke cores with thicknesses of 41 mm and 15 mm, respectively, and has an average estimated age of 35.2 cal. ka BP (**Table 5.3**.). The deposit in the Orakei Basin core is relatively coarse with small-medium lapilli coupled with medium-fine ash, and medium to fine ash within the Pupuke core. Due to the dispersal of the tephra and the coarseness of the deposit at Orakei Basin, this deposit must have been sourced proximal to Orakei, from an eruption large enough in scale to deposit tephra within the Pupuke core as well. As previously discussed for AVF5 only Mt. Cambria (AVF9) (23.9-65.1 ka) is appropriate in location and age (however, with a large error). However, the scale of the eruption, in relation to the dispersal and grain size of the deposit makes this correlation unlikely. The tephra horizons have a large scatter in major element data and only the Orakei Basin tephra deposit has associated trace element data. Some centres have appropriate locations but not necessarily the correct age, including, Mt. Victoria, North Head, Mt. Hobson (AVF5), Mt. St John, Little Rangitoto (AVF14) and Taylors Hill (AVF10). Mt. Victoria, Taylors Hill, Mt. Hobson and Little Rangitoto all have matching geochemical signatures, although only proposed by the spread in major element data coupled with the minimal trace element data for some centres. Scale and location of eruptions, and deposits, therefore become the qualifying criteria for correlation. The correlated horizon in Pupuke is important here as it suggests a location that has to be relatively close to Pupuke and Orakei, thus ruling out Little Rangitoto (when coupled with scale of eruption) and Taylors Hill. Mt. Victoria and Mt. Hobson are therefore both potential candidates for this deposit (and AVF5) however, based primarily on the presence of AVF4 in Pupuke, it is considered more likely to have come from Mt. Victoria rather than Mt. Hobson (based on location). In addition, due to the proximity of Mt. Hobson to Orakei, a slightly thicker deposit would potentially be expected in Orakei Basin core. Therefore **AVF4** is correlated to **Mt. Victoria**, with a confidence level 3 due to the inconclusive geochemistry and age.

AVF3 is the first deposit found below the Rotoehu rhyolitic marker horizon. It is only found within the Orakei Basin core, it has a thickness of 41 mm with coarse tephra shards (>100 μm), and an estimated age of 49.3 cal. ka BP (**Table 5.3.)**. Based on the thickness of the deposit and its occurrence only in Orakei core, volcanoes from the centre and north of the field are considered. Potential centres

that have appropriate ages and locations therefore include Hopua (AVF9) (44.4-56.4 ka), Mt. Cambria (23.9-65.1 ka), Mt. Hobson (AVF5) (44.9-66.9 ka), and Mt. Victoria (AVF4) (46.1-62.9 ka), all of which have matching trace element compositions. Based on the scale of the eruption (inferred by deposit thickness) Mt. Victoria is considered less likely as it would be more likely have deposited material in Pupuke or Onepoto maars. Mt. Hobson is the closest to and largest centre near Orakei, which would potentially result in thicker tephra deposit as outlined for AVF5. Hopua is one of the smallest eruptions in the field with a DRE^{tot} = 0.00086 km^3, is located ca. 7.5 km away from Orakei, and would most likely for a thin deposit in the Orakei Basin. Although Mt. Cambria is even smaller than Hopua (DRE^{tot} = 0.00029 km^3) the centre is located closer (5 km) from Orakei Basin. Therefore, (although geochemistry is inconclusive) based on locality, age, and scale of eruption, **AVF3** is assigned to **Mt. Cambria**, with a confidence rating of 3.

AVF2 is found in the Orakei Basin, Glover Park, and Onepoto cores with thicknesses of 510, 60, and 4 mm respectively. The estimated average age for this horizon is 60.3 cal. ka BP (**Table 5.3**.). The widespread dispersal of AVF2, and the thick deposit in the Orakei Basin core, suggests a large eruption near Orakei Basin. The geochemical composition of AVF2 tephras correlate well to One Tree Hill and the scale and location of the eruption is appropriate for the tephra dispersal and thickness. The proposed horizon age is only slightly higher than the Ar-Ar age range for One Tree Hill at 44.3-59.5 ka (Leonard *et al., in prep*, **Appendix D**). This deposit is therefore correlated with a level 1 confidence to the **One Tree Hill** eruption.

AVF1 is the oldest tephra horizon recorded in the Orakei core at a depth of 80.047 m, with a thickness of 100 mm. It has also been correlated to a 15 mm horizon within the Onepoto core at a depth of 51.3 m (however, shards within this deposit were too small to analyse for trace elements), and as a section of highly disturbed and reworked units within the Glover Park core between 16.5 m and 19.8 m. The three horizons are geochemically indistinguishable (with major elements) and were therefore cross-correlated in **Chapter 3**. The average age of these deposits is estimated at 85.6 cal. ka BP (**Table 5.3**.), although as previously discussed these pre-Rotoehu age estimates might be slightly too high (c.f. **sect. 5.2.2**), therefore respective source centres that are younger than the horizon age are also

considered. The source is thus either a medium eruption in the north of the field, or a large eruption in the central field. Potential source centres that satisfy these age and location criteria therefore include Domain and/or Grafton (Ar-Ar age range of 77.5-122.5 ka), Mt. St John (Ar-Ar age range of 71.5-77.6 ka), and North Head (Ar-Ar age range of 70.8-101.2 ka; Leonard *et al., in prep*, **Appendix D**). Although the major element compositions in samples from all these centres are indistinguishable, the trace element compositions from the Domain/Grafton and Mt. St John are more closely correlated in comparison to North Head (**Appendix E**). Domain and/or Grafton and North Head were smaller eruptions with DRE^{tot}=0.011 and 0.0026 km^3 respectively, compared to DRE^{tot}= 0.028 km^3 of Mt. St John. Although Mt. St John is located furthest away (<3.5 km) from Glover park and Onepoto, it is the largest of the three potential source centres and thus the most likely have produced a 100 mm thick deposit in Orakei Basin and thinner deposits at Onepoto and Glover Park. Therefore, **AVF1** is correlated to **Mt. St John**, however, because of the inclusive geochemical composition, this correlation is given a confidence rating of 3.

AVF1 marks the oldest tephra horizon in the Orakei Basin core. Assuming the previous correlations are accurate, the Glover Park and Onepoto cores extend back further and contain two and three more horizons respectively. These are: in the Glover Park core at 20.78 m (GP1/24, now **AVFa**) with a thickness of 40 mm, and at 23.67 m (GP1/40, now **AVFb**) with a thickness of <10 mm; and in Onepoto core at 62.36 m (now **AVFb**) with a thickness of 8 mm, at 66.94 m with a thickness of 190 mm (now **AVFc**), finally, the Onepoto core ends in large clasts of scoria and lava (not a distal tephra deposit; Shane and Hoverd, 2002) at ca. 69 m (**AVFd**).

AVFa in the Glover Park core contains numerous small (25 μm-100 μm) shards that have a large spread in trace element geochemistry. This heterogeneity makes it difficult to define a source centre based on the geochemistry and correlations are therefore primarily based on locality, scale, and age, with a commensurately low confidence level. Based on extrapolation of the sedimentation rates between AVF 1 and AVFb in the Onepoto cores (discussed in **Sect. 5.2**.) a rough age of 129.2 cal. ka BP is assigned (**Table 5.3**.). The scale of the deposit is indicative of a small-medium sized eruption in the northern part of the field, or alternatively a large eruption in the centre of the field. Based on these factors the possible candidates for

tephra source include, Domain/Grafton (morphostratigraphic age >45.1 ka), Mt. Albert (Ar-Ar age range of 112.4-122.8 ka), Mt. Roskill (Ar-Ar age range of 96.6-111.0 ka), North Head (Ar-Ar age range of 70.8-101.2 ka), and Orakei (morphostratigraphic age range 85.0-130.0 ka). Mt. Albert and Mt. Roskill have quite large DRE^{tot} volume estimates (0.023 km^3 and 0.014 km^3, respectively) but are considered less likely due to their distal location (ca. 13-14 km). North Head (5.4 km distance) and Orakei Basin (5.4 km distance) are potential candidates, with smaller DRE^{tot} volumes calculated 0.0026 km^3 and 0.0067 km^3 respectively, however the geochemistry for both these centres is poorly correlated to the tephra horizon (**Appendix E**). Although the age for Domain/Grafton is poorly constrained, the scale (DRE^{tot} = 0.011 km^3) and location (8 km distance from Glover Park core site) seems appropriate with the shard size and horizon thickness. These criteria coupled with closely correlating major and trace element geochemistry means that **AVFa** is correlated to **Domain/Grafton** with a confidence level 2, due to the poorly constrained age of both deposit and centre(s).

AVFb is found within both the Glover Park core at 23.67 m with a thickness of <10 mm, and the Onepoto core at 62.3 m with a thickness of 8 mm. This horizon has a calculated average sedimentation rate age (by this study) of 140.4 ka. The deposit thicknesses suggest a relatively large/medium eruption mid way between Onepoto and Glover Park in the north or central field. Centres that satisfy these criteria include Albert Park, and Domain/Grafton. The morphostratigraphic constraint for the Domain/Grafton (>45.0 ka) is minimal, however, the locality and geochemistry are well correlated for this centre. Albert Park however, is a better candidate satisfying all the criteria required for this deposit; the Ar-Ar age range for Albert Park is 138.8-150 ka (Leonard *et al., in prep,* **Appendix D**); it was quite a volumetrically large eruption with a total DRE^{tot} 0.028 km^3, and is centred ca. 5 km from Onepoto and ca. 9 km from Glover Park; the geochemistry is well correlated to the tephra deposits in both cores. For these reasons **AVFb** is assigned to **Albert Park** with a confidence level of 2 (not 1, due to the inability to confidently determine the age of the core deposits).

AVFc is the final distal basaltic tephra horizon within the Onepoto core, however it did not yield any appropriate shards for geochemical analysis. The

deposit comprises of poorly sorted large clasts (cm scale) of microcrystalline lava and scoria, with no obvious bedding structures. Due to the thickness of the deposit and the clast sizes it must have originated very close to Onepoto, with the only potential candidates being Pupuke and Tank Farm. Morphostratigraphy shows that Pupuke is older than both Tank Farm and Onepoto, and Tank Farm is only just younger than Onepoto (Hayward *et al.,* 2011). Therefore this deposit must correlate to the eruption of **Tank Farm**, with confidence level of 1, and an age estimate of 173.1 ka.

The final deposit within the Onepoto core is found at its base where the core terminates in thick scoria and lava 2 m below the AVFc horizon. This deposit is thought to represent the base of the maar crater and therefore record the Onepoto eruption itself (Shane and Hoverd, 2002).

Table 5.5. *Outline of correlations for individual tephra horizons to their source centre. Average ages are calculated by this study by sedimentation rates (**Table 5.3.**). Proposed centre is given in bold with certainty value, outlined in the text and in **Figure 5.14**. Ticks indicate where correlation satisfies the criteria of age (within error of Ar-Ar), chemistry, scale, and location. Alternative possible centres are outlined with their certainty value and criteria. Final identifications are outlined in the text, see text also for ambiguities in the table in relation to rating given.*

Core	Sample name	New Horizon#	Depth (m)	Thickness (mm)	Average age (ka)	Proposed Centre(s)	Certainty Value	Confidence rating				Alternative(s)	Certainty Value	Confidence rating			
								Age	Chem	Scale	Location			Age	Chem	Scale	Location
Post Rerewhakaitu (<17.5ka)																	
Pupuke	T21-1-48/58929	24	57.90	22	0.6	**Rangitoto**	**1**	✔	✔	✔	✔	-	-				
Hopua	T4-2-H1-2/58839	23	38.95	3	10	**Mt Wellington**	**1**	✔	✔	✔	✔						
Pukaki	T14 47.72m	22	47.72	1.0	15.4	**Pukeiti**	**2**	✔		✔	✔	-	-				
Rerewhakaitu to Okareka (17.5 - 21.5ka)																	
Pukaki	AT209 49.15m	21	49.15	3.0	19.9	**Mt Smart**	**3**	✔		✔	✔	Panmure Basin	3	✔	✔		
Hopua	T5-2-H1-18/58855(-58856)	21	45.17	290								Pukeiti	3		✔		✔
												Mt Robertson	3			✔	✔
Pukaki	AT210 49.17m	20	49.17	2.0	20.6	**Mt Richmond**	**3**	✔		✔	✔	Waitemokia	3		✔	✔	
Hopua	T6-5-H1-20/58857(-58858)	20	45.51	235								Green Mt	3	✔			
Okareka to Oruanui (21.5- 25.4ka)																	
Pukaki	T43 51.05	19	51.05	1.0	24.2	**Otutaua**	**3**			✔	✔	Green Mt	3	✔		✔	
												Hampton Park	3	✔		✔	
												Otara	3	✔			
												Wiri Mt	3	✔			✔
Orakei Basin	OB1.#30-4-44.22	18	44.22	8	24.3	**Waitemokia**	**2**		✔	✔	✔	Mt Richmond	3	✔			✔
Hopua	T5-6-H1-32-58869	18	47.81	40								Puketutu	2		✔		✔
Pukaki	T45 51.19	18	51.19	0.5								Panmure Basin	3	✔			✔
												Otuataua	2	✔		✔	✔
Orakei Basin	OB1.#30-6-44.652(-44.654)	17	44.65	5	23.4	**Pigeon Mt**	**3**		✔	✔	✔	Little Rangitoto	3	✔	✔		
												Motukorea	2	✔	✔	✔	✔
												Mt Cambria	3	✔			✔
												Mt Richmond	3	✔		✔	
												Panmure Basin	3	✔			
												Taylors Hill	3	✔			✔
Pukaki	T42/45 51.52	16	51.52	50.0	25.3	**Puketutu**	**2**		✔	✔	✔	Otuataua	2	✔			✔
												Mt Robertson	2	✔		✔	✔
												Wiri Mt	2	✔	✔		✔
Orakei Basin	OB1.#30-6-47.715	15	47.72	12	24.5	**Motukorea**	**2**	✔	✔	✔	✔	Pigeon Mt	3		✔	✔	✔
												Mt Cambria	3	✔			✔

Table 5.5. *continued.*

Core	Sample name	New Horizon#	Depth (m)	Thickness (mm)	Average age (ka)	Proposed Centre(s)	Certainty Value	Confidence rating				Alternative(s)	Certainty Value	Confidence rating			
								Age	Chem	Scale	Location			Age	Chem	Scale	Location
Orakei Basin	OB1.#33-2-48.12(-48.128)	14	48.13	12	24.6	**Little Rangitoto**	**1**	✔	✔	✔	✔	-	-				
Orakei Basin	OB1.#33-2-48.19(-48.276)	newB	48.28	10													
Orakei Basin	OB1.#33-4-49.14(-49.46)	newA	49.46	45													
Orakei Basin	OB1.#34-3-50.089(-49.554)	13	50.09	160	25.3	**Panmure Basin**	**1**	✔	✔	✔	✔	Mt Eden	2	✔			✔
												Little Rangitoto	2	✔			✔
												Mt Richmond	2	✔			✔
												Taylors Hill	2	✔			
Oruanui to Rotoehu (25.4 - 45.1 ka)																	
Orakei Basin	OB1.#36-2-52.817(-53.029)	12	53.03	410													
Onepoto	On2.#4-39.06	12	36.09	12													
Pukaki	54.355m	12	54.36		27.2	**Mt Eden**	**1**	✔	✔	✔	✔	-	-				
Pupuke	P23/58947	12	67.59	7													
Hopua	T6-3-H1-39/58876	12	48.80	460													
Pukaki	c. 55.355m	11	55.34		29.3	**Wiri Mt**	**2**	✔		✔	✔	Kohuroa	3	✔			✔
												Otuataua	3			✔	✔
												Mt Robertson	3			✔	✔
												Puketutu	2	✔	✔		✔
Orakei Basin	OB1.#37-2-54.119(-54.213)	10	54.21	407								Panmure Basin	3	✔	✔		
Onepoto	On2.#4-39.47	10	39.47	15	29.9	**Taylor's Hill**	**2**	✔	✔		✔	Mt Hobson	3			✔	✔
Pupuke	T18-7-P26/58951	10	68.09	3								Little Rangitoto	3	✔			✔
Pupuke	P27/58952	9	68.15	6	30.2	**Hopua**	**3**		✔	✔	✔	Mt Cambria	3	✔		✔	✔
												McLennan Hills	3	✔		✔	
Orakei Basin	OB1.#37-2-54.27	8	54.27	45								Kohuora	2	✔		✔	✔
Pupuke	P28/58953	8	68.24	20	31.3	**Crater Hill**	**2**	✔	✔		✔						
Pukaki	c. 56.4m	8	56.40	ca. 720													
Orakei Basin	OB1.#37-2-54.324 (AVF7)	7	54.34	20													
Onepoto	On2.#4-39.905(-39.914)	7	39.90	20	32.5	**Three Kings**	**1**	✔	✔	✔	✔	-	-				
Pukaki	c. 56.8	7	56.90														
Pupuke	T19-3-P29/58954	7	68.49	2													
Pukaki	c.57.0	6	57.10	ca. 500	33.7	**Kohuroa**	**2**	✔		✔	✔	Crater Hill	2	✔	✔		✔
												Puketutu	2	✔	✔		✔
												Wiri Mt	3	✔			✔
												Mt Robertson	3			✔	✔

Table 5.5. *continued.*

Core	Sample name	New Horizon#	Depth (m)	Thickness (mm)	Average age (ka)	Proposed Centre(s)	Certainty Value	Confidence rating				Alternative(s)	Certainty Value	Confidence rating			
								Age	Chem	Scale	Location			Age	Chem	Scale	Location
Orakei Basin	OB1.#39-3-57.342(-57.44)	5	57.34	110	35	**Mt Hobson**	**3**			✔	✔	Little Rangitoto	3			✔	✔
												Mt Cambria	3	✔			✔
												Mt St John	3			✔	✔
												Mt Victoria	3			✔	✔
												North Head	3			✔	✔
												Taylors Hill	3			✔	✔
Orakei Basin	OB1.#39-5-58.11(-58.07)	4	58.11	41	35.2	**Mt Victoria**	**3**		✔	✔	✔	Little Rangitoto	3	✔		✔	✔
Pupuke	P33/58960	4	69.32	15								Mt Cambria	3	✔			✔
												Mt Hobson	3	✔			✔
												Mt St John	3				✔
												North Head	3			✔	✔
												Taylors Hill	3	✔			✔
Pre Rotoehu > 45.1 ka																	
Orakei Basin	OB1.#45-5-67.039(-61.17)	3	67.04	41	49.3	**Mt Cambria**	**3**	✔			✔	Mt Hobson	3	✔			✔
												Mt Victoria	**3**	✔			✔
Orakei Basin	OB1.#50-2-73.555	2	73.56	510													
Glover Park	GP6-8-10.38(-10.6)	2	10.60	60	60.3	**One Tree Hill**	**1**	✔	✔	✔	✔	-	-				
Onepoto	On2.#6-2-43.66	2	43.66	4													
Orakei Basin	OB1.#54-3-80.047	1	80.05	100								Domain/Grafton	3	✔			✔
Onepoto	AB1-On2-#11-51.30	1	54.30	15	85.6	**Mt St John**	**3**			✔	✔	North Head	3	✔			✔
Glover Park	GP16-17.52(&18.15)	1	18.15	12													
Glover Park	GP1/24 - 20.78-21.0	AVFa	21.00	40	129.2	**Domain/Grafton**	**2**	✔	✔	✔	✔	Orakei Basin	3	✔		✔	✔
												Mt Albert	3	✔		✔	
												Mt Roskill	3	✔		✔	
												North Head	2	✔		✔	✔
Onepoto	On2.#18-62.36	AVFb	62.00	45	140.6	**Albert Park**	**2**	✔	✔	✔	✔	Domain/Grafton	2	✔	✔		✔
Glover Park	GP1/40 - 23.67	AVFb	23.67	10													
Onepoto	On2.#21-66.68	AVFc	66.68	270	173.1	**Tank Farm**	**1**	✔		✔	✔	Pupuke	3			✔	✔

5.5. Implications

5.5.1. Tephra dispersal

As a result of tephra horizons being correlated to their source centres, and between core locations, inferences can be made about the tephra dispersal distances (defined as the minimum distance from source which the tephra has travelled, in km) and thickness of the deposits from the AVF eruptions. **Table 5.6** outlines the distance, thickness and (where applicable) the estimated shard sizes for all of the centres that have been assigned a correlation with confidence level 1or 2.

The recorded thicknesses are here considered to be minima values due to potential post-depositional compaction and erosion (Óladóttir *et al.,* 2012). The amount of compaction in the lacustrine deposits is unquantifiable, due to the lack of subaerial deposits in Auckland (discussed in **Chapter 3**). For the confidence level 1 correlations, the maximum dispersal distance is 13.5 km for Three Kings eruption recorded in Pupuke maar, with a thickness of 2 mm and a shard size of ca. 50-100 μm. The thickest deposits (≥100 mm) are all found within ≤6 km from the source, with a sharp decrease in deposit thickness (all <80 mm) at distances >6 km (**Fig. 5.15.A**). This observation correlates well to previously published estimates (Brand *et al.,* 2014) for pyroclastic density current deposits, which are modelled for the AVF to reach a maximum dispersal of 6 km. The maximum thickness recorded in the cores is 510 mm from One Tree Hill eruption in Orakei Basin, suggesting that for a volumetrically large eruption, tephra deposits can be >500 mm thick at distances ca. 6 km, however, this is in a more unusual and extreme case. Shard size also decreases with distance from source (**Fig. 5.15.B**), with 70% of deposits' <5 km from source found to have shards sizes >200 μm, which reduces to 40% of deposit 5-10 km away and 0% >10 km away from source. These findings are particularly applicable as inputs for tephra dispersal simulations, evacuation, and 'clean up' forecasting, planning, and management, all of which are current projects that are running within the DEVORA group (e.g., Tomsen *et al.,* 2014; Wilson *et al.,* 2014).

Table 5.6. *For those deposits with a correlation certainty of 1 or 2, the distance to the deposition site (core) (km), thickness of the deposit within the core (mm) and the average shard size of the tephra (μm) are shown. '?' shows where deposit thickness is unknown, P. Shane pers. comm.*

				Orakei Basin			Glover Park			Onepoto			Pukaki		Hopua			Pupuke		
Centre (eruption)	AVF#	Confidence level	DRE km^3	Distance to (km)	Horizon thickness (mm)	shard size (μm)	Distance to (km)	Horizon thickness (mm)	shard size (μm)	Distance to (km)	Horizon thickness (mm)	shard size (μm)	Distance to (km)	Horizon thickness (mm)	Distance to (km)	Horizon thickness (mm)	shard size (μm)	Distance to (km)	Horizon thickness (mm)	shard size (μm)
Rangitoto	AVF24	1	0.6989	core too old			core too old			core too old			-		-			8.38	22	>200
Mt Wellington	AVF23	1	0.0823	core too old			core too old			core too old			10.44	1	6.96	3	>200	-		
Little Rangitoto	AVF14	1	0.0017	0.9	12	>200	core too old			-			-		-			-		
Panmure Basin	AVF13	1	0.0074	5.2	160	100-200	core too old			-			-		-			-		
Mt Eden	AVF12	1	0.0898	4.4	410	>200	core too old			7.9	12	100-200	12.3	3	6	460	>200	10.7	7	50-100
Three Kings	AVF7	1	0.0693	6.5	20	100-200	core too old			10.6	12	50-100	10.1	2	core too young			13.5	2	50-100
One Tree Hill	AVF2	1	0.2604	4.6	510	>200	9.6	60	>200	10.8	4	100-200	core too young		core too young			core too young		
Tank Farm	AVFc	1	0.0059	core too young			core too young			0.6	270	>200	core too young		core too young			core too young		
Pukeiti	AVF22	2	0.0037	core too old			core too old			core too old			4.7	1	-			-		
Mt Smart	AVF21	2	0.013	core too old			core too old			core too old			7.0	3	2.7	290	>200	-		
Mt Richmond	AVF20	2	0.0057	core too old			core too old			core too old			6.1	2	5	235	100-200	-		
Waitemokia	AVF18	2	0.0098	12.8	8	50-100	core too old			core too old			3.7	0.5	5.6	40	>200	-		
Puketutu	AVF16	2	0.018	-			core too old			core too old			6	50	-			-		
Motukorea	AVF15	2	0.0046	8.4	12	50-100	core too old			core too old			-		-			-		
Wiri Mt	AVF11	2	0.016	-			core too old			-			5.1	?	core too young			-		
Taylors Hill	AVF10	2	0.0051	5.1	407	>200	core too old			12.4	15	100-200	-		core too young			13.2	3	100-200
Crater Hill	AVF8	2	0.024	13.2	45	100-200	core too old			-			1.5	720	core too young			23.5	20	<50
Kohuora	AVF6	2	0.0072	-			core too old			-			2.9	500	core too young			-		
Hopua	AVF3	2	0.00086	7.3	41	50-100	core too old			-			core too young		core too young			core too young		
Albert Park	AVFb	2	0.028	core too young			8.8	10	50-100	5	45	100-200	core too young		core too young			core too young		

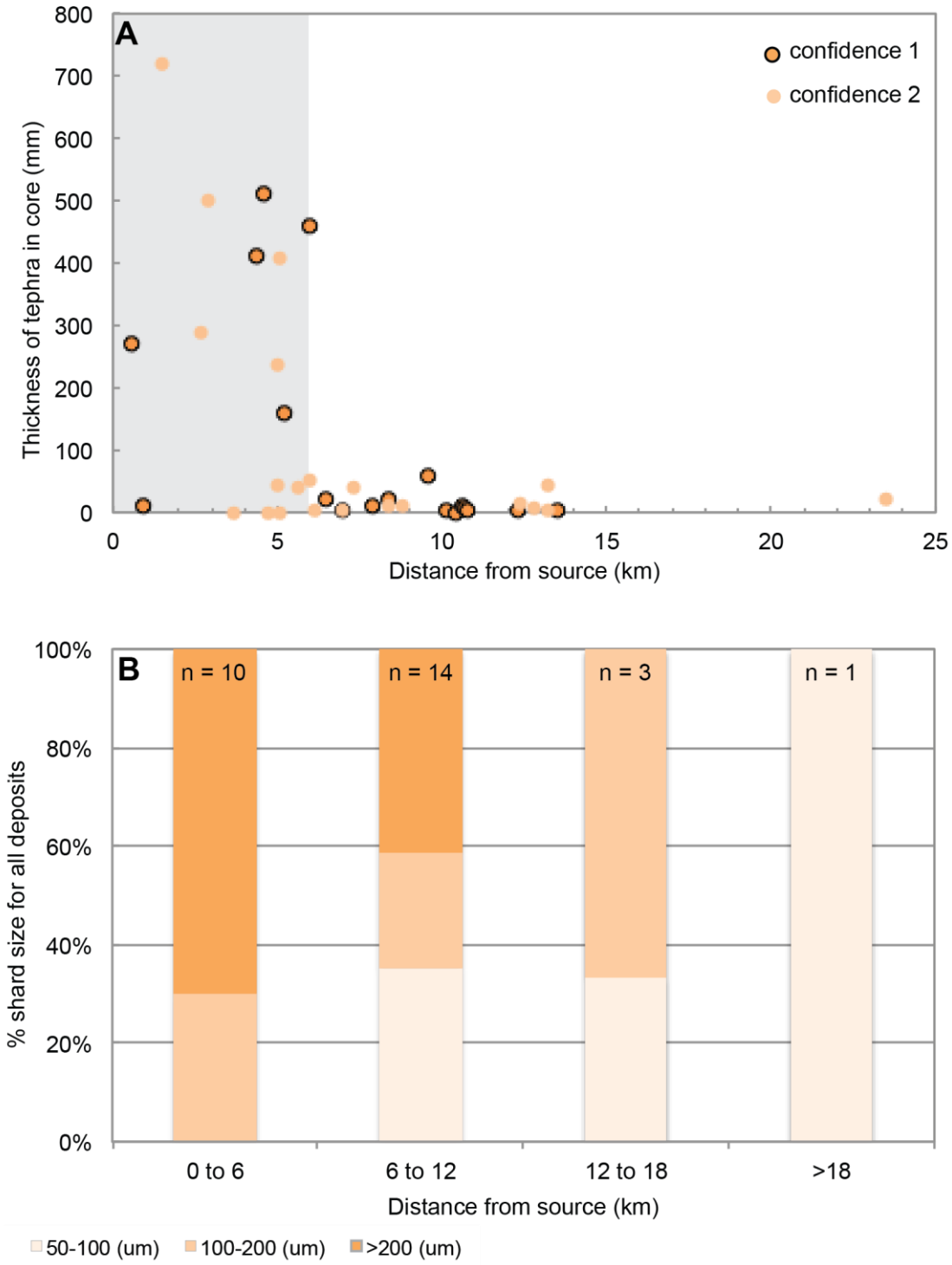

Figure 5.15. *For all correlations with a confidence rating of 1or 2, data detailed in* ***Table 5.6.****; (A) Horizon thickness vs. distance from source, showing the thinning of deposits increases away from source. Grey shaded area marks <6 km, within which all the deposits >100 mm thick are found. (B) % shard size for all deposits vs. distance from source, indicating the fining of shard size away from source.*

Tephra horizon AVF12, correlated to Mt. Eden (highlighted on **Fig. 5.1.**), is one of the most widely dispersed tephra horizons: >10 mm thick in both Pupuke and Pukaki cores, which are 11 km and 12 km from source, respectively. The Mount Eden event is also linked to some of the thickest tephra deposits in the cores with 410 mm in Orakei (4.5 km), and 460 mm in Hopua (6 km from source). **Figure 5.16.A** shows the decrease in tephra thickness away from source, coupled with the reduction in tephra shard size. Mt. Eden is also used here as example to show how the core-to-core and core-to-centre correlations can build isopach maps **Figure 5.16.B** for the dispersal pattern of the eruption. The impact of the prevailing westerly wind (Hayward *et al.,* 2011) is taken into account and produces an elliptical tephra dispersal pattern, and with a calculated total DRE of 0.0898 km^3 the eruption of Mt. Eden was one of the largest in the Auckland Volcanic Field. This example is therefore a more extreme tephra dispersal event from a larger scale eruption, which is not typical of the field.

Accordingly for smaller eruptions the tephra dispersal is restricted to smaller areas, but can form near-source tephra horizons with substantial thicknesses. For example AVF 10, now correlated to the eruption of Taylors Hill (DRE 0.0051 km^3), is restricted to the north of the field with deposits found cross-correlated within Orakei Basin (407 mm at ca. 5 km away), Onepoto (15 mm at ca. 12 km away) and Pupuke (3 mm at ca. 13 km away). Additionally, 13 horizons are found only within a single core, suggesting that for some eruptions tephra would not be dispersed field wide.

Some deposits are not necessarily found in all maars along a dispersal pathway. For example AVF 4 is found in Orakei Basin (41 mm) and Pupuke (15 mm) but is absent in Onepoto, which lies directly between these two. These dispersal patterns are most likely indicative of either discontinuous preservation potential and/or complex distal fall out (Molloy *et al.,* 2009). For more distal sites, the preservation potential of small tephra (<1-2 mm) is much lower, especially when settling through a water column. This can result in differential settling of tephra and thus in discontinuous deposition (Beierle and Bond, 2002).

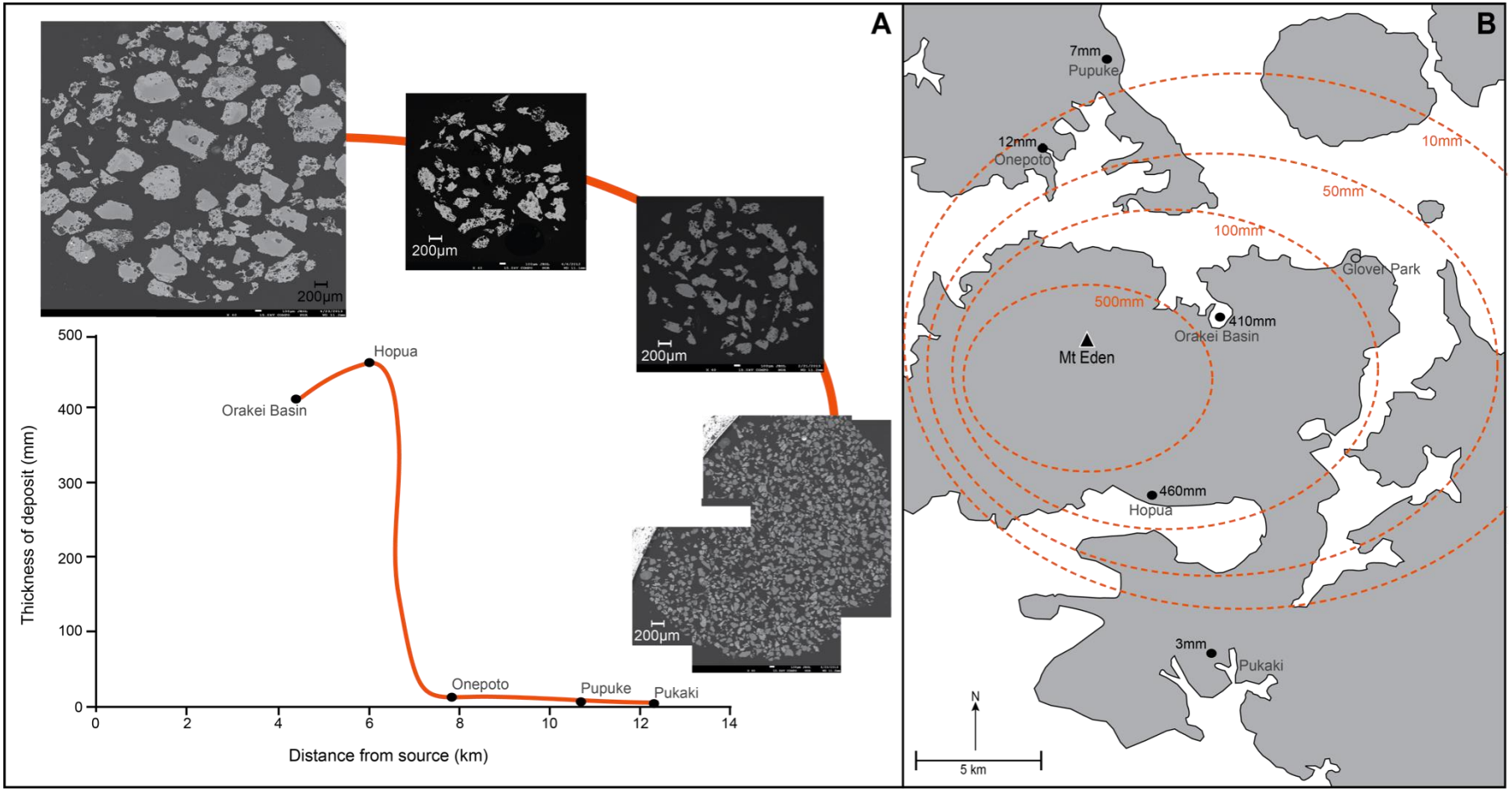

Figure 5.16. *Example of the correlation of Mt. Eden eruption to tephra deposit AVF12. (A) Graph to show change in deposit thickness away from source, note the extreme decline in thickness after ca. 6 km distance. Also shown on (A) are backscatter electron images of the shards from each core site taken on EMP. All pictures are at the same scale with the bar at the base of the images representing 200 µm. (B) inferred isopach map of the tephra dispersal from Mt. Eden based on the deposit thicknesses found in the cores. Dispersal is skewed to the east to reflect the westerly winds likely to have been present at the time of eruption (Hayward et al., 2011).*

Table 5.7 lists tephra dispersal characteristics from basaltic volcanic field worldwide together with those outlined for the AVF centres. Outlined are monogenetic basaltic eruptions that show comparable total eruptive volumes to the AVF centres. The larger (e.g. DRE^{tot} >0.1 km^3) and medium size (e.g. DRE^{tot} >0.01 km^3) eruptions show similar dispersal distances and thicknesses to the AVF eruption deposits. For example Mt. Gambier in the Newer Volcanics province with an estimated DRE^{tot} = 0.198 km^3 (van Otterloo and Cas, 2013) has a measured tephra dispersal of ≤5 cm thick at 10-12 km distance (Lowe and Palmer, 2005). In comparison, One Tree Hill from the AVF has a DRE^{tot} = 0.26 km^3 and a measured tephra thickness and dispersal of 6 cm at 10 km away (**Table 5.7.**). Marcath Volcano in the Luna Crater volcanic field is a similar scale to the mid-range AVF volcanoes, with a DRE^{tot} = 0.06 km^3 (Johnson *et al.,* 2014). It shows a 2 cm thickness at 7 km distance from vent, which is comparable to many similar scale eruptions in the AVF, e.g. Mt. Wellington and Three Kings (**Table 5.7.**). It is difficult to find comparisons for the smaller AVF eruptions. Some show equivalent values to the larger eruptions, for example, Mt. Richmond, with a DRE^{tot} = 0.0057 km^3 depositing tephra a thickness of 0.2 cm at 7 km from vent. However, a number of AVF centres show larger tephra dispersal distances and thicknesses in comparison to the larger eruptions. For example, based on the results of this study, Crater Hill, with a DRE^{tot} = 0.0024 km^3 has dispersed tephra 2 cm thick up to 23 km away, and Hopua, with a DRE^{tot} = 0.00086 km^3, is correlated (this study) to a 4 cm thick, 7 km away.

A number of factors could contribute to the apparent wider dispersal of AVF tephras including,

(1) The occurrence of more explosive phreatomagmatic eruptions leading to wider tephra dispersal e.g., Taylors Hill is calculated at c. 78% volume related to phreatomagmatic phases (Kereszturi et *al.,* 2013),

(2) More favourable wind direction leading to more efficient ash dispersal to the north and north-west of the field e.g., Crater Hill in Orakei or,

(3) Better preservation within the maar deposit sites in comparison to aerial deposits e.g., Orakei Basin maar.

Table 5.7. *Comparative global values for tephra dispersal and thickness for monogenetic basaltic volcanoes. * Cerro Negro is a polygenetic scoria cone, but it has a comparable total volume estimate for the 1995 basaltic eruption, and is therefore deemed applicable for comparison. In bold are examples from this study to allow a direct comparison, note that Three Kings is the 5th largest eruptive centre in the AVF, and Mt. Richmond is the 29th largest.*

Centre Name	Region	Total DRE (km^3)	Tephra thickness (cm)	Dispersal distance (km)	Reference
Paricutin	Michoacán-Guanajuanto volcanic field, Mexico	2.5	25	7	Ort et al., 2008
Sunset Crater	San Francisco volcanic field, Arizona	0.58	10	20	Ort et al., 2008
One Tree Hill	**Auckland volcanic field, New Zealand**	**0.26**	**6**	**10**	**This study**
Mt Gambier	Newer Volcanics province, south-eastern Australia	0.198	≤5	10 to 12	Lowe and Palmer, 2005; van Otterloo and Cas, 2013
Lanthrop Wells	Southwestern Nevada volcanic field	0.12	1	10	Valentine et al., 2008
Cerro Negro*	Nicaragua	0.16	0.5	16	Hill et al., 1998
Three Kings	**Auckland volcanic field, New Zealand**	**0.069**	**2**	**6.5**	**This study**
Marcath Volcano	Lunar Crater volcanic field, Central Nevada	0.06	2	7	Johnson et al., 2014
Mt Richmond	**Auckland volcanic vield, New Zealand**	**0.0057**	**0.2**	**7**	**This study**

5.5.2. Chronostratigraphic age order

As previously outlined, although the recent Ar-Ar dating (Leonard *et al., in prep,* **Appendix D**) has provided a significant improvement on the absolute age constraints for the AVF centres, the associated errors from this method mean that an exact age order for the AVF centres could not be constrained from these data alone. For example, in **Figure 5.17** the centres are presented in order based on their mean Ar-Ar ages, but there then is a large number of centres with overlapping ages that could easily be rearranged in a different order. The correlation of deposits, coupled with Ar-Ar ages and morphostratigraphy enabled us to construction a relative age order for 45 of the 53 centres, thus allowing us to re-assess the numerical ages for all centres. For example, of six previously un-dated centres, the tephra correlation

method can be used to assign ages to the centres Otuataua and Pigeon Mt. But for Boggust Park and Mt. Robertson (Cemetery Hill and Puhinui Craters) no further constraint could be put on their ages. For Mangere Lagoon, Pukaki, and Pukewairiki numerical and relative ages are also not defined by this study, however these have morphostratigraphic constraints. Presented below is a discussion on the relative and numerical age orders proposed, from the youngest to oldest centre.

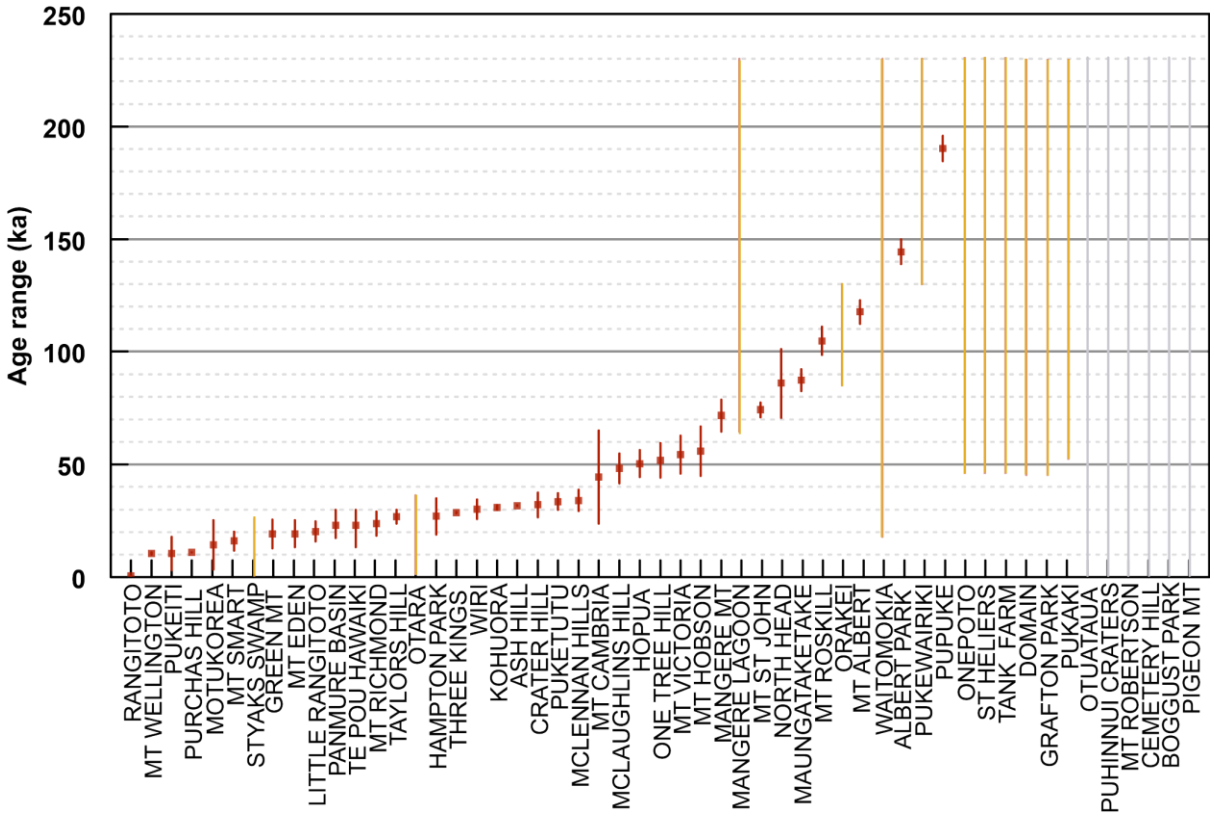

Figure 5.17. *Age range chart for all centres (data from* ***Table 5.1****). Those in red are Ar-Ar (2 sd error) or ^{14}C ages (from Cassata et al., 2008; Leonard et al., in prep., (Ar-Ar); and Lindsay et al., 2011 (^{14}C)). Markers show the mean ages measured by these techniques. Those in orange have their ages based only on morphostratigraphy, and those in grey have no ages associated with them. Of note is the number of centres which, based on errors, could have erupted at a given time. For example at 50 ka there are 18 potential centres (Mt. Cambria, McLaughlins Hill, Hopua, One Tree Hill, Mt. Victoria, Mt. Hobson, Waitomokia, Onepoto, St Heliers, Tank Farm, Domain, Grafton, Otuataua, Puhinui Craters, Mt. Robertson, Cemetery Hill, Boggust Park, and Pigeon Mt.) whose age ranges include 50 ka.*

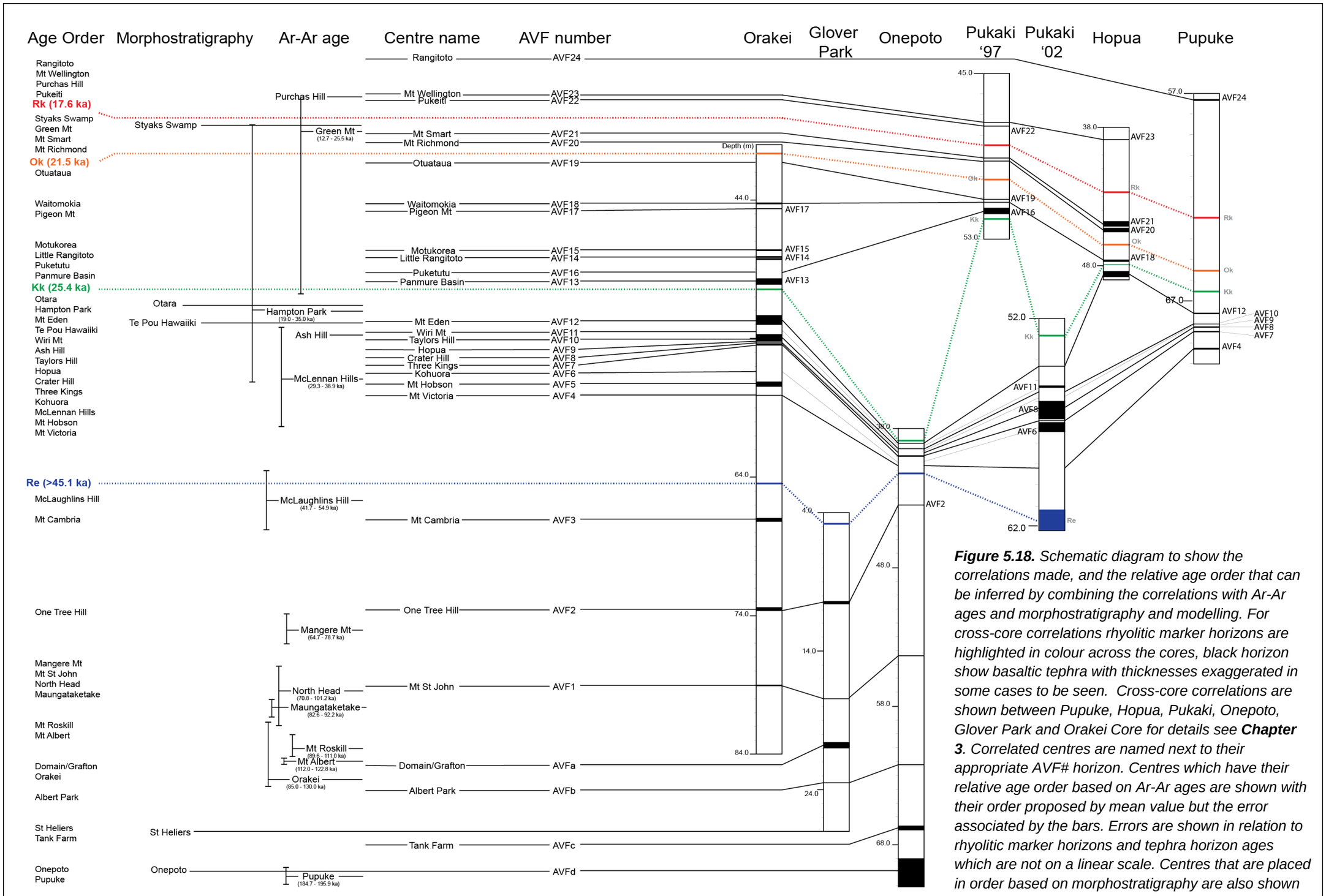

Figure 5.18. *Schematic diagram to show the correlations made, and the relative age order that can be inferred by combining the correlations with Ar-Ar ages and morphostratigraphy and modelling. For cross-core correlations rhyolitic marker horizons are highlighted in colour across the cores, black horizon show basaltic tephra with thicknesses exaggerated in some cases to be seen. Cross-core correlations are shown between Pupuke, Hopua, Pukaki, Onepoto, Glover Park and Orakei Core for details see* ***Chapter 3****. Correlated centres are named next to their appropriate AVF# horizon. Centres which have their relative age order based on Ar-Ar ages are shown with their order proposed by mean value but the error associated by the bars. Errors are shown in relation to rhyolitic marker horizons and tephra horizon ages which are not on a linear scale. Centres that are placed in order based on morphostratigraphy are also shown in the first column.*

Those remaining unconstrained; Mt Robertson, Mangere Lagoon, Pukaki, Pukewairiki, Boggust Park, Cemetery Hill, Puhinnui Craters

Rangitoto volcano is known to be the youngest centre within the Auckland Volcanic Field, with two resolvable eruptive episodes (^{14}C dates of 553 ± 7 and 504 ± 5 cal. yrs. BP; Needham *et al.,* 2011). However, recent geochemical and tephrochronological studies have outlined two conflicting views of the eruption characteristics. Initial research by Needham et al. (2011) suggested evidence for two main eruptive events, identifying a bimodal geochemical signal from both whole rock and tephra deposits (Needham *et al.,* 2011), as well identifying an apparent hiatus between the two. Later research from McGee et al. (2011) supports this observed geochemical bimodality and hiatus, and showed evidence for multiple magma sources through geochemical and isotopic analysis (Pb-Sr-Nd and U-Th-Ra). McGee et al. (2011) termed the eruptions **Rangitoto 1** and **Rangitoto 2** supporting the polymagmatic conclusions of Needham et al. (2011). More recently, Shane et al. (2013) proposed from cryptotephra analysis, that the activity from Rangitoto was constantly intermittent for a much longer time period, 1498 ± 140 to 504 ± 6 cal. yrs. BP, rather than two punctuated events. This debate is currently on-going, but for the purpose of this study the polymagmatic conclusions from Needham et al. (2011) are assumed as the most reliable.

Three more eruptions are identified post-dating the Rerewhakaaitu marker horizon (17.5 ± 0.46 ka; Lowe *et al.,* 2013). The eruptions of **Mt. Wellington** and **Purchas Hill** are well documented and dated as the next youngest eruptions in the AVF. Although there is no evidence in the maar crater tephra layers for the Purchas Hill eruption, which we attribute to its small scale, the morphostratigraphy of Mt. Wellington lavas flowing into the Purchas Hill crater coupled with a ^{14}C date of 11 ± 0.14 ka (Lindsay *et al.,* 2011) confirm that Purchas Hill is ca. 0.5 ka older than Mt. Wellington. Tephra horizon AVF23 is correlated to Mt. Wellington and horizon AVF22 is correlated here to **Pukeiti**, the 4th youngest eruption in the field.

The Rerewhakaaitu and Okareka (21.5 ± 0.29 ka; Lowe *et al.,* 2013) rhyolitic tephra horizons bracket the next group of samples. **Styaks Swamp** and **Green Mountain** (Mt.) are the next eruptions, based on the mean Ar-Ar age for Green Mt. (19.1 ± 3.1 ka) and morphostratigraphic constraint for Styaks Swamp (its tephra directly mantles the Green Mt. lava flows (Hayward *et al.,* 2011). Green Mt. records evidence for a dominantly south-westerly wind in the increased tuff build up to the north and east of the crater. The lack of tephra deposits associated with these

eruptions found within the maar cores is attributed to this dominant wind direction. Only two basaltic horizons are found in this time interval and they are correlated with **Mt. Smart** (AVF21) and **Mt. Richmond** (AVF20), and given sedimentation rate ages of 19.9 and 20.6 ka, respectively.

The next set of deposits is constrained by the Okareka and Kawakawa/Oruanui rhyolitic marker horizons (25.4 ± 0.16 ka; Lowe *et al.,* 2013). Seven basaltic tephras are found within this time window, correlated to **Otuataua** (AVF19), **Waitomokia** (AVF18)**, Pigeon Mt.** (AVF17), **Puketutu** (AVF16)**, Motukorea** (AVF15), **Little Rangitoto** (AVF14), and **Panmure Basin** (AVF13). For Otuataua, Waitomokia, and Pigeon Mt. the correlations provide constraints on the eruption ages, which previously had only been constrained by morphostratigraphy (Waitomokia) or not for all centres (Otuataua and Pigeon Mt.). For Little Rangitoto and Panmure Basin, the correlations are consistent with the Ar-Ar age ranges, but the correlations allow the relative eruptive order of these two centres to be put in place. For Puketutu the Ar-Ar age range is 29.8-37.4 ka (Leonard *et al., in prep.* Appendix D), however, the calculated tephra horizon age is slightly younger than that at 25.3 ka, suggesting a slight discrepancy between the dating techniques. This horizon is however constrained by the Kawakawa/Oruanui and therefore must be younger than 25.4 ± 0.16 ka (Lowe *et al.,* 2013). It is of note that this age put AVF16 out of sync in terms of its nomenclature; this is noted in **Figure 5.18** and discussed in **Section 5.2.2**. Finally, for Motukorea, the age for the tephra horizon (24.5 ka) fits within the Ar-Ar age range (3.3-25.3 ka), although within the older end of the range.

Between the Kawakawa/Oruanui and Rotoehu (45.1 ± 3.3 ka; Danišík *et al.,* 2014) rhyolitic marker horizons there are nine tephra deposits (AVF12 to AVF4). Based on Ar-Ar ages or morphostratigraphy seven other centres can also be added into this age window. **Otara** and **Hampton Park** are potentially the youngest in this age bracket based on the mean Ar-Ar age from Hampton Park (27 ± 8.0 ka; Cassata *et al.,* 2008), and stratigraphic evidence with Otara lava flows directly overlying the Hampton Park tuff ring; Hayward *et al.,* 2011). Again, due to the position of these centres to the east of the field coupled with the predominant westerly wind direction, it is likely that any significant tephra deposits from these centres would occur to the north and east of the centres, supported by the formation of asymmetric tuff rings at the eastern side of Hampton Park. This therefore potentially explains the lack of

tephra deposits found associated with these eruptions, as all maar core sites are found to the west of these centres.

Mt. Eden is proposed to be the next preceding eruption based on the correlation to tephra horizon AVF12. The geochemical composition of all five tephra deposits and the whole rock samples correlate well. However, the position of AVF12 beneath the Kawakawa/Oruanui suggests an age of 27.2 ka that is slightly older than the Ar-Ar age from Mt Eden (13.3-25.3 ka). Because the Te Pou Hawaiki scoria cone and lava flows were identified directly beneath Mt. Eden lava flows (Bartrum, 1928; Kermode, 1975), the eruption **Te Pou Hawaiki** is positioned just prior to Mt. Eden.

With a horizon age of 29.3 ka, the tephra horizon AVF11 is correlated to **Wiri Mt.** with an Ar-Ar age range of 25.7-34.5 ka. Based on morphostratigraphy and a ^{14}C age (31.8 ± 0.2 ka; Lindsay *et al.,* 2011), Ash Hill is suggested to be the next preceding eruption in the field. In similar fashion to the Mt. Eden/Te Pou Hawaiki relationship described above, **Ash Hill** has erupted just before Wiri Mountain, but due to its very small scale Ash Hill is unlikely to be present in the distal tephra record.

Based on the correlation to tephra horizon AVF10, **Taylors Hill** is proposed to be the next preceding eruption in the field with a horizon age of 29.9 ka. Erupting shortly after AVF9, correlated to **Hopua** (horizon age of 30.2 ka), and AVF8 correlated to the **Crater Hill,** (horizon age of 31.3 ka). All of these correlations support the Ar-Ar ages, but again allow us to reliably establish relative age order. This was not previously possible as the Ar-Ar age ranges from all these centres overlap.

AVF 7 is a very extensive deposit found within all the cores that also falls within this age range (Kk to Re). This tephra horizon is correlated to the eruption of **Three Kings**, although sedimentation rate calculations linked to the stratigraphic position of this horizon date it as older (32.5 ka) than the ^{14}C age (28.4-28.8 ka) suggests. The eruption of **Kohuora** centre is proposed to precede this, based on the correlation with tephra horizon AVF 6 which has a calculated age of 33.7 ka. The stratigraphic position for this tephra horizon fits well with the Ar-Ar age range (30-32 ka), is consistent with the morphological restraints and previous radiocarbon and

tephrostratigraphical dates (e.g., Newnham *et al.,* 2007), and confirms, where the Ar-Ar dating could not, that Kohuora is slightly older than Crater Hill.

Based on Ar-Ar dating **McLennan Hills** is proposed to be the next oldest centre with an age of 29.3-38.9 ka; however, tephra from this eruption was not found in any cores. The preceding eruption to McLennan Hills is **Mt. Hobson,** correlated to tephra horizon AVF5 (calculated age of 35.0 ka). Although the stratigraphic positioning of AVF5 would make this eruption younger than the Ar-Ar data suggest (44.9-66.9 ka) it agrees with the morphological constraint that it must be older than Three Kings (**Table 5.1**.). AVF 4, with a calculated horizon age of 35.2 ka, is correlated to the eruption of **Mt. Victoria.** Again, however, the correlation with this horizon would suggest the eruption is younger than the Ar-Ar age measured (46.1-62.9 ka).

The Rotoehu rhyolitic marker horizon marks the final tephra horizon constraint on the age order at older than 45.1 ± 3.3 ka (Danišík *et al.,* 2014). The first preceding eruption has its position based on the Ar-Ar ages recorded, and this is **McLaughlins Hill** (41.7-54.9 ka). Following this is the deposit AVF 3 that is found only within the Orakei Basin core and is best correlated to **Mt. Cambria,** with an age of 49.3 ka for the horizon**.** Prior to this, is the eruption of **One Tree Hill**, based on the correlation to tephra horizon AVF2. This horizon has an average calculated age of 60.0 ka, which is only slightly older than the Ar-Ar age (44.3-59.5 ka), and consistent with the morphological constraints (older than Mt. Hobson, Mt. Eden, Hopua, Mt. Smart and Three Kings all of which erupted through One Tree Hill lava flows; Hayward *et al.,* 2011).

Based on Ar -Ar age range of 64.6-78.7 ka, **Mangere Mt.** is the next older eruption, preceded by tephra horizon AVF1 (84.5 ka) that is correlated to the eruption of **Mt. St John**. Based on the Ar-Ar age of 70.8-101.2 ka and 82.6-92.2 ka **North Head** and **Maungetaketake,** respectively are the next oldest eruptions in order. Due to the lack of tephra deposits or morphological constraints their relative eruption order remains unresolved. With Ar Ar ages of 98.6 – 111.0 and 112.0 – 122.8 ka and based on morphostratigraphy **Mt. Roskill** and **Mt. Albert** are the next oldest AVF centres. There is no overlap associated with the Ar-Ar ages therefore the relative order of these two centres seems accurate.

A newly discovered 129.2 ka old tephra horizon within the Glover Park core (AVFa, **Chapter 3**) most likely records the eruption of **Domain** and/or **Grafton**. Prior to this is considered to be the eruption of **Orakei Basin.** This age sequence is based on sedimentation rates of the core, and morphostratigraphy. The Orakei Basin drill core is not considered to have reached the base of the maar (*G. Leonard pers. comm., 2015),* and therefore the age estimate for the base of the core can only give a minimum age (of 85 ka). Morphostratigraphic constraints give a maximum estimate, based on the lack of evidence for erosion for the last interglacial high-stand (c.f. Pukewairiki; **Table 5.1**), of ca. 130 ka (Hayward *et al.,* 2011).

The 140.6 ka old tephra horizon AVFb preserves the **Albert Park** eruption agreeing with the Ar-Ar age range of 138.8 -150.0 ka. This deposit (AVFb) is very close to the base of the Glover Park core. The base of the Glover Park core represents the maar crater floor and thus **St Heliers (Glover Park)** is proposed to be the next preceding eruption. Although there are no Ar-Ar ages or morphostratigraphic evidence to test this conclusion, based on the sedimentation rates the base of the core at 27 m is calculated to be ca. 164 ka.

Only the Onepoto core records older tephra horizons below this stratigraphic level. Towards the base of the Onepoto core (at ca. 67 m) the first (oldest) 173.1 ka old tephra horizon of the AVF is correlated with the eruption of **Tank Farm**. Two metres deeper than the Tank Farm deposit the Onepoto core terminates in a thick lapilli and lava unit that is likely to represent products of the **Onepoto** eruption itself. As there is no deposit in the Onepoto core from **Pupuke**, the latter is considered to have erupted earlier, supported by morphological evidence and Ar-Ar dates which show an age for Pupuke as 184.7-195.9 ka. The Onepoto deposit is therefore assigned an age of 190.3 ka, as discussed previously in **Section 5.2.2.**

There remain 5 centres that have very limited age constraints, and therefore cannot be accurately included in this chronostratigraphy. These include **Pukaki**, **Mangere Lagoon**, which is morphostratigraphically constrained to be older than Mangere Mt., giving it an minimum age constraint of 64.7 ka, and **Pukewairiki** which has a minimum morphostratigraphic age constraint of 130 ka (**Table 5.1**.). **Boggust Park** and **Mt. Robertson** as discussed previously remain undated.

5.5.3. Temporal Evolution

To assess the temporal eruptive history, the mean ages from the Ar-Ar (Leonard *et al., in prep.* **Appendix D,** and Cassata *et al.,* 2008; **Table 5.1.**) and ^{14}C (Lindsay *et al.,* 2011 and Needham *et al.,* 2011) determinations are taken for twelve of the centres. For twenty-eight centres their ages are assigned based on tephra horizons correlation, and the ages estimated by sedimentation rates for each tephra horizon (**Table 5.2.**). For five centres where morphostratigraphy controls the relative age, a value is assigned from the morphological and correlational constraints. For seven centres there remains not enough information to assign them absolute or relative ages, these are therefore not included in the following evaluations. The ages inferred by this study are outlined in **Table 5.8,** along with the calculated repose periods (time between eruption n and n+1).

Bebbington and Cronin (2011) presented the only existing estimates for both relative and absolute age order based on a Monte Carlo simulation modelling. The input for this model simulation included deposit thickness and age estimation for basaltic tephra within maar cores (from Molloy *et al.,* 2009), and age restrictions from distal tephras from the North Island rhyolitic and andesitic centres, and age estimations for the AVF centres. All of these inputs have now been superseded by more recent findings (e.g., **Chapter 3;** Ar-Ar ages from Leonard *et al., in prep*.). **Figure 5.19** shows a comparison of the outputs from their model and our research. For relative age orders (**Fig. 5.19. A**), there is significant scatter around the 1 to 1 line, which indicates that the data sets are significantly different. In some cases the two data sets agree, with 8 centres put in the same relative positions. However, in their model 22 centres are in slightly older positions, and 14 in slightly younger positions in comparison to this study. There are only a few large (>20 positions) discrepancies between the two; Little Rangitoto, Motukorea, and Te Pou Hawaiki are all given much older positions (42, 35, 43 respectively) than for this study (13, 12, 19), and McLaughlins Mt. and Mt. Mangere given much younger positions by Bebbington and Cronin (2011) (4 and 9 respectively) in comparison to this study (30 and 33 respectively).

For numerical age estimates (**Fig. 5.19. B&C**), the variation between the data sets is much greater: nineteen centres show offsets of <5 ka between the modelled and our age estimates, with the remaining 26 showing much larger offsets between

5.4 ka (Hampton Park) and 124 ka (Te Pou Hawaiki). The Bebbington and Cronin (2011) modelled numerical ages are clustered around 30 ka, whereas this study produces a much greater spread between 20 and 35 ka. The reason for this is that the Bebbington and Cronin model is linked predominantly to tephra deposits, of which most are found within close to 30 ka age range, and thus imparts a bias on the age constraints of their model output. For all centres modelled by Bebbington and Cronin (2011) with ages between 45 and 75 ka, the ages appear to be lower in comparison to this study (e.g. One Tree Hill, Mt. Albert, and Tank Farm). Conversely, modelled centre ages >75 ka seem over estimates (e.g., Little Rangitoto, Orakei Basin and Onepoto). The conflicting results for both relative and absolute age estimates between the two studies (e.g., for Onepoto, Pupuke, and Tank Farm), is proposed to result from discrepancies between the data inputs. As our new method relies on current data, it is considered to have produced more realistic and precise results.

The relative and absolute age results of this study (**Table 5.8**.) suggest that 13 centres erupted in the first ca. 150 kyr of the AVF history (ca. 190.3 – ca. 50 ka), with 31 erupting from ca. 50 ka to 0.5 ka. By using the RMHs as age constraints the number of eruptions per 1000 years (erup/kyr) can be calculated: present to Rerewhakaaitu (Rk) (0 - 17.5 ka) eruption rate of 0.23 erup/kyr; Rerewhakaaitu to Okareka (Ok) (17.5 – 21.5 ka) eruption rate of 1.00 erup/kyr; Okareka to Kawakawa/Oruanui (Kk) (21.5 – 25.4 ka) eruption rate of 2.33 erup/kyr; Kawakawa/Oruanui to Rotoehu (Re) (25.4 – 45.1 ka) eruption rate of 0.71 erup/kyr and Rotoehu to inception (45.1 - 204 ka) eruption rate of 0.10 erup/kyr. These results suggest that in general there was an increase in the eruption frequency through time until ca. 21.5ka (Okareka RMH), followed by a decrease over the last 21.5 ka. Repose periods show a wide range from <0.1 – 13 kyr (**Table 5.8.**), with two outliers of 27.3 and 17.4 kyr, proposed between St Heliers and Albert Park, and Mt. Roskill and Maungetaketake, respectively. Twenty-four centres have repose periods of 1000 years or less, seventeen of which are 500 years or less. In general the longer repose periods were found at the beginning of the field's history, with all of the nine centres with repose periods of >10,000 years appearing in the first 160 kyr. Overall, the general trend for the temporal evolution of the field suggests repose periods of <13 ka, but with an increase of this timing over the last ca. 21 ka.

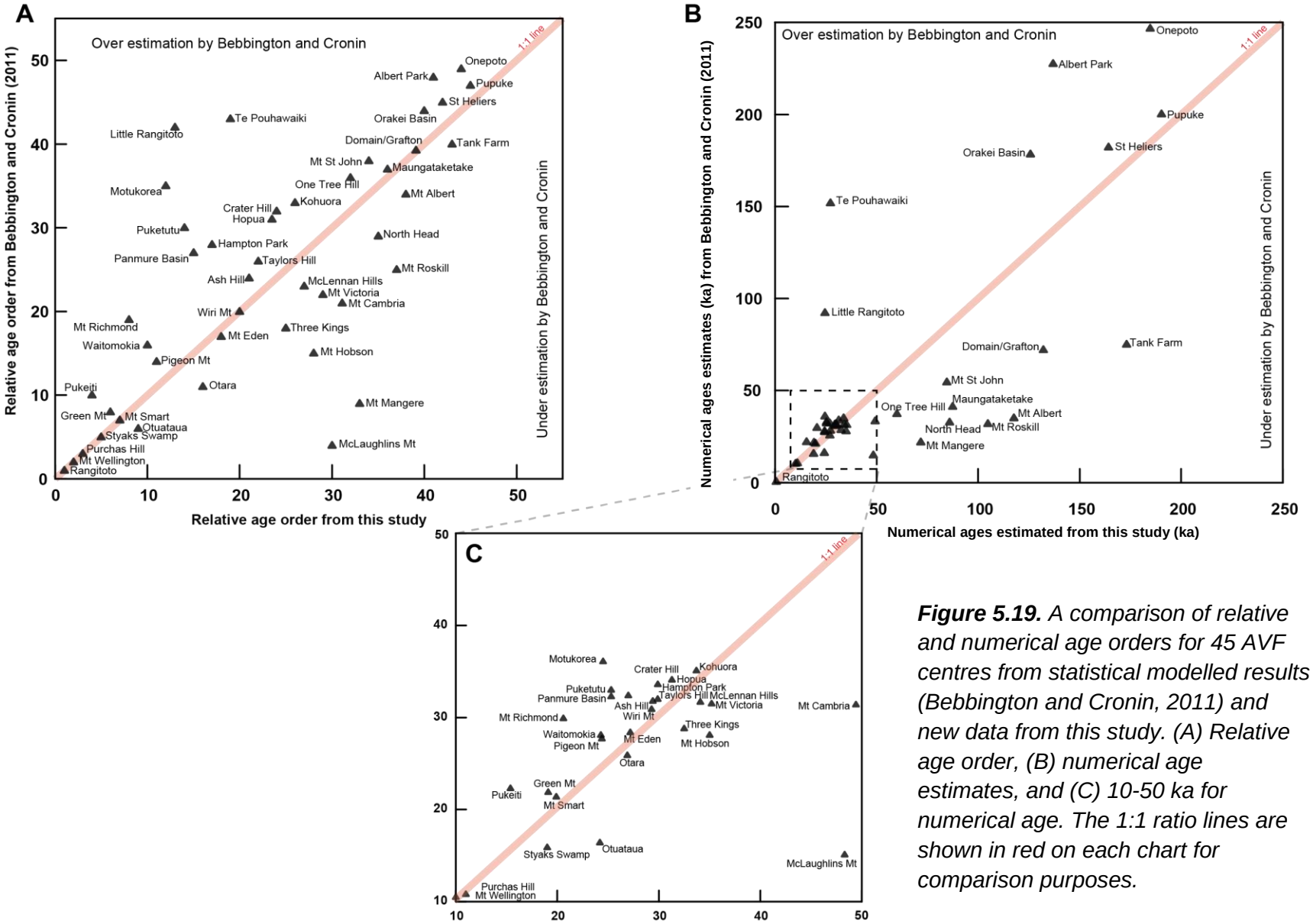

Figure 5.19. *A comparison of relative and numerical age orders for 45 AVF centres from statistical modelled results (Bebbington and Cronin, 2011) and new data from this study. (A) Relative age order, (B) numerical age estimates, and (C) 10-50 ka for numerical age. The 1:1 ratio lines are shown in red on each chart for comparison purposes.*

Table 5.8. *Relative order of eruptions with calculated mean ages, time and distance relationship between the nth, n+1 and n+2 centre. References a. sedimentation rates from this study, b. ^{14}C from Lindsay et al., 2011, c. Ar-Ar from Leonard et al., in prep. d. morphostratigraphic constraints (**Table 5.1.**) with numerical ages evaluated by this study.*

Relative Order	Centre Name	Mean age (t) in ka	Error (1sd)	Ref.	Time relationship t+1 (ka)	Time relationship t+2 (ka)	Distance relationship d+1 (km)	Distance relationship d+2 (km)
	Rangitoto 2	0.5	± 0.05	b			-	
1	Rangitoto	0.6	± 0.07	b	0.05		0.1	
2	Mt Wellington	10.0		a	9.4	9.5	11.9	11.7
3	Purchas Hill	11.0	± 0.05	b	1.0	10.4	0.6	11.1
4	Pukeiti	15.4		a	4.4	5.4	13.4	12.8
5	Styaks Swamp	19.0		d	3.6	8.0	13.9	7.2
6	Green Mt	19.1	± 6.4	c	0.1	3.7	0.5	13.6
7	Mt Smart	19.9		a	0.8	0.9	8.1	8.2
8	Mt Richmond	20.6		a	0.7	1.5	3.0	5.3
9	Otuataua	24.2		a	3.6	4.3	9.7	9.2
10	Waitomokia	24.3		a	0.1	3.7	1.6	8.0
11	Pigeon Mt	24.4		a	0.1	0.2	15.3	17.1
12	Motukorea	24.5		a	0.1	0.2	6.6	19.9
13	Little Rangitoto	24.6		a	0.1	0.2	9.1	8.4
14	Puketutu	25.3		a	0.7	0.8	11.5	20.0
15	Panmure Basin	25.3		a	0.0	0.7	11.4	4.9
16	Otara	26.9		d	1.6	1.6	6.4	13.4
17	Hampton Park	27.0	± 6.0	c	0.1	1.7	0.4	6.5
18	Mt Eden	27.2		a	0.2	0.3	14.3	14.1
19	Te Pou Hawaiiki	27.3		d	0.1	0.3	0.7	13.6
20	Wiri Mt	29.3		a	2.0	2.1	16.1	16.7
21	Ash Hill	29.4		a	0.1	2.1	1.0	16.1
22	Taylors Hill	29.9		a	0.5	0.6	16.0	15.8
23	Hopua	30.2		a	0.3	0.8	10.5	11.4
24	Crater Hill	31.3		a	1.1	1.4	7.4	14.1
25	Three Kings	32.5		a	1.2	2.3	11.3	4.1
26	Kohuora	33.7		a	1.2	2.4	11.6	1.5
27	McLennan Hills	34.1	± 4.8	c	0.4	1.6	5.6	11.6
28	Mt Hobson	35.0		a	0.9	1.3	4.0	12.3
29	Mt Victoria	35.2		a	0.2	1.1	5.8	12.2
30	McLaughlins Hill	48.3	± 6.6	c	13.1	13.3	21.2	15.9
31	Mt Cambria	49.3		a	1.0	14.1	21.4	0.4
32	One Tree Hill	60.3		a	11.0	12.0	8.7	13.8
33	Mangere Mt	71.7	± 7.0	c	11.4	22.4	5.4	14.0
34	Mt St John	85.6		a	13.9	25.3	7.4	2.0
35	North Head	86.0	± 15.2	c	0.4	14.3	6.9	13.8
36	Maungetaketake	87.4	± 4.8	c	1.4	1.8	19.4	12.7
37	Mt Roskill	104.8	± 6.2	c	17.4	18.8	9.1	11.5
38	Mt Albert	117.6	± 5.2	c	12.8	30.2	2.9	11.8
39	Domain/ Grafton	129.2		a	11.6	24.4	6.0	6.6
40	Orakei	130.0		d	0.8	12.4	3.5	8.6
41	Albert Park	136.9		a	6.9	7.7	4.4	1.3
42	St Heliers	164.2		d	27.3	34.2	8.7	5.3
43	Tank Farm	173.1		a	8.9	36.2	11.4	5.6
44	Onepoto	184.7		d	11.6	20.5	0.7	11.3
45	Pupuke	190.3	± 5.6	c	5.6	17.2	3.2	2.4
	Mangere Lagoon	>64.7						
	Pukaki	>52.0						
	Pukewairiki	>130						
	Mt Robertson	-						
	Boggust Park	-						
	Cemetery Hill	-						
	Puhinui Craters	-						

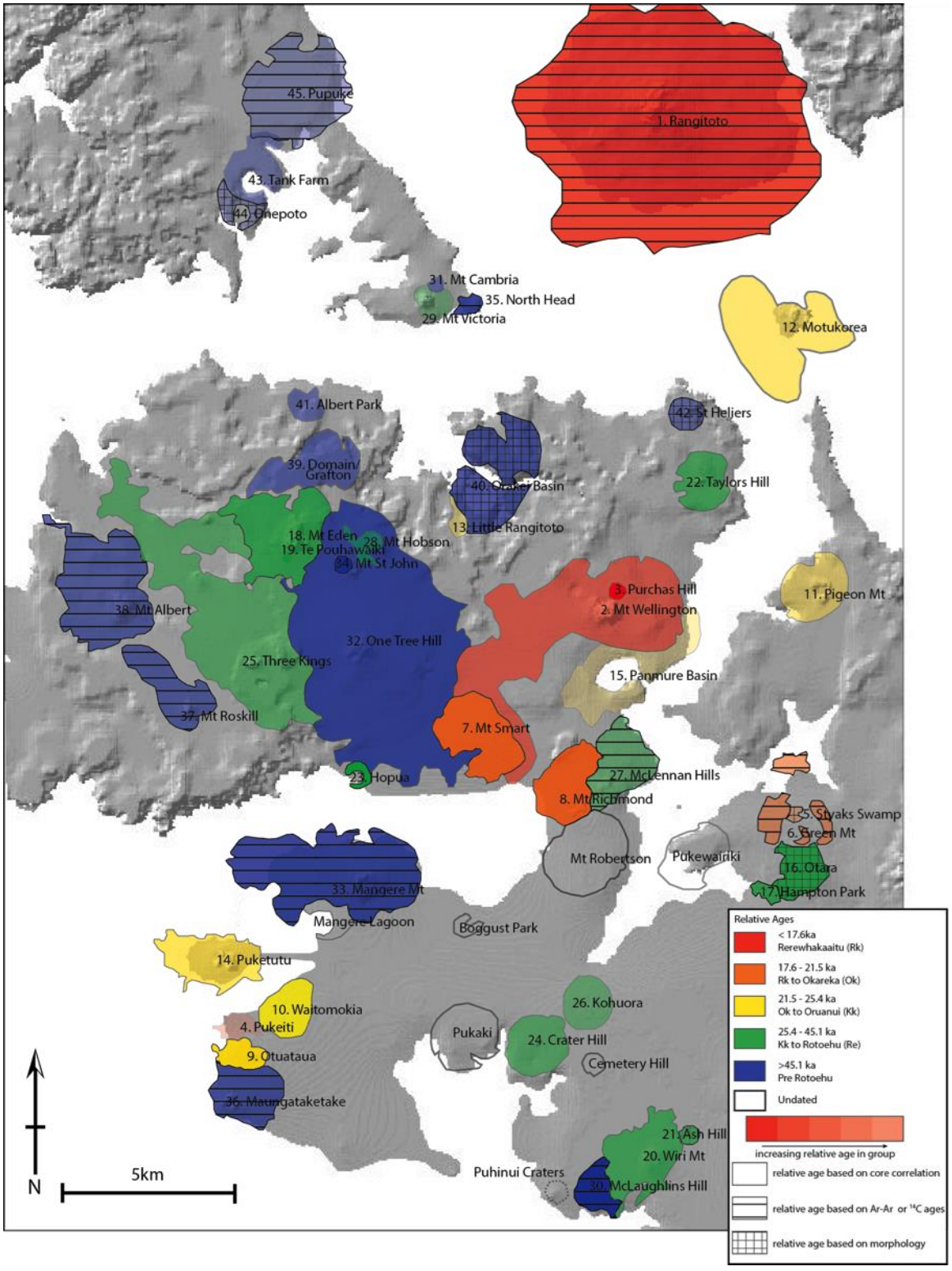

Figure 5.20. *Location map of all the AVF centres in the field divided into colours representing the constraining time zones. The grades of colour represent the relative age within the group with darker colours younger in the group and lighter colours older in the group, and patterns on the colours outlining the way in which the age has been constrained, through core correlation, Ar-Ar dating, or morphostratigraphy. The ages of those without colour remain unconstrained, and the numbers show their relative age order from the oldest (45) to youngest (1).*

5.5.4. Spatial Evolution

Figure 5.20 shows the relative ages of the AVF centres in map view. The distances between successive eruption centres varies from <0.5 km to 21 km. There is alignment of some centres in specific areas (for example McLaughlins Hill – Wiri Mt. – Ash Hill) that have previously been attributed to pre-existing crustal fractures and faults (Magill *et al.,* 2005; von Veh and Németh, 2009; Kereszturi *et al.,* 2014). In general, however, there is no obvious spatial progression or patterns through time.

Previous studies (Le Corvec *et al.,* 2013a; Bebbington, 2013) have suggested that the location of each centre is independent of that of the previous centre, and for the most part the results presented in this study support this suggestion. However, when linked with the temporal evolution, a number of 'coupled' centres appear to have erupted very closely in space *and* time. They are defined as having a repose period of less than 1000 years and vented <1 km away from each other. For example, Mt. Wellington and Purchas Hill are very well dated to 10.5 ka and 11 ka respectively, and are located ca. 0.5 km apart. The other centres include Rangitoto 1 and 2, Styaks Swamp and Green Mt., Mt. Eden and Te Pou Hawaiki, Wiri Mt. and Ash Hill, and Otara and Hampton Park. It would also be possible to have Onepoto and Tank Farm, Mangere Mt. and Mangere Lagoon, and Domain and Grafton included, however the ages of one or both of these couples are poorly constrained and therefore their specific ages are unknown.

In other monogenetic volcanic fields 'clustered' eruptions have been attributed to the mechanism of magma production (Le Corvec *et al.,* 2013b). Similarly, melt production at the AVF has, in some cases, been attributed to multiple sources (discussed below **sect. 5.5.5.1.**), which have differing methods of ascent (McGee *et al.,* 2013), seen most often as zoned single eruptions (e.g. Motukorea; McGee *et al.,* 2012). The first melt batch represents a smaller volume, lower flux melt, representing the initial 'path finder' to the surface, and the second batch represents a much larger higher flux melt, exploiting the pathway established by the first batch (e.g., Strong and Wolff, 2003). It is conceivable that if the magma flux of the initial melt is low that the ascent pathway does not remain open, the second batch will either not make it to the surface, or ascend via a slightly different route to the surface (e.g., Valentine and Krogh, 2006). McGee et al. (2011; 2015) discuss evidence that supports this second suggestion based on U series data. Their study on coupled centres (e.g. Rangitoto 1

and 2) found evidence for ascent through two methods, 1) Initial rapid ascent from depth through high porosity channels indicated by high $^{230}Th/^{232}Th$ but low $^{226}Ra/^{230}Th$, followed by 2) slower, more diffusive flow from shallower depths which developed lower $^{230}Th/^{232}Th$ but higher $^{226}Ra/^{230}Th$ (McGee *et al.,* 2011). The evidence of a minimal time gap between two closely spaced eruptions would support this alternate ascent route. This characteristic is considered to be as a result of the small volumes of magma that are associated with monogenetic volcanoes (Le Corvec *et al.,* 2013b). For this hypothesis to be correct the geochemistry of the two coupled centres would have to reflect the differing geochemistry of the two sources (McGee *et al.,* 2012) (discussed below).

5.5.5. Geochemical evolution

5.5.5.1. Mantle source geochemistry

In **Chapter 4** the geochemical variability of the AVF's eruptive products was discussed, with minor inter-centre variability attributed to the effects of fractional crystallisation on ascending magma (predominantly from olivine and clinopyroxene), and more major within-field variability attributed to the mixing of multiple magma sources. The three proposed sources include,

(1) Ambient MORB-like asthenosphere (≥ 80 km depth), containing

(2) Carbonated peridotite domains (McGee *et al.,* 2015), which mix with

(3) A shallower (≤80 km) subduction metasomatised lithosphere

Evidence for these three mantle sources was primarily based on isotope analyses (McGee *et al.,* 2013). The subduction metasomatised lithosphere was identified based on elevated $^{87}Sr/^{86}Sr$ (indicative of a weak subduction signature), and $^{238}U/^{232}Th$ (coupled with low $^{230}Th/^{232}Th$ ratios), the lowest $^{206}Pb/^{204}Pb$ (<19.1) and low $^{208}Pb/^{204}Pb$ (ca. 38.8) ratios indicating the involvement of a less radiogenic shallow source (e.g. Cook *et al.,* 2005; Hoernle *et al.,* 2006; Timm *et al.,* 2010). In comparison, the carbonated peridotite source was characterised by high $^{206}Pb/^{204}Pb$ (>19.4) and $^{208}Pb/^{204}Pb$ (ca. 39) ratios coupled with high $^{230}Th/^{232}Th$ ratios indicative of an enriched garnet-bearing source. The ambient MORB like signature in the

asthenospheric mantle is identified by intermediate $^{206}Pb/^{204}Pb$ ratios with relatively low $^{207}Pb/^{204}Pb$ ratios in comparison to the other sources (c.f. **Fig. 1.6, Chapter 1**). Isotopes have not however been measured for this study and therefore indicators from major and trace element compositions, and ratios, are more relevant here. Isotope signatures are further discussed and outlined in **Chapter 6**.

The major and trace element compositions that characterise the subduction metasomatised lithospheric source include a positive Sr anomaly and no negative K anomaly, and a decrease in trace element concentrations (McGee *et al.,* 2013, discussed **Chapter 4**). For example high Zr/Nb and K/La, and low $(La/Sm)_N$ ratios are attributed to a depleted source with high levels of previous melt extraction supported by low CaO and MnO concentrations (e.g. Timm *et al.,* 2009). The shallow gradient in HREE is indicative of a garnet-poor source, as discussed in **Chapter 4 section 4.4.2**, attributed to a shallow lithospheric mantle.

The ambient MORB-like asthenosphere is proposed to be the main component in the AVF source (McGee *et al.,* 2013), and it is primarily identified by the Pb isotope compositions as discussed previously. In addition, carbonated peridotite zones were identified within the ambient asthenospheric source (by McGee *et al.,* 2015) based on the similarity of the Purchas Hill signatures to experimental derived values for carbonatites (c.f. Gerbode and Dasgupta, 2010; Beier *et al.,* 2013; Scott *et al.,* 2014). Key sample characteristics include high Si-undersaturated, alkalic, nepheline-normative geochemistry, with elevated CaO/Al_2O_3, low Mg#, and negative correlations between K/La or Ti/Eu vs. La/Yb.

Those centres that exhibit a large negative K anomaly are interpreted to reflect a high proportion of carbonatite in their source (e.g., Purchas Hill is 100% asthenospheric melt (ambient mantle + carbonatite domains); McGee *et al.,* 2013). Conversely those that exhibit a large Sr anomaly are interpreted to reflect a larger proportion of lithospheric source melt (e.g., Rangitoto is ca. 80% lithospheric melt + 20% asthenospheric melt (ambient mantle + carbonatite domains); McGee *et al.,* 2013). Variable proportions of these three sources will produce the range in signatures across the field based on the associated mixing proportions, and thus variably coupled Sr and K anomalies.

It is hypothesised (McGee *et al.,* 2013*,* 2015) that initial melting occurs within carbonated peridotite domains in the asthenosphere due to the lower solidus of the material in comparison to the surrounding non-carbonated peridotite (Pertermann and Hirschmann, 2003; Herzberg *et al.,* 2007). Once the domains of carbonated peridotite are exhausted, the melt source moves to the surrounding ambient mantle peridotite (e.g. McGee *et al.,* 2012), and finally on ascent, the largest volumes of melt are generated through the incorporation of the shallow lithospheric source, which variably dilutes the initial deep-source signature. In order to retain the signature of the deeper source, the ascent of the smaller magma batches must be rapid, and efficient, adding further support to the ascent mechanisms modelled by McGee et al. (2011; 2015) (discussed in **section 5.5.4**).

5.5.5.2. Centre geochemistry and scale relationship

The primitive (MgO ≥8 wt%) AVF whole rock data show a correlation between the volume of the eruptive centre (Kereszturi *et al.,* 2013), and geochemistry, specifically SiO_2, CaO/Al_2O_3, and $(La/Yb)_N$ (**Fig. 5.21;** McGee *et al.,* 2015). Contrary to comments by Brenna and Cronin (2015), in general, the smaller centres show the lowest SiO_2, coupled with high CaO/Al_2O_3, and high $(La/Yb)_N$ ratios, and the converse is true for the larger centres.

McGee et al. (2015) propose that the deeper mantle signature, identified by the high $(La/Yb)_N$, low SiO_2 (wt.%), and high CaO/Al_2O_3 ratio, is produced from a higher proportion of carbonated source within the ambient mantle signature. This correlates with smaller magma batches, and thus smaller eruptions (indicated by DRE^{tot}). In comparison the shallower mantle signature, identified by the low $(La/Yb)_N$, higher SiO_2 (wt%) and lower CaO/Al_2O_3 ratio, produced from the subduction metasomatised lithospheric source, is correlated to the larger eruptions. When combining the new data from this thesis with the pre-existing data used by McGee et al. (2015), Rangitoto remains the 'large' end-member, however, new data from Mt Cambria (and Boggust Park) are the new 'small' end-members, superseding previous 'small' end-member Purchas Hill (**Fig. 5.21**.). The values measured for $(La/Yb)_N$ for Mt Cambria fit the trend, exhibiting higher ratio values than Purchas Hill. The geochemical signatures are not however fully comparable with the previously outlined criteria, for example the SiO_2 values for Mt Cambria are higher and CaO/Al_2O_3 values are lower than for those of Purchas Hill (**Fig. 5.21**). For SiO_2 and

CaO/Al_2O_3 the correlation is clearly less well defined, attributed to the effects of minor amounts of fractional crystallisation on the major elements during magma ascent. The $(La/Yb)_N$ ratio shows a strong correlation because these two elements are incompatible, and are therefore not affected by fractional crystallisation (as discussed in **sect. 5.3.1.**).

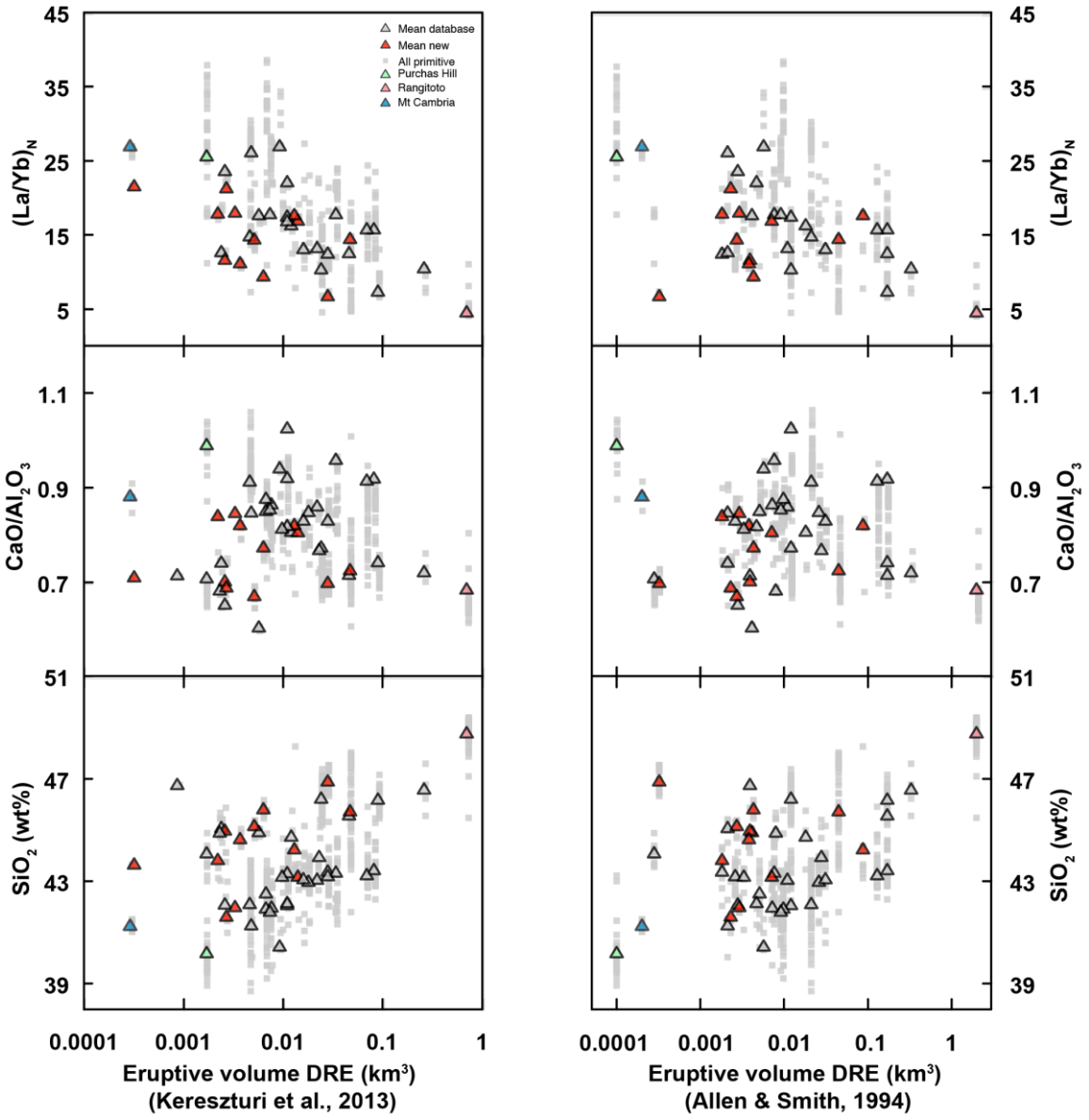

Figure 5.21. *Comparison plots of geochemistry versus eruptive volume. Data are plotted versus both Kereszturi et al. (2013) and Allen and Smith (1994) estimates for* DRE^{tot} *(discussed in* ***sect 5.2.5*** *and outlined in* ***table 5.2****.) Points show the average values for all primitive (>8 wt % MgO) samples for an individual centre: grey symbols showing existing database values, and red symbols show data added by this study, Rangitoto is highlighted in pink, Purchas Hill in green and Mt Cambria in orange.*

Previous studies (e.g. McGee *et al.,* 2013) also indicated a more complex correlation for the centre size based on their multi-element primitive mantle normalised trace element plot trends. All the centres studied (n=10; McGee *et al.,* 2013) were split into three types: 'small' (e.g., Purchas Hill, with large negative K anomaly, no Sr anomaly, steep HREE trend), 'intermediate' (e.g., Wiri Mt, with both negative K and positive Sr anomaly), and 'large' (e.g., Rangitoto, with no negative K anomaly but a large positive Sr anomaly, and shallow HREE trend). For Mt Cambria again however, this geochemical-volume correlation appears to not be consistent with these previous size designations. Mt Cambria is one of the smallest centres in the field, and much smaller than Purchas Hill (DRE 0.00029 km^3 versus 0.0017 km^3, respectively: Kereszturi *et al.,* 2013), but it does not show a much smaller Sr anomaly (0.96-0.98), a more extreme Zr-Hf trough, or steeper REE element trend than Purchas Hill (Sr^*_N = 0.95-1.0; McGee *et al.,* 2013). Conversely, new data from Little Rangitoto shows a small negative K anomaly, a large positive Sr anomaly (1.15-1.19), and a steep REE pattern, considered indicative of an 'intermediate' scale (McGee *et al.,* 2013), but has an estimated DRE volume of 0.0017 km^3, the same size as Purchas Hill. Te Pou Hawaiki, the only new centre to show a similar trend to Rangitoto (large positive Sr anomaly, no K anomaly and a shallow HREE slope), has a DRE of 0.028 km^3, which is not one of the largest centres within the field (9^{th} largest) (see **Fig. 4.5**.).

Assuming the correlation between scale and geochemistry is correct, a number of the new centres exhibit geochemical signatures indicative of larger magma batches than their total eruptive products suggest. Although distal tephra is not accounted for in the Kereszturi et al. (2013) model, this is not considered enough to balance the potential volume discrepancies. It is therefore conceivable to propose that, if the geochemical signatures of the erupted products are more representative of a larger centre than is calculated from the surface deposits, there is a loss in magma volume on ascent. There are two possible explanations for this, 1) some of the magma is simply not erupted and remains within the crust, or 2) some of the magma is lost through minor amounts of fractional crystallisation, coupled with the resultant omittance of crystals in the erupted lavas. This second possibility is supported by the slightly less defined correlations seen between SiO_2 and CaO/Al_2O_3 (**Fig. 5.21.**). However, because many of the AVF lavas have a primitive

geochemical signature, there is only evidence of limited fractional crystallisation occurring (e.g., Smith *et al.,* 2008), which may not be enough to account for the discrepancy between geochemical signature and eruptive scale. Therefore it is most likely that both retention and fractional crystallisation of ascending melts affect the final proportion of magma that is erupted. This assumption highlights a potentially complex relationship between ascending melt and crust.

5.5.5.3. Time resolved geochemistry

Figure 5.22 shows the centres in their proposed relative eruption order (**Table 5.8.**) versus the SiO_2 and $(La/Yb)_N$ content, which, as outlined previously, are analogous with eruption size. This figure suggests that the erupted size over the history of the field is not random. There appears to be cyclicity in the eruption pattern that shows a large eruption (e.g. One Tree Hill) is followed by a small eruption (e.g. Mt. Cambria), which is followed by multiple medium eruptions that increase in scale up to another large eruption (e.g. Crater Hill). In general there is a shorter time period between the two extreme eruptions (e.g. 11 ka between One Tree Hill and Mt. Cambria), than the subsequent period of increasing scale (e.g. 18 ka between Mt. Cambria and Crater Hill). The timing of this periodicity is also concurrent with the repose periods, increasing in time until ca. 21.5 ka then decreasing again to the most recent eruption.

As previously discussed, the eruptive scale and geochemical signatures are produced as a result of variably mixing the mantle source. The cyclicity that is observed over the history of the AVF therefore suggests that the mantle source is variably tapped through time. With a predominant deep source producing the small centre signature, followed by increasing input from a shallow source creating the multiple medium to large eruptions.

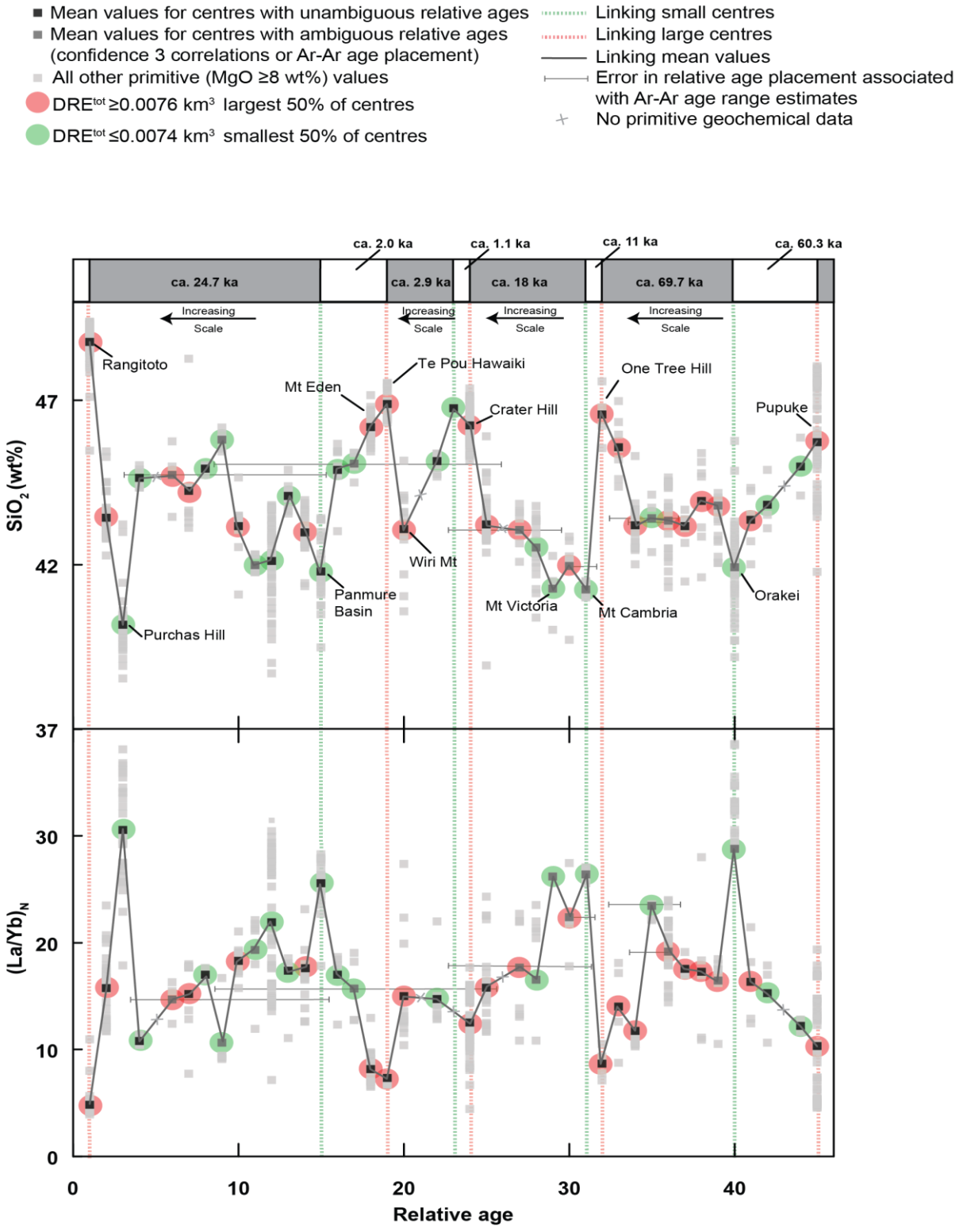

Figure 5.22. *All primitive whole rock samples (MgO ≥8 wt%) from each centre plotted in their newly constrained relative age order (**Table 5.7.**) from 45 (Pupuke) as the oldest to 1 (Rangitoto) as the youngest. Black markers show the calculated mean concentrations for $(La/Yb)_N$ and SiO_2 (wt%). Those centres with slightly ambiguous ordering (e.g. an Ar-Ar age range which means they do not have a definitive position) are show in a lighter grey and have their error in relative age placement detailed.*

Centres that exhibit evidence for coupled eruptions, e.g. Rangitoto 1 and 2, and Mt. Wellington and Purchas Hill, show a systematic decrease in successive eruptions for $(La/Yb)_N$ vs. $(Gd/Yb)_N$, with the first centre having high values and the second centre having low values. This pattern is not however consistent for all the centres identified as 'coupled'. For Domain and Grafton, Otara and Hampton Park, Mt. Eden and Te Pou Hawaiki, both of the centres show geochemical signatures which span the full range of both high and low ratios. This therefore suggests that both source signatures are evident in a single centre, rather than occurring in the successive couplets. For some of the coupled centres there is limited geochemical data available, and therefore observation of the geochemical relationship cannot be made for Tank Farm and Onepoto, Green Mt. and Styaks Swamp, and Wiri Mt. and Ash Hill. Although inconclusive, due to the lack of data for some centres, these results suggest that although there is a temporal and spatial relationship between some of the centres, the hypothesised geochemical relationship for the coupled centres, from primary erupted small volume melts (e.g. low SiO_2 and high $(La/Yb)_N$) to secondary erupted large volume melts (e.g. high SiO_2 and low $(La/Yb)_N$) (**sect. 5.5.4.**) is not seen. This geochemical evolution is however observed within single eruptions (e.g., Motukorea and Crater Hill), suggesting that although geochemically linked couplets may be rare, systematic variation throughout an eruption sequence could also be prevalent in the AVF centres.

From these observations we can conclude that there is evidence for cyclicity relating to the scale of eruptions at the AVF, and that following a large eruption (e.g. Rangitoto) there is most likely to be a very small eruption. There is limited evidence for a systematic evolution in the geochemistry, indicating that the source signature is not evolving through time, rather that the field is variably tapping and mixing multiple magma sources. The geochemical signatures preserved in the eruptive products from the AVF centres provide evidence for the presence of a heterogeneous mantle (asthenospheric and lithospheric) source beneath the AVF. This heterogeneity is reflected as geochemical signature within single centres, coupled centres, and field-wide. The apparent links between scale of eruption and geochemical signature (e.g. SiO_2 and $(La/Yb)_N$), imply that the ascent and eruption of the smaller batches must be highly rapid and efficient in order to preserve their signature. But for some centres

there is also apparent evidence of magma volume loss through fractional crystallisation and/or retention of melt within the crust.

5.6. Conclusions

The collation of whole rock major and trace element data for the field has (with a few exceptions) facilitated the development and testing of a method to correlate the tephra deposits to their source volcanic centre. Correlation between tephra and the glassy matrix of whole rock deposits using geochemistry is proved to be reliable; it produces well-correlated results based on major element signatures, which is strengthened by the use of trace element signatures. Furthermore incompatible trace elements and their ratios (specifically La/Yb, Ce/Yb, Gd/Yb, Zr/Yb, Nb/Yb and Nd/Yb) are representative for individual centres and can therefore be used to correlate basaltic tephra to whole rock samples. Specifically the ratios listed above are the most useful in assigning individual geochemical fingerprints because they are the more variable field wide, the least variable intra-centre, and the least affected by fractional crystallisation processes.

Although geochemistry has proven to be an effective tephra correlation tool, it is not always distinct enough to provide a definitive result. To efficiently correlate tephra layers to their source centres, a multi-faceted approach is required. This combined approach uses age (of both tephra deposit and whole rock deposit) and eruption characteristics (e.g. scale and locality), to assign the source centre to tephra deposits with the highest confidence. Of the twenty eight basaltic tephra horizons in the AVF maar cores, all but two (newA and newB) are correlated to a source; eight with a confidence rating of 1, twelve with a confidence rating of 2, and seven with a confidence rating of 3.

As a result, the level 1 confidence correlations can be used to determine tephra dispersal and thickness from the AVF eruptions. The maximum tephra dispersal distance is 13.5 km with a deposit thickness of 2 mm, and for all deposits with a thickness >100 mm the source is <6 km away. In a number of cases the deposits are restricted to local regions of the field, in close proximity to the source

centre, suggesting that in the event of a future small-scale eruption, the entire Auckland area may not be affected.

The correlations also facilitate construction of a more definitive picture of the evolution of the AVF. Due to the stratigraphic relationships of the tephra horizons within the cores, and their association with the rhyolitic marker horizons, the absolute age order of the centres can be resolved. Because of the errors associated with dating techniques (Ar-Ar and ^{14}C) a relative sequencing of the AVF centres was previously difficult. With our new method 45 centres have a high-confidence age estimate associated with their eruption leaving only seven centres with uncertain ages (Mangere Lagoon, Pukaki, Pukewairiki, Mt. Robertson, Boggust Park, Cemetery Hill and Puhinui Craters).

The temporal eruptive history suggests that the repose periods of the AVF are highly variable, from <0.1 to 13 kyr. In general, the field had a slow initial eruption frequency with 19 eruptions in the first 150 kyr, followed by an increase in eruption frequency until 21.5 ka, after which the eruption rate slowed. Successive eruptions are shown to be spatially highly variable with distances of ca. 0.5-21 km between vents. Some clustering of centres is observed, attributed to exploitation of pre-existing crustal weaknesses or locally fractured crust, although no general spatial evolutionary trend could be determined for the AVF. Coupled eruptions in space and time are identified, however most are not geochemically related. Cyclicity in size and thus geochemistry is also highlighted showing that throughout the history of the AVF three mantle sources have been variably tapped to produce the erupted products of the field.

This study has outlined the method by which a distal basaltic tephra deposit can be correlated to its source signature using geochemical compositions of tephra and whole rock, coupled with a number of other criteria. This information is critical for the assessment and construction of future hazard and risk forecasting of the AVF, which poses a potentially significant threat to large population and complex infrastructure.

Preface to Chapter 6

Chapter 5 outlined the geochemical evolution of the AVF based on the relative age order that was created as a result of the source centre correlation techniques. There is a perceived cyclicity in eruption scale, which is linked to the geochemical signature. Based on the conclusions of previous studies (Huang *et al.,* 1997; McGee *et al.,* 2013) these geochemical signatures were attributed to variations in source input, suggesting increasingly variable mixing proportions of the two sources through time. In general, the increasing input from a shallower, fluid enriched mantle source, was shown to result in volumetrically larger eruptions. This field wide general trend is also mirrored in some coupled eruptions (e.g. Rangitoto 1 and 2), and throughout some single eruptions. **Chapter 5** also highlights evidence for loss of melt volume through fractional crystallisation and/or retention of melt in the crust, hinting at the complex nature of the pre-eruptive processes for the AVF volcanoes. Combined with the mantle processes, crustal processes (e.g. the interplay between ascending melt and crust) are suggested by some authors to be highly complex (e.g. Bryner, 1991; Spörli and Black, 2013; Spörli *et al.,* 2015)**.** However, the role for crustal processes has not been reported within the detailed mantle geochemical studies of Huang et al. (1997) or McGee et al. (2013).

To further investigate the geochemical evolution of the AVF, it was considered necessary to assess the complex pre-eruptive processes that have been indicated by the results from **Chapter 5 and 4,** and from previous studies. Until now only the Sr-Nd-Pb (e.g., Huang *et al.,* 1997; McGee *et al.,* 2013) and U-Ra-Th (McGee *et al.,* 2011) isotope systems have been used to asses the AVF mantle processes. Here I use the Os-Re isotope system, which has been shown to be much more sensitive in tracing crustal (or recycled crustal) products within primitive lavas (e.g., McBride *et al.,* 2001; Jung *et al.,* 2011). **Chapter 6** is presented in the form of a multi-author paper in preparation for submission to Chemical Geology. Authorship contributions include; Timm – development of discussion points and manuscript edits; Millet – facilitated research and manuscript edits; Poirier – training of Hopkins on analytical methods, and some independant analysis of Os, Re, and Os isotopes; Wilson and Leonard – manuscript edits.

Chapter 6

Os isotope constraints on crustal contamination in Auckland Volcanic Field basalts, New Zealand

Jenni L. Hopkins*[a]

Christian Timm[b], Marc-Alban Millet[c], André Poirier[d], Colin J.N. Wilson[a], Graham S. Leonard[b].

[a]School of Geography, Environment and Earth Sciences, Victoria University, PO Box 600, Wellington 6140, New Zealand

[b]GNS Science, PO Box 30368, Lower Hutt 5040, New Zealand

[c]Department of Earth Sciences, Durham University, Durham DH1 3LE, England

[d]Geotop, Université du Québec à Montréal, Montréal, H3C 3P8, Canada

Keywords

Auckland Volcanic Field, Os isotope, crustal contamination, AFC modelling, Dun Mountain ophiolite belt

Abstract

The Auckland Volcanic Field (AVF) represents the youngest and northern-most of three main intraplate volcanic fields on North Island, New Zealand. Previous studies suggested that AVF lava major and trace element, and Sr-, Nd-, Pb-isotope compositions primarily reflect their derivation from asthenospheric and lithospheric mantle sources. We present new Os and Pb isotope data, and Os and Re concentrations for 15 lava samples from 7 centres of the AVF, to further explore mantle and crustal processes. The samples include a selection of the most primitive lavas from the field (Mg# 59-69) and span a range of eruption sizes, ages, locations, and geochemical signatures. The new data show a large range in Os concentrations (6-579 ppt) and $^{187}Os/^{188}Os$ isotope ratios from mantle-like (0.123) to highly radiogenic (0.547). Most samples exhibit highly radiogenic Os signatures together with relatively low Os contents suggesting that ascending melts experienced contamination primarily from metasedimentary crustal rocks with high $^{187}Os/^{188}Os$ (e.g., greywacke). Based on AFC modelling, <1% crustal input into the ascending melt can produce the radiogenic Os isotope signatures. This low level of crustal contamination has no measurable impact on the AVF Sr-Nd-Pb isotope or trace element signatures. In addition, three samples have high Os (Os = 194-578 ppt) contents at mantle-like Os isotope compositions ($^{187}Os/^{188}Os$ = 0.1283-0.1377) suggestive of contamination of the ascending melts with xenocrystic olivine-hosted mantle sulphides. An obvious source is the Permian-Triassic ultramafic Dun Mountain Belt, which traverses the crust beneath the Auckland Volcanic Field. We therefore interpret that the AVF Os isotopic composition and Os contents represent contamination events in a heterogeneous crust composed of Waipapa and Murihiku Terrane metasediments and ultramafic rocks of the Dun Mountain Ophiolite Belt. This demonstrates, contrary to previous models that primitive lavas from the Auckland Volcanic Field interacted variably with the crust.

6.1. Introduction

Monogenetic volcanic fields (MVF) are the surface expression of small-scale magmatic systems found in a number of different tectonic settings, including extensional systems relating to active arcs (e.g., Cascades, USA; Borg *et al.,* 2000), or subduction (e.g., Wudalianchi, China; Hwang *et al.,* 2005), or intraplate settings relating to rifting or plume upwelling (e.g., Eifel, Germany; Shaw, 2004). Monogenetic volcanic centres are linked to individual, often small-volume, batches of magma (<0.1 km^3) (e.g., Connor and Conway, 2000; Németh, 2010; Kereszturi *et al.,* 2013), which erupt over short periods of time (e.g., Németh, 2010), eventually leading to the formation of fields encompassing tens to hundreds of individual centres (e.g., Condit and Connor, 1996; Conway *et al.,* 1998; Connor and Conway, 2000; Valentine *et al.,* 2005). These fields show a range of surface expressions, dependent on the eruption style and magma-water interaction, including tuff rings, maars, scoria cones, and lava flows (e.g., Allen and Smith, 1994; Németh, 2010; Kereszturi *et al.,* 2014). In addition, a link between physical characteristics of monogenetic basaltic volcanism and mantle heterogeneity has recently been proposed (McGee et al., 2015) highlighting the importance to understand the characteristics of different sources contributing to magmas beneath volcanic fields.

Petrological and geochemical studies have shown that basaltic monogenetic fields are the most common petrology type (e.g., Connor and Conway, 2000), which are characterised by the eruption of silica under-saturated basinites, nephelenites and alkaline basalts that are akin to Ocean Island Basalt (OIB) (e.g., Huang *et al.,* 1997; Cook *et al*., 2005; Valentine and Gregg, 2008;). Nevertheless, lavas can show considerable geochemical variations within volcanic fields (e.g., Valentine and Hirano, 2010; Timm *et al.,* 2010; McGee *et al.,* 2013), and within individual centres, the origins of which remain controversial (e.g., Bradshaw and Smith, 1994; Valentine and Gregg, 2008; Needham *et al.,* 2011; Brenna *et al.,* 2010*,* 2011; McGee *et al.,* 2012). Several studies have attributed variations in geochemical and isotopic signatures, both for individual eruptions and on a field wide scale, to mantle heterogeneity (e.g., Huang *et al.,* 1997; McBride *et al.,* 2001; Cook *et al.,*

2005; McGee *et al.,* 2013), or magma modification at various depths by wall rock assimilation and contamination or fractional crystallisation (e.g., Lassiter and Luhr, 2001; Alves *et al.,* 2002; Chesley *et al.,* 2002; Jamais *et al.,* 2008; Timm et al., 2009). Any crustal assimilation and contamination may be facilitated by storage or ponding within the crust (e.g., Bohrson *et al.,* 1997), however lava erupted in monogenetic volcanic fields are generally mafic (>8 wt.% MgO), suggesting that they have undergone little fractional crystallization and arguing against long magma storage in the crust. Variations mainly in the trace element, and Sr-, Nd-, and Pb-isotopic composition of lavas from monogenetic volcanic fields are therefore proposed to primarily resemble the composition of the underlying lithospheric and asthenospheric mantle (e.g., Valentine and Perry, 2007; McGee *et al.,* 2012, McGee *et al.,* 2013; McGee *et al.,* 2015).

Nevertheless, a prerequisite first step for the interpretation of geochemical data from continental intra-plate basalts is to distinguish between the geochemical signature of mantle heterogeneity and crustal contamination (e.g., Blondes *et al.,* 2008; Jung *et al.,* 2011). To understand the role of the crust and mantle petrogenesis beneath a continental monogenetic volcanic field we use the ^{187}Re-^{187}Os decay system. This isotope system was chosen as it is highly sensitive to crustal contamination due to a significant difference in $^{187}Os/^{188}Os$ between continental crust and the mantle. It therefore provides a unique tool to study subtle signs of crustal influence (e.g. Central European Volcanic Province (CEVP), Jung *et al.,* 2011; Newer Volcanics Province (NVP), McBride *et al.,* 2001) and mantle heterogeneity in lavas. The significant differences of $^{187}Os/^{188}Os$ in the crust and mantle result from contrasting behaviour of Re and Os during partial melting. Because Os behaves compatibly in mantle sulphides it primarily remains in the mantle whereas Re is moderately incompatible, and it preferentially enters the melt. The difference in the behaviour of Re and Os therefore results in extreme fractionation (e.g. high Re/Os in melt and crust, and low Re/Os in the mantle). Radioactive decay of ^{187}Re to ^{187}Os generates highly radiogenic $^{187}Os/^{188}Os$ values in old crustal rocks (up to $^{187}Os/^{188}Os = 5.0$; McBride *et al.,* 2001) and unradiogenic $^{187}Os/^{188}Os$ in the mantle (ca. 0.12; McBride *et al.,* 2001). Thus,

the contamination of a melt through either crustal assimilation (or recycled crustal derived material in a heterogeneous mantle) will cause an unusually radiogenic Os isotope signature.

Here we present new Os and Re concentrations and $^{187}Os/^{188}Os$ and $^{206}Pb/^{204}Pb$, $^{207}Pb/^{204}Pb$, $^{208}Pb/^{204}Pb$ isotope data for 15 mafic lavas from the Auckland Volcanic Field. The collection of this new data is aimed at identifying the relative importance of mantle heterogeneity (including crustal recycling) and the role of crustal contamination into ascending melts to give new insights into dynamics of melt generation and ascent beneath the city of Auckland.

6.2. The Auckland Volcanic Field

This study focuses on the monogenetic basaltic Auckland Volcanic Field (AVF), North Island, New Zealand. The AVF is located 400 km to the west behind the currently active arc, the Hikurangi Margin (Seebeck e*t al.,* 2014). The arc is thought to have regressed and rotated clockwise during the Miocene towards the south-east (Kear, 2004), but since 16 Ma the arc front is proposed to have migrated parallel to the subducting plate as a result of slab rollback along the Tonga-Kermadec subduction system (Seebeck *et al.,* 2014). The AVF is the northernmost of three intraplate monogenetic volcanic fields active in, and since, the Pliocene (Ngatutura and Alexandra ca. 2.7-1.5 Ma; Briggs *et al.,* 1994, and South Auckland ca.1.59-0.51 Ma; Cook *et al.,* 2005) (**Fig. 6.1.A**).

The AVF consists of ca. 53 individual centres (**Fig. 6.1.C**; Hayward *et al.,* 2011) that are emplaced over an area of ca. 360 km^2 (Figure 1; Allen and Smith, 1994). The centres comprise explosion craters, tuff rings (now maar lakes), scoria cones and lava flows. The edifices are interpreted to have formed through single eruptions of small magma batches (e.g., Allen and Smith, 1994), except for the youngest and largest volcano Rangitoto, where two eruption episodes were identified (Rangitoto 1 [553±7 cal. yrs. BP] and Rangitoto 2 [504±5 cal. yrs. BP]; Needham *et al.,* 2011). The total volume of erupted material in the AVF field is estimated at 1.7 km^3 total dense rock equivalent (DRE^{tot}), ca. 41% of which (0.7 km^3) formed Rangitoto (Kereszturi

et al., 2013). Previous studies have shown that basaltic volcanism commenced ca. 190 ka ago (**Chapter 5**) and shows some distinct changes in eruption frequency over time, with eruption rate increasing to ca. 21.5 ka (**Chapter 5**) and then decreasing up to the Rangitoto eruption. In **Chapter 5** it is also concluded that there is no obvious spatial evolution of the field through time.

The crust underlying the AVF is 20-30 km thick, composed of Waipapa and the Murihiku-Dun Mountain Maitai-Brook Street terranes (**Fig. 6.1.B**) (e.g., Kermode 1992; Eccles *et al.,* 2005; Horspool *et al.,* 2006), overlain by up to 1-2 km of Miocene Waitemata group sediments. The Waipapa and Murihiku terranes consist of ca. 227.5 to 148.5 Ma old late Triassic to late Jurassic low-grade meta-sediments. The Dun Mountain terrane represents a Permian to late Cretaceous oceanic arc ophiolite obduction event at the eastern Gondwana margin (e.g., Kimbrough *et al.,* 1992). The Dun Mountain terrane consists of ultramafic rocks and includes dunites, lherzolites, harzburgites and werhlites (McCoy-West *et al.,* 2013). The terrane forms a distinct positive magnetic lineament - the Junction Magnetic Anomaly (JMA). The JMA can be traced continuously through the North and South islands of New Zealand (Hatherton and Sibson, 1970) and crosses the Auckland Volcanic Field as a narrow (ca. 2-5 km), linear series of anomalies interpreted to be eastward-dipping serpentinised shear zones, extending to depths of 20-30 km (Eccles et al., 2005). Direct evidence of the Dun Mountain Ophiolite Belt (DMOB) beneath the AVF occurs in the form of serpentinite xenoliths within volcanic rocks in tuff rings from Pupuke, St. Heliers and Taylors Hill volcanoes (e.g., Searle, 1959a; Bryner, 1991; Jones, 2007; Spörli *et al.,* 2015). The basement rocks that make up the region of the study area have been extensively investigated (e.g., Bryner, 1991; Kermode, 1992; Eccles *et al.,* 2005; McCoy-West *et al.,* 2013), allowing potential sources of crustal contamination to be well characterised. Although the Auckland Volcanic Field has been the focus of many geochemical and petrological studies (Smith *et al*., 2008; Needham *et al.,* 2011; McGee *et al.,* 2011, 2012, 2013), questions about the origin of the observed geochemical composition of the lavas remain. In order to understand the complexity of melt dynamics in the AVF it is

important not only to understand where partial melting occurs in the mantle, but also how the geochemical composition of melts evolve and change during ascent.

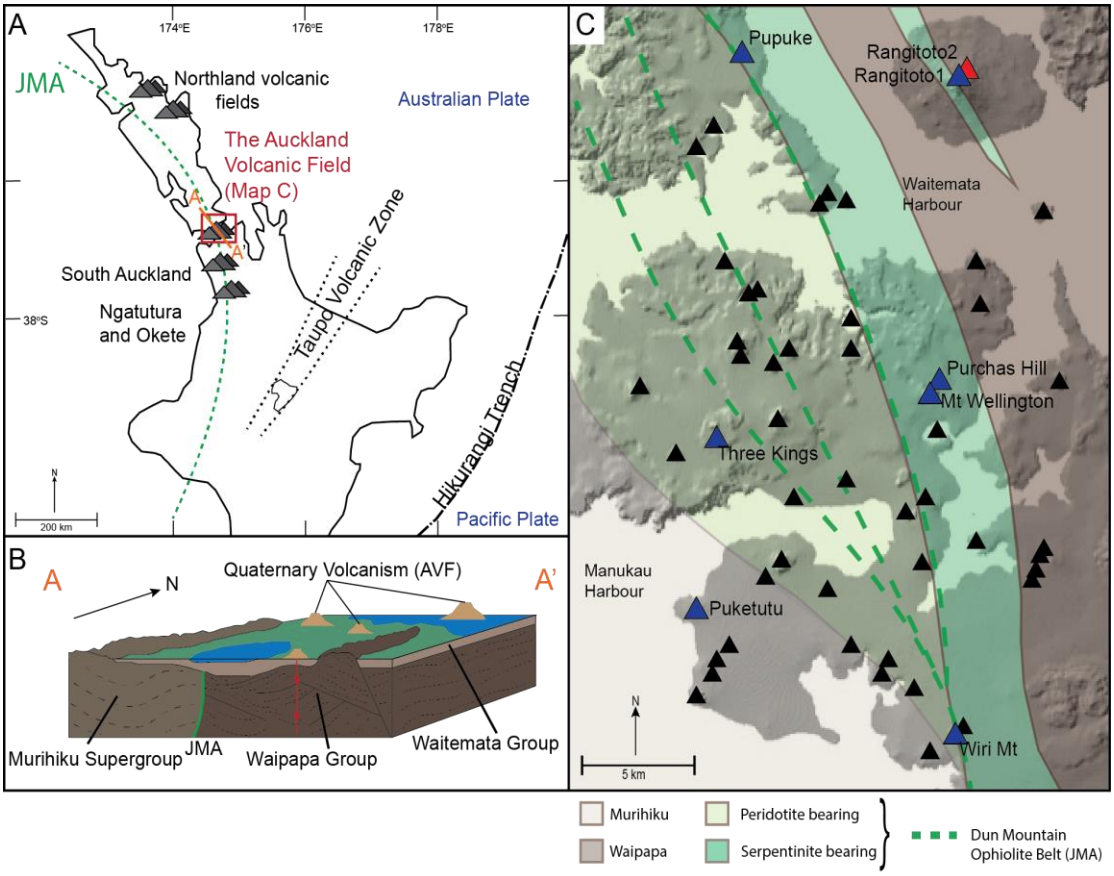

***Figure 6.1**. Schematic map of the Auckland Volcanic Field (AVF). (A) Location of the AVF within the North Island, New Zealand. The green dashed line indicates the Dun Mountain Ophiolite belt identified by the Junction Magnetic Anomaly (JMA) (Eccles et al., 2005), the Taupo Volcanic Field (TVZ) is shown with the dotted line, and the Hikurangi Trench between the Australian and Pacific plates is shown with a dash-dot line. The migrating monogenetic volcanic fields are also marked, Ngatutura and Okete ca.2.7-1.5 Ma (Briggs et al., 1994) and South Auckland ca.1.59-0.51 Ma (Cook et al., 2005). (B) Schematic diagram adapted from Kermode (1992) and Eccles et al. (2005) outlining the basement geology beneath the AVF: cross section A-A' is shown in diagram A. (C) DEM map of the AVF, black triangles indicate the sites of the volcanic centres. Those sampled for this study are highlighted by name, and the geochemical groups assigned denoted by blue – Low-SiO_2 group, and red – High-SiO_2 group (outlined in **section 6.4.1.** in the text). Proposed terranes at 1.5 km depth are shown (from Eccles et al., 2005).*

6.3. Samples and Analytical techniques

The major- and trace-element chemistry and Sr-, Nd-, and Pb isotopic composition of selected volcanic centres from the Auckland Volcanic Field have previously been discussed (McGee et al., 2011, 2012, 2013, 2015). For the purpose of this study 15 samples from Mt Wellington, Purchas Hill, Three Kings, Wiri Mt, Puketutu, the oldest centre Pupuke (190 ± 5.6 ka; Leonard *et al., in prep.* Appendix C) and the youngest Rangitoto 2 (504 ± 5.0 calendar (cal.) yrs BP; Needham *et al.,* 2011) were chosen to complement existing Pb isotope data and generate new Os content and isotope analysis. The samples chosen are some of the most primitive of the AVF lavas (Mg# = 59-69) from a range of eruption centres covering the field's areal extent, centre size, and age (**Table 6.1.**). Generally the selected samples contain minor olivine phenocrysts (≤ 3mm across) in a plagioclase, pyroxene, olivine-bearing groundmass, except for samples from Pupuke, which contain abundant large olivines ≥ 5mm across.

All new samples were prepared for chemical and isotopic analysis at Victoria University of Wellington, New Zealand (VUW). Fresh samples were chipped using a Rocklabs Boyd crusher to <15 mm in size and then reduced to powder in an agate ring mill. Major elements were analysed by XRF analysis at the Open University, Milton Keynes, UK on an ARL® 8420+ dual goniometer spectrometer. Powdered samples were fused with lithium metaborate and subsequently analysed following methods of Ramsey et al. (1995). Whin sill dolerite (WS-E) was run as an internal standard with associated accuracy of <1% except for Na_2O (2.37%) and P_2O_5 (1.59%) and precision of <2%. For trace element concentrations the powdered samples were digested in hot concentrated HF and HNO_3 for 4 days, and then dried to incipient dryness and taken up in concentrated HCl to reduce sample loss through the production of insoluble fluorides. Following this, samples were converted back into HNO_3 then left for 3 days in hot 1M HNO_3 to form the final analytical solution. Sample dilutions were measured on an Agilent 7500CS ICP-MS at Victoria University, Wellington, using BHVO-2 as a primary standard, and BCR-2 as a secondary standard. Precision on BCR-2 (n=15 from five digestions) was <6.5 % 2sd% except for Nb, Cs, and Ba (all ≤8 %),

and Ta, Pb, and Nb (≤20.5 %), and values were all within <6 % of the reference value, except for Cu, Cs, and Ta. All standard values are reported in **Appendix B**.

Pb isotope samples were prepared and purified in an ultra-clean chemical separation laboratory at VUW. For Pb isotope analysis 200 mg of powdered sample was leached in ultrapure 6M HCl for 1 hour at 120°C, rinsed with Millipore water, and digested in ultrapure conc. HNO_3 coupled with ultrapure conc. HF, then turned into solution with 0.8M HBr. The solution was then centrifuged and loaded onto 5mm columns equipped with AG1-X8 resin and Pb was extracted in a double-pass using 6M HCl. Pb isotopic compositions were analysed using a Neptune MC-ICP-MS at Durham University, UK. International standard NBS-981 was used to monitor machine drift, with internal precisions (2SE) of $^{206}Pb/^{204}Pb$ <±0.0012, $^{207}Pb/^{204}Pb$ <±0.0013, $^{208}Pb/^{204}Pb$ <±0.0044. All values of NBS-981 are outlined in **Appendix B**, and measured data are reported in **Table 6.1**.

Os isotope compositions and Re and Os contents were determined at GEOTOP, Université du Québec à Montréal (UQÀM), Canada following the method of Meisel et al. (2003). For these analyses 0.8 g aliquots of whole rock powder were spiked with a known enriched tracer solution of ^{190}Os - ^{185}Re, and digested in Teflon-sealed quartz tubes with 3 ml 6M HCl and 3 ml conc. HNO_3 at 300°C and 100 bar in a high-pressure asher unit (HPA-S, Anton-Parr-Perkin Elmer Instruments). After digestion Os was extracted using the Paris Br_2 technique. 2 ml of chilled Br_2 was added to sample and left on a hot plate at 90°C for 2 hours. This scavenges the oxidised Os (OsO_4) from the aqueous solution into the liquid Br_2, leaving Re (and PGEs) within the aqueous solution. 20 drops of HBr was added to the isolated liquid Br_2 (including Os) to reduce Os from volatile Os^{8+} (OsO_4) to non-volatile Os^{4+} ($OsBr_6^{2-}$), and evaporated down. A final step of micro-distillation using Cr^{VI} containing H_2SO_4 was used to purify the Os, and make sure it was quantitatively separated from isobaric Re (after Birck *et al.,* 1997). Samples were then measured using a Triton TIMS in negative-ion mode for Os (Creaser *et al.,* 1991) and on a Sector Field (SF)-ICP-MS for Re. Os and Re concentrations were calculated by isotope dilution from known spike solution

values. Os blanks for total procedure are 0.3 pg, and 7 pg for Re, this value is subtracted from the sample totals in data processing, along with oxygen interference correction and spike-sample unmixing. The widely used standard DROsS was also analysed, with an internal precision (2SE) for $^{187}Os/^{188}Os$ of average measurements of <±0.00012. For Re, the standard NIST SRM 3143 was used, with an internal precision (2SE) for average $^{187}Re/^{185}Re$ measurements of <±0.05. All values for DROsS and NIST SRM 3143 are outlined in **Appendix B**.

6.4. Results

6.4.1. Major and trace elements

Volcanic rocks from the AVF range in composition from sub-alkaline silica under-saturated basanites to alkaline basalts (e.g., SiO_2 = 39.8-48.8 wt.%) following the rock classification of LeMaitre (2002). Most AVF lavas form broad negative trends with MgO (wt.%) vs. SiO_2, and Al_2O_3 (wt.%) and positive trends with CaO FeO^t, TiO_2, and P_2O_5 (wt.%) indicative of olivine and pyroxene fractionation (**Fig. 6.2.**). The only exception are lavas from Rangitoto (in particular Rangitoto 2 samples) having consistently lower wt. % FeO^t, TiO_2, CaO and P_2O_5 and higher SiO_2 and Al_2O_3 at given wt.% MgO. Here we therefore define two groups a high SiO_2 group (Rangitoto 2 samples), and a low SiO_2 group (all other samples). Cook et al. (2005) identify a similar variability in major element compositions in lavas from the South Auckland Volcanic Field.

All AVF samples show primitive mantle normalised trace element distributions similar to ocean island basalt (OIB) (normalisation values after McDonough and Sun, 1995), with typical positive Nb and negative K anomalies on multi-element diagrams (**Fig. 6.3.**). Compared to the high-SiO_2 group lavas, the low-SiO_2 group lavas shows higher Nb and Ta (e.g., Nb/Ba ≥ 0.2) relative to the large ion lithophile elements (LILE; Rb, Ba, K). The low SiO_2 group lavas furthermore have higher light rare earth elements (LREE; La, Gd, Nd) but low heavy rare earth elements (HREE; Yb) in comparison to

the high SiO_2 group lavas resulting in high LREE/HREE values (e.g., $(La/Yb)_N$ >20). In addition the low SiO_2 group shows high ratios of more to less incompatible elements, for example Th/HREE (e.g., Th/Yb ≥2), higher Ce/Pb (>10), lower K/Nb (<300) and Sr/Nb (<5). Conversely the high-SiO_2 group lavas show only minor enrichment in Nb and Ta relative to the LILE (e.g., Nb/Ba ≤ 0.2), have lower LREE but similar to slightly higher HREE (e.g., $(La/Yb)_N$ <20). These lavas have higher Th relative to HREE (e.g. Th/Yb <1), lower Ce/Pb (<10), yet higher K/Nb (>300) and Zr/Nb (>7). The distinct REE patterns and Nb and Ta contents are comparable to those outlined by Cook et al. (2005), who noted higher Nb, $(La/Yb)_N$ and Th/HREE values, for their Group B (equivalent to the low-SiO_2 group here) and low Nb, $(La/Yb)_N$ and Th/HREE for their Group A (c.f. our high-SiO_2 group) and contrasting incompatible trace element ratios (e.g. K/Nb, Zr/Nb and Ce/Pb). The low-SiO_2 group lavas show strong negative K anomalies that are increasingly subdued in the high-SiO_2 group lavas, which show positive Sr anomalies and are in turn less prominent in the low-SiO_2 group. These observations are also consistent with Hoernle et al. (2006) and Timm et al. (2009 and 2010) who also divided their data from New Zealand intraplate volcanic centres and fields into 'low-SiO_2' and 'high-SiO_2' groups, showing similar differing major and trace element geochemical compositions to the AVF low- and high-SiO_2 groups.

Table 6.1. *Selected geochemical data for AVF centres, * denotes data from lavas previously analysed by McGee et al., 2013. 'i, ii, iii etc' denotes duplicate analyses from the same sample but different digestion. Full data can be found in Appendix C.*

Centre	Sample	$^{187}Os/^{188}Os$ (±2σerror)	Os (ppt)	Re (ppt)	SiO_2 (wt%)	MgO (wt%)	Ni (ppm)	$^{206}Pb/^{204}Pb$ (±2σerror)	$^{207}Pb/^{204}Pb$ (±2σerror)	$^{208}Pb/^{204}Pb$ (±2σerror)
Rangitoto	AU59308	0.5470 ± 0.0013	5.8	411.9	45.47*	11.49*	239*	19.224 ± 0.001*	15.594 ± 0.001*	38.485 ± 0.003*
	AU59311	0.3901 ± 0.0016	10.9	45.2	48.80	9.75	147	19.071 ± 0.001	15.615 ± 0.001	38.801 ± 0.003
	AU59309-i	0.4041 ± 0.0023	10.4	225.9	48.53	8.65	217	19.064 ± 0.001	15.612 ± 0.001	38.787 ± 0.003
	AU59309-ii	0.2525 ± 0.0004	22.2							
	AU59309-iii	0.123 ± 0.065	122.6	218.7						
Mt. Wellington	AU62391	0.3204 ± 0.0013	9.3	25.9	43.12*	12.77*	367*	19.302 ± 0.001	15.587 ± 0.001	38.872 ± 0.003
	AU62411-i	0.3166 ± 0.0019	8.6	411.0	43.30*	12.74*	314*	19.293 ± 0.001*	15.582 ± 0.001*	38.858 ± 0.003*
	AU62411-ii	0.3951 ± 0.0003	10.8							
Purchas Hill	AU44711	0.2831 ± 0.0005	23.7	90.5	39.79*	11.4*	312*	19.132 ± 0.002	15.613 ± 0.002	38.841 ± 0.005
	AU44707-i	0.4235 ± 0.0011	9.7		42.98*	12.26*	248*	19.383 ± 0.002	15.589 ± 0.002	38.929 ± 0.006
	AU44707-ii	0.2994 ± 0.0038	10.8	187.4						
	AU44707-iii	0.2752 ± 0.0065	9.1	196.6						
	AU44707-iv	0.2539 ± 0.0009	8.9							
Three Kings	AU59443	0.2422 ± 0.0006	9.9	98.3	43.04*	11.85*	267*	19.293 ± 0.001*	15.582 ± 0.001*	38.855 ± 0.002*
	AU59453	0.1623 ± 0.0006	27.5	189.3	43.00*	12.17*	286*	19.298 ± 0.002*	15.592 ± 0.001*	38.886 ± 0.003*
Wiri	AU43943	0.2730 ± 0.0025	14.1	231.5	43.58*	11.18*	253*	19.225 ± 0.001*	15.576 ± 0.001*	38.791 ± 0.002*
	AU43931-i	0.2242 ± 0.0020	8.5	153.7	44.03*	11.00*	229*	19.219 ± 0.001*	15.579 ± 0.001*	38.795 ± 0.002*
	AU43931-ii	0.2449 ± 0.0012	8.5							
	AU43931-iii	0.3299 ± 0.0017	14.7	133.8						
	AU43931-iv	0.1987 ± 0.0007	15.0							
	AU43931-v	0.1283 ± 0.0001	194.0							
Puketutu	AU62379	0.2328 ± 0.0004	7.3	91.7	42.87*	12.19*	331*	19.282 ± 0.001*	15.580 ± 0.001*	38.839 ± 0.003*
	AU62383-i	0.2659 ± 0.0011	10.4	140.4	42.84*	12.30*	342*	19.330 ± 0.001*	15.595 ± 0.006*	38.918 ± 0.003*
	AU62383-ii	0.2122 ± 0.0003	7.3							
Pupuke	AU58657	0.1374 ± 0.0008	578.4	207.3	44.75*	13.93*	463*	19.218 ± 0.001	15.613 ± 0.001	38.924 ± 0.005
	JH005	0.1377 ± 0.0002	195.5	235.7	45.48	14.22	538	19.247 ± 0.001	15.615 ± 0.001	38.931 ± 0.004

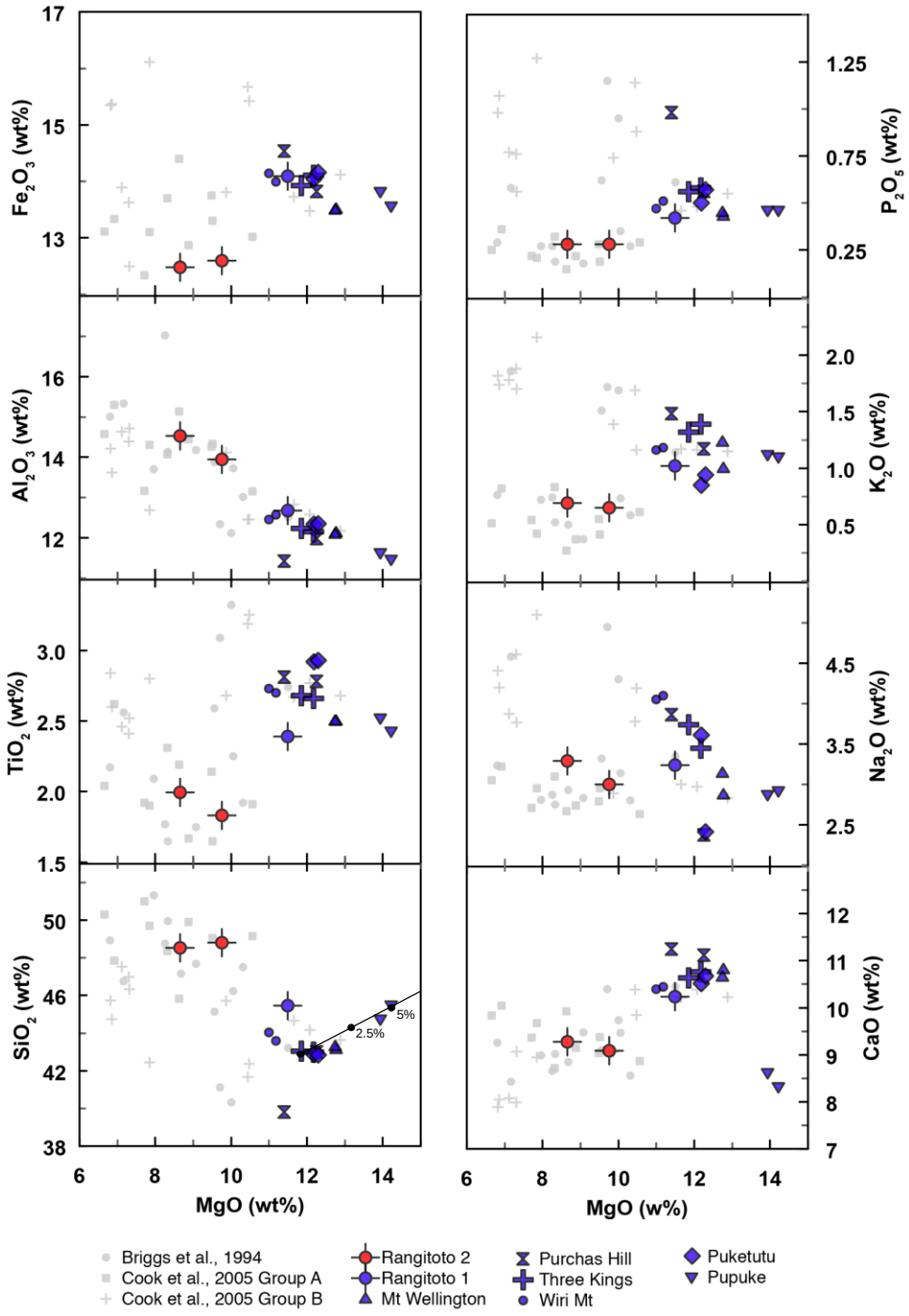

Figure 6.2. *Diagram panels showing major elements vs. MgO (wt.%). Blue symbols denote group 1 and red symbols denote group 2 samples. Grey symbols represent previously published data from the South Auckland volcanic field, with squares denoting Group A and crosses denoting Group B as assigned by Cook et al.(2005); and spots showing data from Briggs et al. (1994), which were ungrouped. Our low-SiO_2 group (blue) generally correlates to Group B, and our high-SiO_2 group (red) to Group A. Also shown in the SiO_2 vs. MgO panel is the impact of mixing olivine into the samples, showing the addition of 5% olivine (values from Deer et al., 1992) could produce the Pupuke sample signatures.*

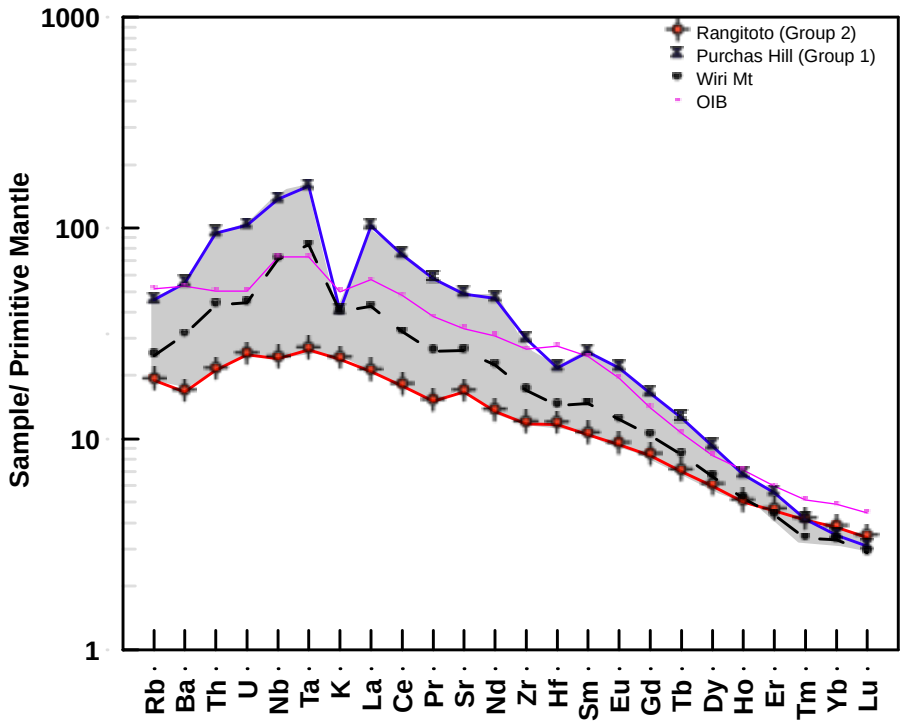

Figure 6.3. *Diagram showing representative primitive mantle-normalised multi-element distribution to present the AVF trace element data range (after McGee et al., 2013). The lava end members are exemplified by Purchas Hill (Group 1; blue) and Rangitoto 2 (Group 2; red). Wiri Mt. lavas show intermediate trace element distribution in black. Grey field marks the range from the AVF field, and pink shows a typical OIB-type signature (OIB and normalisation values from McDonough and Sun, 1995).*

6.4.2. Sr-Nd-Pb isotopes

Isotopic data for the AVF lavas are reported in **Table 6.1**. Seven new Pb isotope data have been generated supplementing previously published AVF Pb isotope data of McGee et al. (2013). In general the AVF lava Pb isotopic composition show limited variation ($^{206}Pb/^{204}Pb$ = 19.060-19.383, $^{207}Pb/^{204}Pb$ = 15.576-15.617, and $^{208}Pb/^{204}Pb$ = 38.787-38.931). On Pb isotope variation diagrams (**Fig. 6.4.**) the AVF data plot between the mid ocean ridge basalt (MORB), HIMU (high μ = high time integrated U/Pb) and enriched mantle (EM I or II) end-members (following the classification of Zindler and Hart, 1986).

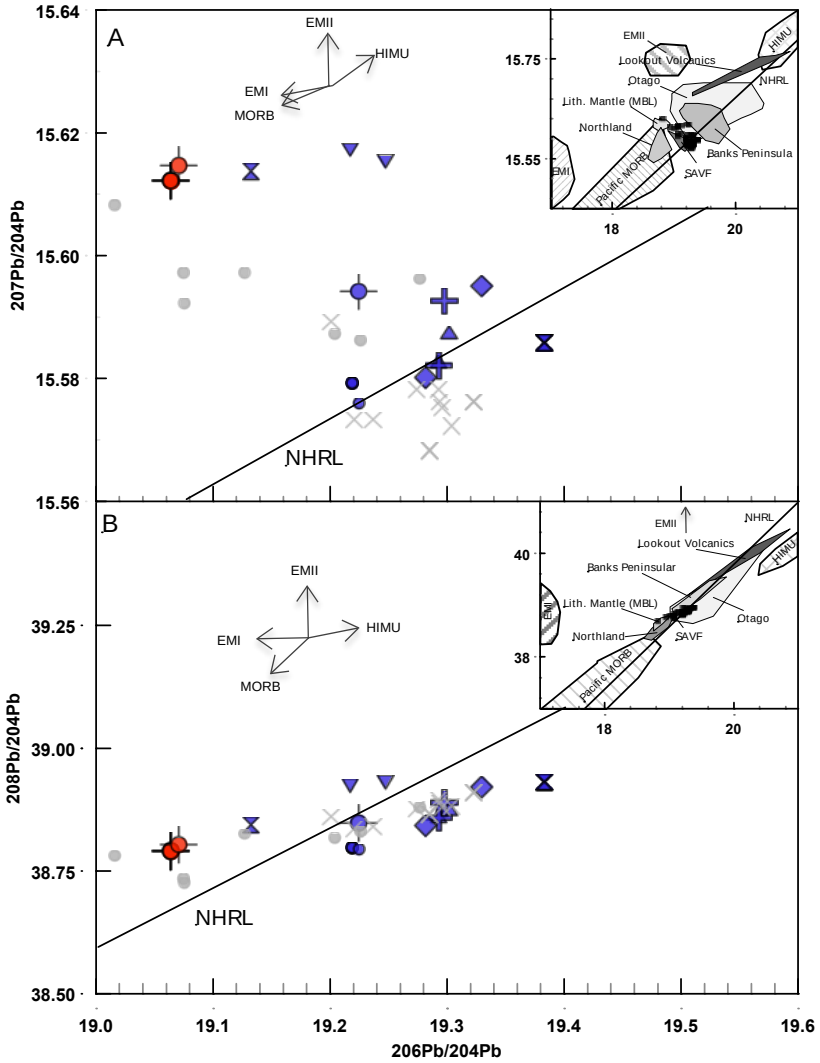

Figure 6.4. *A) $^{206}Pb/^{204}Pb$ vs. $^{207}Pb/^{204}Pb$ and B) $^{208}Pb/^{204}Pb$ vs. $^{206}Pb/^{204}Pb$ for all lavas from the Auckland Volcanic Field, in comparison to the Northern Hemisphere Reference Line (NHRL) from Hart (1984). On the inset plots the mantle reservoir end members are from Zindler and Hart (1986): Enriched Mantle (EMI and EMII), Pacific MORB Mantle, Lith. Mantle (MBL), and HIMU. Values for Northland from Huang et al. (2000), for Otago from Timm et al. (2010), for Banks Peninsular from Timm et al. (2009), and for Lookout Volcanics from McCoy-West et al. (2010). Also shown are values for the SAVF from Cook et al., 2005 (Group A are grey spots, and group B grey crosses). Symbols for the AVF data are as in* ***Figure 6.2.*** *again, our low-SiO_2 group (blue) generally correlates to Group B, and our high-SiO_2 group (red) to Group A from Cook et al. (2005).*

The spread in Pb isotope compositions observed in AVF lavas generally overlap with Pb isotope values from the South Auckland Volcanic Field ($^{206}Pb/^{204}Pb$ = 18.950-19.323; $^{207}Pb/^{204}Pb$ = 15.568-15.613, and $^{208}Pb/^{204}Pb$ = 38.723-38.906; Cook *et al.,* 2005; **Fig. 6.4.**). Purchas Hill lava AU44711 (low-SiO_2) show elevated $^{206}Pb/^{204}Pb$ (19.383) and $^{208}Pb/^{204}Pb$ (38.929), but $^{207}Pb/^{204}Pb$ similar to lavas from other AVF centres. Conversely, Rangitoto 2 (high-SiO_2) shows the lowest $^{206}Pb/^{204}Pb$ (e.g., 19.064), low $^{208}Pb/^{204}Pb$ (e.g., 38.485), coupled with some of the highest $^{207}Pb/^{204}Pb$ values of all AVF volcanic rocks (**Fig. 6.4**.).

Previously published Sr and Nd isotope data from the AVF lavas show a restricted range from $^{87}Sr/^{86}Sr$ = 0.702710 to 0.703125 and from $^{143}Nd/^{144}Nd$ = 0.512939 to 0.512956 (McGee *et al.,* 2013). Although no obvious trend has been identified between Sr and Nd isotopic compositions, the AVF and SAVF high-SiO_2 lavas have distinctly higher $^{87}Sr/^{86}Sr$ (=0.7032) than the lavas from the other centres at similar $^{143}Nd/^{144}Nd$ values (=0.5129). Similarly there is no clear correlation observed between $^{206}Pb/^{204}Pb$ and $^{143}Nd/^{144}Nd$, although $^{206}Pb/^{204}Pb$ and $^{87}Sr/^{86}Sr$ show a broad negative trend (McGee *et al.,* 2013; Cook et al., 2005).

The isotope data therefore support and reiterate the groups discussed for the concentration data and these groupings are also consistent with Cook et al. (2005). Their 'Group B' type (our low SiO_2) was defined by lower $^{87}Sr/^{86}Sr$ values (= ≤0.7028) at similar $^{143}Nd/^{144}Nd$ values (=0.51296-0.51298), coupled with higher $^{206}Pb/^{204}Pb$ values (=19.201-19.323), higher $^{208}Pb/^{204}Pb$ (=38.833-38.892) and lower $^{207}Pb/^{204}Pb$ values (15.568-15.589). In comparison to their 'Group A' type (our high-SiO_2), which has higher $^{87}Sr/^{86}Sr$ values (= ≥0.7029) and similar $^{143}Nd/^{144}Nd$ values (= 0.51294-0.51298), coupled with lower $^{206}Pb/^{204}Pb$ values (=18.950-19.277), lower $^{208}Pb/^{204}Pb$ (= 38.723-38.876), and higher $^{207}Pb/^{204}Pb$ values (= 15.586-15.613).

6.4.3. Re, Os, and $^{187}Os/^{188}Os$

$^{187}Os/^{188}Os$ values and Re and Os concentrations are given in **Table 6.1**. The AVF lavas show a wide range in Os and Re concentrations (Os = 5.8-578 ppt, Re = 25.9-411 ppt). These concentrations fall within the range of Os contents reported from other OIB-type lavas (Os = ca.1-600ppt; Schiano *et al.,* 2001, Re = ca.100 to 642 ppt; Hauri and Hart, 1997). The Os isotope compositions from AVF volcanic

rocks also show a significant range from mantle values ($^{187}Os/^{188}Os$ = 0.1283; cf. Meisel *et al.,* 2001) to radiogenic values ($^{187}Os/^{188}Os$ = 0.5470). The majority of samples (n = 19) have $^{187}Os/^{188}Os$ ≥0.15, higher than the range assumed for mantle-derived lavas (Lassiter and Hauri, 1998; Widom *et al.,* 1999; Rasoazanamparany *et al.,* 2015). In general no obvious correlations between Os and Re concentrations, $^{187}Os/^{188}Os$ and MgO, Ni, Cu or Zr are observed. The exception is samples from Pupuke showing high MgO, Ni, and Os concentrations but low $^{187}Os/^{188}Os$ values (**Fig. 6.5**.).

The overall range in $^{187}Os/^{188}Os$ in the AVF lavas is larger than that observed in most OIB-like basalts (**Fig.6.6.A**) (Reisberg *et al.,* 1993; Hauri and Hart, 1993; Roy-Barman and Allegre, 1995; Marcantonio *et al.,* 1995; Lassiter and Hauri, 1998; Schiano *et al.,* 2001; Day *et al.,* 2010). Most AVF $^{187}Os/^{188}Os$ values however overlap with the Os isotopic composition of alkali basaltic and tholeiitic lavas from other continental intraplate volcanic fields, such as the Newer Volcanic Province, SE Australia ($^{187}Os/^{188}Os$ = 0.1342-0.4456; McBride *et al.,* 2001); CEVP, Germany ($^{187}Os/^{188}Os$ = 0.1487-0.7526; Jung *et al.,* 2011) and East African Rift System ($^{187}Os/^{188}Os$ = 0.1239-0.4366; Nelson *et al.,* 2012) (**Fig.6.6.A**). **Figure 6.7** shows that there is a large range in $^{187}Os/^{188}Os$ in relation to the narrow range in $^{206}Pb/^{204}Pb$. Lavas with more radiogenic Os isotopic composition generally contain less Os (e.g. Rangitoto sample AU59309: $^{187}Os/^{188}Os$ = 0.5470, Os = 5.8 ppt), and those with lower $^{187}Os/^{188}Os$ contain more Os (e.g. Wiri Mt. sample AU43931: $^{187}Os/^{188}Os$ = 0.1283, Os = 194 ppt). In addition, low Os concentration lavas (<40 ppt) generally have more variable Os isotope signatures (0.1623-0.5470), becoming less variable (0.1230-0.1374) with increasing Os contents. On an $^{187}Os/^{188}Os$ versus 1/Os diagram the AVF samples form a broad positive trend (**Fig. 6.6.B**) generally plotting between crustal and mantle end member fields. Of note is that samples from Purchas Hill, Rangitoto and Three Kings form individual positive trend lines at varying gradients, whereas samples from Wiri Mt. and Mt. Wellington show no clear trends between $^{187}Os/^{188}Os$ and 1/Os (**Fig. 6.6.B**). These mixing trends converge on a similar end member with $^{187}Os/^{188}Os$ = 0.1231 ~0.1283 and Os concentration of ca. 50-200 ppt, similar to primitive upper mantle (e.g., Meisel *et al*., 2000), and thus are interpreted to represent the mantle end member for the AVF.

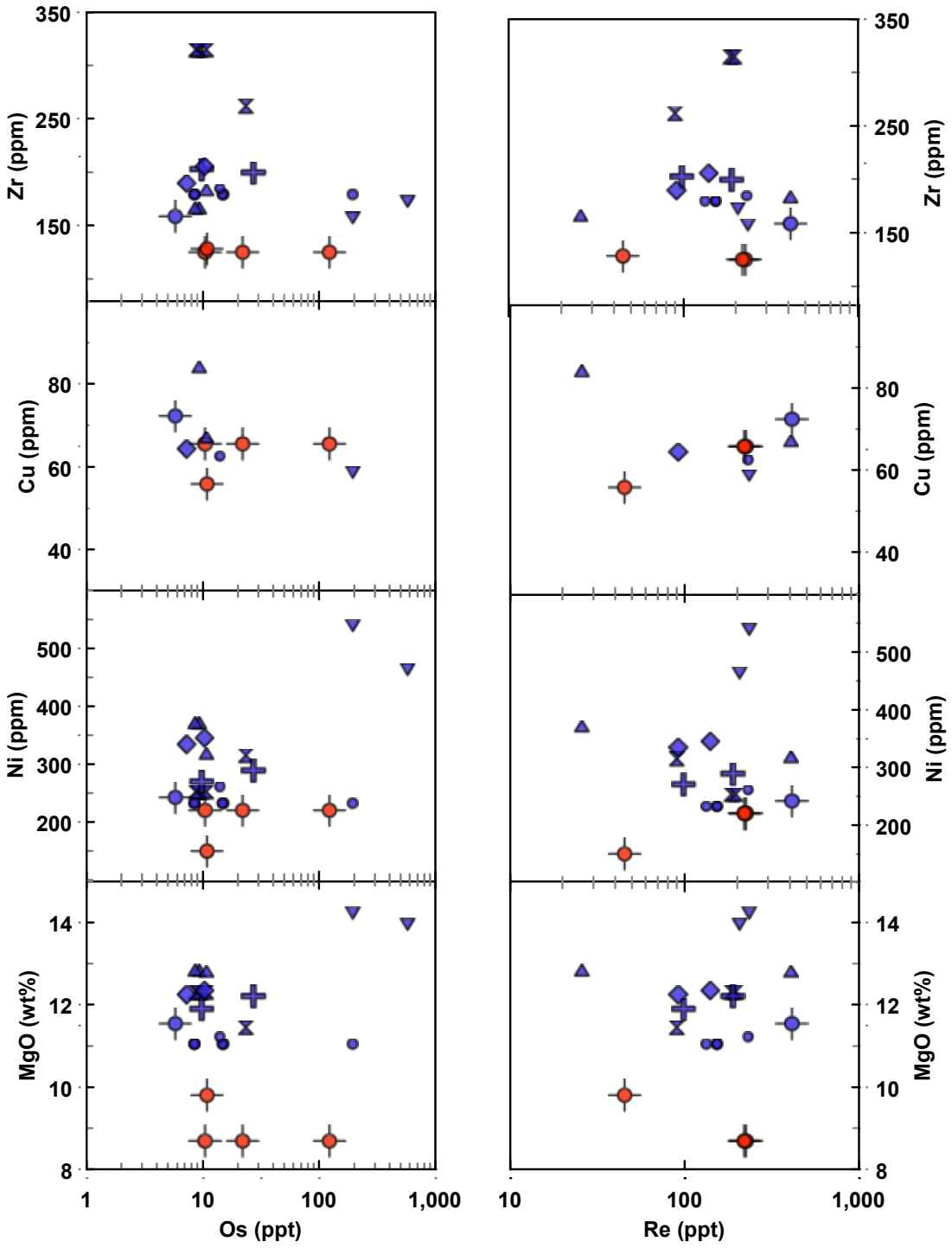

Figure 6.5. *Os and Re concentrations versus MgO (in wt.%), Ni, Cu and Zr (all in ppm) contents. Symbols are as in* ***Figure 6.2****.*

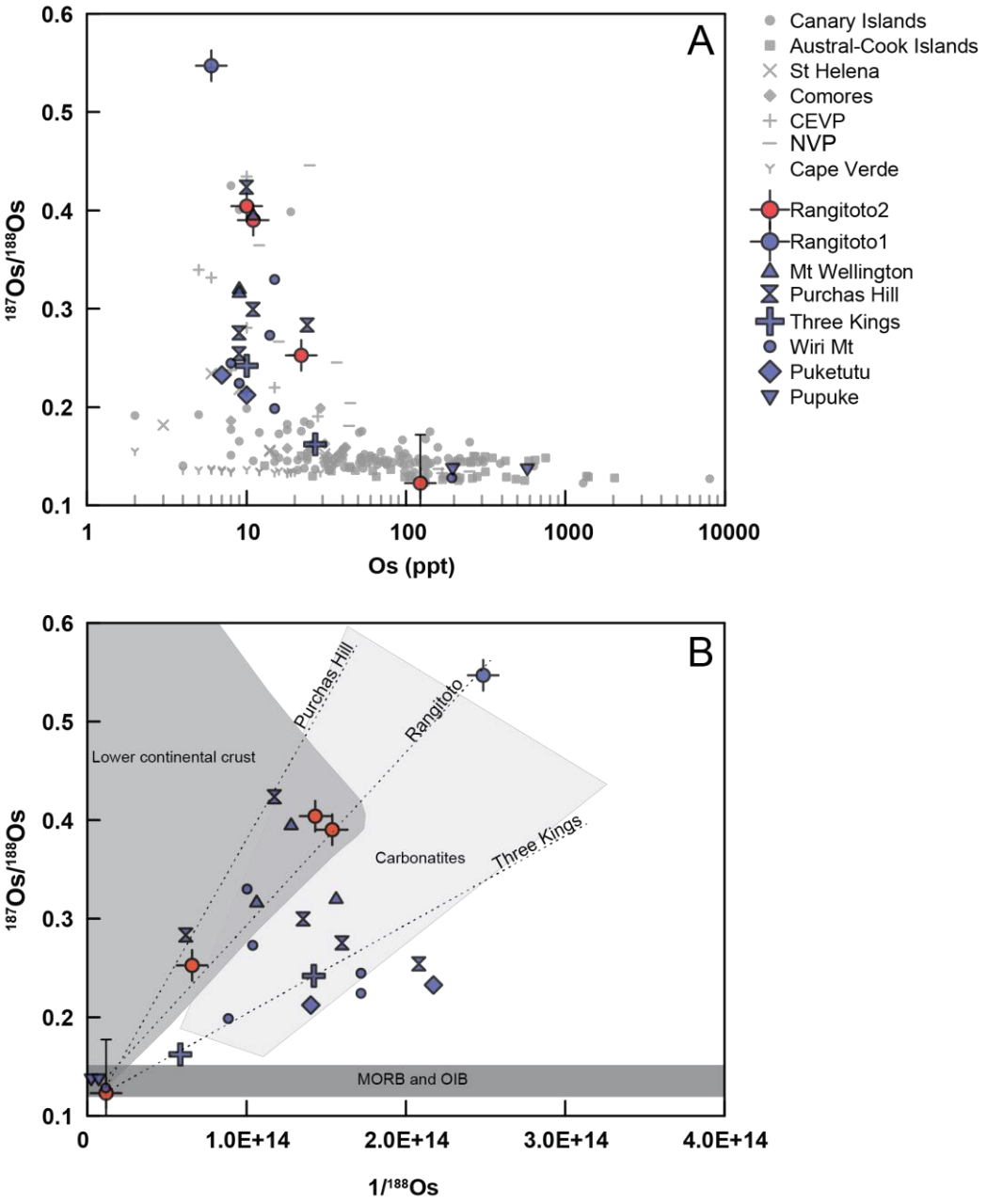

Figure 6.6. *(**A**) $^{187}Os/^{188}Os$ vs Os (ppt) for all samples from the AVF. Also shown in grey symbols are global OIB values for the Canary Islands (Marcantonio et al., 1995; Widom et al., 1999; Day et al., 2010); the Austral Cook Islands (Hauri and Hart, 1993; Reisberg et al., 1993); St Helena and Comores (both from Reisberg et al., 1993); Central European Volcanic Province (CEVP; Jung et al., 2011); Newer Volcanic Province, Australia (NVP; McBride et al., 2001); Cape Verde (Escrig et al., 2005). (**B**) $^{187}Os/^{188}Os$ vs $1/^{188}Os$ for all AVF samples, with global fields for lower continental crust (Esser and Turekian, 1994; Rudnick and Fountain, 1995; Saal et al., 1998; Rudnick and Gao, 2003), and MORB and OIB (Hauri and Hart 1993; Roy-Barman and Allegre, 1995; Schiano et al., 1997; Schiano et al., 2001; Peucker-Ehrenbring and Jahn, 2001), and Carbonatites (Escrig et al., 2005; Widom et al., 1999). Error bars are shown for Rangitoto sample AU59309, for all other analyses the errors are smaller than the symbol.*

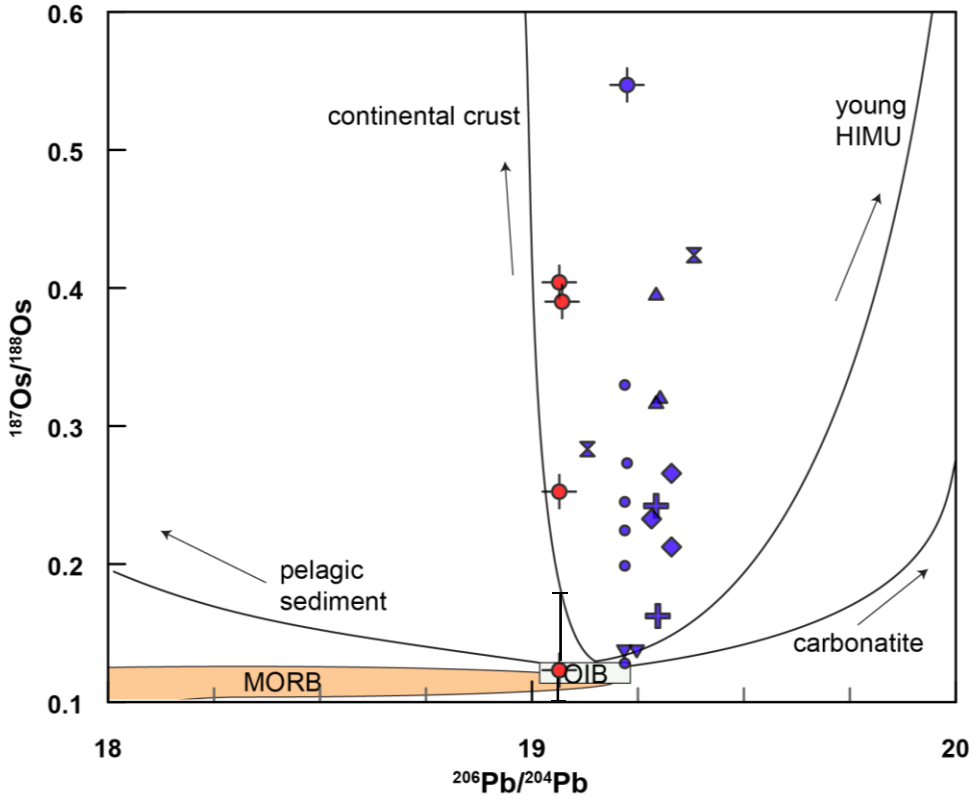

***Figure 6.7**. Diagram after Day (2013), to show mixing relationships for various potential contaminants in $^{206}Pb/^{204}Pb$ vs. $^{187}Os/^{188}Os$ isotope space. Data values for MORB and OIB from Widom et al. (1999) and Day et al. (2010); pelagic sediments from Roy-Barman and Allegre (2005); carbonatite from Escrig et al. (2005) and Widom et al. (1999); young HIMU from Day et al. (2009); and continental crust from Saal et al. (1998) and Widom et al. (1999).*

6.5. Discussion

6.5.1. Mantle source heterogeneity

Intraplate basalts with OIB-like characteristics typically contain isotope signatures from multiple sources including depleted MORB mantle (DMM), HIMU (through addition of ancient recycled oceanic crust), and enriched mantle end members (EMI, cause by terrigeneous sediment assimilation, and EMII caused by pelagic sediment assimilation; cf. Zindler and Hart 1986; outlined on **Fig. 6.4.**). The petrogenesis of the AVF basalts has been the subject of a number of geochemical and isotopic studies (Huang *et al.,* 1997; Needham *et al.,* 2011; McGee *et al.,* 2011, 2012, 2013, 2015). In general, published Sr-, Nd-, Pb-isotope data from AVF

samples plot intermediate between Pacific MORB and HIMU (e.g., $^{206}Pb/^{204}Pb$ = 19.0-19.4; Huang *et al.,* 1997; McGee *et al.,* 2013, **Fig. 6.4**.). Compared to a 'true' HIMU Pb isotope composition (e.g., $^{206}Pb/^{204}Pb$ >20.5), which requires ≥0.8 Ga to evolve from a typical MORB mantle (e.g., Thirlwall *et al.,* 1997), the much less radiogenic Pb isotopic compositions in the AVF lavas were attributed to the presence of a 'young' HIMU signature by Huang et al. (1997). Similarly Cook et al. (2005) proposed that ≤12% melting of a garnet-bearing asthenospheric mantle containing young (<0.2 Ga) HIMU-like isotope signature can explain the geochemical composition of the SAVF low SiO_2 group lavas. In addition the low SiO_2 group AVF lavas contain high CaO/Al_2O_3, Na_2O and K_2O at low Nb/U and elevated Ce/Pb, Nb/Ce, and U/Pb suggestive of the presence of carbonated garnet peridotite domains (McGee *et al.,* 2015) hosted in MORB-like peridotitic asthenosphere (McGee *et al.,* 2013). The geochemical and isotopic signatures of the high-SiO_2 group lavas are attributed (by McGee et al., 2013) to additional input from an EMII-type lithospheric source metasomatised by subduction-related fluids and melts into the ascending asthenospheric melt at shallower depth. Similarly, low-degree partial melting (≤8 %) of shallow, spinel bearing EMII-type subduction metasomatised lithosphere has been invoked to explain the low total alkali (TAS), Nb contents, $(La/Yb)_N$ ratios and e.g., $^{206}Pb/^{204}Pb$ of the high-SiO_2 group in the SAVF (Cook et al., 2005).

Figure 6.7 shows the relationship between $^{206}Pb/^{204}Pb$ and $^{187}Os/^{188}Os$. Despite the large $^{187}Os/^{188}Os$ range $^{206}Pb/^{204}Pb$ is fairly restricted, indicating that different processes control each isotope system. As outlined above the AVF lava major and trace element, and Sr-, Nd-, and Pb-isotope data were previously interpreted to reflect asthenospheric and lithospheric mantle sources (e.g., Huang et al., 1997; McGee et al., 2013). The high $^{187}Os/^{188}Os$ at low Os contents however point towards the influence of a component with radiogenic Os isotopic composition and low Os content. The different behaviour of the two isotope systems questions that a heterogeneous mantle source alone is responsible for the AVF Os signatures, and this hypothesis is further investigated below in regards to other potential sources.

The interpretation of Sr-, Nd-, and Pb-isotope systematics of AVF lavas relies on the assumption that erupted basalts are directly representative of their mantle

sources, as proposed by McGee et al. (2013). Nevertheless, a number of studies have noted xenolithic material (e.g., crustal schistose fragments) within tuff rings from the AVF maar craters (e.g. St Heliers, Taylors Hill, Mangere Mt; Spörli and Black, 2015), providing direct evidence for the interaction of ascending magmas with the country rock (e.g., Bryner, 1991). Because of its sensitivity to identify whether the AVF lavas have experienced crustal or lithospheric mantle contamination, we will use the Re, Os and $^{187}Os/^{188}Os$ systematics to evaluate this conundrum.

6.5.2 Origin of sulphides in AVF lavas

Platinum Group Elements (PGE), including Os, are chalcophile and thus are concentrated in sulphide minerals. Although Os and Re are incompatible in olivine and clinopyroxene (e.g. Burton *et al.,* 2002), Os is more chalcophile than Re and therefore highly compatible with sulphides during mantle melting (D_{Os} ~ 10^4 between sulphides and silicate melt; Roy-Barman *et al.,* 1998; Jamais *et al.,* 2008). Therefore minimal sulphide fractionation can effectively remove Os from a melt. Despite the incompatibility of Os in olivine (±spinel), the crystallisation of olivine can cause sulphur saturation and consequent precipitation of base metal sulphide formation (BMSs; Alard *et al.,* 2002), thereby causing a co-variation between olivine and Os (Burton *et al.,* 2002). In addition, olivine-hosted sulphides can form either through combined olivine and sulphide crystallisation (e.g. Bézos *et al.,* 2005; Lorand *et al.,* 2010; Day *et al.,* 2010) or can be incorporated through accumulation of xenocrystic olivine during ascent (e.g. Alard *et al.,* 2002). Sulphides formed through fractional crystallisation are either retained in residual minerals in the mantle (e.g. olivine; Lorand *et al*., 2010) or can segregate and form sulphides during magma transport and emplacement (e.g. Bézos *et al*., 2005). The PGE concentrations in the melt depends on the degree of partial melting, as only high degrees of partial melting (> 16%) will completely remove sulphur from the mantle source, resulting in a PGE-rich melt (Day *et al.,* 2010). Accordingly, low-degree partial melts (≤ 6%) show lower, but more variable HSE contents due to incomplete breakdown of sulphide in the mantle source (e.g. Day *et al.,* 2010). Conversely, Re is less compatible to modestly incompatible in sulphides and thus is not preferentially incorporated into them.

As low-degrees of partial melting have been suggested to occur beneath the AVF (≤6 %; McGee *et al.,* 2011, 2012, 2013) variable Os contents are expected. Furthermore, the concentrations of Os and Re in the AVF lavas show no obvious correlation with Mg, Ni, Cu and Zr; **Fig. 6.5**.), suggesting that fractional crystallisation of olivine and pyroxene have had no or only a minor influence on Os and Re concentrations in most AVF lavas. In addition, because no significant trends between the above-mentioned elements are observed, partial melting, and silicate plus sulphide phase fractionation, cannot alone cause the Os content variability seen in the AVF lavas. Other primary phases controlling PGEs include PGE-rich alloys and possibly Cr-spinels (e.g., Day 2013). However PGEs reveal an even more complex behaviour depending on $ƒO_2$, $ƒS_2$, temperature and pressure prevailing during mantle melting, crystal fractionation and during melt ascend and eruption. Regardless, due to low melting temperatures and low viscosities of BMSs, they are strongly soluble in basaltic melts, and can therefore be preferentially incorporated into the ascending magmas (Alard *et al.,* 2002). It is therefore likely that ascending magma becomes contaminated with mantle or crustal sulphides if the magma passes through an appropriate source.

Assimilation of oceanic or continental crust into the mantle in subduction settings increases the radiogenic Os signature of the mantle through input of high $^{187}Re/^{188}Os$, and thus high $^{187}Os/^{188}Os$ contents (e.g., Alves *et al.,* 1999; Borg *et al.,* 2000; Dale *et al.,* 2007; Suzuki *et al.,* 2011). Furthermore at or near subduction zones, fluids derived from a subducting plate metasomatise the subcontinental lithospheric mantle and hence increase $ƒO_2$ and $ƒS_2$ creating more oxidising conditions in the mantle. Mantle sulphides, stable under reduced mantle condition, then partially oxidize to sulphates (e.g., Carroll and Rutherford, 1985) releasing previously sulphide-bonded metals facilitating the movement and concentration of Os in partial melts (e.g., Jurgo, 2009; Suzuki *et al.,* 2011). Assuming partial melts or supercritical fluids redistribute Os, both of these processes can increase the Os concentrations in the subduction metasomatised lithosphere (and melt), and can result in a more radiogenic Os isotope signature over time.

The lithosphere beneath the AVF was exposed to subduction in the Oligocene to Miocene between c. 20 and 30 Ma (Seebeck *et al.,* 2014). Through radioactive decay of ^{187}Re to ^{187}Os the Os isotope composition of the lithospheric mantle

beneath the AVF would have increased in 30 Ma to ca.$^{187}Os/^{188}Os$ = 0.1473-0.1524 (assuming a $^{187}Re/^{188}Os$ = 50 in recycled crust, Widom *et al.,* 1999; and a mantle value of $^{187}Os/^{188}Os$ = 0.123-0.1283, this study). The only AVF lavas that contain values similar to the $^{187}Os/^{188}Os$ = 0.14 proposed to represent the lithospheric mantle are from Pupuke. Previously up to 80 % contribution from the subduction metasomatised lithospheric mantle (SMLM) to the ascending asthenospheric melts has been proposed to explain the major and trace element and Sr-, Nd- and Pb isotopic composition of the high SiO_2 AVF lavas (McGee *et al.,* 2013). Therefore to create the Os signature of the Pupuke samples, that accumulated olivine ($^{187}Os/^{188}Os$ = 0.1374-0.1377, Os = 196-578 ppt) through addition of olivine-hosted SMLM sulphides, (assuming a ≤80 % contribution from the SMLM and using a simple binary mixing model), the Os concentration in the SMLM would have to be ≥700 ppt, with $^{187}Os/^{188}Os$ = 0.1391-0.1472. This value is however higher than those values recorded in lithospheric mantle xenoliths from Zealandia (e.g. McCoy-West *et al.,* 2013; Liu et al., 2015). In addition, if the lithospheric mantle is the source of Os isotopic signature and high Os contents in the Pupuke lavas it would be expected that these samples are part of the high-SiO_2 group samples, contrary to what is observed.

Other than the SMLM beneath the AVF, there is at least one alternative source potentially contaminating the Pupuke samples with sulphide-bearing olivine; the ultramafic rocks (primarily serpentinised dunite and harzburgite) of the Permian-Triassic Dun Mountain ophiolite belt (DMOB; e.g., Coombs et al., 1976; Sivell and McCulloch, 2000). Parts of the DMOB cross directly beneath Pupuke at shallow levels (≥ 1.5 km depth, **Fig.6.1.C.)** making the ultramafic rocks of the Dun Mountain ophiolite belts a likely melt contaminant.

Although there are currently no Os isotope measurements on the DMOB rocks, O'Driscoll et al. (2012) reports Os content and isotope values from the Shetland ophiolite complex, which although older (429 Ma), has similarities to the DMOB in formation (obduction at arc collision zone) and lithology (serpentinised dunite and harzburgite). $^{187}Os/^{188}Os$ isotope values reported range from 0.1204 to 0.1502 with Os concentrations ranging from 300-8000 ppt (O'Driscoll *et al.,* 2012). Assuming mean values of $^{187}Os/^{188}Os$ = 0.1353 and Os = 4150 ppt (based on the Os isotope values and contents from the Shetland ophiolite complex) simple binary

mixing modeling (**Fig. 6.8**.) requires <10% input from the Dun Mountain ultramafic rocks into our proposed ambient mantle values of $^{187}Os/^{188}Os$ = 0.123-0.1283 and Os = 50-200 ppt to explain the $^{187}Os/^{188}Os$ values and Os content observed in the Pupuke samples. However only ca. 5% olivine accumulation is required to explain the higher MgO, Ni and Cr contents of these samples. This suggests that the concentration of Os in the contaminant needs to be ≥ 6000 ppt Os, which is within the range reported by O'Driscoll et al. (2012). Nevertheless, 5-10% olivine accumulation can not only explain the $^{187}Os/^{188}Os$ values and Os, but also the MgO and Ni contents observed in the Pupuke samples (see mixing line on **Fig. 6.2.**). Contamination from the Dun Mountain ultramafic rocks cannot however explain the highly radiogenic Os isotope signatures ($^{187}Os/^{188}Os$ = 0.1623-0.5470) and low Os concentrations (<50 ppt) in most other AVF samples.

6.5.3. Contamination and assimilation

On an $^{187}Os/^{188}Os$ versus $1/^{188}Os$ diagram most AVF lavas plot on a broad positive array between the OIB and continental crust, and overlap with the signature for carbonatites, indicative of a mixing end member with a high Os isotope ratio and a low Os concentration (**Fig.6.6.B**.).

Carbonatites have often been associated with the subcontinental lithospheric mantle sources in New Zealand (e.g., Scott et al., 2014), with a lithospheric mantle source, affected by carbonatitic metasomatism, used to explain the geochemistry of mantle xenoliths from beneath South Island, New Zealand (e.g., Scott *et al.,* 2014; McCoy-West *et al.,* 2015). Carbonatites typically have low Os concentrations and elevated Os isotope ratios, and therefore could represent a mantle end-member causing the highly radiogenic signature seen for the AVF lavas. The only carbonatites measured globally range in Os isotope ratios from 0.18-0.6 with Os concentrations of 4-23 ppt (Widom et al., 1999; Escrig et al., 2005). However, because of the low Os contents in carbonatites, Widom et al. (1999) highlight that carbonatitic metasomatism will have limited effect on the Os isotope composition of the mantle. In addition, if carbonatite metasomatism were responsible for the elevated Os isotope ratios and low Os concentrations, the proportion of assimilated volume would need to be minor as there is no correlation between the Os signatures and elements indicative of carbonatite metasomatism (including CaO, Sr, and Nd;

Cooper *et al.,* 2015). Because the Os isotopic composition of carbonatite is ≤0.6, with low Os contents, parts of the lithospheric mantle source would need to be of carbonatitic composition to be an effective contaminant. Even then, either an unrealistically high amount of assimilation into ascending melts is required to explain the elevated $^{187}Os/^{188}Os$ of >0.25, or direct melting of the carbonatite-domained mantle is required, which should have a notable effect on the major and trace element composition.

These results support previous conclusions by Handler et al. (1997) who also show, for wherlite and apatite-bearing peridotites, interaction with carbonatitic melt has no effect on the Os isotope composition or concentrations of Os or Re. In addition, a more recent study by McCoy-West et al. (2015) identified that metasomatism beneath Zealandia does contain a carbonatitic component, but that does not affect the PGE budget in peridotite, which is controlled by residual sulphides. Therefore an alternative end-member with high $^{187}Os/^{188}Os$ and low Os content is required to explain the radiogenic Os isotopic composition of most AVF lavas.

Crustal rocks (e.g., metasediments) typically show highly radiogenic $^{187}Os/^{188}Os$ values (ca. 0.165-2.323; Saal *et al.,* 1998) and low Os contents (ca. 20 to 100 ppt; Saal *et al.,* 1998; Widom *et al.,* 1999). Although the Sr-, Nd-, and Pb-isotopic composition from the AVF lavas show no detectable evidence for crustal contamination, the highly radiogenic $^{187}Os/^{188}Os$ isotope ratios in some of the AVF lavas exceed most values reported from the lithospheric mantle and carbonatitic sources, as previously discussed. This suggests that an end-member with $^{187}Os/^{188}Os$ >0.6 is required to create the radiogenic Os isotopic composition seen in the AVF samples, indicating a radiogenic crustal source.

Lavas from single centres (Rangitoto, Three Kings, Purchas Hill, Mt Wellington and Puketutu) plot mostly along individual linear mixing trends for each centre (**Fig.6.6.B**.). The variability observed within a single sample however, is more complex; duplicate analyses of the same sample using different digestions show variable results. This variability is attributed to the ‘nugget effect’ (Alves *et al.,* 2002), which suggests variability of individual digestions is caused by sampling varying amounts of mineral-hosted sulphides or oxide micro-inclusions with either inherited

crustal or mantle signatures from a single powdered sample. Dale et al. (2012) show that, due to preferential sampling of radiogenic source or crustal components in low degree melts, the Os isotope composition of mantle melts may not truly represent the bulk mantle Os isotope composition. The 'nugget effect' likely represents this preferential sampling of radiogenic components. Neverthless the data can be used to constrain the amount of crustal contamination in the AVF lavas.

6.5.5. AFC modelling

As simple binary mixing and/or fractional crystallisation cannot explain the $^{187}Os/^{188}Os$ and Os values from the AVF lavas (see **Fig. 6.8**.) we used the combined assimilation fractional crystallisation (AFC) model of DePaolo (1981) to quantify the amount of contamination (**Fig. 6.8**.). Potential contaminants have to satisfy the following criteria: 1) be a known basement lithology, and 2) have highly radiogenic Os isotope signature and low Os concentration. In addition constraining factors that the model has to satisfy includes 1) the lavas have undergone low levels of fractional crystallisation (<10%; McGee *et al.,* 2013; **Chapter 4**), and 2) mixing proportions between contaminant and melt have to be low enough to have little or no effect on trace element or Sr-Nd-Pb isotope systems.

Field studies mapping of the basement terranes and crustal xenoliths in lavas indicate, in addition to DMOB rocks, that both the Waipapa and the Murihiku terrane greywacke meta-sedimentary rock lithologies are found beneath the AVF (**Fig. 6.1.B**; e.g., Kermode, 1992). Although no Os isotope analysis has been undertaken on these terranes specifically, similar greywacke sediments have been studied in both Australia (Saal *et al.,* 1998) and India (Wimpenny *et al.,* 2007), and show that greywacke metasediments generally have highly radiogenic $^{187}Os/^{188}Os$ of 1.2832 to 5.1968 and low Os concentrations of 40-100 ppt (Wimpenny *et al.,* 2007). AFC modelling suggests that <1% bulk assimilation of greywacke metasediments with Os = 44.5 ppt and $^{187}Os/^{188}Os$ = 1.2832 (Saal *et al.,* 1998) into a mantle melt ($^{187}Os/^{188}Os$ = 0.1283; Os = 194 ppt; Wiri Mt value from this study), coupled with ≤ 5% fractional crystallisation, can produce the range of observed radiogenic Os isotope signatures (and low Os contents) in the AVF lavas (**Fig 6.8.**). Such low levels of crustal assimilation has no significant effect on the traditional trace element and Sr-, Nd-, Pb- isotope compositions.

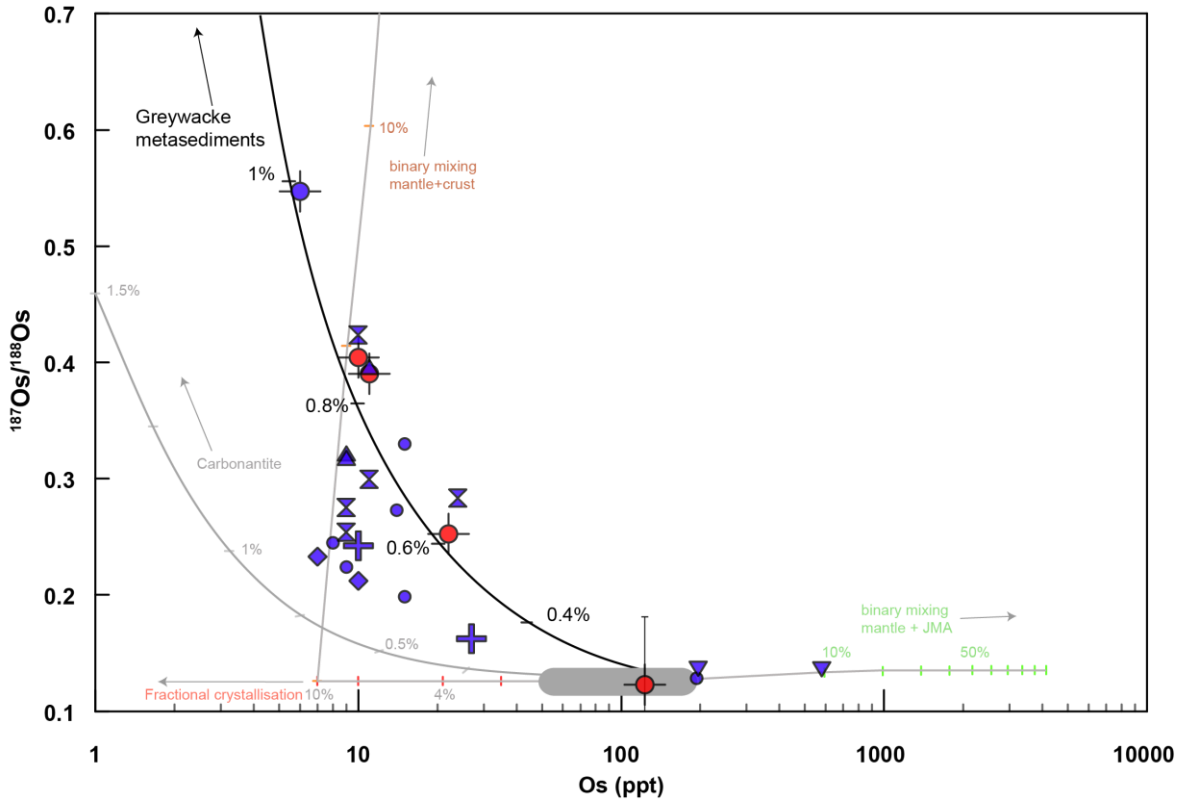

Figure 6.8. *Whole rock $^{187}Os/^{188}Os$ vs Os concentration (ppt) for OIB with proposed methods of signature formation. Sulphide assimilation is modelled (green line) using binary mixing from AVF mantle values with values measured for sulphides found in dunite within Shetland Ophiolite complex ($^{187}Os/^{188}Os$ = 0.1353, Os = 4150 ppt: O'Driscoll et al., 2012). Fractional crystallisation is modelled (red text and tick marks) using the Raleigh equation for samples from 50 to 7 ppt, showing that it requires ≤10% fractional crystallisation to reduce the Os concentrations. Crustal assimilation is modelled (orange text and tick marks) through binary mixing of post 30% fractional crystallisation of the mantle-derived melt ($^{187}Os/^{188}Os$ = 0.128, Os = 7 ppt) with <10 % crust, with values reflective of greywacke ($^{187}Os/^{188}Os$ = 1.283, Os = 44.5 ppt; Saal et al., 1998). Finally assimilation fractional crystallisation (AFC) is modelled (black text and tick marks) (after DePaolo, 1981) for mantle values ($^{187}Os/^{188}Os$ = 0.128, Os = 194 ppt; this study, Wiri Mt value) with crustal values of greywacke ($^{187}Os/^{188}Os$ = 1.283, Os = 44.5 ppt; Saal et al., 1998), D_{Os}= 20 (Widom et al., 1999), r (rate of fractional crystallisation) = 0.95.*

6.5.6. Implications for magma origin, generation and ascent

Based on our new Os isotope data we demonstrate that almost all AVF lavas analysed have interacted at ≤30 km depth with continental crust beneath Auckland. Aeromagnetic surveys over the Auckland area shows that the subsurface Dun Mountain Ophiolite Belt is almost universally present beneath the AVF (Eccles et al., 2005). Despite this, only few lavas show clear indication of significant mantle olivine accumulation based on their high Os concentrations and low mantle-like Os isotope ratios. Interestingly the centres that have petrographic and geochemical evidence for mantle olivine accumulation (Wiri Mt, Pupuke and Rangitoto) are located near or on faults separating the Dun Mountain Belt from adjacent sediments within the Matai Terrane (c.f. **Fig. 6.1.C**; Eccles et al., 2005). These observations strongly suggest the accumulation of olivines from mantle lithologies as magma ascends along faults cutting the ultramafic rocks of the Dun Mountain Belt between 1.5 km and 30 km depth (Eccles *et al.,* 2005).

The location of the intraplate basaltic fields on North Island, New Zealand (since 2.7 Ma) have remained static during minor arc migration during this time arguing against a direct relationship between intraplate volcanism and the subduction zone (Heming, 1980 and Smith *et al.,* 1993). This led Heming (1980) and Smith et al. *(*1993) to proposed the presence of a mantle plume to cause partial mantle melting and upwelling beneath the AVF. More recently, partial melting of a geochemically depleted asthenospheric mantle source containing HIMU-type carbonated peridotite domains has been used to explain the elevated Pb isotopic composition in magmas derived from >80 km depth (e.g., McGee *et al.,* 2015). These authors furthermore proposed that the asthenospheric melts variably interact with the overlying EMII-like lithosphere, metasomatised by long-lasting subduction throughout the Mesozoic, similar to the model put forward to explain intraplate volcanism on Zealandia (e.g., Timm et al., 2010). We generally concur with these models, and note the decoupling between the mantle source signatures and the Os isotope signatures. These observations demonstrate that lavas previously interpreted to represent ‘purely’ mantle melts must have experienced some degree of crustal contamination.

A low velocity zone, suggested to represent partial melt, has been identified by seismic tomography between 70-90 km depth beneath the Auckland region (e.g., Horspool *et al.,* 2006). These low velocity zones are attributed to regions of partial

melt within the mantle caused by crustal extension associated with the slab rollback (Horspool *et al.,* 2006), resulting in upwelling of hot asthenopheric mantle and subsequent partial decompression melting. We note that the other intraplate volcanic fields (Ngatutura and Okete; Briggs *et al.,* 1994, and the South Auckland volcanic field; Cook *et al.,* 2005) also are spatially correlated to the position of the DMOB (**Fig.6.1.C.**), and suggest that these melts may also exploit the DMOB as a weakness in the crust through which low degree melts can easily ascend (**Fig. 6.9**.). This avenue is beyond the scope of this research, however would be a useful direction for further study.

In summary, we show that almost all AVF lavas studied show Os isotopic compositions higher than typical mantle values of ≤0.13 and Os contents lower than 50 ppt, suggesting that most AVF lavas carry a crustal signature. This suggests, contrary to previous interpretation, that batches of melt beneath the AVF interacted with the continental crust, which has radiogenic $^{187}Os/^{188}Os$ and low Os contents, such as metasedimentary greywacke. Conversely, the unradiogenic Os isotopic ratios coupled with high (>150 ppt) Os concentrations of the samples from Pupuke, Wiri and Rangitoto, are attributed to contamination through olivine-bearing sulphide assimilation from the Dun Mountain Ophiolite Belt. The presence of mantle-derived sulphide hosting olivines in lavas from eruption centres located above the Dun Mountain Ophiolite Belt strongly argues for their derivation from crustal levels (**Fig. 6.9.**). We therefore propose that, although there is no evidence for long residence time of melts within the crust, crustal contamination does occur beneath most of the Auckland Volcanic Field and impacts the erupted products.

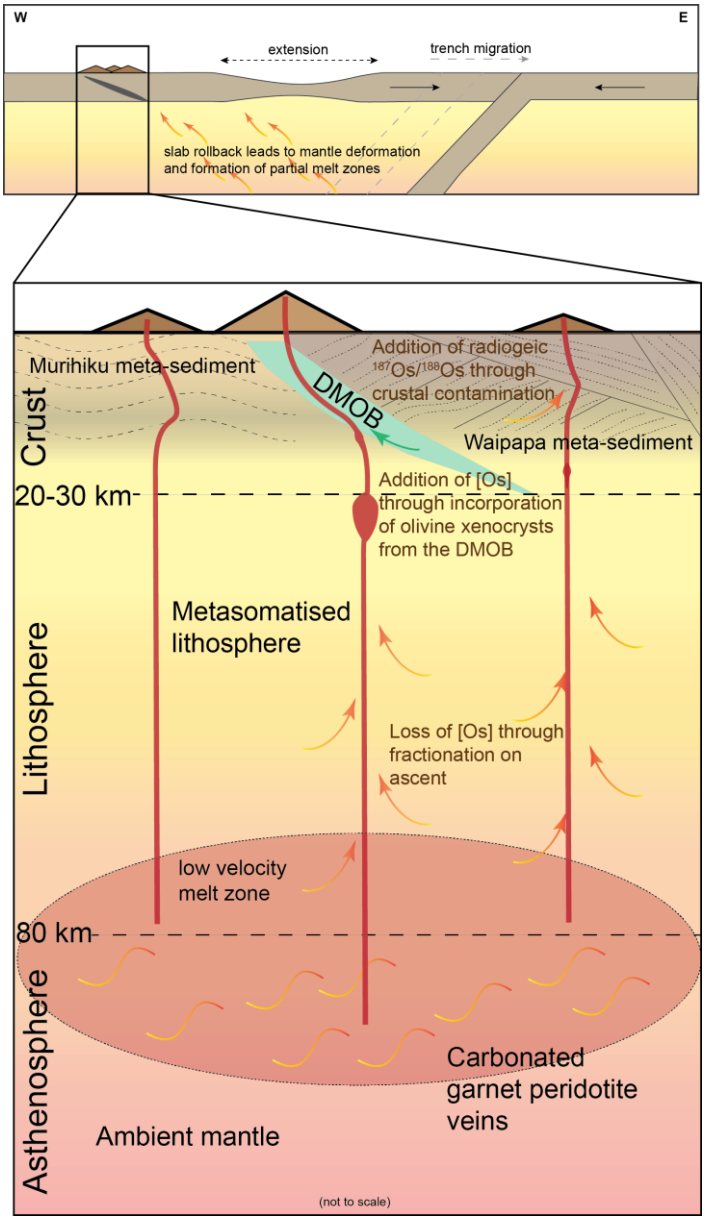

Figure 6.9. *Schematic model to illustrate the proposed magma ascent for the AVF eruptions. Melts are derived from a heterogeneous source, including ambient peridotite mantle containing HIMU-like carbonated peridotite veins (McGee et al. (2015) at a depth of >80 km depth, and a subduction metasomatised lithosphere at <80 km depth, all of which give the ascending magma its Sr-, Nd-, Pb-isotopic and major and trace element signatures (McGee et al., 2013). Minimal fractionation occurs on ascent, efficiently reducing the Os concentration from mantle values, followed by preferential assimilation of olivines from the Dun Mountain Ophiolite Belt (DMOB) as xenocrystic material causing increase in Os concentration, and finally minor crustal contamination of magmas causing the radiogenic isotope signatures. A crustal depth of 20-30 km and the positions of the low velocity melt zone region are from tomography by Horspool et al. (2006), and upper cross section adapted from Seebeck et al. (2014).*

6.6. Conclusions

The Os concentrations and isotopic systematics in lavas from the AVF show no obvious correlation to the tracers of mantle sources, implying that the Os signatures are not primarily caused by source heterogeneity, but have resulted from crustal contamination. Two differing types of crustal contamination are identified. 1) Metasediments (e.g. Waipapa and Murihiku Terranes) which contain highly radiogenic Os coupled with minimal elemental Os and, 2) xenocrystic olivine hosted sulphides (from the Dun Mountain Belt) with unradiogenic mantle-like $^{187}Os/^{188}Os$ and high Os contents. Less than 1% contamination from the crust coupled with ≤5% fractional crystallisation, and ≤10% contamination from xenocrystic olivine-bearing sulphide is sufficient to produce the $^{187}Os/^{188}Os$ and high Os contents measured in the AVF lavas. The evidence for crustal contamination has important implications for magma ascent characteristics, suggesting that 1) there is interaction with the crust and, 2) that the Dun Mountain Ophiolite Belt may act as a principle pathway for the rapid ascent of these highly primitive lavas.

Acknowledgements

Financial support for this work was provided by DEVORA project. The authors would like to thank Lucy McGee for use of lava samples and some unpublished data. JLH would like to thank Elaine Smid and the University of Auckland (UoA) rock collection for sample loan, and GEOTOP at UQAM for use of analytical facilities, and Monica Handler for helpful reviews and discussion of the text.

Chapter 7

Synthesis and Conclusions

Auckland cityscape from Mt Eden crater with Mt Victoria and North Head outlined in front of Rangitoto (Image by Hopkins, J.L.).

7.1. Introduction

The primary aim of this research was to improve the tephrostratigraphic framework for the Auckland Volcanic Field, New Zealand, and develop a method to link these tephra horizons to their source. A secondary aim was to use this information to constrain the spatial, temporal, and geochemical evolution of the monogenetic basaltic AVF. In this chapter I will outline the original contributions that are made by this thesis. I will revisit the research questions that were originally identified in **Chapter 1** and outline how this research has tackled these questions. I will then discuss the outstanding questions that have come to light as a result of this thesis and outline potential for future research.

7.2. Original Scientific Contributions

Most tephrostratigraphic studies in New Zealand have focused on the active eruptive centres of Taupo Volcanic Zone (e.g., Howorth, 1975; Froggatt, 1982; Froggatt and Lowe, 1990; Dunbar and Kyle, 1992; Alloway *et al.,* 2004; Shane *et al.,* 2006 Allan *et al.,* 2008; Danisik *et al.,* 2012) or Taranaki Volcano (e.g., Alloway *et al.,* 1994; Alloway *et al.,* 1995; Shane, 2005; Turner *et al.,* 2009; Turner *et al.,* 2011). This is due to their shorter repose period and larger eruptions posing a greater volcanic hazard to New Zealand. Relatively few studies have therefore focused primarily on the basaltic eruptions from the Auckland Volcanic Field (AVF) (e.g., Molloy *et al*., 2009; Needham *et al.,* 2011; Shane and Zawalna-Geer, 2011; Shane et al., 2013).

This study (**Chapter 3)** has, for the first time, used X-ray and magnetic susceptibility techniques combined with visual observations to pinpoint basaltic tephra horizons in the Orakei Basin and Onepoto cores. Using this new approach, I have found 1) previously un- or misidentified horizons, 2) provided new insight into the characteristics of the basaltic tephra deposits within the cores, and 3) outlined how re-worked and primary horizons can be reliably identified. I coupled these results with the first extensive trace element analysis obtained on the basaltic tephra shards for the AVF (**Chapter 3**), to allow new insights into the use of trace elements to create more distinct geochemical fingerprints for specific deposits. The combination of these new methods allowed me to establish a more reliable

tephrostratigraphic framework for the AVF, and to better assess tephra dispersal and eruption frequency (**Chapter 3**). This study furthermore has global implications by outlining the benefits of using trace element signatures of tephra shards to further define and fingerprint specific tephra deposits, a concept which is only beginning to be exploited.

In **Chapter 4** I present new major and trace element whole rock data for previously un- or under- sampled centres of the AVF. I also collate for the first time all reliable data from previous studies, both published (e.g., McGee *et al.,* 2013), unpublished (particularly that collected and curated by I.E.M. Smith), and MSc project data (e.g., Hookway, 2000). In doing this I bring the total number of centres with both major and trace element geochemical data from 22 to 46 out of the 53 proposed centres.

In **Chapter 5**, the newly constructed tephrostratigraphic framework is combined with the newly collated whole rock database, and a new suite of $^{40}Ar/^{39}Ar$ age determinations (Leonard *et al., in prep.* **Appendix D**), to develop a method for the correlation of basaltic tephra horizons to their source centres. Although it is standard protocol to attempt to correlate distal tephra to source, this is most commonly facilitated through well-characterised proximal tephra deposits. The newly developed method allows the correlation of basaltic tephra to whole rock compositions, something that has not previously been attempted. Although the investigation relies predominantly on the trace element signatures of both the tephra and the whole rock, for the AVF this study found that geochemistry alone couldn't reliably fingerprint 53 centres individually. The study therefore shows that the use of multiple lines of evidence is required to correlate the tephra horizons to their source centre. In using this approach, I have conducted and reported the first study to not only correlate tephra horizons to their source centre by correlating tephra with whole rock chemistry, but also to correlate the distal basaltic AVF tephra deposits to their source. The tephra dispersal from individual centres can be mapped and used in future hazard and risk forecasting. For the AVF this process has produced the first relative and absolute eruptive history for 45 of 53 AVF centres for the last ca. 200 ka. As a result of this, I also, for the first time, show evidence for coupled eruptions in space and time, a potential cyclicity to the eruption characteristics (geochemistry and scale), and evidence for melt volume loss on ascent.

Finally, in **Chapter 6**, I use the Re/Os isotope system coupled with trace element geochemistry to provide the first geochemical evidence for crustal contamination of the ascending magma batches for a number of the AVF centres. The contamination is linked to both the sedimentary country rock (meta-greywackes of the Murihiku and Waipapa terranes), and also the rocks of the Dun Mountain ophiolite belt through which the magma ascended. This is the first time geochemical evidence for crustal contamination has been noted, and has potential implications for magma ascent that has previously not been identified.

7.3. Research Questions

7.3.1. Can a more detailed basaltic tephra stratigraphy for the AVF be produced for the maar deposits using newly developing analysis methods?

7.3.1.1. X-ray and Magnetic Susceptibility

The use of X-ray and magnetic susceptibility analysis techniques are shown to be exceptionally powerful and accurate tools to identify the location and assessing the characteristics of basaltic tephra deposits within lacustrine maar sediment cores. X-ray imagery identifies basaltic tephra shards due to the high abundance of heavy X-ray absorbing elements (e.g., FeO) contained within the shards, and therefore in comparison to the lacustrine sediments, the parts of the core that contain basaltic shards appear very bright on the imagery. The abundance of Fe-rich magnetic minerals within the basaltic tephra also results in large peaks in magnetic susceptibility where tephra shards are located. Therefore, a positive indication from both these analyses allows even the thinnest (1-2 mm) basaltic horizons, which may have had ambiguous identification based on visual observations previously, to be accurately identified within the cores. These techniques reveal details about the density of shards, the shard size, and shape, coupled with the characteristics of the horizon itself, which includes the bedding type, structure and any deformation. This method allows initial identification through non-invasive techniques of primary and reworked horizons or section of horizons.

7.3.1.2. Tephra Geochemistry

Prior to this study, trace element analysis of the basaltic tephra shards within the AVF had not been undertaken. The trace element analyses provided the ability to more accurately constrain and fingerprint the geochemical signature of the tephra horizons and thus to correlate horizons less ambiguously. Selected trace element concentrations, and trace element ratios, were proven to produce a more distinctive geochemical signature for a specific horizon compared to major element compositions of the same centres/lavas, facilitating better identification and designation of specific horizons. The trace elements and trace element ratios, in comparison to the corresponding major element signatures, proved to 1) constrain a highly variable signature, 2) constrain a bimodal signature and, 3) split overlapping signatures for two horizons, thereby allowing more precise correlations to be made. This study therefore has produced a highly detailed tephrostratigraphy for the AVF maar cores through the combined use of new, non-invasive, observational techniques, coupled with detailed geochemical analysis.

7.3.2. Can individual horizons be linked to their source centre?

7.3.2.1. Tephra-derived glass to whole rock correlations

This study has demonstrated that tephra horizons can be linked to their source centre based on the correlation between medial-distal tephra deposits and proximal lava-scoria deposits. The correlation between tephra-derived glass samples and whole rock-derived glass samples was shown to be the simplest way of correlating, with a number of major elements successful at providing comparable geochemical signatures (e.g., MgO vs. full major element suite plus trace elements Rb, Zr, Cs, Ni, Cr, Y, Er, and SiO_2 vs. Al_2O_3, Na_2O, K_2O and; CaO vs. Al_2O_3, Na_2O). However in many cases glassy lava samples were (and are often) not available, therefore a more complex correlation method was developed. For the AVF the incompatible trace elements and their ratios (specifically La/Yb, Gd/Yb, Zr/Yb, Nd/Yb, Nb/Yb, and Ce/Yb) are show to be 1) the most variable element or ratios across the AVF eruption products, 2) the most distinctive for individual eruptions, 3) the least affected by partial melting and fractional crystallisation and therefore, 4) the most comparable in values between bulk whole rock and tephra-derived glass. This

method proved successful in correlating the tephra deposits to source centre, however, in some cases geochemistry could not be a defining factor in the correlation, and therefore for these cases additional criteria had to be used.

7.3.2.2. Additional Criteria

A multifaceted approach to correlation is required to not only 1) strengthen correlations highlighted by the geochemistry but also 2) resolve any ambiguities remaining from the geochemical signatures alone. For this study I combined age and location (of both tephra and centre) and scale of eruption and calculated tephra volume, with geochemistry. The combination of these criteria allows the confidence of a correlation to be given a scale, where correlations gain a higher confidence by satisfying a higher number of criteria. Of the twenty-eight tephra horizons identified, twenty have a correlation confidence rating of 2 or 1, meaning they satisfy three or more of the four criteria used.

Therefore in conclusion, it is possible to correlate tephra deposits to source centre. However, a detailed understanding of the geochemistry of the centres involved and the potential defining geochemical signatures is required and, where geochemistry is not enough to distinguish between centres, other criteria need to be included to allow refinement of the source correlation.

7.3.3. What is the spatial, temporal and geochemical evolution of the AVF?

7.3.3.1. Temporal Evolution

By combining the tephra correlations with Ar-Ar and ^{14}C ages (Leonard *et al., in prep.* **Appendix D**), and morphostratigraphic constraints, 45 of 53 of the AVF centres are put into a relative age order, with absolute age estimates also presented. This age order allows the assessment of the temporal evolution of the field. The results suggest that in general the repose periods for eruptions increased from inception of the field to ca. 21.5 ka, and have now decreased to the eruption of Rangitoto, with a ca. 10 ka hiatus between Mt Wellington and Rangitoto 1. The repose periods are however, highly variable from <0.1 ka to 13 ka (with two outliers at 17 and 27 ka), with fourteen of the centres with repose periods <0.5 ka, and nine with repose periods >10 ka. Therefore, based on these results it is possible to

suggest that the next eruption from the AVF will most likely occur in <13 ka yrs. after Rangitoto's latest eruption, but most likely to be at the less frequent limit of this, if the deceleration of repose periods is correctly inferred.

7.3.3.2. Spatial Evolution

In general there are no overarching trends to the spatial evolution of the AVF eruptions, although there are some patterns in terms of grouping of centres. The term 'aligned' is used to describe when more than 2 centres are found in geographical alignment but without any age relationships, and the term 'coupled' is used when 2 centres are found in close proximity in both space and time. Aligned centres are attributed to the magma exploiting pre-existing weaknesses (faults or fractures) within the crust. In contrast the appearance of coupled centres is attributed to the dual ascent styles that are found within the AVF (e.g., McGee *et al.,* 2011; McGee *et al.,* 2015). As a result of these observations the ability to predict where the next eruption from the AVF will occur is limited. However it is considered more likely that an eruption will occur along a pre-existing fault line (e.g., Kereszturi *et al.,* 2014) and, if dual magma batches are ascending, separated by a time gap, the secondary eruption may not necessarily occur through the primary conduit.

7.3.3.3. Geochemical Evolution

The geochemistry of the products of the field are show to represent the variable mixing from multiple magma sources at various depths within the mantle (e.g., McGee *et al.,* 2013; McGee *et al.,* 2015). These geochemical signatures, and thus source proportions, generally correlate to the size of the subsequent eruption. Small centres are shown to often have higher $(La/Yb)_N$ ratios coupled with lower SiO_2 concentrations, and the converse true for the larger centres. When these geochemical signatures for each centre are plotted in relative age order, there is possibly an apparent cyclic nature to the eruption sizes and thus geochemistries for the AVF products. This cyclicity suggests that throughout the history of the AVF the mantle source has remained constant, but variably tapped, to produce the signatures seen in the AVF products.

7.3.4. What can the eruptive products of the AVF tell us about the pre-eruptive processes which act on the upwelling magma?

Evidence for a loss of magma volume is highlighted by the eruption of lavas that have the geochemical signatures of much larger melt body. This loss of magma volume is attributed to fractional crystallisation of the ascending melt, and/or retention of melt within the crust. Evidence of crustal interaction is further supported by the Os isotope systematics, which show the influence of both metasedimentary terranes (Waipapa and Murihiku) and the Dun Mountain ophiolite belt (DMOB) can be found within the AVF eruptive products. The metasedimentary terranes have a modelled input of <1%, but due to their highly radiogenic Os isotope ratios, this minor amount of contamination has a major effect on the AVF lavas Os signatures, increasing the $^{187}Os/^{188}Os$ ratios from mantle values (ca. 0.1230) to more extreme values (e.g., ca. 0.2-0.5). Previous isotope studies have therefore not identified this contamination, as the proportions are too small to have an impact on the less sensitive isotopic systems (e.g. Pb-Sr-Nd). The contamination from the DMOB has a different signature leading to elevated Os concentrations (e.g., from mantle values of ca. 50 ppt to values of ca. 400 ppt seen in the Pupuke samples) but little change in Os isotope values). This is attributed to contamination of ≤ 10% xenocrystic olivine supporting findings from Sporli and Black (2015). As both these signatures are observed within single centres, it is proposed that the ascending magma interacts with both the metasedimentary terranes, and the DMOB. With the DMOB tentatively proposed as a principle pathway to facilitate rapid ascent of these primitive lavas through the crust.

7.4. Further Research

7.4.1. Application of newly developed methods on other cores

The multi-method analyses of the cores from the AVF have proved to accurately and efficiently identify basaltic tephra within the cores. In terms of a local application, the AVF cores that were not assessed using these methods (Panmure Basin and Pukaki) would benefit from this analysis. The Pukaki core would particularly benefit from this due to the currently ambiguous analysis and correlation of multiple cores, and basaltic tephra horizons from within this maar (**Chapter 1**; Sandiford *et al.,* 2001; Shane, 2005; Zawalna-Geer, 2012). All of the basaltic tephra deposits within the Pukaki core currently only have limited major element analysis. Therefore, by re-sampling the tephra horizons within this core, trace-element analysis could be undertaken on the glass shards, allowing centre correlations of a higher confidence rating to be produced (**Chapter 5**). This core also extends back further than the current research outlines (Shane, 2005), and therefore new horizons could be (and almost certainly would be) found below the Rotoehu rhyolitic marker horizon. The Pukaki core is of specific importance as it is the only core that likely records more of the eruptions from the south of the field. Therefore the information gathered from re-analysing this core would strengthen some of the previous correlations and add new details about eruptions in the southern AVF.

From a global perspective, the X-ray and magnetic susceptibility method is transferrable to marine, peat and ice cores, and is a valuable way to quickly and non-invasively identify regions of interest (with regards to tephra horizons) in the cores. If the matrix sediment is less dense (for X-ray) and contains less magnetic minerals than the tephra, the horizons will be easily identified by this method. Similarly these methods will be useful in identifying if units appear to be reworked or disturbed in any way.

The use of trace elements, outlined within **Chapter 3,** as a more geochemically unique fingerprint for tephra horizons is also highly transferrable. Where previous studies have highlighted major element concentrations that are indistinguishable between tephra horizons (e.g., Davies *et al.,* 2014) this methodology can be applied to provide a more individual signature for the deposits, and potentially resolve any geochemical ambiguities in correlations.

7.4.2. Age refinement of tephra horizons and thus eruptive centres

Currently the ages of the tephra horizons, especially those below the Rotoehu marker horizon are poorly constrained. In **Chapter 3** I outline the ambiguities that arise in sedimentation rate calculations that cause major discrepancies between, and within, the cores. I recalculate these sedimentation rate ages in **Chapter 5** using the new data gained from this study, however these are only calculated, rather than definitive ages. It would therefore be of use to investigate the ability to further refine the ages of the tephra horizons. This would be exceptionally important in the case of the Rotoehu tephra, the age of which remains controversial, and thus the basaltic horizons, which pre-date this deposit, are also poorly constrained. In addition, if the basaltic horizons themselves could be better dated (potentially through statistical modelling) for those horizons with a high confidence rating, a better constraint could potentially be applied to the eruption from an individual centre itself.

7.4.3. A further application of tephra horizon correlation

Analysis and comparison of volatile contents (e.g., H_2O, CO_2, sulphur) within olivine hosted melt inclusions (MIs) between tephra (horizons with a confidence level 1) and the correlated centre's whole rock compositions, will allow the amount of degassing associated with the individual eruptions to be evaluated. Following on from this, if the correlation between centre size (Kereszturi *et al.,* 2013) and geochemistry (McGee *et al.,* 2015) holds true for centre size and degassing (volatile difference), the total degassing from the field could be calculated. This process has previously been used to assess if there is a link between amount of degassing and the eruption style (Cervantes and Wallace, 2003), which could also be applied to the AVF volcanoes, as the tephra horizons correlated (with level 1 confidence) come from a range of eruption types. The ability to constrain the effects of degassing on the eruption style could important information for forecasts of the characteristics of future eruptions.

7.4.4. Centre and field geochemical evolution

Chapters 5 and 6 outlined results of the geochemical evolution of the AVF. There are a number of outstanding questions that need to be addressed in order to further knowledge of the mantle processes for the field. McGee et al. (2011, 2012) detailed the evolution throughout individual eruptions assessing the eruptions of both Rangitoto and Motukorea. The results for these centres suggest that individual eruptions evolve geochemically through time as a result of a shallowing magma source. However, this evolution has only been measured in these two systems and, to determine whether these two centres are unusual or represent 'the norm', a number of other centres should be assessed. This pattern of geochemical evolution is also noted for some of the 'coupled centres' (**Chapter 5**), with the older centre showing the initial deeper mantle signature and the younger centre showing the shallower mantle signature. In contrast, Smith et al. (2008) suggested a geochemical variation throughout a single eruption (Crater Hill) was consistent with fractionation on ascent from a single source, thereby providing an element of controversy that could be tested. Further investigation of these relationships could hold important information about magma ascent processes and the mantle sources.

Similarities between the geochemistry of the AVF and the South AVF (SAVF) are also noted (**Chapter 6**) and the ability to assess the geochemical evolution of the SAVF (and potentially the older Ngatutura and Alexandra fields) could allow more details about the evolution of the AVF to be highlighted. These data would allow further investigation of the mantle source (are they the same or different?), whether there are variations across the fields in the degrees of partial melting, and also for the geochemical evolution of the fields (are they the same or different? Is this 'within field' evolution consistent?).

The key overarching aim for all these aspects of further research is to provide more details about the AVF, thus increasing our ability to accurately forecast the characteristics and mechanisms of a future eruption. Auckland city, the people, and the infrastructure are at risk from a future eruption, and therefore accurate and realistic information is required to build effective disaster management strategies.

References

Affleck, D.K., Cassidy, J., Locke, C.A., 2001. Te Pou Hawaiki volcano and pre-volcanic topography in central Auckland: volcanology and hydrogeological implications. New Zealand Journal of Geology and Geophysics 44, 313-321.

Agustín-Flores, J., Németh,K., Cronin, S.J., Lindsay, J.M., Kereszturi, G., Brand, B.D., Smith, I.E.M., 2014. Phreatomagmatic eruptions through unconsolidated coastal plain sequences, Maungataketake, Auckland Volcanic Field (New Zealand). Journal of Volcanology and Geothermal Research 276, 46-63.

Alard, O., Griffin, W.L., Pearson, N.J., Lorand, J-P., O'Reilly, S.Y., 2002. New insights into the Re-Os systematics of sub-continental lithospheric mantle from in situ analysis of sulphides. Earth and Planetary Science Letters 203, 651-663.

Albarède, F., 1995. Introduction to Geochemical Modeling. Cambridge University Press, Cambridge, UK.

Allan, A.S.R., Baker, J.A., Carter, L.,Wysoczanksi, R.J., 2008. Reconstructing the Quaternary evolution of the world's most active silicic volcanic system: insights from an ~1.65 Ma deep ocean tephra record sourced from the Taupo Volcanic Zone, New Zealand. Quaternary Science Reviews 27, 2341-2360.

Allen, S.R., Smith I.E.M., 1994. Eruption styles and volcanic hazard in the Auckland Volcanic Field, New Zealand. Geoscience Reports of Shizuoka University 20, 5-14.

Alloway, B.V., Lowe, D.J., Chan, R.P.K., Eden, D.N., Froggatt, P.C., 1994. Stratigraphy and chronology of the Stent tephra, a c.a. 4000 year old distal silicic tephra from Taupo Volcanic Centre, New Zealand. New Zealand Journal of Geology and Geophysics 37, 37-47.

Alloway, D., Neall, V.E., Vucetich, C.G., 1995. Late Quaternary (post 28,000 year BP) tephrostratigraphy of the northeast and central Taranaki, New Zealand. Journal of the Royal Society of New Zealand 25, 385-458.

Alloway, B.V., Westgate, J.A., Pilans, B.J., Pearce. N.J.G., Newnham, R.M., Byrami, M.L., Aarburg, S.E., 2004. Stratigraphy, age and correlation of middle Pleistocene silicic tephra in the Auckland region, New Zealand: a prolific distal record of Taupo Volcanic Zone volcanism. New Zealand Journal of Geology and Geophysics 47, 447-479.

Alves, S., Schiano, P., Campas, F., Allegre, C.J., 2002. Osmium isotope binary mixing arrays in arc volcanism. Earth and Planetary Science Letters 198, 355-369.

Baker, J., Peate, D., Waight. T., Meyzen, C., 2004. Pb isotopic analysis of standards and samples using a ^{207}Pb-^{204}Pb double spike and thallium to correct for mass bias with a double-focusing MC-ICP-MS. Chemical Geology 211, 275-303.

Bartrum. J.A., 1928. Lava slickenslides at Auckland. The New Zealand Journal of Science and Technology 10, 23-25.

Bebbington, M.S., 2013. Assessing probabilistic forecasts of volcanic eruption onsets. Bulletin of Volcanology 252, 14-28.

Bebbington, M.S., Cronin, S.J., 2011. Spatio-temporal hazard estimation in the Auckland Volcanic Field, New Zealand, with a new event-order model. Bulletin of Volcanology 73, 55-72.

Beckett , W., 2000. Occupational respiratory disease. New England Journal of Medicine 342, 406-413.

Beier, C., Mata, J., Stöckhert, F., Mattielli, N., Brandl, P., Madureira, P., Genske, F., Martins, S., Madeira, J., and Haase. K., 2013. Geochemical evidence for melting of carbonated peridotite on Santa Maria Island, Azores. Contributions to Mineralogy and Petrology 165, 832-841.

Beierle, B., Bond, J., 2002. Density-induced settling of tephra through organic lake sediments. Journal of Paleolimnology 28, 433-440.

Berghuijs, J.F., Mattson H.B., 2013. Magma ascent, fragmentation and depositional characteristics of “dry” maar volcanoes: similarities with vent-facies kimberlite deposits. Journal of Volcanology and Geothermal Research 252, 53-72.

Bertrand, S., Daga, R., Bedert, R., Fontijn, K., 2014. Deposition of the 2011-2012 Cordón Caulle tephra (Chile, 40°S) in lake sediments: implications for tephrochronology and volcanology. Journal of Geophysical Research: Earth Surface 119, 2555-2573.

Bézos, A., Lorand, J-P., Humler, E., and Gros, M., 2005. Platinum-group element systematic in Mid-Ocean Ridge basaltic glasses from the Pacific, Atlantic and Indian Oceans. Geochimica et Cosmochimica Acta 69, 2613-2627.

Birck, J-L., Roy-Barman, M., Capmas, F., 1997. Re-Os isotopic measurements at the femtomole level in natural samples. Geostandards Newsletter 21, 19-27.

Blondes, M.S., Reiners, P,W., Ducea, M.N., Singer, B.S., Chesley, J., 2008. Temporal-compositional trends over short and long tmie scales in basalts of Big Pine Volcanic Field, California. Earth and Planetary Science Letters 269, 140-154.

Bohrson, W., Davidson, J., Wolff, J.A., 1997. Rethinking the chemical heterogeneity of the mantle. EOS Transactions, American Geophysical Union 78, 257-262.

Borg, L.E., Brandon, D.A., Clynne M.A., Walker, R.J., 2000. Re-Os isotopic systematics of primitive lavas from Lassen region of the Cascade arc, California. Earth and Planetary Science Letters 177, 301-317.

Bourne, A.J., Davies, S.M., Abbott, P.M., Rasmussen, S.O., Steffensen, J.P., Svensson, A., 2013. Revisiting the Faroe Marine Ash Zone III in two Greenland ice cores: implications for marine-ice correlations. Journal of Quaternary Science 28, 641-646.

Boygle, J., 1999. Variability of tephra in lake and catchment sediments, Sínavatn, Iceland. Global and Planetary Change 21, 129-149.

Bradshaw, T.K., Smith, E.I., 1994. Polygenetic Quaternary volcanism at Crater Flat, Nevada. Journal of Volcanology and Geothermal Research 63, 165-182.

Brand, B.D., Gravely, D.M., Clarke, A.B., Lindsay, J.M., Bloomberg, S.H., Agustín-Flores, J., Németh, K., 2014. A combined field and numerical approach to understanding dilute pyroclastic density current dynamics and hazard potential: Auckland Volcanic Field, New Zealand. Journal of Volcanology and Geothermal Research 276, 215-232.

Brendryen, J., Haflidason, H., Sejrup, H.P., 2010. Norwegian Sea tephrostratigraphy of marine isotope stages 4 and 5: prospects and problems for tephrochronology in the North Atlantic region. Quaternary Science Reviews 29, 847-864.

Brenna, M., Cronin, S.J., 2015. Mantle heterogeneity controls on small-volume basaltic volcanism. Forum comment on McGee *et al.,* 2015, Geology doi 10.1130/G37023C.1.

Brenna, M., Cronin, S.J., Smith, I., Sohn, Y., Németh, K., 2010. Mechanisms driving polymagmatic activity at a monogenetic volcano, Udo, Jeju Island, Korea. Contributions to Mineralogy and Petrology 160, 931-950.

Brenna, M., Cronin, S.J., Németh, K., Smith, I.E.M., Sohn, Y.K., 2011. The influence of magma plumbing complexity on monogenetic eruptions, Jeju Island, Korea. Terra Nova 23, 70-75.

Briggs, R.M., Okada, T., Itaya, T., Shibuya, H., Smith, I.E.M., 1994. K-Ar ages, paleomagnetism, and geochemistry of the South Auckland volcanic field, North Island, New Zealand. New Zealand Journal of Geology and Geophysics 37, 143-153.

Bryant, E., 2005. Natural Hazards, Cambridge University Press, New York, USA. pp. 1-13.

Bryner, V., 1991. Motukorea: the evolution of an eruption centre in the Auckland Volcanic Field. MSc thesis, University of Auckland, New Zealand.

Burton, K, W., Gannoun, A., Birck, J.L., Allègre, C.J., Schiano, P., Clocchiatti, R., Alard, O., 2002. The compatibility of rhenium and osmium in natural olivine and their behavior during mantle melting and basalt genesis. Earth and Planetary Science Letters 198, 63-76.

Carroll, M.R., Rutherford, M.J., 1985. Sulphide and sulphate saturation in hydrous silicate melts. Journal of Geophysical Research 90, 601-612.

Cassata, W.S., Singer, B.S., Cassidy, J., 2008. Laschamp and Mono Lake geomagnetic excursions recorded in New Zealand. Earth and Planetary Science Letters 268, 76-88.

Cervantes, P., Wallace, P., 2003. Magma degassing and basaltic eruption styles: a case study of ~ 2000 year BP Xitle volcano in central Mexico. Journal of Volcanology and Geothermal Research 120, 249-270.

Chesley, J.T., Ruiz, J., Righter, K., Ferrari, L., Gómez-Tuena, A., 2002. Source contamination versus assimilation: an example from the Trans-Mexican Volcanic Arc. Earth and Planetary Science Letters 195, 211-221.

Condit, C.D., Connor, C.B., 1996. Recurrence rates of volcanism in basaltic volcanic fields: An example from the Springerville volcanic field, Arizona. Geological Society of America Bulletin 108, 1225-1241.

Connor, C.B., 1990. Cinder cone clustering in the Trans-Mexican Volcanic Belt: implications for structural and petrologic models. Journal of Geophysical Research 95 (B12) 19395-19405.

Connor, C.B., Conway, F.M., 2000. Basaltic volcanic fields, in Sigurdsson, H. et al., ed., Encyclopedia of Volcanoes, San Diego, Academic Press pp331-343.

Conway, F.M., Connor, C.B., Hill, B.E., Condit, C.D., Mullaney, K., Hall, C.M., 1998. Recurrence rates of basaltic volcanism in SP cluster, San Francisco volcanic field, Arizona. Geology 26, 655-658.

Cook, C., Briggs, R.M., Smith, I.E.M., Maas, R., 2005. Petrology and geochemistry of the intraplate basalts in the South Auckland Volcanic Field, New Zealand: evidence for two coeval magma suites from distinct sources. Journal of Petrology 46, 473-503.

Coombs, D.S., Landis, C.A., Norris, R.J., Sinton, J.M., Borns, D.J., Craw, D., 1976. Dun Mountain ophiolite belt, New Zealand, its tectonic setting, constitution, and origin, with special reference to the southern portion. American Journal of Science 276, 561-603.

Cooper, A.F., Collins, A.K., Palin, J.M., Spratt, J., 2015. Mineralogical evolution and REE mobility during crystallisation of ancylite-bearing ferrocarbonatite, Haast River, New Zealand. Lithos 216-217, 324-337.

Creaser, R.A., Papanastassiou, D.A., Wasserburg, G.J., 1991. Negative thermal ion mass spectrometry of osmium, rhenium and iridium. Geochimica et Cosmochimica Acta 50, 397-401.

Dale, C.W., Gannoun, A., Burton, K.W., Argles, T.W., Parkinson, I.J., 2007. Rhenium-osmium isotope and elemental behavior during subduction of oceanic crust and the implications for mantle recycling. Earth and Planetary Science Letters 253, 211-225.

Dale, C.W., Macpherson, C.G., Pearson, D.G., Hammond, S.J., Arculus, R.J., 2012. Inter-element fractionation of highly siderophile elements in the Tonga Arc due to flux melting of a depleted source. Geochimica et Cosmochimica Acta 89, 202-225.

Danišík, M., Shane, P., Schmitt, A.K., Hogg, A., Santos, G.M., Storm, S., Evans, N.J., Fifield, L.K., Lindsay, J.M., 2012. Re-anchoring the late Pleistocene tephrochronology of New Zealand based on concordant radiocarbon ages and combined $^{238}U/^{230}Th$ disequilibrium and (U-Th)/He zircon ages. Earth and Planetary Science Letters 349-350, 240-250.

Davies, S.M., Abbott, P.M., Meara, R.H., Pearce, N.J.G., Austin, W.E.N., Chapman, M.R., Svensson, A., Bigler, M., Rasmussen, T.L., Rasmussen, S.O., Farmer, E.J., 2014. A North Atlantic tephrostratigraphical framework for 130-60 ka b2k: new tephra discoveries, marine-based correlations, and future challenges. Quaternary Science Reviews 106, 101-121.

Day, J.M.D., 2013. Hotspot volcanism and highly siderophile elements. Chemical Geology 341, 50-74.

Day, J.M.D., Pearson, D.G., Macpherson, C.G., Lowry, D., Carracedo, J.C., 2009. Pyroxenite-rich mantle formed by recycled oceanic lithosphere: Oxygen-osmium isotope evidence from Canary Island lavas. Geology 37, 555-558.

Day, J.M.D., Pearson, D.G., Macpherson, C.G., Lowry, D., Carracedo, J.C., 2010. Evidence for distinct portions of subducted oceanic crust and lithosphere in HIMU-type mantle beneath El Hierro and La Palma, Canary Islands. Geochimica et Cosmochimica Acta 74, 6565-6589.

Deer, W.A., Howie, R.A., Zussman, J., 1992. An introduction to the rock forming minerals. Wiley, New York.

de Klerk, P., Janke, W., Kühm, P., Theuerkauf, M., 2008. Environmental impact of the Laacher See eruption at a large distance from the volcano: integrated palaeoecological studies from Vorpommern (NE Germany). Palaeogeography, Palaeoclimatology, Palaeoecology 270, 196-214.

Delcamp, A., van Wyk de Vries, B., Stéphane, P., Kervyn, M., 2014. Endogenous and exogenous growth of the monogenetic Lemptégy volcano, Chaîne des Puys, France. Geosphere 10, 998-1019.

Demidjuk, Z., Turner, S., Sandiford, M., George, R., Foden, J., Etheridge, M., 2007. U-series isotope and geodynamic constraints on mantle melting processes beneath the New Volcanic Province in South Australia. Earth and Planetary Science Letters 261, 517-533.

DePaolo, D.J., 1981. Trace element and isotopic effects of combined wallrock assimilation and fractional crystallization. Earth and Planetary Science Letters 53, 189-202.

Dirksen, O., van den Bogaard, C., Danhara, T., Diekmann, B., 2011. Tephrochronological investigation at Dvuh-yurtochnoe lake area, Kamchatka: Numerous landslides and lake tsunami, and their environmental impacts. Quaternary International 246, 298-311.

Dohrenwend, J.C., Wells, S.G., Turrin, B.D., 1986. Degradation of Quaternary cinder cones in the Cima volcanic field, Mojave Desert, California. Geological Society of America Bulletin 97, 421-427.

Dunbar, N.W., Kyle, P.R., 1992. Volatile contents of obsidian clasts in tephra from the Taupo Volcanic Zone, New Zealand: Implications to eruptive processes. Journal of Volcanology and Geothermal Research 49, 127-145.

Eade, J., 2009. Petrology and correlation of lava flows from the central part of the Auckland Volcanic Field. MSc thesis, University of Auckland, New Zealand.

Eccles, J.D., Cassidy, J., Locke, C.A., Spörli, K.B., 2005. Aeromagnetic imaging of the Dun Mountain Ophiolite Belt in northern New Zealand: insight into the fine structure of a major SW Pacific terrane suture. Journal of the Geological Society, London 162, 723-735.

Engwell, S.L., Sparks, R.S.J., Carey, S., 2014. Physical characteristics of tephra layers in the deep-sea realm: the Campanian Ignimbrite eruption. Geological Society of London Special Publication 398, 47-64.

Erlund, E.J., Cashman, K.V., Wallace, P.J., Poili, L., Rosi, M., Johnson, E., Delgado Granados, H., 2010. Compositional evolution of magma from Parícutin Volcano, Mexico: the tephra record. Journal of Volcanology and Geothermal Research 197, 167-187.

Escrig, S., Doucelance, R., Moreira, M., Allegre, J.C., 2005. Os isotope systematics in Fogo Island: evidence for lower continental crust fragments under the Cape Verde Southern Islands. Chemical Geology 219, 93-113.

Esser, B.K., Turekian, K.K., 1994. The osmium isotopic composition of the continental crust. Geochimica et Cosmochimica Acta 57, 3093-3104.

Fergusson, G., Rafter, T.A., 1959. New Zealand C14 age measurements – 4. New Zealand Journal of Geology and Geophysics 2, 208-241.

Francis, P., Oppenheimer, C., 2004. Volcanoes. Oxford, Oxford University Press pp521.

Franklin, J.T., 1999. Geology of the Orakei Basin area. MSc thesis, University of Auckland, New Zealand.

Froggatt, P.C., 1982. Review of methods of estimating rhyolitic tephra volumes – applications to the Taupo Volcanic Zone, New Zealand. Journal of Volcanology and Geothermal Research 14, 301-318.

Froggatt, P.C., Lowe, D.J., 1990. A review of late Quaternary silicic and some other tephra formations from New Zealand – their stratigraphy, nomenclature, distribution, volume, and age. New Zealand Journal of Geology and Geophysics 33, 89-109.

Gerbode, C., Dasgupta, R., 2010. Carbonate-fluxed melting of MORB-like pyroxenite at 2.9 GPa and genesis of HIMU ocean island basalts. Journal of Petrology 51, 2067-2088.

Govindaraju, K., 1994. Compilation of working values and sample description for 383 geostandards. Geostandards Newsletter 18 (special issue).

Gramlich, J.W., Murphy, T.J., Garner, E.L., Shields, W.R., 1973. Absolute isotopic abundance ratio and atomic weight of a reference sample of rhenium. Journal of Research of the National Bureau of Standards 77A, 691-698.

Green, J.D., Lowe, D.J., 1985. Stratigraphy and developments of c.a. 17,000 year old Lake Maratoto, North Island, New Zealand, with some inferences about post glacial climatic change. New Zealand Journal of Geology and Geophysics 28, 675-699.

Green, R.M., Bebbington, M.S., Cronin, S.J., Jones, G., 2014. Automated statistical matching of multiple tephra records exemplified using five long maar sequences younger than 75ka, Auckland, New Zealand. Quaternary Research 82, 405-419.

Guilbaud, M.-N., Siebe, C., Layer, P., Salinas, S., 2012. Reconstruction of the volcanic history of the Tacámbaro-Puruarán area (Michoacán, México) reveals high frequency of Holocene monogenetic eruptions. Bulletin of Volcanology 74, 1187-1211.

Gutmann, J.T., 2007. Geologic Studies in the Pnacate Volcanic Field. Journal of the Southwest 49, 189-243.

Haase, K.M., Devey, C.W., 1996. Geochemistry of labas from the Ahu and Tupa volcanic fields, Easter Hotspot, southeast Pacific: implications for intraplate magma genesis near a spreading axis. Earth and Planetary Science Letters 137, 129-143.

Handler, M.R., Bennett, V.C., Esat, T.M., 1997. The persistence of off-cratonic lithospheric mantle: Os isotopic systematics of variably metasomatised southeast Australian xenoliths. Earth and Planetary Science Letters 151, 61-75.

Hart, S.R., 1984. A large-scale isotope anomaly in the Southern Hemisphere mantle. Nature 309, 753-757.

Hasebe, N., Fukutani, A., Sudo, M., Tagami, T., 2001. Transition of eruptive styles in an arc-arc collision zone: K-Ar dating of Quaternary monogenetic and polygenetic volcanoes in the Higashi-Izu region, Izu peninsula, Japan. Bulletin of Volcanology 63, 377-386.

Hasenaka, T., Carmichael, I.S.E., 1987. The cinder cones of Michoacan-Guanajuao, Central Mexico: Petrology and chemistry. Journal of Petrology 28, 241-269.

Hatherton, T., Sibson, R.H., 1970. Junction Magnetic Anomaly north of Waikato River. New Zealand Journal of Geology and Geophysics 13, 655-662.

Hauri, E.H., Hart, S.R., 1993. Re-Os isotope systematics of HIMU and EMII oceanic island basalts from the South Pacific Ocean. Earth and Planetary Science Letters 114, 353-371.

Hauri, E.H., Hart, S.R., 1997. Rhenium abundance and systematics in oceanic basalts. Chemical Geology 139, 185-205.

Hayward, B.W., Morley, M.S., Sabaa, A.T., Grenfell, H.R., Daymond-King, R., Molloy, C., Shane, P.A., Augustinus, P.A., 2008. Fossil record of the post-glacial marine breaching of Auckland's volcanic maar craters. Records of the Auckland Museum 45, 73-99.

Hayward, B.W., Murdoch, G., Maitland, G., 2011. Volcanoes of Auckland, The Essential Guide. Auckland University Press, Auckland, New Zealand.

Heming, R.F., 1980. Patterns of Quaternary basaltic volcanism in the northern North Island, New Zealand. New Zealand Journal of Geology and Geophysics 23, 335-344.

Heming, R.F., Barnet, P.R., 1986. The petrology and petrochemistry of the Auckland volcanic field. In: Smith, I.E.M., (Ed), Late Cenozoic Volcanism in New Zealand. Royal Society of New Zealand Bulletin 23, 64-75.

Herzberg, C., Asimow, P.D., Arndt, N., Niu, Y., Lesher, C.M., Fitton, J.G., Cheadle, M.J., and Saunders, A.D., 2007. Temperatures in ambient mantle and plumes: Constraints from basalts, picrites, and komatiites. Geochemistry, Geophysics, Geosystems 8, doi: 10.1029/2006GC0001390.

Hill, B.E., Connor, C.B., Jarzemba, M.S., La Femina, P.C., Navarro, M., Strauch, W., 1998. 1995 eruptions of Cerro Negro volcano, Nicaragua, and risk assessment for future eruptions. Geological Society of America Bulletin 110, 1231-1241.

Hoernle, K., White, J.D.L., van den Bogaard, P., Hauff, F., Coombs, D.S., Werner, A.F., Timm, C., Garbe-Schönberg, D., Reay, A., Cooper, A.F., 2006. Cenozoic intraplate volcanism on New Zealand: upwelling induced by lithospheric removal. Earth and Planetary Science Letters 248, 350-367.

Hookway, M., 2000. The geochemistry of Rangitoto. MSc thesis, University of Auckland, New Zealand.

Horspool, N.A., Savage, M.K., Bannister, S., 2006. Implications for intraplate volcanism and back arc deformation in northwestern New Zealand, from joint inversion of receiver functions and surface waves. Geophysical Journal International 166, 1466-1483.

Horwell, C.J., Baxter, P.J., 2006. The respiratory health hazards of volcanic ash: a review for volcanic risk mitigation. Bulletin of Volcanology 69, 1-24.

Horwell, C.J., Fenglio, I., Ragnarsdottir, K.V., Sparks, R.S.J., Fubini, B., 2003. Surface reactivity of volcanic ash from the eruption of Soufrière Hills volcano, Monserrat, with implications for health hazards. Environmental Research 93, 202-215.

Houghton, B.F., Wilson, C.J.N., Rosenberg, M.D., Smith, I.E.M., Parker, R.J., 1996. Mixed deposits of complex magmatic and phreatomagmatic volcanism: an example from Crater Hill, Auckland, New Zealand. Bulletin of Volcanology 58, 59-66.

Houghton, B.F., Wilson, C.J.N., Smith, I.E.M., 1999. Shallow-seated controls on styles of explosive basaltic volcanism: a case study from New Zealand. Journal of Volcanology and Geothermal Research 91, 97-120.

Houghton, B.F., Bonadonna, C., Gregg, C.E., Johnston, D.M., Cousins, W.J., Cole, J.W., Del Carlo, P., 2006. Proximal tephra hazards: recent eruption studies applied to volcanic risk in the Auckland Volcanic Field, New Zealand. Journal of Volcanology and Geothermal Research 155, 138-149.

Hoverd, J.L., Shane, P.A., Smith, I.E.M., Smith, V.C., Wilson, C.J.N., 2005. Towards an improved understanding of local and distal volcanic stratigraphy in Auckland: stratigraphy of a long core from Glover Park (St Helier's Volcano) in Auckland. Institute of Geological & Nuclear Sciences Science Report 2005/31, pp45.

Howorth, R., 1975. New formations of late Pleistocene tephras from the Okataina Volcanic Centre, New Zealand. New Zealand Journal of Geology and Geophysics 18, 683-712.

Huang, Y., Hawkesworth, C., van Calsteren, P., Smith, I., Black, P., 1997. Melt generation models for the Auckland volcanic field, New Zealand: constraints from U-Th isotopes. Earth and Planetary Science Letters 149, 67-84.

Huang, Y., Hawkesworth, C., Smith, I., van Calsteren, P., Black, P., 2000. Geochemistry of late Cenozoic basaltic volcanism in Northland and Coromandel, New Zealand: implications for mantle enrichment processes. Chemical Geology 164, 219-238.

Hwang, S.K., Jin, X., Ahn, U.S., 2005. Volcanic forms and eruption processes of Laiheishan and Huoshaoshan in the Wudalianchi volcanics, NE China. Journal of Petrological Society Korea 14, 251-263.

Jamais, M., Lassiter, J.C., Brügmann, G., 2008. PGE and Os-isotopic variations in lavas from Kohala Volcano, Hawaii: constraints on PGE behaviour and melt/crust interaction. Chemical Geology 250, 16-28.

Jochum, K.P., and Nehring, 2006. GeoRem preferred values. http://georem.mpch-mainz.gwdg.de/sample_query_pref.asp.

Jochum, K.P., Willbold, M., Raczek, I., Stoll, B., Herwig, K., 2005. Chemical characteristics of the USGS reference glasses GSA-1G, GSC-1G, GSE-1G, BCR-2G, BHVO-2G, and BIR-1G using EMPA, ID-TIMS, ID-ICP-MS, and LA-ICP-MS. Geostandards and Geoanalytical Research 29, 285-302.

Johnson, E.R., Wallace, P.J., Cashman, K.V., Granados, H.D., Kent, A.J.R., 2008. Magmatic volatile contents in degassing-induced crystallisation at Volcan Jorullo, Mexico: implications for melt evolution and the plumbing systems of monogenetic volcanoes. Earth and Planetary Science Letters 269, 478-487.

Johnson, E.R., Wallace, P.J., Cashman, K.V., Granados, H.D., 2010. Degassing of volatiles (H_2O, CO_2, S, Cl) during ascent, crystallisation, and eruption of mafic monogenetic volcanoes in central Mexico. Journal of Volcanology and Geothermal Research 197, 225-238.

Johnson, P.J., Valentine, G.A., Cortés, J.A., Tadini, A., 2014. Basaltic tephra from monogenetic Marcath Volcano, centre Nevada. Journal of Volcanology and Geothermal Research 281, 27-33.

Jones, J., 2007. The amphibolite xenoliths of St Heliers. MSc thesis, University of Auckland, New Zealand.

Jung, S., Pfänder, J.A., Brauns, M., Maas, R., 2011. Crustal contamination and mantle source characteristics in continental intra-plate volcanic rocks: Pb, Hf and Os isotopes from central European volcanic province basalts. Geochimica et Cosmochimica Acta 75, 2664-2683.

Jugo, P.J., 2009. Sulfur content at sulfide saturation in oxidized magmas. Geology 37, 415-418

Kamber, B.S., Collerson, K.D., 2000. Zr/Nb systematics of ocean island basalts reassessed - the case for binary mixing. Journal of Petrology 41, 1007-1021.

Kear, D., 2004. Reassessment of Neogene tectonism and volcanism in North Island, New Zealand. New Zealand Journal of Geology and Geophysics 47, 361-374.

Kenny, J., Lindsay, J., Howe, T., 2011. Large scale faulting in the Auckland Region, DEVORA project. Institute of Earth Science and Engineering technical report 1-2011.04.

Kereszturi, G., Németh, K., Cronin, S.J., Agustin-Flores, J., Smith, I.E.M., Lindsay, J., 2013. A model for calculating eruptive volumes for monogenetic volcanoes – Implications for the

Quaternary Auckland Volcanic Field, New Zealand. Journal of Volcanology and Geothermal Research 266, 16-33.

Kereszturi, G., Németh, K., Cronin, S.J., Procter, J., Augustin-Flores, J., 2014. Influences on the variability of eruption sequences and style transitions in the Auckland Volcanic Field, New Zealand. Journal of Volcanology and Geothermal Research 286, 101-115.

Kermode, L.O., 1975. Urban geology of Mt Eden borough. New Zealand Geological Survey, unpublished report G17.

Kermode, L.O., 1992. Geology of the Auckland urban area. Scale 1:50,000. Institute of Geological and Nuclear Sciences geological, map 2. IGNS, Lower Hutt.

Kermonde, L.O., Smith I.E.M., Moore, C.L., Stewart, R.B., Ashcroft, J., Nowell, S.B., Hayward, B.W., 1992. Inventory of quaternary volcanoes and volcanic features of Northland, South Auckland and Taranaki. Geological Society of New Zealand Miscellaneous Publications 61, p100.

Kimbrough, D.L., Mattinson, J.M., Coombs, D.S., Landis, C.A., Johnston, M.R., 1992. Uranium-lead ages from the Dun Mountain ophiolite belt and Brook Street Terrane, South Island, New Zealand. Geological Society of America Bulletin 104, 429-443.

Kraus, S., Kurbatov, A., Yates, M., 2013. Geochemical signatures of tephras from Quaternary Antarctic Peninsula volcanoes. Andean Geology 40, 1-40

Kuntz, M.A., Champion, D.E., Spiker, E.C., Lefebre, R.H., 1986. Contrasting magma types and steady-state, volume-predictable, basaltic volcanism along the Great Rift, Idaho. Geological Society of America Bulletin 97, 597-594.

Lassiter, J.C., Hauri, E.H., 1998. Osmium-isotope variations in Hawaiian lavas: evidence for recycled oceanic lithosphere in the Hawaiian plume. Earth and Planetary Science Letters 164, 483-496.

Lassiter, J.C., Luhr, J.F., 2001. Osmium abundance and isotope variations in mafic Mexican volcanic rocks: Evidence for crustal contamination and constraints on the geochemical behaviour of osmium during partial melting and fractional crystallisation. Geochemistry, Geophysics, Geosystems 2, paper number 2000GC000116.

Le Corvec, N., Bebbington, M.S., Lindsay, J.M., McGee, L.E., 2013a. Age, distance and geochemical evolution within a monogenetic volcanic field: Analysing patterns in the

Auckland Volcanic Field eruption sequence. Geochemistry, Geophysics, Geosystems 14, 3648-3665.

Le Corvec, N., Spörli, K.B., Rowland, J., Lindsay, J., 2013b. Spatial distribution and alignments of volcanic centres: Clues to the formation of monogenetic volcanic fields. Earth-Science Reviews 124, 96-114.

LeMaitre, R.W., 2002. Igneous Rocks: Classification and Glossary of Terms. 2nd Edition, Cambridge University Press, pp236.

Leonard, G.S., Calvert, A.T., Wilson, C.J.N., Smid, E., Lindsay, J., Champion, D., Hopkins, J.L., *in prep.* High precision ^{40}Ar-^{39}Ar dating of late Quaternary basalts: the complex accelerating eruption rate of Auckland Volcanic Field, New Zealand.

Lindsay, J.M., Leonard, G.S., Smid, E.R., Hayward, B.W., 2011. Ages of Auckland Volcanic Field: a review of existing data. New Zealand Journal of Geology and Geophysics 54, 379-401.

Liu, J., Scott, J.M., Martin, C.E., Pearson, D.G., 2015. The longevity of Archean mantle residues in the convecting upper mantle and their role in young continent formation. Earth and Planetary Science Letters 424, 109-118.

Lorand, J-P., Alard, O, Luguet, A., 2010. Platinum-group element micronuggets and refertilisation process in Lherz orogenic peridotite (northeastern Pyrenees, France). Earth and Planetary Science Letters 289, 298-310.

Lowe, D.J., 1988a. Stratigraphy, age, composition and correlation of late Quaternary tephras interbedded with organic sediments in Waikato lakes, North Island, New Zealand. New Zealand Journal of Geology and Geophysics 31, 125-165.

Lowe, D.J., 1988b. Late Quaternary volcanism in New Zealand: towards an integrated record using distal airfall tephras in lakes and bogs. Journal of Quaternary Science 3, 111-120.

Lowe, D.J., 2011. Tephrochronology and its application: a review. Quaternary Geochronology 6, 107-153.

Lowe, D.J., Newnham, R. M., 2004. Role of tephra in dating Polynesian settlement and impact, New Zealand. Past Global Changes News 12, 5-7.

Lowe, D.J., Palmer, D.J., 2005. Andisols of New Zealand and Australia. Journal of Integrated Field Science 2, 39-65.

Lowe, J.J., Rasmussen, S.O., Björck, S., Hoek, W.Z., Steffensen, J.P., Walker, M.J.C., Yu, Z.C., 2008. Synchronisation of palaeoenvironmental events in the North Atlantic region during the Last Termination: a revised protocol recommended by the INTIMATE group. Quaternary Science Reviews 27, 6-17.

Lowe, D.J., Blaauw, M., Hogg, A.G., Newham, R.M., 2013. Ages of 24 widespread tephras erupted since 30,000 years ago in New Zealand, with re-evaluation of the timing and palaeoclimatic implications of the Lateglacial cool episode recorded in the Kaipo bog. Quaternary Science Reviews 74, 170-194.

Luguent, A., Nowell, G.N., Pearson, D.G., 2008. $^{184}Os/^{188}Os$ and $^{186}Os/^{188}Os$ measurements by negative thermal ionisation mass spectrometry (N-TIMS): effects of interfering elements and mass fractionation corrections on data accuracy and precision. Chemical Geology 248, 342-362.

Magill, C.R., McAneney, K.J., Smith, I.E.M., 2005. Probabilistic assessment of vent locations for the next Auckland Volcanic Field event. Mathematical Geology 37, 227-242.

Manville, V., Wilson, C.J.N., 2004. Vertical density currents: a review of their potential role in the deposition and interpretation of deep-sea ash layers. Journal of the Geological Society London 161, 947-958.

Marcantonio, F., Zindler, A., Elliott, T., Staudigel, H., 1995. Os isotope systematics of La Palma, Canary Islands; evidence for recycled crust in the mantle source of HIMU ocean islands. Earth and Planetary Science Letters 133, 397-410.

McBride, J.S., Lambert, D.D., Nicholls, I.A., Price, R.C., 2001. Osmium isotopic evidence for crust-mantle interaction in the genesis of continental intraplate basalts from the Newer Volcanics Province, Southeastern Australia. Journal of Petrology 42, 1197-1218.

McCoy-West, A.J., Baker, J.A., Faure, K., Wysoczanski, R., 2010. Petrogenesis and origins of Mid-Cretaceous continental intraplate volcanism in Marlborough, New Zealand: Implications for the long-lived HIMU magmatic mega-province of the SW Pacific. Journal of Petrology 51, 2003-2045.

McCoy-West, A.J., Bennett, V.C., Puchtel, I.S., Walker, R., 2013. Extreme persistence of cratonic lithosphere in the southwest Pacific: Paleoproterozoic Os isotopic signatures in Zealandia. Geology 41, 231-234.

McCoy-West, A.J., Bennett, V.C., O'Neill, H St. C., Hermann, J., Puchtel, I.S., 2015. The interplay between melting, refertilisation and carbonatite metasomatism in off-cratonic

lithospheric mantle under Zealandia: an integrated major, trace and platinum group element study. Journal of Petrology 56, 563-604.

McDonough, W.F., Sun, S.-s., 1995. The composition of the Earth. Chemical Geology 120, 223-253.

McGee, L.E., 2012. Melting processes in small basaltic systems: the Auckland Volcanic Field, New Zealand. Ph.D. thesis, University of Auckland, New Zealand.

McGee, L.E., Beier, C., Smith, I.E.M., Turner, S., 2011. Dynamics of melting beneath a small-scale basaltic system: a U-Th-Ra study for Rangitoto volcano, Auckland Volcanic Field, New Zealand. Contributions to Mineralogy and Petrology 162, 547-563.

McGee, L.E., Millet, M.-A., Smith, I.E.M., Németh, K., Lindsay, J.M., 2012. The inception and progression of melting in a monogenetic eruption: Motukorea Volcano, the Auckland Volcanic Field, New Zealand. Lithos 156, 360-374.

McGee, L.E, Smith, I.E.M., Millet, M.-A., Handley, H., Lindsay, J., 2013. Asthenospheric control of melting processes in a monogenetic basaltic system: a case study of the Auckland Volcanic Field, New Zealand. Journal of Petrology 54, 2125-2153.

McGee, L.E., Millet, M.-A., Beier, C., Smith, I.E.M., Lindsay, J.M., 2015. Mantle heterogeneity controls small-volume basaltic eruption characteristics. Geology 43, 551-554.

McKenzie, D., O'Nions, R.K., 1991. Partial melt distributions from inversion of rare earth element concentrations. Journal of Petrology 32, 1021-1091.

Meisel, T., Walker, R.J., Irving, A.J., Lorand, J-P., 2000. Osmium isotopic compositions of mantle xenoliths: A global perspective. Geochimica et Cosmochimica Acta 65, 1311-1323.

Meisel, T., Reisberg, L., Moser, J., Carignan, J., Melcher, F., Brugmann, G., 2003. Re-Os systematics of UB-N, a serpentinized peridotite reference material. Chemical Geology 201, 161-179.

Miller, C.A., 1996. Geophysical and geochemical characteristics of the Auckland Volcanic Field. MSc thesis, University of Auckland, New Zealand.

Miller, T.P., Casadevall, T.J., 2000. Volcanic ash hazards to aviation, in Sigurdsson, H. et al., ed., Encyclopedia of Volcanoes, San Diego, Academic Press pp331-343.

Mochizuki, N., Tsunakawa, H., Shibuya, H., Tagami, T., Ozawa, A., Cassidy, J., Smith, I.E.M., 2004. K-Ar ages of the Auckland geomagnetic excursions. Earth, Planets and Space 56, 283-288.

Molloy, C.M., 2008. Tephrostratigraphy of the Auckland maar craters. MSc thesis, University of Auckland, New Zealand.

Molloy, C.M., Shane, P., Augustinus, P., 2009. Eruption recurrence rates in a basaltic volcanic field based on tephra layers in maar sediments: implications for the hazards in the Auckland volcanic field. Geological Society of America Bulletin 121, 1666-1677.

Moufti, M.R., Moghazi, A.M., Ali, K.A., 2012. Geochemistry and Sr-Nd-Pb isotopic composition of the Harrat Al-Madinah volcanic field, Saudi Arabia. Gondwana Research 21, 670-689.

Needham, A., 2009. The eruptive history of Rangitoto volcano, Auckland Volcanic Field, New Zealand. MSc thesis, University of Auckland, New Zealand.

Needham, A.J., Lindsay, J.M., Smith, I.E.M., Augustinus, P., Shane, P.A., 2011. Sequential eruption of alkaline and subalkaline magmas from a small monogenetic volcano in the Auckland Volcanic Field, New Zealand. Journal of Volcanology and Geothermal Research 201, 126-142.

Nelson, W.R., Furman, T., van Keken, P.E., Shirey, S.B., Hanan, B.B., 2012. Os-Hf istopic insight into mantle plume dynamics beneath the East African Rift System. Chemical Geology 320-321, 66-79.

Németh, K., 2010. Monogenetic volcanic fields, origin, sedimentary record, and relationship with polygenetic volcanism. In Canon-Tapia, E., Szakacz, A., (Ed.), What is a Volcano? Geological Society of America Special Papers 470, 43-66.

Németh, K., White, J.D.L., Reay, A., Martin, U., 2003. Compositional variation during monogenetic volcano growth and its implications for magma supply to continental volcanic fields. Journal of the Geological Society, London 160, 523-530.

Németh, K., Cronin, S., Smith, I.M., Agustin-Flores, J., 2012. Amplified hazard of small volume monogenetic eruptions due to environmental controls, Orakei Basin, Auckland, Volcanic Field, New Zealand. Bulletin of Volcanology 74, 2121-2137

Newnham, R.M., Lowe, D.J., 1999. Testing the synchroneity of pollen signals using tephrostratigraphy. Global and Planetary Change 21, 113-128.

Newnham, R.M., Lowe, D.J., Alloway, B.V., 1999. Volcanic hazards in Auckland, New Zealand: a preliminary assessment of the threat posed by central North Island silicic volcanism based on the Quaternary tephrostratigraphical record. Geological Society London, Special Publications 161, 27-45.

Newnham, R.M., Lowe, D.J., Giles, T.M., Alloway, B.V., 2007. Vegetation and climate of Auckland, New Zealand, since ca. 32 000 cal. yr ago: support for an extended LGM. *Journal of Quaternary Science* 22, 517-534.

New Zealand Transport Agency, 2011. Submission report in support of application for variation under conditions. ACCC-Ash-Cloud.

Nicholls, I.A., Joyce, E.B., 1989, Newer Volcanics, in Johnson, R.W., ed., Intraplate volcanism in Eastern Australia and New Zealand: Cambridge University Press, Cambridge, pp. 137-140.

O'Driscoll, B., Day, J.M.D., Walker, R.J., Daly, S., McDonough, W.F., Piccoli, P.M., 2012. Chemical heterogeneity in the upper mantle recorded by peridotites and chromitites from the Shetland Ophiolite Complex, Scotland. Earth and Planetary Science Letters 333-334, 226-237.

Óladóttir, B.A., Sigmarsson, O., Larsen, G., Devidal, J-L., 2011. Provenance of basaltic tephra from Vatnajökull subglacial volcanoes, Iceland, as determined by major- and trace-element analyses. The Holocene 21, 1037-1048.

Óladóttir, B.A., Larsen, G., Sigmarsson, O., 2012. Deciphering eruption history and magmatic processes from tephra in Iceland. Jökull 62, 21-38.

Ort, M.H., Elson, M.D., Anderson, K.C., Duffield, W.A., Hooten, J.A., Champion, D.E., Waring, G., 2008. Effects of scoria-cone eruptions upon nearby human communities. Geological Society of America Bulletin 120, 476-486.

Ortega-Gutiérrez, F., Gómez-Tuena, A., Elías-Herrera, M., Solari, L.A., Reyes-Salas, M., Marcías-Romo, C., 2014. Petrology and geochemistry of the Valle de Santiago lower crust xenoliths: Young tectonothermal processes beneath the central Trans-Mexican volcanic belt. Lithosphere 6, 335-360.

Oxford Economics, 2010. The economic impacts of air travel restrictions due to volcanic ash. Report for Airbus. Oxford, Oxford Economics.

Paton, C., Hellstrom, J., Paul, B., Woodhead, J., Hergt, J., 2011. Iolite, freeware for the visualisation and processing of mass spectrometric data. Journal of Analytical Atomic Spectrometry 26, 2508-2518.

Payne, R.J., Gehrels, M.J., 2010. The formation of tephra layers in peatlands: an experimental approach. Catena 81, 12-23.

Pearce, N.J.G., Westgate, J.A., Perkins, W.T., Preece, S.J., 2004. The applications of ICP-MS methods to tephrochronological problems. Applied Geochemistry 19, 289-322.

Pearce, N.J.G., Denton, J.S., Perkins, W.T., Westgate, J.A., Alloway, B.V., 2007. Correlation and characteristation of individual glass shards from tephra deposits using trace element laser ablation ICP-MS analyses: current status and future potential. Journal of Quaternary Science 22, 721-736.

Pearce, N.J.G., Alloway, B.V., Westgate, J.A., 2008. Mid-Pleistocene silicic tephra beds in the Auckland region, New Zealand: their correlation and origins based on the trace element analyses of single glass shards. Quaternary International 178, 16-43.

Pertermann, M., Hirschmann, M.M., 2003. Partial melting experiments on MORB-like pyroxenite between 2 and 3 GPa: Constraints on the presence of pyroxenite in basalt source regions from solidus location and melting rate. Journal of Geophysical Research – Solid Earth 108 (B2), 12-29.

Peucker-Ehrenbrink, B., and Jahn, B., 2001. Rhenium-osmium isotope systematics and platinum group element concentrations: loess and the upper continental crust. Geochemistry, Geophysics, Geosystems 2, doi:10.1029/2001GC000172.

Pickrill, R.A., Nelson, C.S., Stoffers, P., Craig, G.G.P., 1991. Influence of late Holocene pyroclastic eruptions on the sedimentary geochemistry of Lake Rotoiti, North Island, New Zealand. Journal of Paleolimnology 6, 173-192.

Pyle, D.M., 1989. The thickness, volume and grain size of tephra fall deposits. Bulletin of Volcanology 51, 1-15.

Ramsey, M.H., Potts, P.J., Webb, P.C., Watkins, P., Watson, J.S., Coles, B.J., 1995. An objective assessment of analytical method precision: comparison of ICP-AES and XRF for the analysis of silicate rocks. Chemical Geology 124, 1-19.

Rasoazanamparany, C., Widom, E., Valentin, G.A., Smith, E.I., Cortés, J.A., Juentz, D., Johnsen, R., 2015. Origin of chemical and isotopic heterogeneity in a mafic, monogenetic

volcanic field: A case study of the Lunar Crater Volcanic Field, Nevada. Chemical Geology 397, 76-93.

Reisberg, L., Zindler, A., Marcantonio, F., White, W., Wyman, D., Weaver, B., 1993. Os isotope systematics in ocean island basalts. Earth and Planetary Science Letters 120, 149-167.

Robinson, J.A., Wood, B.J., 1998. The depth of the spinel to garnet transition at the peridotite solidus. Earth and Planetary Science Letters 164, 277-284.

Roy-Barman, M., Allègre, C.J., 1995. $^{187}Os/^{186}Os$ in oceanic island basalts; Tracing oceanic crust recycling in the mantle. Earth and Planetary Science Letters 129, 145-161.

Roy-Barman, M., Wasserburg, G.J., Papanastassiou, D.A., Chaussidon, M., 1998. Osmium isotope concentrations and Re-Os concentrations in sulphide globules from basaltic glasses. Earth and Planetary Science Letters 154, 331-347.

Rudnick, R.L., Fountain, D.M., 1995. Nature and composition of the continental crust – a lower crustal perspective. Reviews of Geophysics 33, 267-309.

Rudnick, R.L., Gao, S., 2003. Composition of the continental crust. Treatise on Geochemistry 3, 1-64.

Rymer, H., 2000. Volcanic Hazards. In Sigurdsson, H. et al., (Ed), Encyclopedia of Volcanoes, San Diego, Academic Press, pp. 895-896.

Saal, A.E., Rudnick, R.L., Ravizza, G.E., Hart, S.R., 1998. Re-Os isotope evidence for the composition, formation and age of the lower continental crust. Nature 393, 58-61

Sandiford, A., Alloway, B., Shane, P., 2001. A 28,000-6600 cal yr record of local and distal volcanism preserved in a paleolake, Auckland, New Zealand. New Zealand Journal of Geology and Geophysics 44, 323-336.

Schiano, P., Birck, J.-L., Allègre, C.J., 1997. Osmium-strontium-neodymium-lead isotopic covariations in mid-ocean ridge basalt glasses and the heterogeneity of the upper mantle. Earth and Planetary Science Letters 150, 363-379.

Schiano, P., Burton, K.W., Dupre,B., Birck, J.-L., Guille, G., Allegre, C.J., 2001. Correlated Os-Pb-Nd-Sr isotopes in the Austral-Cook chain basalts: the nature of mantle components in plume sources. Earth and Planetary Science Letters 186, 527-537.

Scott, J.M., Hodgkinson, A., Palin, J.M., Waight, T.E., Van der Meer, Q.H.A., Cooper, A.F., 2014. Ancient melt depletion overprinted by young carbonatitic metasomatism in the New Zealand lithospheric mantle. Contributions to Mineralogy and Petrology 167, 963.

Searle, E.J., 1959a. Schistose rocks from St Heliers Bay, Auckland. New Zealand Journal of Geology and Geophysics 2, 368-379.

Searle, E.J., 1959b. The volcanoes of Ihumatao and Mangere, Auckland. New Zealand Journal of Geology and Geophysics 2, 870-888.

Searle, E.J., 1961a. The age of the Auckland volcanoes. New Zealand Geographer 17, 52-63.

Searle, E.J., 1961b. The petrology of the Auckland basalts. New Zealand Journal of Geology and Geophysics 4, 165-204.

Searle, E.J., 1964. City of volcanoes: A geology of Auckland. Auckland, Pauls Book Arcade.

Searle, E.J., 1965. Auckland volcanic district. In Thompson, B.N., and Kermode, K.O., (Eds), New Zealand volcanology: Northland, Coromandel, Auckland. New Zealand, Department of Scientific and Industrial Research Information Series 49, 90-103.

Seebeck, H., Nicol, A., Giba, M., Pettinga, J., Walsh, J., 2014. Geometry of the subducting Pacific plate since 20 Ma, Hikurangi margin, New Zealand. Journal of the Geological Society, London 171, 131-143.

Shane, P., 2000. Tephrochronology: a New Zealand case study. Earth-Science Reviews 49, 223-259.

Shane, P., 2005. Towards a comprehensive distal andesitic tephrostratigraphic framework for New Zealand based on eruptions from Egmont Volcano. Journal of Quaternary Science 20, 45-57.

Shane, P., Smith, I.E.M., 2000. Geochemical fingerprinting of basaltic tephra deposits in the Auckland Volcanic Field. New Zealand Journal of Geology and Geophysics 43, 569-577.

Shane, P., Hoverd, J., 2002. Distal record of multi-sourced tephra in Onepoto Basin, Auckland, New Zealand: implications for volcanic chronology, frequency and hazards. Bulletin of Volcanology 64, 441-454.

Shane, P., Sandiford, A., 2003. Paleovegetation of marine isotope stages 4 and 3 in Northern New Zealand and the age of the widespread Rotoehu tephra. Quaternary Research 59, 420-429.

Shane, P., Zawalna-Geer, A., 2011. Correlation of basaltic tephra from the Mt. Wellington volcano: implications for the penultimate eruption from the Auckland Volcanic Field. Quaternary International 246, 374-381.

Shane, P.A., Black, T.M., Eggins, S.M., Westgate, J.A., 1998. Late Miocene marine tephra beds: recorders of rhyolitic volcanism in North Island, New Zealand. New Zealand Journal of Geology and Geophysics 41, 165-178.

Shane, P., Sikes, E.L., Guilderson, T.P., 2006. Tephra beds in deep-sea cores off northern New Zealand: implications for the history of Taupo Volcanic Zone, Mayor Island and White Island volcanoes. Journal of Volcanology and Geothermal Research 154, 276-290.

Shane, P., Gehrels, M., Zawalna-Geer, A., Augustinus, P., Lindsay, J., Chaillou, I., 2013. Longevity of a small shield volcano revealed by crypto-tephra studies (Rangitoto volcano, New Zealand): Change in eruptive behaviour of a basaltic field. Journal of Volcanology and Geothermal Research 257, 174-183.

Shapley, M.D., Finney, B.P., 2015. Lake morphometry controls the remobilization and long term geochemical imprint of distal tephra deposition. Journal of Paleolimnology 53, 309-320.

Shaw, C.S.J., 2004. The temporal evolution of three magmatic systems in the West Eifel volcanic field, Germany. Journal of Volcanology and Geothermal Research 131, 213-240.

Sivell, W.J., McCulloch, M.T., 2000. Reassessment of the origin of the Dun Mountain ophiolite, New Zealand: Nd-isotopic and geochemical evolution of magma suites. New Zealand Journal of Geology and Geophysics 43, 133-146.

Smith, I.E.M., Okada, T., Itaya, T., Black, P.M., 1993. Age relationships and tectonic implications of late Cenozoic basaltic volcanism in Northland, New Zealand. New Zealand Journal of Geology and Geophysics 36, 385-393.

Smith, I.E.M., Blake, S., Wilson, C.J.N., Houghton, B.F., 2008. Deep-seated fractionation during the rise of a small-volume basalt magma batch: Crater Hill, Auckland, New Zealand. Contributions to Mineralogy and Petrology 155, 511-527.

Smith, I.E.M., McGee, L.E., Lindsay, J.M., 2009. Review of the petrology of the Auckland Volcanic Field. Institute of Earth Science and Engineering technical report, University of Auckland, Auckland 1-2009.03

Sorrentino, L., Stilwell, J.D., Mays, C., 2014. A model of tephra dispersal from an early Palaeogene shallow submarine Surtseyan-style eruption(s), the Red Bluff Tuff Formation, Chatham Island, New Zealand. Sedimentary Geology 300, 86-102.

Spargo, S.R.W., 2007. The Pupuke volcanic centre: polygenetic magmas in a monogenetic field. MSc thesis, University of Auckland, New Zealand.

Spörli, K.B., Black, P.M., 2013. Catalogue of crustal xenoliths from the St Heliers Volcanoes, Auckland Volcanic Field, New Zealand. Institute of Earth Science and Engineering technical report, University of Auckland, Auckland 1-2013.01.

Spörli, K.B., Black, P.M., Lindsay, J.M., 2015. Excavation of buried Dun Mountain-Maitai terrane ophiolite by volcanoes of the Auckland Volcanic field, New Zealand. New Zealand Journal of Geology and Geophysics doi:10.1080/00288306.2015.1035285.

Striewski, B., Shulmeister, J., Augustinus, P.C., Soderholm, J., 2013. Late Holocene climate variability from Lake Pupuke maar, Auckland, New Zealand. Quaternary Science Reviews 77, 46-54.

Strong, M., Wolff, J., 2003. Compositional variations within scoria cones. Geology 31, 143-146.

Sun, S.-s., McDonough, W.F., 1989. Chemical and isotopic systematics of oceanic basalts: implications for mantle composition and processes. In Saunders, A.D., and Norry, M.J., (Eds.), Magmatism in the Ocean Basins. Geological Society, London, Special Publications 42, 313-345.

Suzuki, K., Senda, R., Shimizu, K., 2011. Osmium behaviour in a subduction system elucidated from chromian spinel in Bonin Island beach sands. Geology 39, 999-1002.

Tanaka, K.L., Shoemaker, E.M., Ulrich, G.E., Wolfe, E.W., 1986. Migration of volcanism in the San Francisco volcanic field, Arizona. Geological Society of America Bulletin 97, 129-141.

Thirlwall, M.F., 1997. Pb isotopic and elemental evidence for OIB derivation from young HIMU mantle. Chemical Geology 139, 51-74.

Thompson, M., Potts, P.J., Kane, J.S., Webb, P., Watson, J.S., 2000. GeoPT4 International proficiency test for analytical geochemistry laboratories. Geostandards Newsletter 24, E1-37.

Timm, C., Hoernle, K., van den Bogaard, P., Bindeman, I., Weaver, S., 2009. Geochemical evolution of intraplate volcanism at Banks Peninsular, New Zealand: interaction between asthenospheric and lithospheric melts. Journal of Petrology 50, 989-1023.

Timm, C., Hoernle, K., Werner, R., Hauff, F., van de Bogaard, P., White, J., Mortimer, N., Garbe-Schönberg, D., 2010. Temporal and geochemical evolution of the Cenozoic intraplate volcanism of Zealandia. Earth-Science Reviews 98, 38-64.

Tomsen, E., Lindsay, J.M., Gahegan, M., Wilson, T.M., Blake, D.M., 2014. Evacuation planning in the Auckland Volcanic Field, New Zealand: a spatio-temporal approach for emergency management and transportation network decisions. Journal of Applied Volcanology 6, 1-22.

Turner, M.B., Bebbington, M.S., Cronin, S.J., Stewart, R.B., 2009. Merging eruption data sets: building an integrated Holocene eruptive record for Mt Taranaki, New Zealand. Bulletin of Volcanology 71, 903-918.

Turner, M.B., Cronin, S.J., Bebbington, M.S., Smith, I.E.M., Stewart, R.B., 2011. Relating magma composition to eruption variability at andesitic volcanoes: A case study from Mount Taranaki, New Zealand. Geological Society of America Bulletin, 123, 2005-2015.

Valentine, G.A., Gregg, T.K.P., 2008. Continental basaltic volcanoes – processes and problems. Journal of Volcanology and Geothermal Research 177, 857-873.

Valentine, G.A., Hirano, N., 2010. Mechanisms of low-flux intraplate volcanic fields – Basin and Range (North America) and northwest Pacific Ocean. Geology 38, 55-58.

Valentine, G.A., Keating, G.N., 2007. Eruptive styles and inferences about plumbing systems at Hidden Cone and Little Black Peak scoria cone volcanoes (Nevada, USA). Bulletin of Volcanology 70, 105-113.

Valentine, G.A., Krogh, K.E.C., 2006. Emplacement of shallow dikes and sills beneath a small basaltic volcanic center – the role of pre-existing structure (Paiute Ridge, southern Nevada, USA. Earth and Planetary Science Letters 246, 217-230.

Valentine, G.A., Krier, D., Perry, F.V., Heiken, G., 2005. Scoria cone construction mechanisms, Lathrop Wells volcano, southern Nevada, USA. Geology 33, 629-632.

Valentine, G.A., Krier, D., Perry, F.V., Heiken, G., 2008 Eruptive and geomorphic processes at the Lathrop Wells scoria cone volcano. Journal of Volcanology and Geothermal Research 161, 57-80.

Vandergoes, M.J., Hogg, A.G., Lowe, D.J., Newnham, R.M., Denton, G.H., Southon, J., Barrell, D.J.A., Wilson, C.J.N., McGlone, M.S., Allan, A.S.R., Almond, P.C., Petchey, F., Dabell, K., Dieffenbacher-Krall, A.C., Blaauw, M., 2013. A revised age for the Kawakawa/Oruanui tephra, a key marker for the last glacial maximum in New Zealand. Quaternary Science Reviews 74, 195-201.

van Otterloo, J., Cas, R.A.F., 2013. Reconstructing the eruption magnitude and enery budgets for the pre-historic eruption of the monogenetic ~5 ka Mt. Gambier Volcanic Complex, south-eastern Australia. Bulletin of Volcanology 75, 769.

von Veh, M. W., Németh, K., 2009. An assessment of the alignments of vents based on geostatistical analysis in the Auckland Volcanic Field, New Zealand. Géomorphologie 3, 175-186.

Vogel, D.C., Keays, R.R., 1997. The petrogenesis and platinum-group element geochemistry of the Newer Volcanic Province, Victoria, Australia. Chemical Geology 136, 181-204.

Walker, G.P.L., 2000. Basaltic volcanoes and volcanic systems, in Sigurdsson, H. et al., ed., Encyclopaedia of Volcanoes, San Diego, Academic Press, pp283-289.

Walczyk, T., Hebeda, E.H., and Heumann, K.G., 1991. Osmium isotope ratio measurements by negative thermal ionisation mass spectrometry (NTI-MS). Improvement in precision and enhancement in emissions by introducing oxygen and freons into the ion source. Fresenius' Journal of Analytical Chemistry 344, 537-541.

Westgate, J.A., Gorton, M.P., 1981. Correlation techniques in tephra studies. In Self, S., Sparks, R.S.J., Editors, Tephra studies. Dordrecht, D. Reidel, 73-94.

Westgate, J.A., Perkins, W.T., Fuge, R., Pearce, N.J.G., Wintle, A.G., 1994. Trace element analysis of volcanic glass shards by laser ablation inductively coupled mass spectrometry: application to Quaternary tephrochronological studies. Applied Geochemistry 9, 323-335.

Widom, E., Hoernle, K.A., Shirey, S.B., Schmincke, H.-U., 1999. Os Isotope Systematics in the Canary Islands and Madeira: lithospheric contamination and mantle plume signatures. Journal of Petrology 40, 279-296.

Wilson, C.J.N., Rhoades, D.A., Lanphere, M.O., Calvert, A.T., Houghton, B.F., Weaver, S.D., Cole, J.W., 2007. A multi-approach radiometric age estimate for the Rotoiti and Earthquake flat eruptions, New Zealand, with implications for the MIS 4/3 boundary. Quaternary Science Reviews 26, 1861-1870.

Wilson, G., Wilson, T.M., Deligne, N.I., Cole, J.W., 2014. Volcanic hazard impacts to critical infrastructure: A review. Journal of Volcanology and Geothermal Research 286, 148-182.

Wimpenny, J., Gannoun, A., Burton, K.W., Widdowson, M., James, R.H., Gíslason S.R., 2007. Rhenium and osmium isotope and elemental behaviour accompanying laterite formation in the Deccan region of India. Earth and Planetary Science Letters 261, 239-258.

Winter, J.D., 2010. Principles of igneous and metamorphic petrology. 2nd ed. Pearson Prentice Hall, New Jersey.

Zawalna-Geer, A., 2012. Towards a tephra framework for the Auckland Maar lake sediments and the potential of applying cryptotephra techniques. Phd Thesis, University of Auckland, New Zealand.

Zindler, A., Hart, S., 1986. Chemical Geodynamics. Annual Review of Earth and Planetary Sciences 14, 493-571.

Zou, H., Fan, Q., Yao, Y., 2008. U-Th systematics of dispersed young volcanoes in NE China: Asthenosphere upwelling cause by piling up and upward thickening of stagnant Pacific slab. Chemical Geology 255, 134-142.